

CRANFIELD UNIVERSITY

GARETH EVANS

SEABED PROTECTION SYSTEMS

TO PREVENT SCOUR FROM

HIGH SPEED SHIPS

CRANFIELD DEFENCE AND SECURITY

PhD

CRANFIELD UNIVERSITY

CRANFIELD DEFENCE AND SECURITY
DEPARTMENT OF ENGINEERING SYSTEMS AND
MANAGEMENT

PhD

2009

Gareth Evans

Seabed Protection Systems to prevent Scour from High-Speed Ships

Supervisors: Dr C K Jolly/Dr K R McNaught

January 2010

Abstract

This document reviews the scour protection systems required around port structures where these are to be used for the berthing of vessels powered by water jet systems. The development of a scour protection system at Poole Harbour in Dorset has been documented and reviewed and a series of laboratory investigations were then undertaken. This has enabled a greater understanding of the scour mechanisms from the water jet propulsion systems of High Speed Ships. This work has shown that current design guidance on scour protection is not appropriate for use on berths used by High Speed Ships, that failure of these systems can occur rapidly and catastrophically, and secondary effects from water jets may promote the failure of quay walls. The scour protection system should comprise two individual elements, a filter layer and an armour layer. It has been found that systems involving individual isolated armour units are inappropriate and prone to failure and that shaped linked armour blocks need to be used. The loads on the armour layer were also found to be oscillatory and the materials used for both the armour and filter layers need to be designed for cyclic fatigue loading and fretting. Water jets are also capable of reducing the strength of permeable, seabed strata.

CONTENTS

| | |
|---|-----|
| CONTENTS | iii |
| LIST OF FIGURES | vii |
| GLOSSARY | xi |
| Chapter 1 | 1 |
| INTRODUCTION | 1 |
| 1.1 Background..... | 1 |
| 1.2 Project aims | 3 |
| 1.3 Project objectives | 4 |
| Chapter 2 | 5 |
| LITERATURE SURVEY AND BACKGROUND THEORY | 5 |
| 2.1 Growth and Trends of High Speed Ships | 5 |
| 2.2 Scour..... | 7 |
| 2.3 Structure – Scour interaction | 9 |
| 2.4 Soil Liquefaction | 15 |
| 2.5 Scour Protection Systems | 16 |
| 2.6 Scour Modelling | 22 |
| 2.7 Background Theory | 30 |
| 2.8 Air Entrainment..... | 32 |
| 2.9 Hydraulic Similitude | 32 |
| Chapter 3 | 36 |
| DISCUSSION ON CURRENT DESIGN GUIDANCE | 36 |
| 3.1 Current Design | 36 |
| 3.2 Design Guidance | 38 |
| Chapter 4 | 42 |
| THE CHARACTERISTICS OF HIGH SPEED SHIPS | 42 |
| 4.1 General Features..... | 42 |
| 4.2 Water Jet Drives | 45 |
| 4.3 Jet Vectors | 46 |

| | | |
|--|---|-----|
| 4.4 | Intakes | 47 |
| Chapter 5 | | 50 |
| POOLE HARBOUR SEABED PROTECTION SYSTEM | | 50 |
| 5.1 | Background | 50 |
| 5.2 | Development Sequence for the Seabed Protection..... | 52 |
| 5.3 | Phase I..... | 54 |
| 5.4 | Seabed Monitoring | 56 |
| 5.5 | Phase II Works | 60 |
| 5.6 | Phase II Monitoring..... | 62 |
| 5.7 | Phase III Works | 62 |
| 5.8 | Phase IV Works..... | 64 |
| 5.9 | Discussion on the Poole Harbour Works | 65 |
| Chapter 6 | | 68 |
| LABORATORY MODELLING | | 68 |
| 6.1 | Introduction | 68 |
| 6.2 | Description of the Physical Model..... | 68 |
| 6.3 | Discussion on the model and calibration procedures..... | 80 |
| 6.3 | Scale Factors | 87 |
| Chapter 7 | | 92 |
| Model Test Results and Data Analysis | | 92 |
| 7.1 | Introduction | 92 |
| 7.2 | Data Handling | 92 |
| 7.2 | Data Preparation | 97 |
| 7.3 | Data analysis and integrity checking | 100 |
| 7.6 | Example test run commentary | 105 |
| 7.5 | Static pressure readings..... | 108 |
| Chapter 8 | | 112 |
| Discussion of MODEL TEST Results | | 112 |
| 8.1 | Introduction..... | 112 |
| 8.2 | Force oscillations | 112 |

| | | |
|--|---|-----|
| 8.3 | Jet velocity | 118 |
| 8.4 | Air entrainment | 121 |
| 8.5 | Static Pressures..... | 125 |
| Chapter 9 | | 128 |
| DISCUSSION ON THE SCOUR PROTECTION SYSTEM | | 128 |
| 9.1 | Introduction..... | 128 |
| 9.2 | Block ejection | 129 |
| 9.3 | Block migration and movement | 137 |
| 9.4 | Fatigue failure of the filter membrane..... | 142 |
| Chapter 10 | | 144 |
| CONCLUSIONS | | 144 |
| 10.1 | General comments..... | 144 |
| 10.3 | Armour layer | 146 |
| FUTURE WORK | | 148 |
| References | | 150 |
| APPENDIX 1 - Model Test Details and Run Analyses | | |

LIST OF FIGURES

| | |
|--|----|
| Figure 1: Section through a gravity quay wall showing overturning and stabilising forces | 10 |
| Figure 2: Schematic diagram of an open piled quay and deck slab | 11 |
| Figure 3: Schematic diagram of a sheet piled wall showing the overturning and restoring forces..... | 12 |
| Figure 4: Showing interconnected Armorflex concrete units | 17 |
| Figure 5 Showing stone pitching being bonded by asphalt and an interlocking concrete block system | 18 |
| Figure 6: Section through a grouted mattress | 18 |
| Figure 7: Laying a grouted mattress | 19 |
| Figure 8: Showing concrete ‘dolos’ | 20 |
| Figure 9: Concrete Tetrapod..... | 20 |
| Figure 10: Development stages of a water jet entering a plunge pool | 25 |
| Figure 11: Diagram showing the scour formation cycle from a free falling jet..... | 26 |
| Figure 12: Pressures causing rock ejection..... | 30 |
| Figure 13: Drag coefficient versus Reynolds number | 31 |
| Figure 16: Maximum bed velocity from a single propeller | 39 |
| Figure 17: Mean stone size required for a given flow velocity | 40 |
| Figure 18: Typical High Speed Ferry | 43 |
| Figure 19: Illustration of jet drive installation | 44 |
| Figure 20: S type Jet Drive unit manufactured by Rolls Royce | 45 |
| Figure 21: A Type jet Drive unit manufactured by Rolls Royce | 45 |
| Figure 22: Deployment of deflector bucket for manoeuvring | 47 |
| Figure 23: Jet vector for steerage | 47 |
| Figure 24: Location of Poole Harbour Ferry Terminal..... | 51 |
| Figure 25: Schematic diagram showing the seabed clearances for the HSS..... | 52 |
| Figure 26: Pre-construction survey..... | 53 |
| Figure 27: Phase 1 works at Poole Harbour Terminal 2..... | 54 |
| Figure 28: Seabed profiles at the linkspan after installation of the phase 1 works | 56 |
| Figure 29: Instrumentation and technique used for rock levelling | 57 |
| Figure 30: Concrete block installation by divers using purpose made lifting frame | 61 |
| Figure 31: Arrangement of concrete blocks phase 3 (NB Phase 2 similar but with only 4 block sets in the corner of the berth) | 63 |

| | |
|--|-----|
| Figure 32: The improved sheet pile scour protection detail | 64 |
| Figure 33: Schematic view on test tank showing seabed plated and model blocks | 69 |
| Figure 34: Schematic diagram showing concrete block supports and load measuring system..... | 70 |
| Figure 35: General view of test tank..... | 73 |
| Figure 36: Loading Frame | 74 |
| Figure 37: Steel formwork for the model scour protection blocks | 74 |
| Figure 38 : Drawing of Model Scour Protection | 75 |
| Figure 39: General view of loading frame showing gauge bars | 75 |
| Figure 40: View on bridge amplifier and ‘Pad’ data logger | 76 |
| Figure 41: Pump unit and connection hose..... | 76 |
| Figure 42: Jet pipe and air feed | 77 |
| Figure 43: Load gauge..... | 77 |
| Figure 44: Gauge bar and strain gauge | 78 |
| Figure 45: Showing model concrete blocks and connection rods..... | 79 |
| Figure 46: Diagram of static pressure measurement system | 79 |
| Figure 47: Layout of lower seabed platform and position of static pressure tapings..... | 80 |
| Figure 48: Calibration graph gauge 3 | 82 |
| Figure 49: Graph showing the secondary gauge deflections when support 1 only is loaded..... | 85 |
| Figure 50: Jet flow versus pump speed..... | 88 |
| Figure 51: Air valve setting versus air flow rate | 89 |
| Figure 52: Air valve setting versus air entrainment % by volume for various pump speeds..... | 90 |
| Figure 53: Conversion of raw data | 97 |
| Figure 54: Frequency analysis procedure | 98 |
| Figure 55: Data analysis carried out on the data for each test run | 99 |
| Figure 56: Example of Data Analysis Summary | 101 |
| Figure 57: Example of load v time graph for a gauge (Run 2 Load gauge 9) | 102 |
| Figure 58: Example of a load v time graph showing total loads on blocks (Run 2 block loads)..... | 103 |
| Figure 59: Example of a load time graph used to check frequency analysis | 104 |
| Figure 60: Example of a load v time graph (Run 1 Load gauge 3)..... | 107 |
| Figure 61: Showing the ejected block set following test run 1 | 108 |
| Figure 62: Single load gauge reading on block 2 Run 2 Load gauge 4)..... | 114 |

| | |
|--|-----|
| Figure 63: Block loads v time for multiple blocks (Run 2 Block Loads) | 115 |
| Figure 64: Gauge loads v time single block (Run 22) | 116 |
| Figure 65: Illustration of secondary graph oscillations for a load v time (Run 3 gauge 5 including a 10 period moving average) | 117 |
| Figure 66: Load transfer mechanism between blocks | 118 |
| Figure 67: Block Force vs. jet velocity | 119 |
| Figure 68: Air entrainment v force for 1.46 m/s jet flow | 121 |
| Figure 69: Air entrainment v force for 2.00 ms ⁻¹ jet flow | 122 |
| Figure 70: Air entrainment v force for 2.49 m/s jet flow | 122 |
| Figure 71: Air entrainment v force range for 1.46 m/s jet flow | 123 |
| Figure 72: Air entrainment v force range for 2.00 m/s jet flow | 124 |
| Figure 73: Air entrainment v force range for 2.49 m/s jet flow | 124 |
| Figure 74: Static pressure reading v jet flow with no air entrainment | 125 |
| Figure 75: Static pressure readings v jet flow with air entrainment | 126 |
| Figure 76: Schematic diagram showing mechanism for potential pressure increase beneath concrete blocks | 130 |
| Figure 77: Showing the load gauge readings before and after the ejection of an adjacent block set... 132 | 132 |
| Figure 78: Illustrating mechanism for uplift pressures on blocks | 133 |
| Figure 79: Showing maximum pressure under blocks as a result of jet flow | 134 |
| Figure 80: Required concrete block thicknesses for a given jet flow (Prototype) | 136 |
| Figure 81: Time v force to achieve ejection of block | 140 |
| Figure 82: Required concrete block thicknesses for a given jet flow | 147 |

GLOSSARY

| | |
|----------|---|
| A_p | <i>difference between the mass density of the sediment and the fluid</i> |
| b | <i>pier width</i> |
| B | <i>air / water ratio</i> |
| C | <i>clearance distance between the propeller tip and the seabed</i> |
| C_t | <i>propeller thrust coefficient</i> |
| d | <i>diameter of wire</i> |
| d | <i>grain size</i> |
| d_{50} | <i>median sediment grain size</i> |
| D_M | <i>equivalent spherical diameter for the unit 1.6 Dm for Toskanes</i> |
| D_m | <i>mean size of bed material</i> |
| D_p | <i>propeller diameter</i> |
| E | <i>Young's modulus</i> |
| E_m | <i>maximum depth of scour</i> |
| f | <i>frequency</i> |
| f_c | <i>Nyquist frequency</i> |
| F_0 | <i>Densimetric Froude number</i> |
| g | <i>gravitational constant</i> |
| h | <i>tailwater depth above unscoured bed</i> |
| H_p | <i>distance from propeller centreline to top of scour protection/seabed</i> |
| I | <i>second moment of area</i> |
| K_a | <i>active earth pressure coefficient</i> |
| K_p | <i>passive earth pressure coefficient</i> |
| L | <i>largest dimension of the precast concrete scour unit</i> |
| n | <i>number of propeller revolutions per second</i> |
| P_d | <i>dynamic pressure</i> |

| | |
|---------------|---|
| P_{ub} | <i>water Pressure beneath scour blocks</i> |
| q | <i>discharge per unit width of plane jet</i> |
| R_e | <i>Reynolds number</i> |
| R_{ej} | <i>Reynolds number of the jet</i> |
| R_p | <i>pressure coefficient for scour protection design</i> |
| s | <i>specific gravity of the bed sediment</i> |
| sg | <i>specific gravity</i> |
| S | <i>maximum equilibrium scour depth without a rudder</i> |
| T | <i>scour depth</i> |
| u | <i>pore water pressure</i> |
| U_0 | <i>initial velocity</i> |
| U_{max} | <i>maximum velocity at bed level</i> |
| Vo | <i>average approach flow velocity</i> |
| V_0 | <i>efflux velocity</i> |
| W | <i>weight</i> |
| W_i | <i>self weight</i> |
| W_l | <i>waterline length of a vessel</i> |
| z | <i>water of soil depth</i> |
| ϑ | <i>undisturbed Shields parameter</i> |
| τ_∞ | <i>bed shear stress for the undisturbed flow</i> |
| ρ'_a | <i>active soil pressure due to effective stress</i> |
| ρ'_p | <i>passive soil pressure due to effective stress</i> |
| ρ | <i>density of fluid</i> |
| γ | <i>density of the soil</i> |
| ν | <i>kinematic viscosity of the fluid</i> |
| δ_{st} | <i>initial displacement</i> |
| λ | <i>geometric scale factor</i> |

Chapter 1

INTRODUCTION

This report is a PhD research project, the purpose of which is to investigate the scour effects from High Speed Ships (HSS) around port structures and to consider the requirements for scour protection systems.

This project has been conducted at Cranfield University (Defence Academy) by Gareth Evans.

1.1 Background

The project was initiated from construction works carried out at Poole Harbour, Dorset where a traditional scour protection scheme was designed to current design criteria and which subsequently proved inadequate. Following this failure a new scour protection scheme was developed and constructed that was found to be capable of resisting the scour forces. A physical model of the scour protection system used at Poole Harbour was developed to study the behaviour and gain a greater understanding of the system. The relationship between the water jet flow and the scour protection system has been investigated and better understanding of the design criteria obtained.

Since the 1990's there has been tremendous growth in the deployment and use of high speed ships (HSS). The effect that these craft are having on the industry is being compared with the change to container ships in the 1960's, and the predictions suggest this growth will continue (Baird & Martin, 1998). These vessels operate at speeds in excess of 28 knots which is around 1½ to 2 times that of conventional ferries. This speed advantage is a critical factor in the growth in operation of these vessels, which are now predicted as being able to provide effective competition against overloaded road and rail transport links in the near future.

The design of high speed ships varies from conventional vessels both in terms of their hull shape and propulsion systems due to the use of catamaran (wave piercing hulls) and water jet technology.

The designers of the new high speed ferries have configured the vessels to enable them to operate from the berths originally intended for the conventional vessels, using normal Roll on Roll off (Ro Ro) facilities. Similarly their draught is typically the same or less than already available so dredging is not usually required and their gross tonnage is typically less than similar size conventional vessels enabling the existing fender systems to be retained. Consideration is being given to the design of temporary floating berthing facilities for these vessels to allow their use in strategically important locations for short periods (Baird & Martin, 1998).

The current generation of high speed ferries may be characterised as wide beam with catamaran hulls and water jet propulsion. They tend to be of aluminium construction with wave piercing hulls, and stern loading ramps. The move away from conventional propeller drive is primarily due to the greater efficiency of jet drive units when operating at high speeds. The use of water jet drive systems has also meant that the directional control of these vessels is no longer achieved by a rudder but by direct vectoring of the propulsion jets. The configuration of the vector system enables a proportion of the jet flow to be directed downwards at approximately 40 to 60 degrees to the horizontal onto the seabed. This is their normal position when drive is engaged but no translational thrust is required and the rearward thrust is balanced by the component of the jet that is vectored downwards and forwards. It is this arrangement that is giving rise to serious scour problems around port structures.

Scour problems arising from conventional propeller driven ships has been widely appreciated for many years and conventional protection systems have been normally alleviated the problem (Berg & Cederwall, 1981), (Hamill, 1988). The introduction of high speed ferries with their water jet propulsion systems has given rise to scour problems on berths previously used by conventional ships at a number of UK ports. These problems have also shown that conventional scour protection systems installed to protect against propeller driven vessels are unlikely to prove adequate in protecting

against high speed ferries. Quantitative records for scour are difficult to obtain because there is often reluctance on the part of port authorities to publicise these problems (Whitehouse, 1998).

In order to reduce the costs incurred by using tugs to assist in berthing and unberthing operations even the modern conventional propeller driven vessels are now being fitted with large powerful bow thrusters or vectored nozzles that are producing similar thrusts and wash to the jet units. This is particularly the case for ferries and other vessels on regular service. During the preparation of this report the displacement vehicle ferry operating out of Poole Harbour was replaced by a new larger vessel equipped with ducted nozzles as opposed to conventional propellers. Within days of commencing operations this new vessel caused acute scour problems within the Port.

1.2 Project aims

The following project aims have been developed to provide design parameters to assist in the design of new scour protection systems for HSS berths and manoeuvring areas.

- To review the scour protection systems used at Poole Harbour and identify both the problems that occurred and the solutions that were adopted and to draw conclusions for the future design of scour protection systems.
- To develop a physical model of the scour protection system used to allow the measurement of the hydraulic forces on the protection system.
- To review the current design guidance for engineers on appropriate protection systems taking into account:
 - * The propulsion system.
 - * The nature of the seabed.
 - * The selection of materials and systems

1.3 Project objectives

The project objectives and deliverables are set out below.

- 1 To fully document and analyse the staged development of the Poole Harbour scour protection system in order to identify the critical parameters for future design.
- 2 To investigate localised effect of water jets on the scour protection system by physical modelling in a laboratory tank. The model tank was used to investigate the displacement forces on the scour protection blocks generated over a range of water jet velocities and for permeable and impermeable seabed conditions.
- 3 To examine the effect of air entrainment in the water jet.
- 4 A review of the suitability of the scour protection used at Poole Harbour and provide recommendations for further investigation work.

Chapter 2

LITERATURE SURVEY AND BACKGROUND THEORY

This chapter provides background on the growth of high speed ships and expected future trends both in deployment and design changes to these vessels. No previous work into modelling the scour effects from high speed ferries has been found. Therefore previous works have been examined relating to scour protection systems, scour effects from conventional propeller driven vessels and modelling work carried out on water jets from dam spillways.

2.1 Growth and Trends of High Speed Ships

Conventional ferries are displacement vessels and as such their maximum through water velocity, according to Froude's laws, is a function of their waterline length. This speed is given by the formula:

$$\text{Hull speed (knots)} = 2.427 \sqrt{W_l} \quad \dots\dots\dots \text{Equation 1}$$

Where W_l is the waterline length of the vessel in metres

Since conventional ferries have typical length in the range 80 to 140 metres it can be seen that their maximum cruising speeds will be in the range:

20 Kts. – 28 Kts.

This hull speed is also known as the 'hump' speed and is discussed by Lewis (1988), it forms a natural speed restriction for conventional vessels. For vessels to exceed their natural hull speed they need to have sufficient power to climb over their bow wave and lift clear of the wave trough that is formed by a displacement hull. This can be achieved by applying a large amount of power to a vessel with a planing hull or as in the case of the high speed ferries by using a wave piercing hull together with the aerodynamic lift from the catamarans deck.

High Speed Vessels with speeds typically greater than 28 knots represent a trend in shipping that is affecting both short and deep-sea traders (National Ports and Waterways Institute Louisiana State University, 2000). Tremendous growth in the use of these vessels has occurred since the early 1990's with these craft providing competition to conventional ferries on most of the main ferry routes around the UK, Europe and in many parts of the rest of the world (Karayannis et al., 2000).

When these craft were initially put into service they were heralded as the most significant change in sea transport since the introduction of container vessels. However, predicted growth trends for these vessels have not been met in recent years. This has been due to the rising fuel costs, environmental and sea keeping issues. Notwithstanding this it is clear from recent developments that vessel designers are solving these problems and that the growth in the use of these vessels will continue. It is also likely that a new generation of high speed Ro Ro cargo vessels will be brought into service that will allow a modal shift of cargo that is currently carried on congested highways. (Akagi, 1991)

The developments taking place are likely to offer alternatives to the gas turbine motive power units that are currently used in the HSS (Wood, 2000). But the current proposals by ship designers are based upon retaining the existing water jet propulsion units.

2.2 Scour

The scour process is described by Sumer and Fredsoe (2002) as the loss of material resulting from the insertion of a structure in a flow. This is to differentiate from erosion which is considered as loss of material under 'natural' flow conditions. Scour has then been categorized into two forms

- clear water scour when no sediment motion takes place far from the structure, $\theta < \theta_{cr}$
- live bed scour when sediment transport occurs over the entire bed, $\theta > \theta_{cr}$

where θ is the undisturbed Shields parameter defined by;

$$\theta = \frac{U_f}{g(s-1)d} \dots\dots\dots \text{Equation 2}$$

and

$$U_f = \sqrt{\tau_\infty / \rho} \dots\dots\dots \text{Equation 3}$$

(In the case of waves τ_∞ should be replaced by $\tau_{max,sc}$ the maximum value of the undisturbed bed shear stress.)

Where;

τ_∞ = the bed shear stress for the undisturbed flow

s = specific gravity of the bed sediment

g = gravitational constant

d = grain size

and θ_{cr} is the critical value of the Shields parameter (Shields, 1936) corresponding to sediment motion

This categorization has been extended to include;

- Global scour
- Local scour

Where global scour occurs over the whole structure location and local scour is confined around individual elements of the structure. It is often the case that local scour is additive to the global scour. Examples of local compared to global scour are given for offshore structures by Angus and Moore (1982). These terms can become somewhat blurred in the case where repeated local scour events can appear to cause progressive global scour (Whitehouse, 1998)

In the case of vessel movements we can apply a similar definition, but in this case scour can be defined as the loss of natural seabed material as a result of the hydraulic flows generated by the vessels propulsion and manoeuvring systems.

In many instances the occurrence of scour is minor and has no significant affect on the function and stability of the adjacent structures. To establish the importance of scour it is necessary to determine the likely effect on the environment, or adjacent structures, which in the case of seabed scour will involve predicting the depth and area of the scour, the likely duration and frequency of the scour source and the possible structural or functional implications. The initial study should identify all forms of scour as described above that may be present to enable the ‘in combination’ effect of likely scour to be assessed.

2.3 Structure – Scour interaction

Due to the hidden nature of scour where it gives rise to structural failure this can be instantaneous with little or no prior indications of distress. In the case of bridge structures this has resulted in significant loss of life and has been the subject of national concern (Standing Committee on Structural Safety, 1994). Following this report, inspection regimes were adopted within the UK to carry out assessment and routine monitoring for scour on both highway and rail bridges. At the same time many port operators have also become concerned over the potential of scour damage and many have introduced regular monitoring regimes.

In the design of marine structures the current guidance (British Standards Institute, 1984) the only allowance for loss of bed material is a requirement to include for an over-dredge of 1 metre of bed material. Therefore unless the designer recognises the potential for scour there is no tolerance allowed in a design to accommodate anything other than minor bed loss adjacent to the structure.

In the case of port structures the basic structural forms are described below, together with the potential failure mechanisms due to both scour and soil liquefaction or weakening.

Gravity Structures

These structures are founded at a relatively shallow embedment and derive their lateral and overturning stability from their mass. Typical examples are mass concrete walls and caissons. Due to the shallow foundations they are vulnerable to scour and potential failure mechanisms include direct under scour of the foundations, toe scour causing either rotational failure of the structure, or rotational shear failure of the soil. Figure 1 shows the typical structural arrangement of a gravity quay wall together with the overturning and stabilising forces acting on the wall. It can be seen that any significant loss of seabed from the toe of the wall will result in a reduction in sliding resistance and gross loss can result in the development of a soil slip plane which would promote failure in overturning.

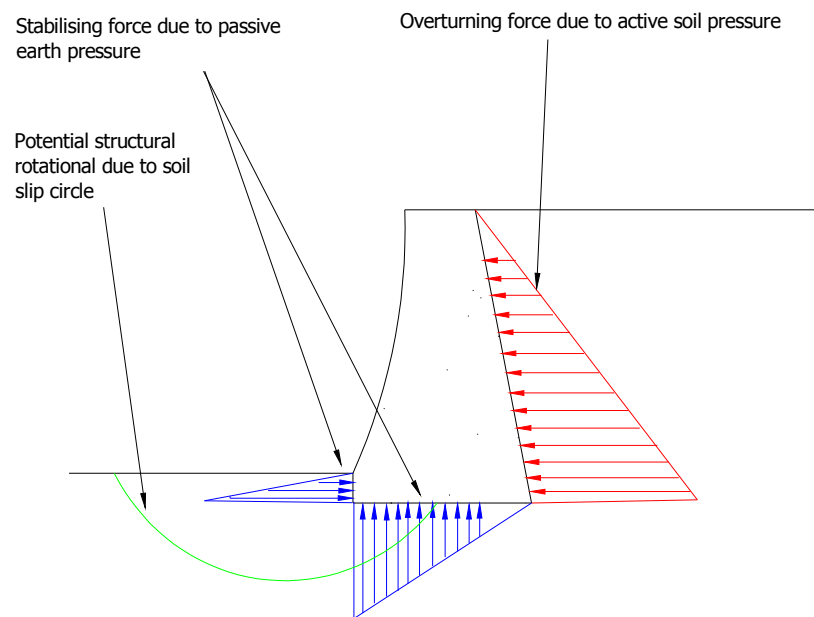


Figure 1: Section through a gravity quay wall showing overturning and stabilising forces

Open Piled Structures

The revetment slope beneath an open piled structure is prone to scour, toe scour can give rise to slip failure of the embankment and consequential lateral loading and shear failure of the piles

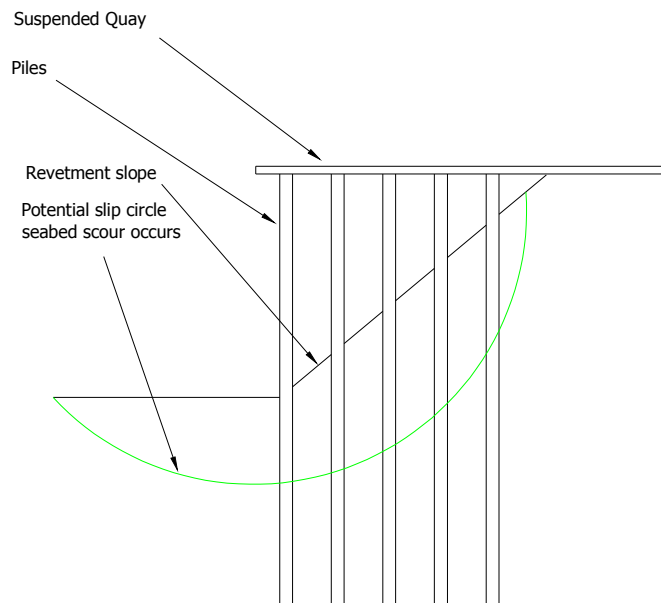


Figure 2: Schematic diagram of an open piled quay and deck slab

Sheet Piled Walls

This is a common form of construction for modern berths where the ground conditions permit. This form of construction often uses horizontal ties positioned at the level of Mean Low Water Spring tides and connected to anchor pile or blocks located behind the sheet piling and outside the zone of influence.

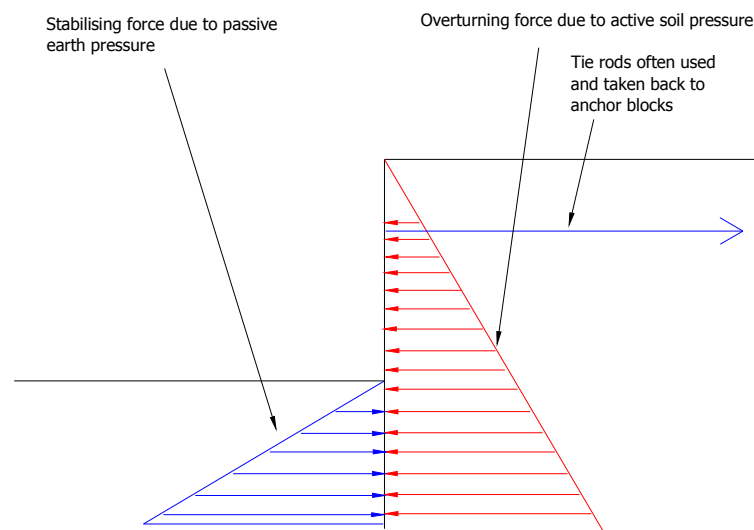


Figure 3: Schematic diagram of a sheet piled wall showing the overturning and restoring forces

These structures derive their stability from passive earth pressure of the seabed on the seaward side of the sheet piling. Even temporary removal of seabed material will cause loss of passive earth pressure as a stabilizing force on the sheet piling which cannot then be readily re-established (Simpson & Driscoll, 1998). This is illustrated by comparing the typical coefficients of earth pressure.

In non cohesive soils the effective active pressure behind a retaining wall is given by

$$\rho_a' = K_a(\gamma z - u) \dots \dots \dots \text{Equation 4}$$

The passive earth pressure is similarly calculated using the coefficient of passive earth pressure (Tomlinson & R, 2001, pp.199-206)

$$\rho_p' = K_p(\gamma z - u) \dots \dots \dots \text{Equation 5}$$

Where;

ρ_a' = Active soil pressure due to effective stress

ρ_p' = Passive soil pressure due to effective stress

K_a and K_p are the active and passive earth pressure coefficients respectively

γ is the bulk density of the soil

z is the depth

u is the pore water pressure

Typical values of the active soil pressure coefficients for non cohesive soils are tabulated below:

Table 1: Typical values for Active and Passive Earth Pressure coefficients

(Tomlinson & R, 2001)

| ϕ' (Angle of shearing resistance) | K_a | K_p |
|--|-------|-------|
| 20 | 0.5 | 2.1 |
| 25 | 0.42 | 2.5 |
| 30 | 0.35 | 3 |
| 35 | 0.27 | 3.8 |
| 40 | 0.22 | 4.6 |

Following a scour event due to a ship propulsion system the scour hole will typically refill. This is especially true with HSS scour since the holes formed tend to be deep and steep sided. Where the scour occurs in front of a sheet piled wall the stabilizing force from the soil will reduce as the coefficient of passive earth pressure is no longer valid and tends towards the lower bound coefficient of active earth pressure.

2.4 Soil Liquefaction

When the pore water pressure in a non cohesive soil increases, it reduces the effective stress between the soil particles. This process is fundamental to the study of geotechnical engineering and variation in the pore water pressure within a soil can be brought about by a number of factors for example ground water flows, loading and waves. Any increase in pore water pressure in a non cohesive soil will give rise to a reduction in the soil strength, and the ultimate stage is when the pore pressure equals the overburden pressure giving rise to soil liquefaction. It is important however to recognise that prior to reaching liquefaction there is a progressive loss in soil strength as can be seen from equation 5. The effect of surface waves in certain circumstances has also been found to give rise to significant pore pressure variation to cause soil liquefaction in the marine environment. This effect has caused movement and failure of subsea pipelines and scour protection blocks (Sakai et al., 1992) (Sakai & Gotoh, 1994).

This problem has been studied in detail by Sumer and Fredsoe (2002) in respect of wave induced liquefaction on pipelines and armour blocks. This work was focussed on the cyclic build up of soil pore pressure induced by a wave train. In some cases the pressure increase was sufficient to cause liquefaction of the soil. Where this occurs in proximity to structures as demonstrated in section 2.3 even a modest increase in pore pressure can reduce the Factor of Safety of the structure. It is also the case that even a temporary rise in pore pressure within a soil can cause a permanent loss of soil strength. It is not current design practice to allow reduction in soil strength parameters due to this effect (British Standards Institute, 1984).

In the case of the work at Poole Harbour the original rock armour blocks not in the direct scour area were found to have been buried deeper than their original placement depth. It is thought that this was caused by the blocks sinking into the seabed following soil liquefaction caused by the water jets.

In addition if it is proved that the HSS jets are giving rise to an increase in pore pressure within the seabed strata this process would have a similar effect to that described above in reducing the passive soil resistance in front of port structures.

2.5 Scour Protection Systems

Any scour protection system is required to fulfil two functions:

- 1) Reduce the action of the water velocity causing the scour.
- 2) Increase the resistance of the natural strata to erosion.

To achieve these requirements, most systems comprise two components, a cover (or armour) layer and a filter layer. The exception to this is where the cover layer is impermeable and a filter layer is therefore not required.

Impermeable cover layers should only be used where excess pore pressure (which could give rise to uplift) within the substrata can be ruled out. In the case of marine structures this is very unlikely to be the case since pore pressure variations are likely to occur from:

- * Waves
- * Pressures within the seabed strata generated by the combination of low permeability and tidal lag.
- * Inflows through the seabed under adjacent dock structures due to ground water flows and tidal lag.

Cover Layers

Typical cover layers include rip-rap (placed natural stone), concrete blocks, concrete bagwork, stone filled gabion baskets and geocontainers. The resistance of all single element systems against hydrodynamic forces increases with the weight of the element, but this weight increase is usually linked to an increase in size. These systems are typically layered 1.5 to 2 units in thickness. Where individual units become very large this tends to increase the voids between the units placing greater demands on the filter layer. This size requirement also proves a limiting factor in design where navigational clearances are to be met or involves greater seabed excavation and increases the design retention height of any adjacent structures.

In order to minimise the thickness of the armour layer but retain an adequate resistance against hydrodynamic forces, Heibaum (2000) recommends the use of connected armour elements. This can be achieved by connecting individual units together as in gabions or binding units together by partial grouting or by use of open textured asphalt. An interlocking paved system will also provide a degree of interconnectivity but this will lose all resistance once a small section starts to fail.



Figure 4: Showing interconnected Armorflex concrete units

(Reproduced from the Armorflex™ catalogue)



Figure 5 Showing stone pitching being bonded by asphalt and an interlocking concrete block system

(Reproduced from the Hesselberg-hydro Ltd and the Armorflex™ catalogues)

The oldest forms of scour protection are fascine mattresses which are willow bundles of 100-400mm diameter tied together.

Continuous layer protection can also be provided by geosynthetic mattresses filled with concrete or mortar, their placement can be endless because mattresses can be zipped or sewn together. (see Figure 4 and Figure 5).

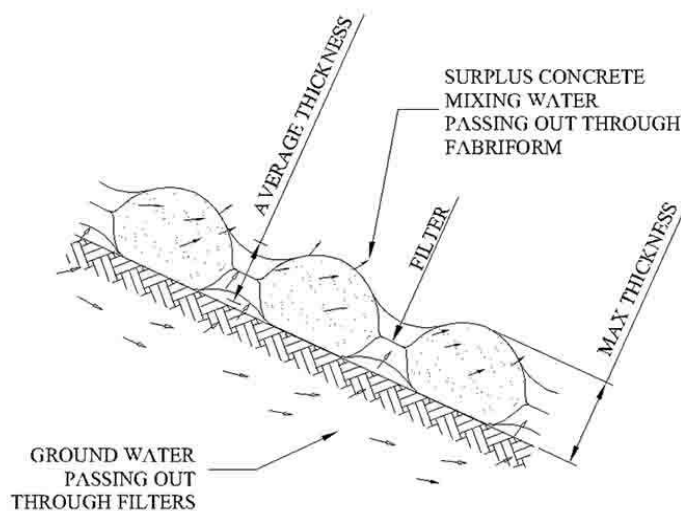


Figure 6: Section through a grouted mattress

(Reproduced from the Intrusive Prepakt catalogue)



Figure 7: Laying a grouted mattress

(Reproduced from the Intrusive Prepakt catalogue)

Filter Layers

Traditionally filter layers have been provided by controlled placement of layered granular material. However, due to the difficulty of effectively placing fine material underwater, often in current flows, these systems have had limited success. In recent years the use of geotextile filters has made placement of effective filter layers more easily achievable. Where high frictional resistance is required between the underlying strata and the filter, layer the use of non woven geotextile is recommended by Heibaum (2000)

Studies have been carried out by Fotherby and Ruff (1998) on shaped concrete armour units. Where used in breakwater situations the shaped units such as Tetrapods or Dolos have a high porosity which has been shown to provide more energy dissipation and allow greater unit stability (Figure 8 and Figure 9). In river and marine scour protection systems this high porosity promotes scour and the pumping of fine materials from under the units which will place a higher load on the filter system (Sumer et al., 2001).



Figure 8: Showing concrete ‘dolos’

(Reproduced from the Pierce County WA.org website)



Figure 9: Concrete Tetrapod

(Reproduced from Flickr website; photo by d ha rm e sh Mumba India)

Tests carried out on 'Dolos' (Brebner 1978) and 'Toskanes' (Fotherby & Ruff, 1998) revealed that these units had no advantages over normal rip rap when placed on a horizontal bed under steady state turbulent flow. When the same units were laid on slopes there were advantages due to the natural angle of repose of these units being greater than rip rap.

A design equation was developed by Fotherby (1995) for local scour protection at bridge piers using shaped concrete armour units:

$$\frac{V_0^2}{g(sg-1)D_M} = 0.7 + 20\left[\frac{L}{b}\right] \dots\dots\dots \text{Equation 6}$$

where

L = largest dimension of the unit

V_0 = average approach flow velocity

D_M = equivalent spherical diameter for the unit 1.6 Dm for Toskanes

b = pier width

sg = specific gravity

g = gravitational constant

Fotherby (1995) summarises her work with the statement:

'Analysis of the little data available indicates that the complex shape of the amour unit does not have significantly increased stability over rip rap of equal weight when installed in the bed of a channel.'

The research work to date into scour protection systems has been to cater for flow velocities normally experienced in rivers and estuaries which are of the order of 2ms^{-1} to 5ms^{-1} . These flows are substantially less than those generated by the water jets from HSS. In addition, the nature of the failure of the conventional rock armouring at Poole Harbour suggested that the forces imposed on the rock units were considerably underestimated when using the current design guidance.

2.6 Scour Modelling

The scour effects from water jet propulsion systems do not appear to have been the subject of any published research papers. From discussions within the industry it is understood that special investigations have been undertaken by the Wolfson unit at Southampton University to establish some limited design parameters for the design of HSS scour protection at Portsmouth Harbour but this work is not in the public domain.

Due to the lack of previous research into this topic, papers on the following subjects have been reviewed in order to provide background information for this work:

- 1) Scour effects from conventional propellers.
- 2) Scour effects from plane jets from dam spillways.
- 3) Design parameters for scour protection systems.

Scour effects from conventional propellers

The disturbance and scour from conventional propellers has been appreciated for many years. The resulting damage has been reported by several researchers, Quarrain (1994) who found that 42% of major British Ports had encountered propeller induced bed scour and that of this 29% were classified as being of a serious nature. A similar study by Berg & Cederwall (1981) on Swedish ports found that 16 out of 18 ports had suffered damage due to propeller scour.

Research by Hamill (1988) into the scour effects of conventional propellers have enabled predictions to be made of the maximum depth of scour (E_m)

$$E_m = f(V_0, D_p, d_{50}, C, \rho, g, A_p, \nu)$$

Where E_m = *Maximum depth of scour*

- V_0 = efflux velocity
- D_p = propeller diameter
- d_{50} = median sediment grain size
- C = clearance distance between the propeller tip and the seabed
- ρ = density of fluid
- g = gravitational acceleration
- A_p = difference between the mass density of the sediment and the fluid
- ν = kinematic viscosity of the fluid

In the above:

$$V_0 = nD_p\sqrt{C_t}$$

where n = number of propeller revolutions per second

C_t = propeller thrust coefficient

and

$$\frac{V_0}{\sqrt{\frac{gd_{50}A_p}{\rho}}} = F_0 \dots\dots\dots \text{Equation 7}$$

Where

F_0 = Densimetric Froude number

And

$$\frac{V_0D_p}{\nu} = R_{ej} \dots\dots\dots \text{Equation 8}$$

Where

R_{ej} = Reynolds number of the jet

Based on the work by Rajaratnam (1981) on erosion produced by a plane wall jet (in this case the plane wall jet described by Rajaratnam is a rectangular shaped jet emerging from a dam spillway as opposed to a circular jet) it was demonstrated that provided:

$$R_{ej} > 10^4$$

the scale effect of the Reynolds number could be neglected.

From the above it can be deduced that model jet flows can be applied to full scale jets without significant scale effects provided the jet Reynolds numbers are above the threshold values determined by Rajaratnam.

Hamill (1988) also comments that where plane momentum jets were used for models of conventional propellers these did not produce a good representation of propeller wash.

In later work taking into account the effect of the rudder the following empirical equation was proposed for the prediction of equilibrium scour depth;

$$\frac{Sn}{S} = 0.75 - 0.07 F_0 + 0.02 \left(\frac{D_p}{d_{50}} \right) - 0.15(1 + \alpha) \dots \dots \dots \text{Equation 9}$$

Where

S = the maximum equilibrium scour depth without a rudder.

It was noted by other researchers that the presence of the rudder could cause an increase in the final equilibrium erosion depth by a factor of 3 (Sumer & Fredsoe, 2002)

Scour formation in plunge pools

The research carried out in this area is mainly focused upon the scour development in non cohesive granular soils, and whilst useful from the aspect of modelling most of

these papers, do not provide insight into this current work where it is the protection system that is being examined rather than the development of scour within a natural river bed. They do however provide insight into the behaviour of turbulent jets.

Jet development

When the jet enters the tailwater pool the water jet undergoes a various transition stages to its fully developed stage this process has been analysed by (Ervine & Falvey, 1987) this is illustrated in Figure 10 below. It can be seen that although the jet remains intact upon entry into the pool there is expansion of the outer boundary of the jet and contraction of the core. It has been found that erosive capacity of the jet is maximised after it becomes fully developed in the pool. The water jet from the HSS is formed directly from the manoeuvring buckets of the vessel so the initial flow can be expected to be fully turbulent however the development stages will be similar to those found in Figure 10

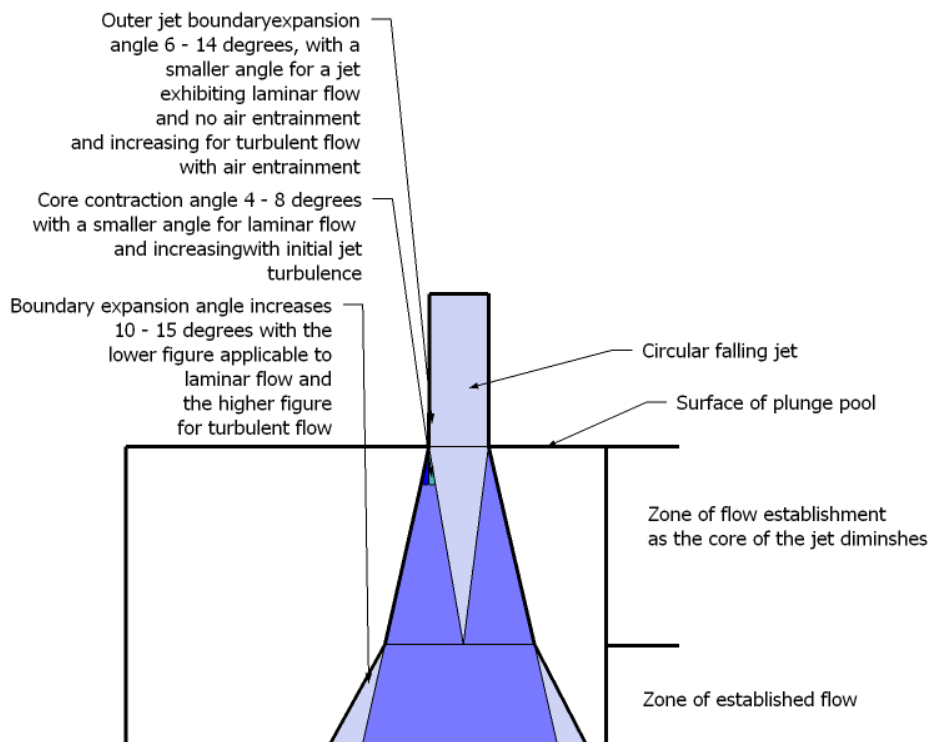


Figure 10: Development stages of a water jet entering a plunge pool

(Ervine & Falvey, 1987)

In his paper Bollaert (2004) examines the process by which scour holes form in rock, and models the effect of a water jet impacting on various sizes of rock joint.

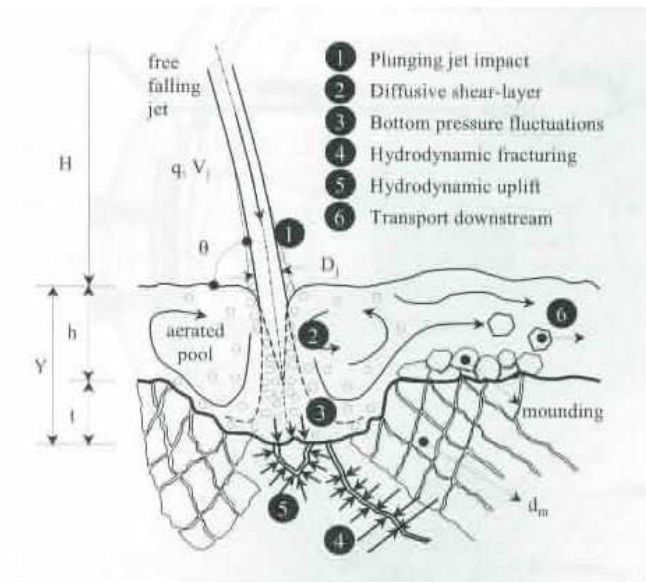


Figure 11: Diagram showing the scour formation cycle from a free falling jet

(Bollaert & Schleiss, 2001)

The process of scour formation as described by Bollaert is shown in Figure 11. This diagram illustrates the scour cycle where the water jet entrains air during its entry into the plunge pool. This entrained air gives rise to two effects which are dynamic pressure variations and change in velocity of the jet. The dynamic pressure variations may enter the rock joints, progressively extending these joints until the joint network surrounds an elemental piece of rock. Then an instantaneous net pressure difference acting across all faces may eject the element of rock from the surrounding mass. Once ejected, the element of rock can be moved by the high turbulent flows. This effect had not been documented in any of the previous papers and offered an explanation to some of the problems and failure observed during the installation of the scour protection at Poole Harbour.

Scour evaluation methods derived from research carried between 1932 and 2001 as analysed by Bollaert and Schleiss (2001) can be seen to be primarily either empirical or semi empirical as demonstrated in Table 2.

Table 2: Showing scour depth prediction methods proposed by researchers in the last 78 years

| Ref No | Scour evaluation method | Number of researchers adopting each approach |
|---------------|---|---|
| 1 | Empirical approach based upon laboratory and field observations | 19 |
| 2 | Analytical-empirical methods combining laboratory and field observations with some physics | 12 |
| 3 | Approaches based upon extreme values of fluctuating pressures at the plunging pool bottom | 7 |
| 4 | Techniques based upon time-mean and instantaneous pressure difference and accounting for rock characteristics | 7 |
| 5 | Scour model based upon fully transient water pressures in rock joints | 1 |

The empirical formulae were typically in the form:

$$Y = t + h = K \frac{H^y q^x h^w}{g^v d_m^z} \dots\dots\dots \text{Equation 10}$$

Where *t* is the scour depth below the initial bed depth

K is a constant

q is the jet discharge rate (per unit width of the jet

H is the fall height of the jet (through air)

h is the tailwater depth (measured from the initial river bed level

d is the characteristic sediment size or rock block diameter

Mason and Arumugam (1985) calibrated this formula against a large number of scour results and suggested the following parameters as providing the best fit for both model and prototype conditions.

$$K = (6.42 - 3.1H^{0.1})$$

$$V = 0.3$$

$$W = 0.15$$

$$X = (0.6 - H/300)$$

$$Y = (0.15 - H/200)$$

$$Z = 0.1$$

Further work on scour in plunge pools had been carried out by Mason (1989) where the scour depth formulae at the time were summarised and found to have some notable discrepancies. These were thought to arise as a result of neglecting the aeration effect within the water jets. Through a series of laboratory tests Mason developed a new equation for scour depth:

$$T = \frac{3.39^{0.6} q (1+B)^{0.3} h^{0.16}}{g^{0.3} D_m^{0.06}} \quad \dots\dots\dots \text{Equation 11}$$

Where: T = *scour depth*

q = *discharge per unit width of plane jet*

h = *tailwater depth above unscoured bed*

g = *gravitational constant*

D_m = *mean size of bed material*

B = *air / water ratio*

Semi empirical equations have been developed by a number of researchers combing field and laboratory data with some physics and a detailed overview of these is provided by Bollaert (2002) who also provided an approach based upon the extreme values of fluctuating pressures at the plunge pool bottom.

In his work Bollaert found the simultaneous application of extreme minimum (and maximum bottom pressures above and underneath the rock can result in net pressure differences of up to 7 times the root mean square value or 1.5 to 1.75 the kinetic energy of the incoming jet (Figure 12). These figures do not include the violent transient pressures that can be present in the rock joints as mentioned by Bollaert (2002). In his work on the transient pressures Bollaert does mention that the maximum and minimum pressures should be defined at the centre of the block for a long enough time interval but does not elaborate on the extent of that time interval.

Since the maximum and minimum pressures are not occurring at the same time interval the pressure difference as defined represents the upper limit of dynamic loading. The work by Caroni, E et al (2002) where direct force measurements were take on a spillway slab shows an increase in the maximum force measured with increasing time interval. In this case the test conditions were maintained for long periods and as suggested by Bollaert the likelihood of maximum and minimum pressures coinciding increase with the time duration of the event.

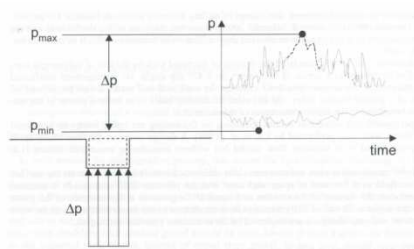


Figure 12: Pressures causing rock ejection

(Bollaert & Schleiss, 2002)

2.7 Background Theory

To gain a better understanding of the forces acting on the scour protection system some basic concepts in fluid mechanics will be considered.

A body subject to an incompressible flow will be subject to drag which can be split into pressure drag and profile rag (Douglas et al., 2005). Total drag on a body is often described in terms of its drag coefficient which is a combination of pressure and profile drag. Diagrams for drag coefficients for a cylinder and a sphere are shown in Figure 13

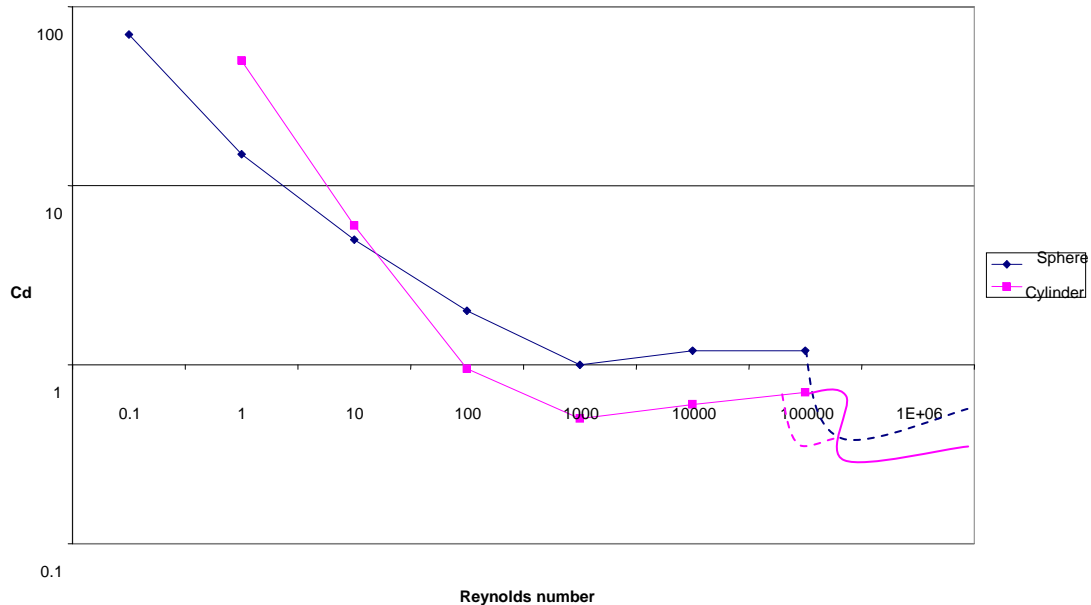


Figure 13: Drag coefficient versus Reynolds number

At very low Reynolds numbers the flow past a body is a laminar, the inertial effects small, and the pressure recovery almost complete so pressure drag is small and profile drag is nearly all due to skin friction. For Reynolds numbers between 10^3 and 10^5 the drag factor is nearly constant. At Reynolds of around 10^5 the boundary layers changes from laminar to turbulent before flow separation and there is a marked drop in C_d . In the case of the concrete blocks the values shown on Figure 13 will not be correct but the general shape of the curves will be similar. Where air is entrained this will reduce the effective density of the fluid, the combined medium will become compressible which will give dynamic pressure effects.

On a cylinder within an incompressible flow for Reynolds numbers greater than 90 and up to 2×10^5 vortex shedding can be expected to occur. This effect produces alternating lateral loads on the cylinder which induce vibration. The frequency of this forced vibration can be calculated from an empirical formula due to Vincent Strouhal in 1878 and is known as the Strouhal number.

$$f = 0.198 \frac{U_0}{d} \left\{ 1 - \frac{19.7}{R_e} \right\} \dots\dots\dots \text{Equation 12}$$

Where

U_0 = Initial velocity

d = diameter of wire

R_e = Reynolds number

This formula is valid for $250 < R_e < 10^5$

2.8 Air Entrainment

Previous work on the jets into plunge pools has indicated that air entrainment within the water subject has a significant affect on scour (Bollaert & Schleiss, 2001)

It has also been noted that there are significant problems in modelling air entrainment using scale models due to the scale effect of the air bubbles within the water.

In addition bubble formation in a salt water environment varies from that in a fresh water (Craig et al., 1993)

2.9 Hydraulic Similitude

The factors of similarity that are normally required to be considered in hydraulic modelling for this these flows are based upon achieving Froude number similitude. For this work in common with other researchers (Caroni et al., 2002), (Bollaert, 2002) a geometric scale of 1:20 was chosen and the modelling carried out to Froude similarity.

Table 3: Factors for Hydraulic Similitude

| Type | Defining Characteristic |
|-------------|---|
| Geometric | <p>Shape:</p> <p>All the significant elements of the scour protection system will be reproduced in the model. Scale factor is the relationship of linear measurements between the model L_m and the prototype L_p</p> $\lambda = \frac{L_m}{L_p}$ |
| Kinematic | <p>Motion:</p> <p>Velocity and direction of flow are reproduced to scale in the model. The scale factor for velocity is the relationship between the Froude numbers for the model (F_{rm}) and the Prototype (F_{rp})</p> $F_{rm} = F_{rp}$ $V_m / (gL_m)^{0.5} = V_p / (gL_p)^{0.5}$ $V_m / V_p = (gL_m)^{0.5} / (gL_p)^{0.5}$ $V_m / V_p = L_m^{0.5} / L_p^{0.5} = (L_m / L_p)^{0.5}$ |
| Dynamic | <p>Forces:</p> <p>At similar points all forces are reproduced to scale in the model. In this case it is necessary to establish the relationship between the model and the prototype for the following cases:</p> <p>Dynamic pressure from water flows:</p> $P_{dyn} = \frac{1}{2} \rho g v^2$ |

| Type | Defining Characteristic |
|-----------------------|--|
| Static water pressure | <p>→ $\frac{P_m}{P_p} = \frac{\frac{1}{2} \rho g v_m^2}{\frac{1}{2} \rho g v_p^2}$</p> <p>→ $\frac{L_m^2}{L_p^2}$</p> <p>→ $\frac{L_m}{L_p}$</p> <p>$P_{STAT} = \rho g h$</p> <p>→ $\frac{P_m}{P_p} = \frac{\rho g h_m}{\rho g h_p}$</p> <p>→ $\frac{P_m}{P_p} = \frac{L_m}{L_p}$</p> |
| Reynolds number | <p>Reynolds number</p> <p>$Re = \rho v L / \mu$</p> <p>Where:</p> <p>$\rho =$ Density</p> <p>$v =$ velocity</p> <p>$\mu =$ dynamic fluid viscosity (for water $\mu = 0.89 \times 10^{-3}$ Pa.s)</p> <p>Where the value of Reynolds number is large the kinematic viscosity has a lesser influence on flow behaviour. Therefore the respective Reynolds numbers for both the prototype and the model will be considered. For pipe flows a Reynolds number</p> |

| Type | Defining Characteristic |
|-------------|--|
| | <p>greater than 2300 is generally considered as indicating turbulent flow. Therefore this would be a threshold value below which the model would have to take into account differences in Reynolds number.</p> <p>For prototype</p> $Re = 1.1236 \times 10^7$ <p>For the model</p> $Re = 1.264 \times 10^5$ <p>Therefore in both cases the flow can be considered to be fully turbulent and the difference in the Reynolds number between the model and the prototype will have little effect in relation to the jet flows. This concurs with the work by Rajaratnam¹⁴ who demonstrated where $Re_j > 10^4$ the effect could be neglected. However this parameter must still be considered and care taken when comparing local flow effects on the model and the prototype. In the case of water flows between the concrete blocks case the Reynolds numbers could be 3.370×10^3 (model) and 2.690×10^5 (Prototype)</p> |

Chapter 3

DISCUSSION ON CURRENT DESIGN GUIDANCE

3.1 Current Design

Current design of scour protection systems is limited to the prediction of scour depths for a given flow and bed particle size and the design of rip-rap protection to resist fluvial or tidal currents and for scour resulting from propeller driven vessels.

The design guidance has been developed from physical modelling and in most cases subsequent numerical modelling. Design guidance has been provided for flat bed conditions Mason (1989) and the protection of armoured slopes under open piled quay walls is discussed in a PIANC guidance note (1997)

Since they currently represent the principle solutions available, the design equations from Mason (1989) have been examined over a range of variables up to those expected from high speed ferries. It should be noted that these equations were never intended to be used for the design flows illustrated below but this serves to illustrate why additional design guidance is required.

Taking the equations from Mason (1989) and extrapolating gives the results shown in Figure 14 and Figure 15. In both cases the percentage air entrainment has been taken as zero. It should be noted that extrapolation of these tables is not valid since they are derived from empirical formulae however in the absence of proper guidance this is being used for design.

In Figure 14 a jet velocity of 10ms^{-1} was used and it can be seen that the scour hole depth is sensitive to the particle size of bed material over the range 0.1mm to 200mm but at greater particle sizes there is about the same change in scour depth (for particle sizes up to 1800mm.)

In Figure 15 a particle size of 1000mm was used and this shows virtually straight line relationship between jet flow rate and scour depth.

Whilst the application of existing numerical models to the scour from high speed ferries provides some trend information, it clearly shows that extrapolation of these equations is not correct, since the scour depth to particle size curve gives hardly any change in scour depth once the particle size exceeds 0.2m. Clearly when compared with the limited full scale data from Poole Harbour this is not the case.

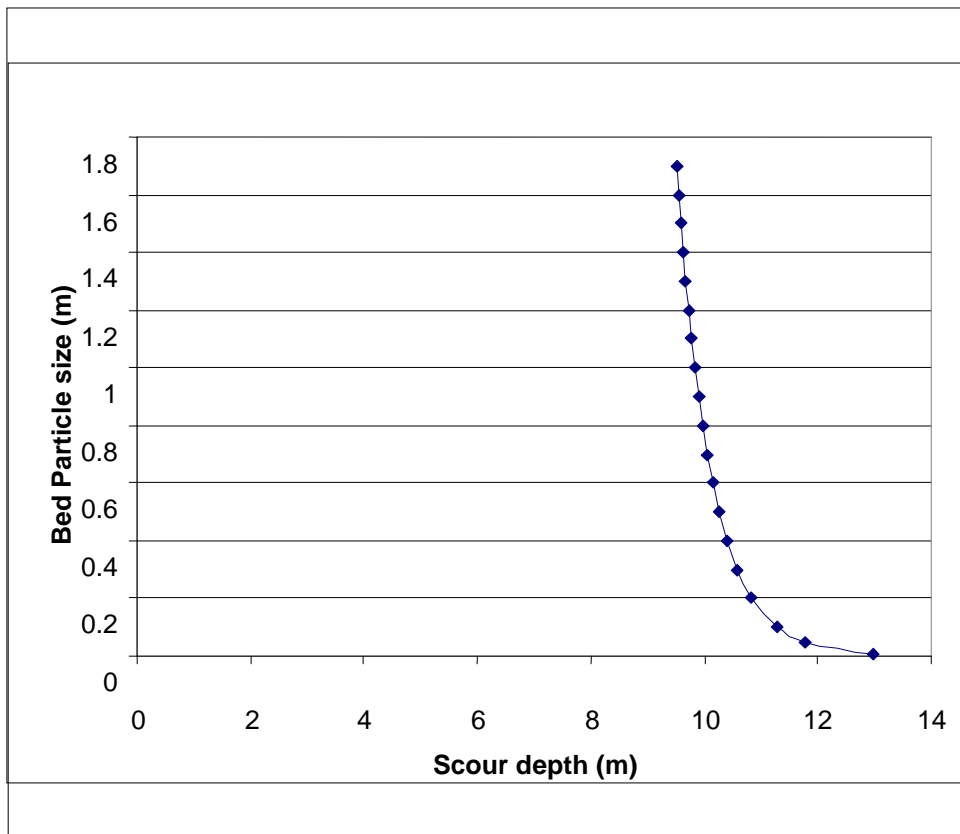


Figure 14: Scour depth predictions from Mason 1989 (Particle size v scour depth)

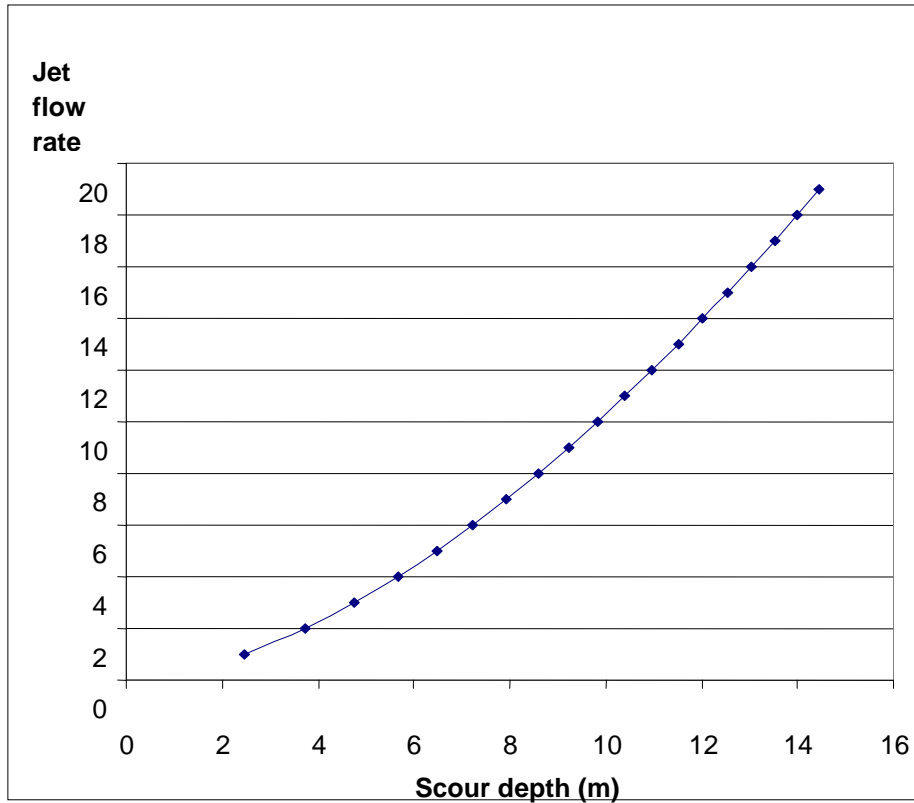


Figure 15: Scour depth predictions from Mason 1989 (Flow rate v scour depth)

3.2 Design Guidance

In the PIANC Document design guidance is provided to size the ‘Rip Rap’ stones as follows:

$$U_0 = c \left[\frac{P_d}{D_p^2} \right]^{1/3} \dots\dots\dots \text{Equation 13}$$

Where U_0 = centreline jet velocity from the propeller

$\epsilon = 1.48$ for a non ducted propeller and 1.17 for a ducted propeller

P_d = Installed engine power

D_p = Propeller diameter

The initial jet diameter is given by the equations:

$D_p = 0.71D_0$ for a non-ducted propeller

$D_0 = D_p$ for a ducted propeller

The maximum bed velocity generated from a propeller is shown in Figure 16

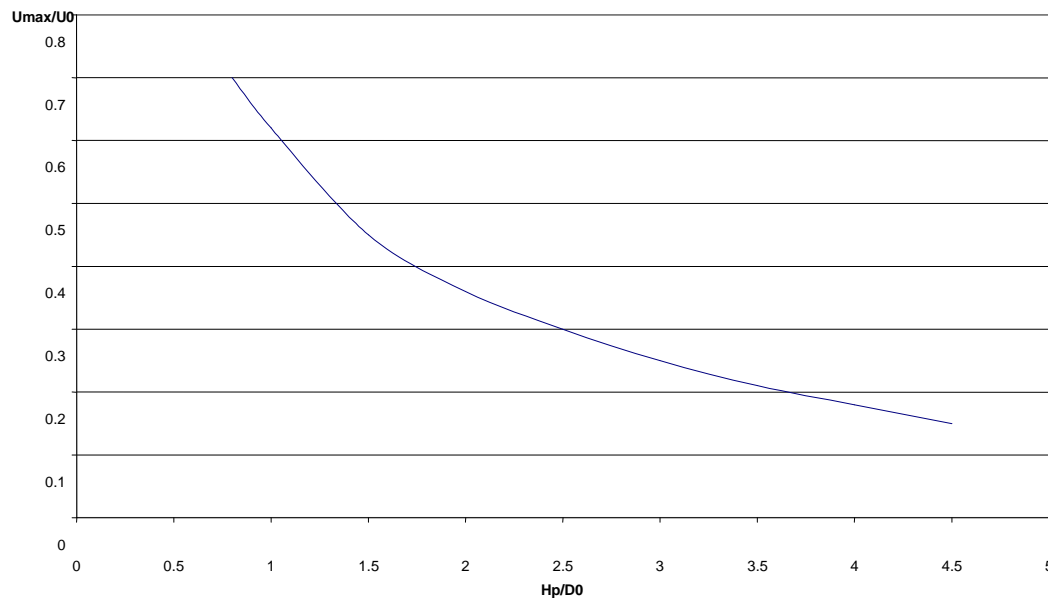


Figure 16: Maximum bed velocity from a single propeller

Where H_p = distance from propeller centreline to top of scour protection/seabed

U_{max} = Maximum velocity at bed level

The calculated value of U_{max} is then used in the following graph to determine the

(D_{50})

the mean stone size required:

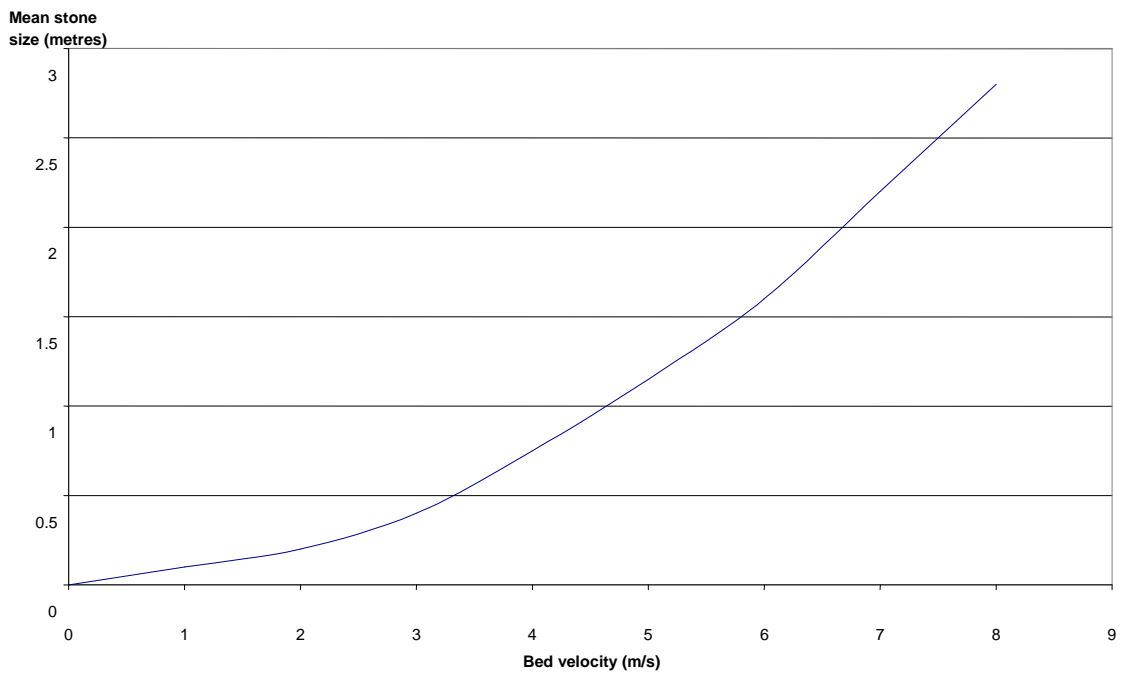


Figure 17: Mean stone size required for a given flow velocity

The above graph is based upon a density for the rocks of 2650 kg/m^3 and a density for the seawater of 1026 kg/m^3

For sloping banks it is recommended to increase the mean stone size by 50%

A worked example in the document shows that for a 50000 dwt container ship with the following specifications:

$$\begin{aligned} D_p &= 7.4\text{m} \\ P_d &= 33000\text{kW} \end{aligned}$$

With an under keel clearance of 1 metre then the Rip Rap protection would comprise 2 layers of rock 0.9m to 1.1m diameter.

This represents a scour protection for a vessel with approximately five times the displacement tonnage of a large high speed ferry. The experience at Poole Harbour has shown that this system would prove to be completely inadequate to protect against scour from even the smaller high speed ferries.

Chapter 4

THE CHARACTERISTICS OF HIGH SPEED SHIPS

4.1 General Features

The high speed ships referred to in this report are characterised by their propulsion systems.

The current generation of vessels are typically in the range of 30m to 80m in length with operating speeds in excess of 28 knots. Their propulsion systems are usually gas turbine engines driving a water jet unit.

The form of the vessel is a catamaran wave piercing hull with a linking deck and usually the deck linking the hulls is aerodynamically configured to provide lift forces during high speed operation, see Figure 18. Lifting the vessel in this manner reduces the “wetted” area of the hull and consequently the hydraulic resistance and also assists with overcoming the conventional speed restraints of conventional vessels.

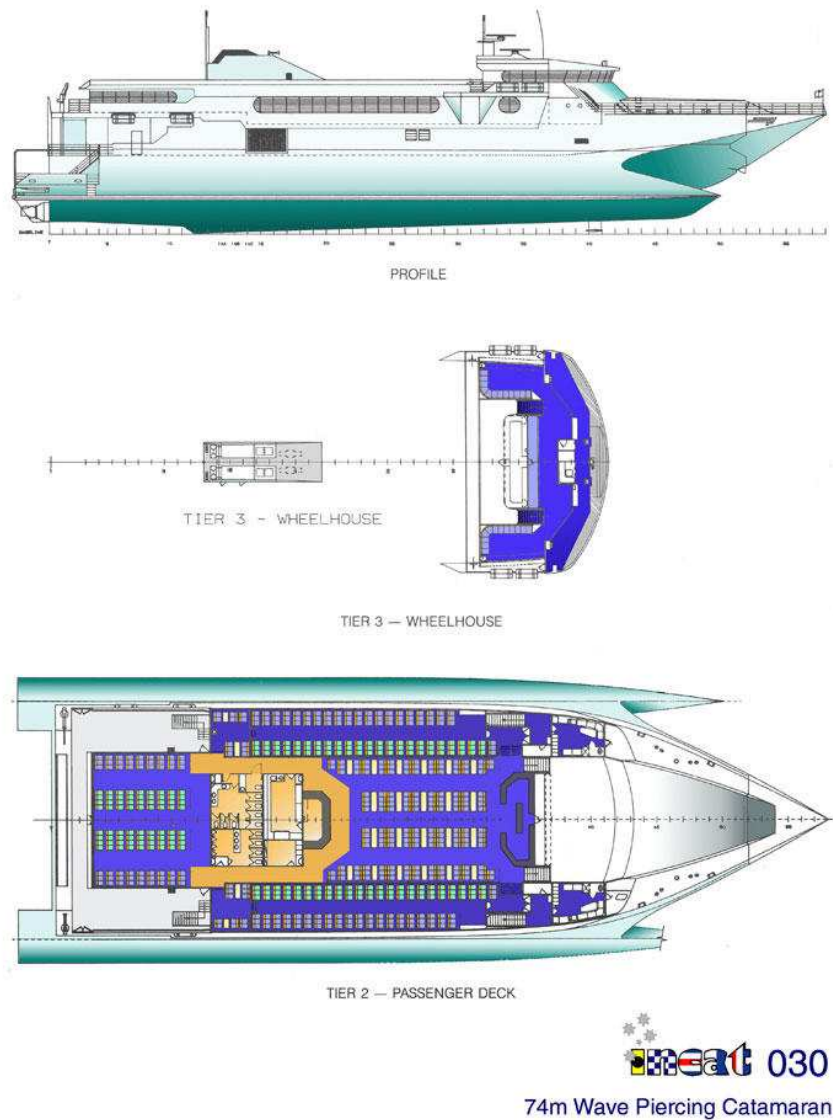


Figure 18: Typical High Speed Ferry
(Reproduced from the Incat catalogue)

Of particular interest in this report are the water jet drive units which there are located in the hulls. An illustration of this is shown in Figure 19, although the vessel shown is not a catamaran hull.

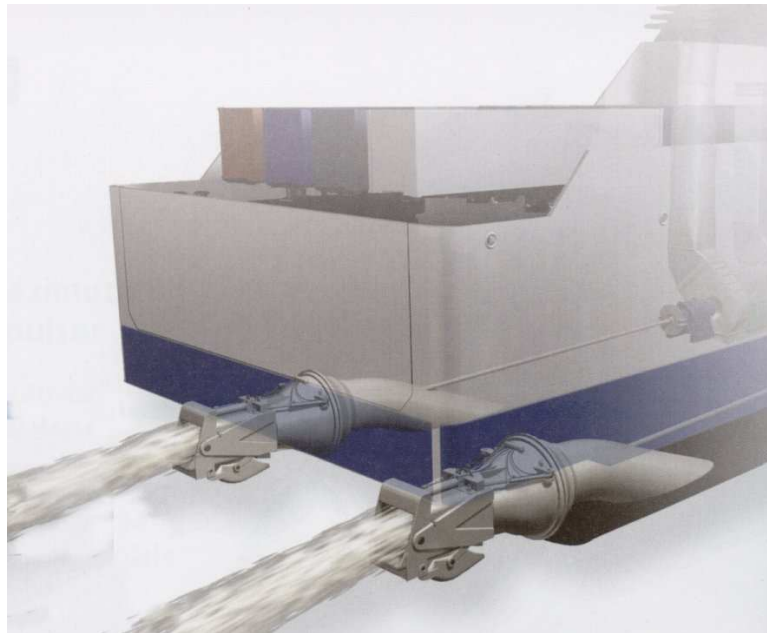


Figure 19: Illustration of jet drive installation

(Reproduced from the Rolls Royce Marine Propulsion catalogue)

The construction of these vessels has until recently been limited to two companies in Australia, Austel and Incat, although they have been constructed in various parts of the world under licence. As a result of this the ship designs are very similar.

The layout of 74 metre high speed ferry is shown in Figure 18. This layout is typical for vessels of this type with the water jet drive units located at the rear of the catamaran hulls. These vessels are constructed from aluminium to reduce the dead weight tonnage since their performance is greatly affected by displacement.

4.2 Water Jet Drives

The basic configuration of the water jet drives are shown in Figure 20 and Figure 21. The important factor in the drive system is that the jet drives operate at constant speed during manoeuvring. This speed is typically limited to 70% of full power. The jet flows and velocities are shown in Table 4, the size of the jet orifice is 1m diameter (= 0.785m²).



Figure 20: S type Jet Drive unit manufactured by Rolls Royce

(Reproduced from the Rolls Royce Marine Propulsion catalogue)

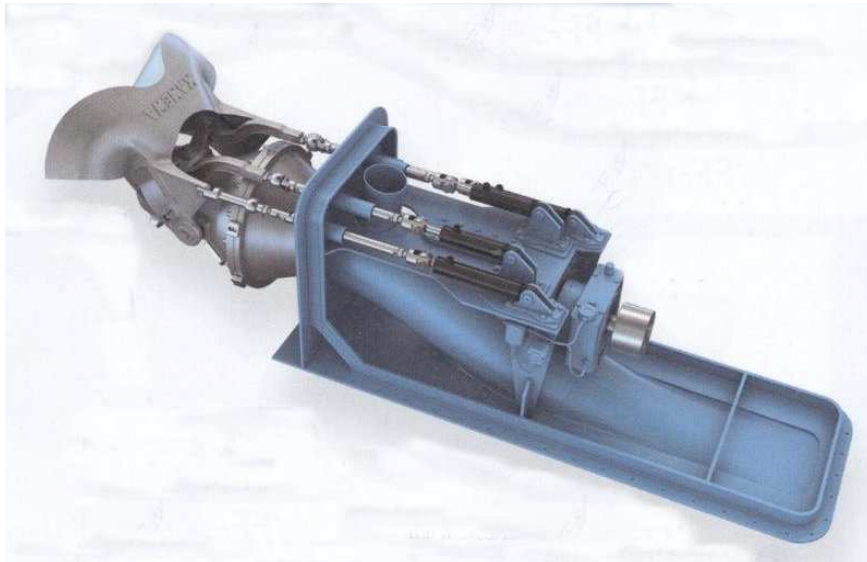


Figure 21: A Type jet Drive unit manufactured by Rolls Royce

(Reproduced from the Rolls Royce Marine Propulsion catalogue)

Table 4: Typical jet flow and velocities for High Speed Ships*(Reproduced from the Rolls Royce Marine Propulsion catalogue)*

| Power | Flow Rate | Average Jet Velocity |
|--------------------|------------------------------------|-----------------------------|
| Cruise | 15m ³ s ⁻¹ | 19.1ms ⁻¹ |
| Manoeuvring | 10.5m ³ s ⁻¹ | 13.3ms ⁻¹ |

4.3 Jet Vectors

The possible jet water permutations are shown in Figure 22 and Figure 23. The jet nozzles rotate up to 30° either side of the straight ahead position in order to allow yaw control. In order to produce no translational force manoeuvring cowls (often referred to as ‘buckets’) are used to deflect a proportion of the jet rearwards and downwards onto the sea bed. Where reverse is required, further use of the buckets deflects a larger proportion of the jet back under the vessel.

When the manoeuvring cowls are used, the water jet velocity is governed via the engine speed to 70% of full power (or less). It can be seen that the vessel can be operating its water jets at 70% maximum thrust, but will remain stationary by using the partially deployed manoeuvring cowls to balance the forward and reverse thrusts. It appears to be normal practice when manoeuvring for berthing to operate the water jets at the maximum allowable (i.e. 70% full power) in order to minimise operational ‘turnaround’ times. Maintaining the highest possible jet velocity during manoeuvring gives the vessel a much greater control response and is particularly likely to be used during conditions of high winds.

An additional factor during the operation of the manoeuvring cowls is air entrainment within the water jet. Due to the jet nozzles being located close to the free water

surface when the cowls are deployed, they induce air from the surface into the cowls. The effect is clearly visible during the vessels' operation but no quantitative information is available showing the percentage of air entrainment that occurs. It will, however, be a variable figure related to cowl position and jet velocity.

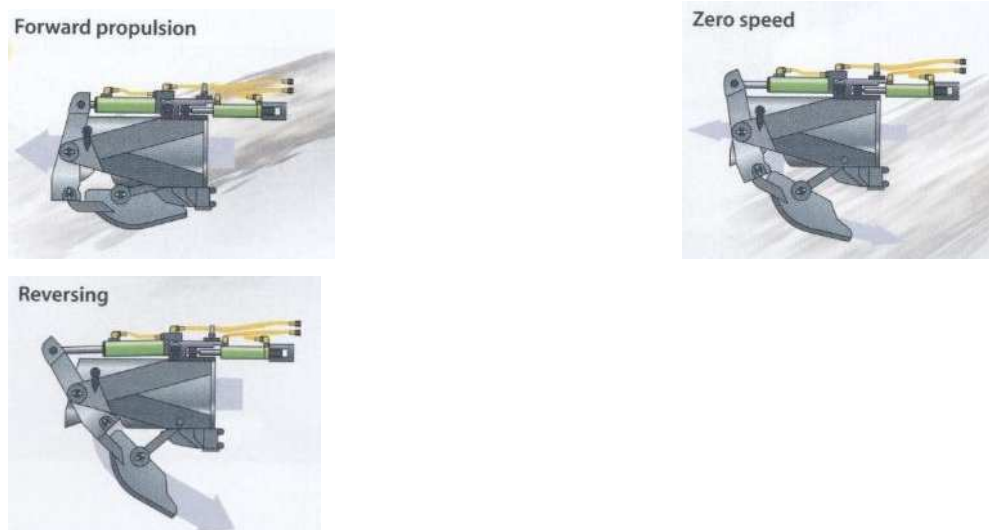


Figure 22: Deployment of deflector bucket for manoeuvring

(Reproduced from the Rolls Royce Marine Propulsion catalogue)

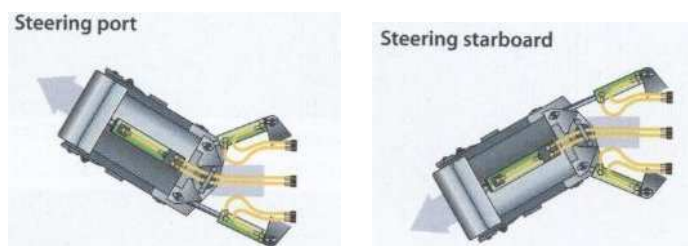


Figure 23: Jet vector for steerage

(Reproduced from the Rolls Royce Marine Propulsion catalogue)

4.4 Intakes

The water jet intakes are located on the underside of the hull. These intakes typically have 3 to 5 times the cross sectional area of the jet nozzles so the velocities are

proportionally less. Although these elements clearly influence the water flows around the vessel they are not considered as noticeably contributing to the scour effect of the jets.

It should be recognised however, that any silt and small debris thrown into suspension may be taken into the jet unit which will cause accelerated wear on the turbines and nozzles. In addition the jet output will be grit entraining and this will greatly increase the risk of impingement corrosion to the dock structures.

Chapter 5

POOLE HARBOUR SEABED PROTECTION SYSTEM

In 1997 a high speed ferry commenced service operating between Poole Harbour and St Helier in the Channel Islands. Poole Harbour is located on the south coast of the UK and due to the distances involved had operated a single service each day to the Channel Islands with one conventional ferry. The high speed service was able to operate two sailings a day with one vessel.

The service carries passengers and light vehicles with two sailings per day over the summer period between April and October.

5.1 Background

Prior to the start of the ferry service, Poole Harbour Engineers identified the requirement for several modifications to the existing RoRo terminal (Terminal 2). These included the modification of the end of the link span to accommodate the new vessel and provision of seabed protection within the berth area. The location of this berth is shown in Figure 24. The requirement for seabed protection was identified by Poole Harbour Engineers as a result of scour damage that occurred to the berth previously used by the same vessel at Weymouth Harbour.



Figure 24: Location of Poole Harbour Ferry Terminal

Reproduced from the 1:50000 Landranger series with the permission of the Ordnance Survey© Crown copyright. All rights reserved Licence AL 100010731

The required works were designed by Royal Haskonning and the seabed protection system was installed by Sub-Surface Engineering.

The ferry is a 74 metre catamaran with wave piercing hulls and constructed from aluminium. The propulsion units are two water jet drives, one located in each hull. Manoeuvring is achieved by rotating the water jet nozzles in the horizontal plane and deflector cowls to change from forward to reverse.

The natural seabed in Poole Harbour was a coarse sand with occasional pockets of soft clay. It was a key client requirement that any works to the seabed could be easily removed using conventional plant and equipment. This was to maintain flexibility for any future works required in the port. The distance between the seabed and the vessel jet outlets is shown in Figure 25. On the assumption that the jet is highly turbulent on its exit from the bucket the jet core contraction will be around 8 degrees which will give a fully developed

jet within a water depth of 3.6 metres and greater which will be the case on most states of tide (Ervine & Falvey, 1987)

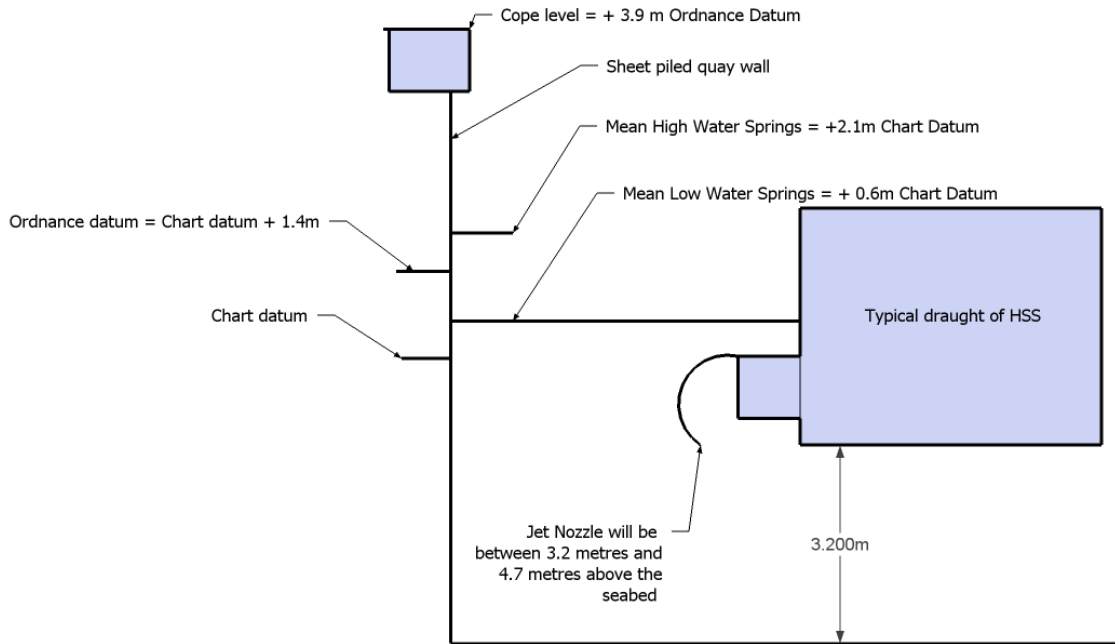


Figure 25: Schematic diagram showing the seabed clearances for the HSS

5.2 Development Sequence for the Seabed Protection

Reduced scale Figures have been included in this section of the report and the full size drawings appended. Pre-construction survey of the berth was carried out in October 1996, see Figure 26.

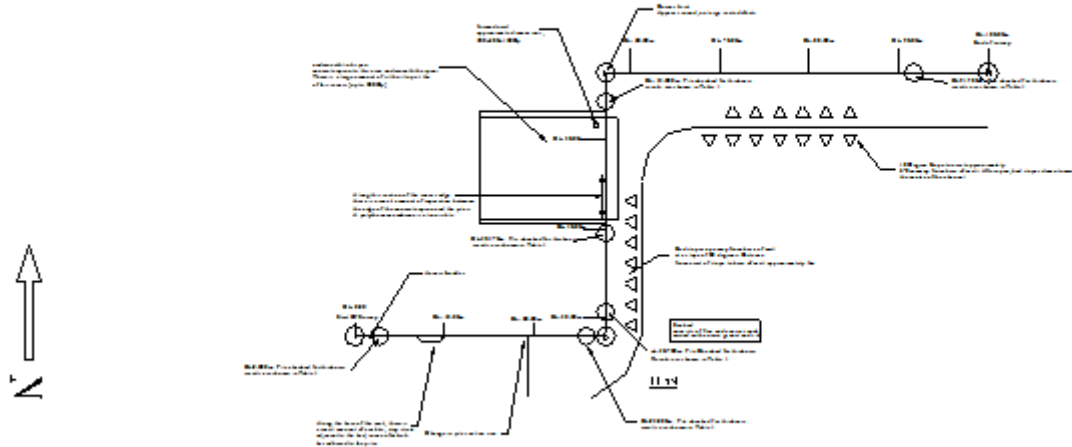


Figure 26: Pre-construction survey

Phase 1 - The original scour protection system was designed and installed in 1997 followed by an extended period of monitoring and associated remedial works see Figure 27. In addition to the seabed monitoring, occasional checks were made on the steel thicknesses of the sheet piles. The protection works proved inadequate in the area of the linkspan as the installed rocks were subject to gross movement during each berthing operation. These movements gave rise to both scour problems and seriously reduced navigational clearances due to mounding of the rocks.

Phase 2 - During 2001 it was decided that a revised system of seabed protection was required immediately adjacent to the link span. This new system was designed by this researcher in close consultation with Poole Harbour Engineers. The test panels were installed in the winter period whilst the ferry was out of service.

Phase 3 - Following installation, the monitoring process continued, after a further two years service the installed system was extended and an improved protection system at the seabed/sheet-pile interface constructed.

The layout form of the protection systems is shown on the appended drawings and described in detail below.

5.3 Phase I

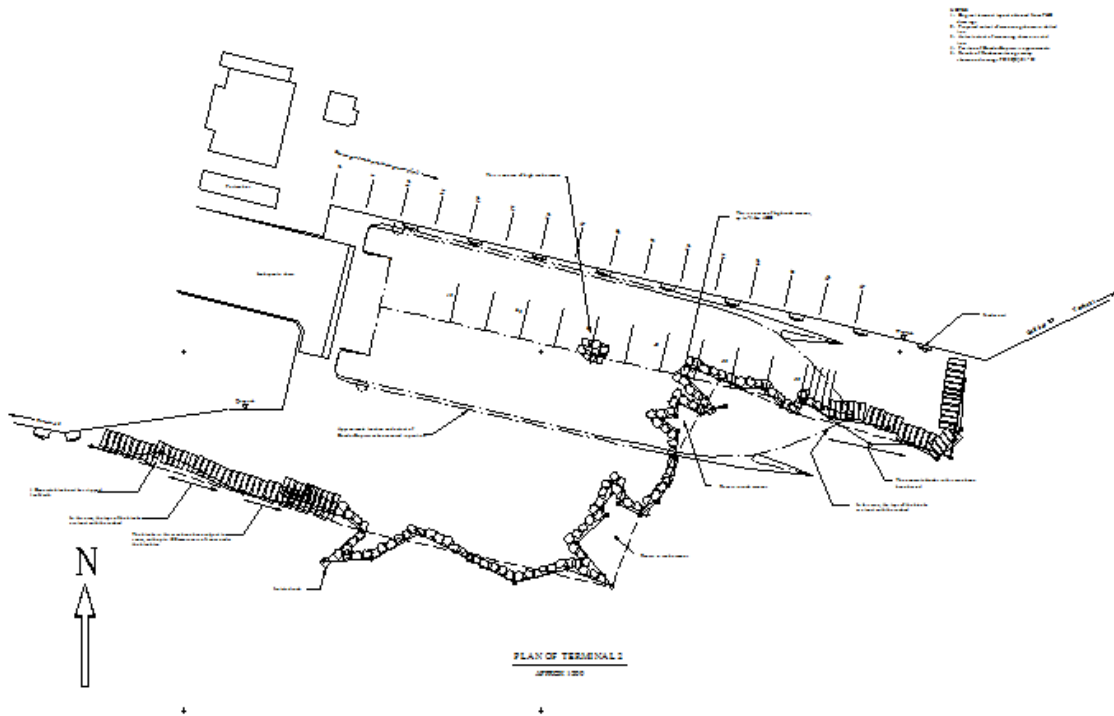


Figure 27: Phase 1 works at Poole Harbour Terminal 2

The system comprised natural rock (Portland Stone), with an average weight of 4 tonnes (air weight) and an average size of 1.5m long x 1.5m wide x 0.9m high, obtained from a local quarry. The construction tolerance for the finished seabed level after placing of the rocks was ± 150 mm. This tight tolerance was essential in order to achieve the necessary navigational depths without removing passive soil resistance to the seaward face of the steel sheet piling. The natural seabed was dredged to construction level using a combination of diver dredging, and grab dredging from a barge. Following this, a close woven geotextile was laid on the seabed and a double layer of rocks placed on top. Around sections of the perimeter of the protected area, concrete blocks were laid to form a kerb line. This kerb line was an additional requirement specified by the Harbour Engineer to limit the migration of the rocks away from the protection area.

The kerb units and second layer of rocks were placed by a crane located on the quayside with divers controlling the positioning. Due to the reach/lift limitations of the crane outermost kerb and blocks had to be placed using a crane on a dredge barge.

This method of construction was adopted to achieve the tight vertical tolerances necessary. The levels underwater were checked using a system developed specifically for this project. The system comprised two high accuracy pressure transducers which were calibrated to give comparative depth measurement between the two transducers. Waves in the area of the terminal were generally of small height and wavelength. With the wave heights involved and when working at depth the wave effects on static pressure changes were high attenuated. Despite this wave height compensation was built into the system by taking a series of static pressure readings and averaging these over a rolling sample period on both the reference transducer and the mobile transducer. The sampling rate was set at 0.1 seconds and the sampling period set at 5 seconds to suit the wave period within the harbour. Although the system had the facility to vary the sampling period it was not necessary to alter this during the works. The pressure transducers measured absolute pressure and atmospheric pressure variations were not relevant since it was a comparative measurement device that was checked for calibration each time it was used. This system was able to produce repeatable level readings to within an accuracy of 50mm underwater. The works took approximately 8 weeks to complete on site.

5.4 Seabed Monitoring

Following the placement, a programme of routine monitoring was set up to check for any significant movement of the rocks. Initially when the ferry first started operating from the berth the monitoring was carried out every few days to verify the effectiveness of the protection. The results of this monitoring survey are summarised in Figure 28 and the numerical results appended.

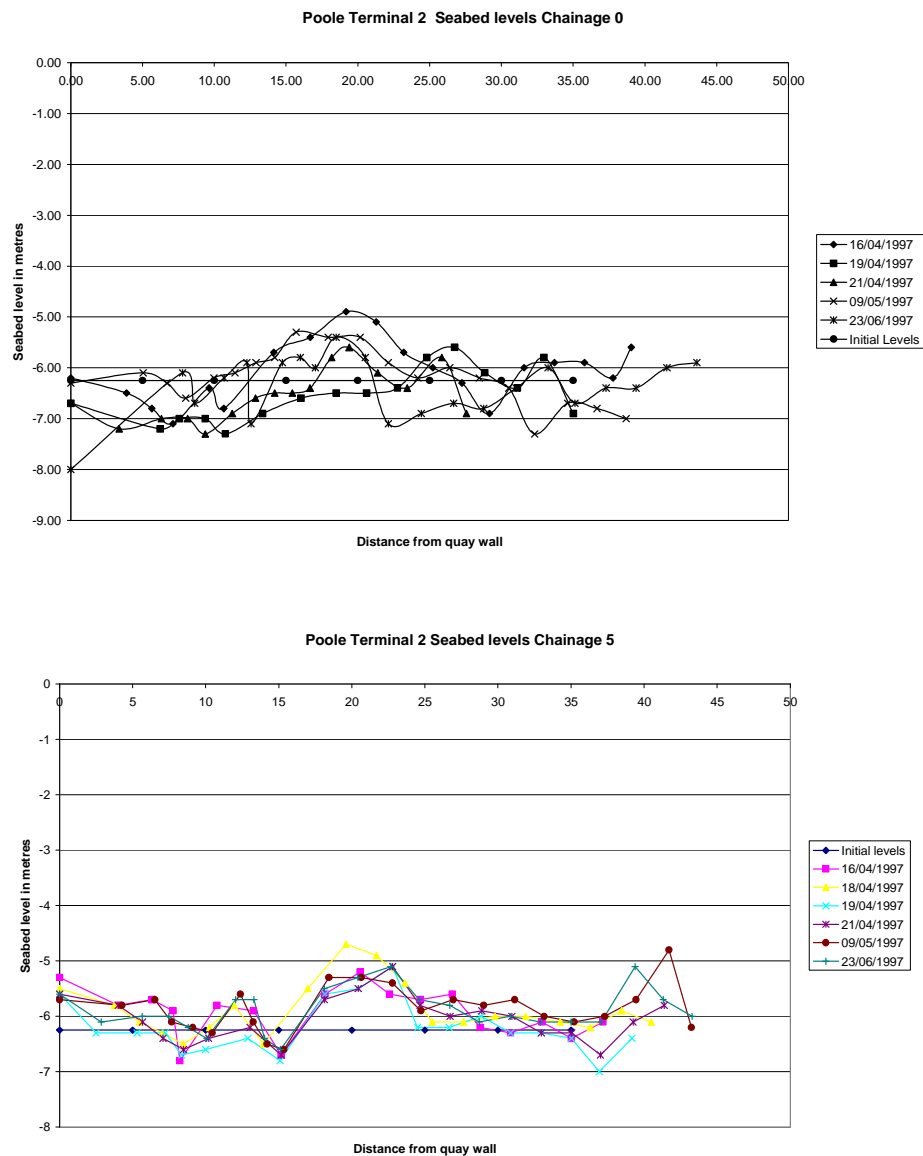


Figure 28: Seabed profiles at the linkspan after installation of the phase 1 works

The presence of large discrete rocks meant that conventional single beam echo sounding would not provide a sufficiently accurate plot of any movements. In particular the initial

formation of voids between rocks would not be identified at an early stage. It was therefore decided that the seabed monitoring would be carried out by divers.

The system adopted is indicated in Figure 29 where divers were required to walk out across the seabed at 5 metre chainages along the berth, and take depth readings at approximately every 2 metres out from the berth. The method proved to be accurate and able to produce highly repeatable results. A further advantage was the diver was able to provide a visual description of detected movement of the rocks.

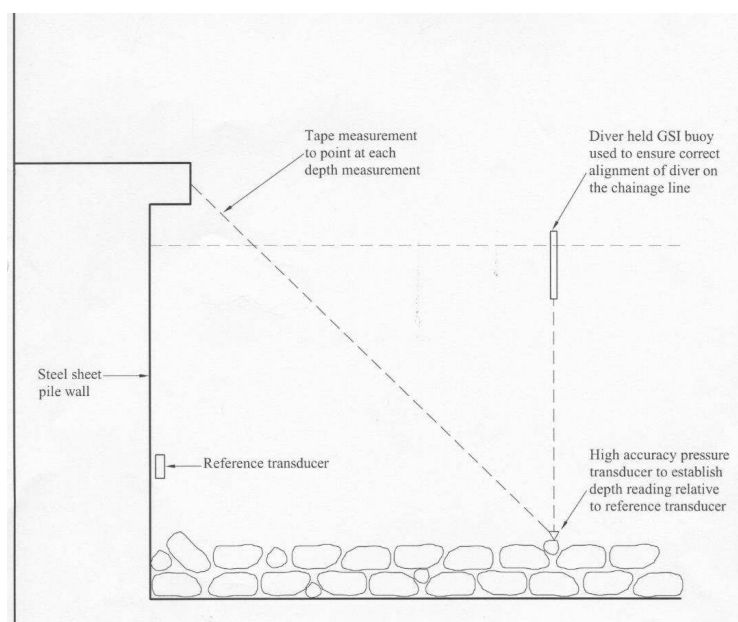


Figure 29: Instrumentation and technique used for rock levelling

Initially the monitoring was carried out over the full length of the berth but it was quickly established that the area of concern was limited to the first 30 metres adjacent to the link span. The remainder of the berth was then only checked occasionally and no detailed measurements taken. In addition, in the areas adjacent to the link span where substantial rock displacements were occurring, the divers were used to strop up and relocate rocks when navigational clearances were lost and additional rocks/blocks were placed in areas where all the rocks were missing and the geotextile exposed.

Significant movement of rocks was detected around the link span area after each ferry berthing operation. In one instance a 5 metre deep scour hole was found immediately outside the area of rock armouring. This was partially filled when the adjacent section of concrete kerb blocks and rocks slumped into the hole.

It became apparent that the rocks themselves were not offering any significant scour protection, and it was only when the geotextile mat remained in place that scour was prevented. The formed concrete blocks were proving significantly more stable than the rocks, but even these units were moving when subject to direct impact from the ships water jets.

From the routine monitoring and remedial works it was clear that the natural seabed (sand) was being displaced wherever there was any loss in the integrity of the geotextile. A particular area of concern was in the corner of the berth adjacent to the link spans. The scour in this location was occurring within the in-pans to the sheet piling, the voids formed by the displaced sand were being filled by the adjacent rocks falling into the scour holes although in some locations rocks were found buried below their original placement level even though they were outside the zone of jet impingement. After the first 12 months operation, a scour hole of around 3 metres depth had developed in this area, although this had not shown up on the level monitoring data due to the adjacent rocks moving into the scour hole as it formed. The depth of scour was detected by probing at the in-pan positions and determining the depth to the sand strata. The movement of the original rocks that formed the scour protection into the scour hole had been compensated for over the period by adding additional concrete blocks to the bare areas of geotextile. Three other problems were noted during the monitoring program. Where the geotextile was exposed, it was found to be suffering from considerable abrasion damage. Where sand was being picked up in the jets, this was causing impingement corrosion on the steel sheet piles. If any sections of geotextile became free they would pose a significant threat to the high speed ferry if taken into the coolant pumps or water jet intakes.

At this stage a comprehensive review of alternative protection methods was undertaken in close liaison with Poole Harbour Engineers and this is briefly summarised in Table 5.

Table 5: Review of Alternative Scour Protection Methods

| Type | Description | Advantages | Disadvantages |
|-------------------------|--|---|--|
| Fabriform | Concrete filled grout mattress 75mm to 350mm thick. | Relatively easy to construct. Large coverage for relatively low cost. | Very vulnerable at edges and once underscour would require complete replacement. |
| Amourflex | Precast concrete units up to 350mm thick connected together with rope or wire. | Mat units easy to lay. | Similar to fabriform but connecting the adjacent mats underwater is expensive. |
| Rock | As quarried rock obtainable in most sizes. | Readily available. | No control on shape, proven as ineffective. |
| Insitu Concrete | Concrete placed directly on seabed. | Quick to place. | Difficult to control. Environmentally difficult to use cannot be removed. Thickness difficult control. |
| Precast Concrete Blocks | Precast blocks joined together. | Easy to place deform to bed profile. | Requires significant diver intervention. |
| Gabions | Stone/rock in wire baskets. | Deform to bed. | Specialist placing required. |
| Steel Plates | Steel plates laid on seabed. | Quick to place. | Expensive. Corrodes. |

5.5 Phase II Works

From the monitoring of the Phase I works it was evident that concrete cuboid blocks were considerably more stable than the rocks, especially when they were laid in a tight geometric pattern.

It was decided to carry out a small scale test using concrete blocks in the area of greatest scour. The general arrangement of the blocks is shown in Figure 31.

The blocks were cast on the quayside with lifting eyes formed in their top surfaces. Running through the centre of the blocks were 100mm diameter plastic ducts that were used to connect the blocks together in groups of 5. Spacer washers were used between the blocks to allow for articulation. These groups were formed by tensioning 20mm diameter stainless steel cable which was looped through the centre ducts. The objective of the system was to allow the groups of blocks to articulate to follow the existing seabed profile but to prevent significant gaps opening up between the blocks. This system was also designed to allow for movement should minor scour occur under the blocks.

A purpose made lifting frame was manufactured and tested to allow the blocks to be craned into position as a complete group, with lifting chains attached to each individual block in the group, see Figure 30.

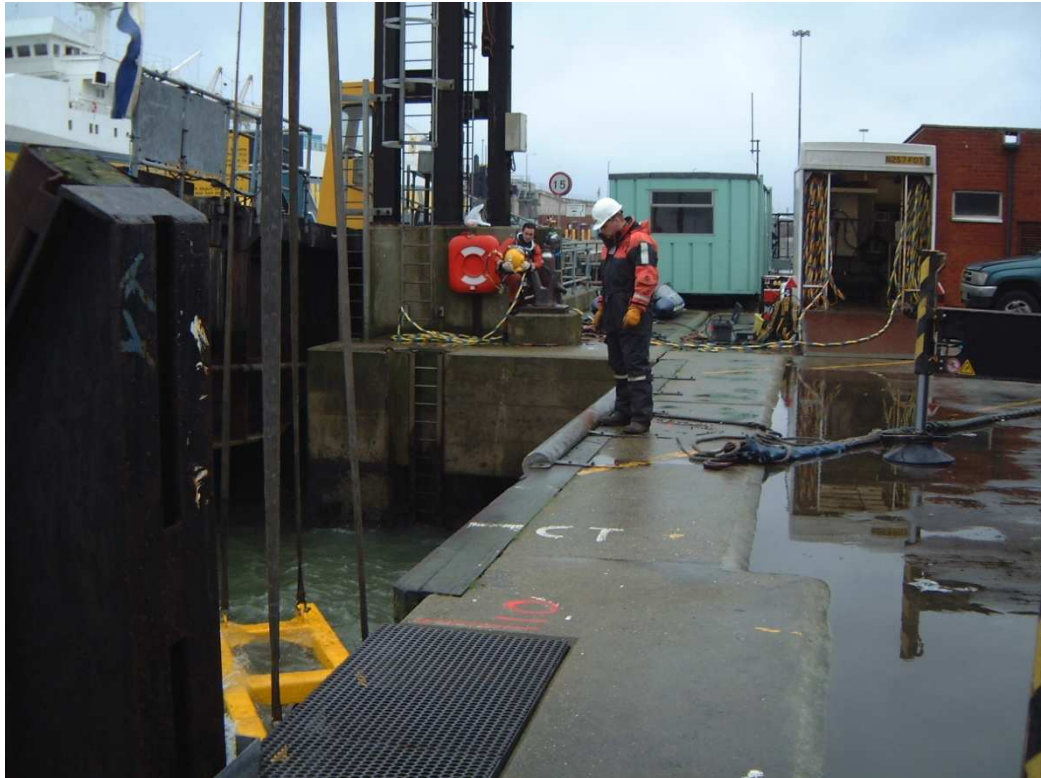


Figure 30: Concrete block installation by divers using purpose made lifting frame

Prior to the installation, the seabed was re-surveyed and any existing rocks that would obstruct the new works were individually stropped and craned clear. The seabed was levelled by dumping sand and new geotextile placed over the top of the sand.

The new groups of blocks were then positioned by divers on the seabed, and the groups were connected to each other by shackles and chains.

The area covered by these works was the area of greatest seabed scour to the corner of the berth and only 6 groups of the concrete blocks used.

5.6 Phase II Monitoring

The Phase II works were monitored for two years. The blocks were found to be successful with the blocks remaining in position whilst subject to direct impact from the ships' jets. The problem that was found was extensive scour around the edge of the blocks which caused washout of most of the sand fill beneath the whole area. In addition there was still a scour problem at the location of the sheet pile in-pans.

It was also noted that despite the seabed having been levelled prior to laying the blocks, there were localised works and gaps between the underside of the blocks and the seabed.

After two years of monitoring it was decided to extend the concrete block-work protection and to carry out further works to prevent scour at the in-pan locations.

5.7 Phase III Works

The arrangement and extent of the Phase III works is shown on Figure 31. This system was similar to the Phase II works but included better edge details, used insitu concrete to provide scour protection at the in-pan locations and connected the blocks to the sheet piling to prevent any gaps opening up. The detail used is shown in Figure 32.

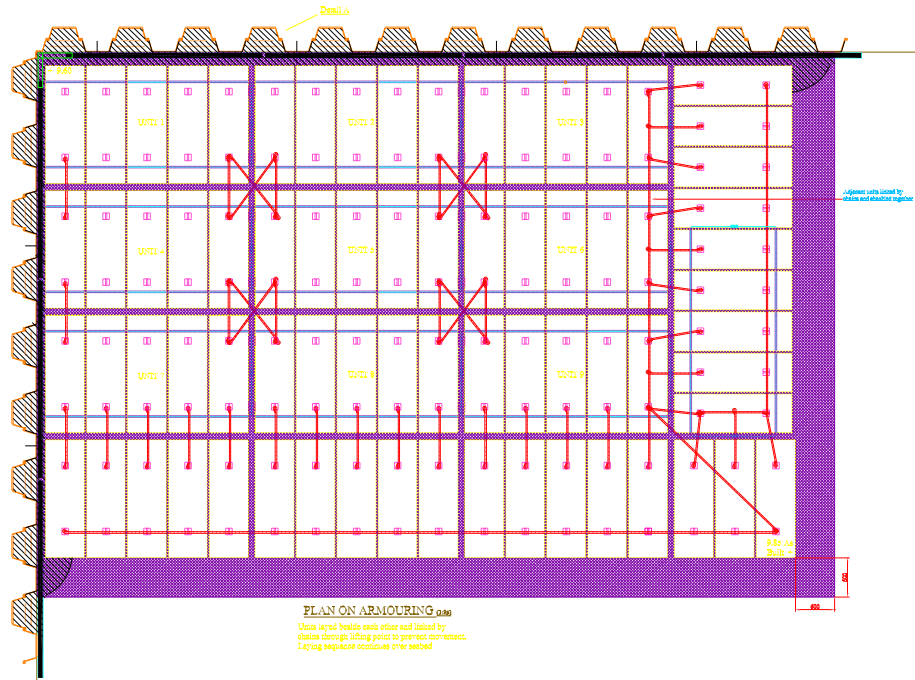


Figure 31: Arrangement of concrete blocks phase 3 (NB Phase 2 similar but with only 4 block sets in the corner of the berth)

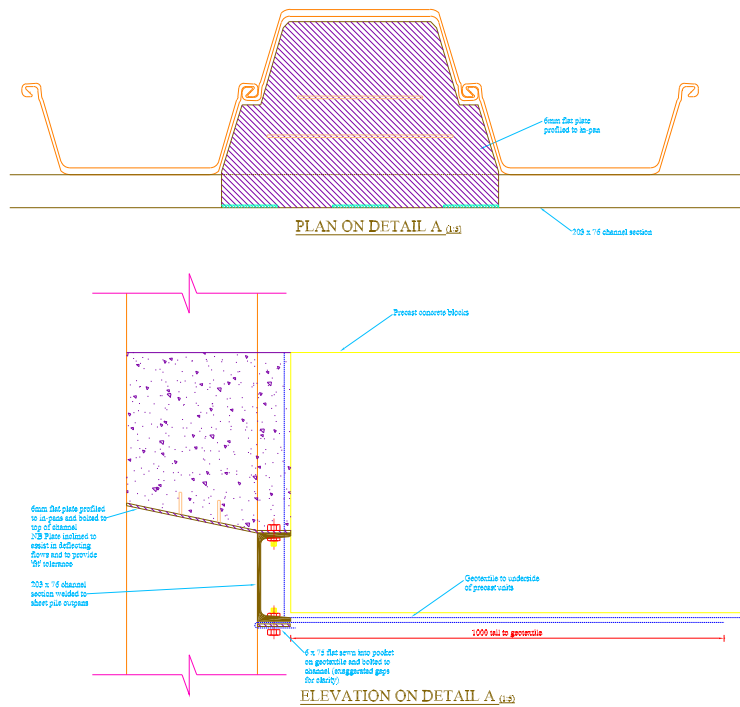


Figure 32: The improved sheet pile scour protection detail

The blocks used for Phase II were recovered from the seabed, cleaned and re-used. The seabed was re-levelled using sand fill, and a steel waling welded underwater to the sheet piles around the area of the works.

From the experience gained from the earlier works the job was completed over a 2 week period.

5.8 Phase IV Works

In December 2007 further inspections of the seabed protection system were carried out. The inspections revealed that failure of the geotextile membrane had occurred at the junction between the sheet pile wall and some fretting of the membrane had occurred under the edges of the blocks suggesting that some cyclic movement of the membrane or the blocks had occurred. Where the failure of the geotextile had occurred at the sheet pile

wall junction, the loss of the sand substrata had caused a localized void that was 2.5 metres in depth. This in turn had caused the concrete blocks over this area to settle and slope down towards the corner. The original rocks were found at depth under the new scour protection system at depths of up to 2 metres below their original placement levels. The inspection also revealed that the wire cables that had been used to connect the block sets together had fretted through at the corners of the outer blocks. Remedial works were undertaken to fill the void and repair the scour protection. This involved the removal of the blocks, infilling the void with sand, and then levelling and renewing the geotextile and repositioning the original blocks.

5.9 Discussion on the Poole Harbour Works

The works carried out at Poole revealed the following problems:

- 1) Conventional scour protection measures used with docks and harbours are not adequate to cope with the vectored jets from high speed ferries and current design guidance does not exist. Conventional design criteria used for Rip Rap are not appropriate and provide an unsafe solution. The failures being observed could not be easily explained when solely considering the hydrodynamic forces
- 2) The critical area for protection is the immediate manoeuvring area on the berth. In this case the area was found to occur between the sheet piling below the link span and up to 35 metres along the berth.
- 3) Edge and toe protection around scour protection systems is critical for the integrity of the whole system. This is particularly true at the sheet pile/seabed interface.
- 4) Even where the seabed is levelled prior to placing a seabed protection system it must be assumed that local voids will develop beneath the units.

- 5) Where rock protection was used, not only did it fail to protect against scour but the movement of the rocks caused localized mounds of rocks on the seabed which caused navigational clearances to be reduced below the minimum requirements.
- 6) The weight and depth of any blocks used needs to be reduced as much as possible to minimize material usage, excavation depth, cost of placement and to reduce the “design” retained height of any adjacent structures.
- 7) Following a review of the survey data it was noted that some of the original rock armouring was found buried up to 2 metres below its original placement level even where this was outside the immediate areas of scour.

From the experience at Poole it is clear that any scour protection system would not only be subject to direct forces from the jet drive units. Where voids exist and develop between and under the protection system, the water jets will raise the water pressure in these areas giving rise to uplift and ejection forces.

This problem was appreciated at the time of the Phase II design which is why lightweight mats such as Armourflex or similar were not used. It was decided that although these systems could be anchored to the seabed these anchorages would have to be continuous at edge locations and that conventional toeing in, covered by rock dumping, would not prove adequate.

From the model testing that was carried out, it was found that there were additional factors to be considered in the design of the scour protection system. These resulted from the response of the blocks when subject to loading by the water jets. The forces generated in the blocks were found to be highly variable oscillating loads which could give rise to oscillation of the individual blocks on the seabed. In the light of this, when further inspections were carried out on the scour protection system, particular attention was paid to the geotextile mat and the block connection system. It was found that both of these elements had failed as a result of this action.

During the December 2007 inspections, the failure of the geotextile membrane appears to have resulted from the geotextile flexing against the corners of the concrete blocks. This action suggests that the jet is causing a fluctuating load to occur on the geotextile and blocks to generate the problem. This indicates that any future designs will need to allow for this cyclic load in the materials specification and block design. The fretting of the wire rope suggests that the cyclic movement was not limited to the geotextile but that the individual blocks themselves were also subject to cyclic movement.

The burial of the original rocks from the phase 1 works is now thought to be due to a combination of loss of original seabed by scour and self burial due to liquefaction of the seabed due to the jets raising the seabed pore pressure.

Chapter 6

LABORATORY MODELLING

6.1 Introduction

From the research carried out no previous attempts were found to measure the forces on model blocks from a water jet. Therefore all aspects of the physical model had to be designed and detailed specifically for this project. All the testing frames, support systems and load gauges were drawn up and manufactured in the university workshops.

6.2 Description of the Physical Model

A model of the seabed protection system at Poole Harbour was constructed to enable laboratory simulation of the action of a water jet on concrete armour blocks. This model allowed the vertical loads on the concrete blocks to be measured when a water jet was directed from various angles, at differing flow rates and with varying air entrainment in the jet.

The general arrangement is shown in Figure 33. The components used in the model are described in Table 6, and illustrated by the sketches, drawings and photographs. This section is followed by a discussion on the way the model was configured together with a description of calibration procedures and calculations carried out to quantify possible errors.

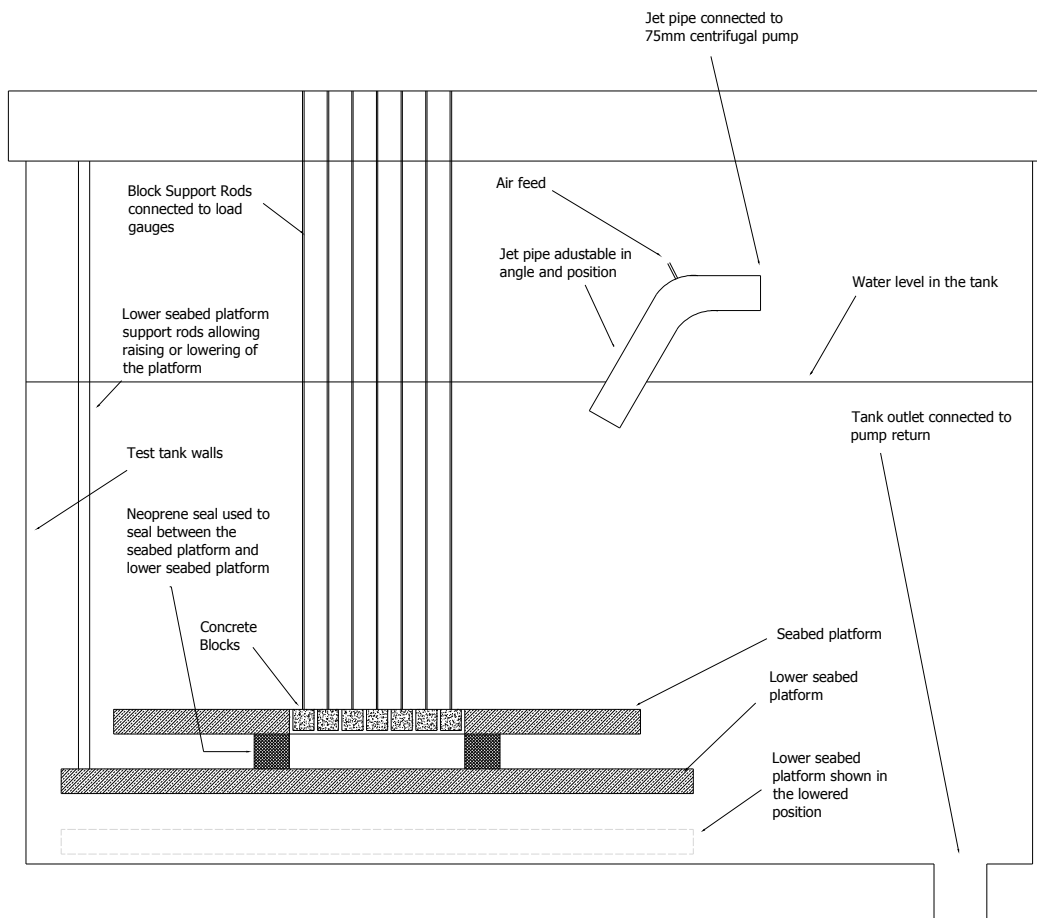


Figure 33: Schematic view on test tank showing seabed plated and model blocks

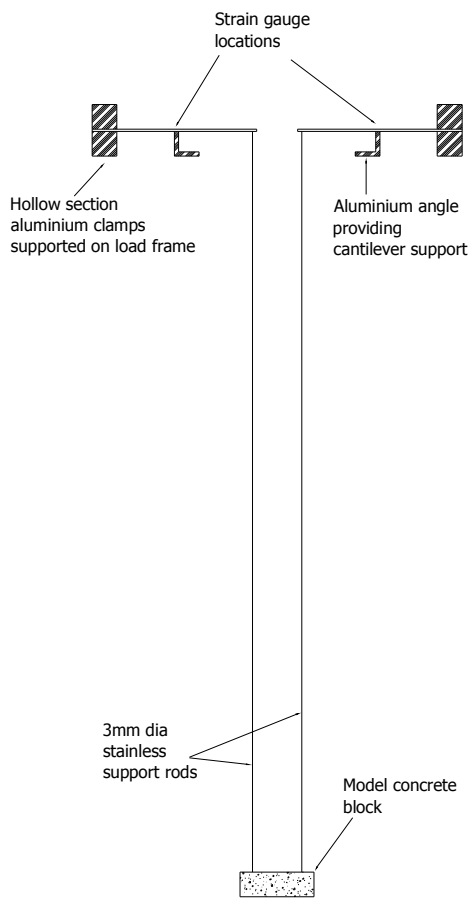


Figure 34: Schematic diagram showing concrete block supports and load measuring system

The elements used in the physical model are summarised in Table 6 below:

Table 6: Summary of model components

| Element | Description | Comments |
|--------------------|---|-------------------------|
| Test Tank | 1.8metre x 1.2metre x 1.2metre riveted steel water tank braced with external scaffolding | Figure 35 |
| Load gauges | 15mm wide by 225mm long by 3mm thick stainless steel strips incorporating Vishay strain gauge (type CEA-06-250UN-120) | Figure 43 and Figure 44 |
| Load frame | Purpose made aluminium frame formed from box and channel sections. The frame was designed to be highly robust and rigid to minimise any distortion under load | Figure 39 |
| Upper seabed plate | 35mm thick engineering plastic 900mm by 900mm with central machined hole to take model blocks | Figure 33 |
| Lower seabed plate | 35mm thick engineering plastic 1200mm by 900mm | Figure 33 |
| Jet pipe | 50mm internal diameter steel pipe machined to take 3mm internal diameter steel pipe to allow air to be introduced into the water jet (75mm to 50mm reducer used to connect to the pump supply pipe) | Figure 42 |
| Water Pump | 75mm centrifugal pump driven by a petrol engine Rated at 1300 litres per minute | Figure 41 |

| Element | Description | Comments |
|-----------------------|--|-------------------------|
| Connection pipes | 75mm spiral reinforced plastic | Figure 41 |
| Static pressure | 6mm diameter holes were drilled and tapped into the lower seabed plate and plastic air tubes lead back to a pressure gauge | Figure 46 |
| Concrete model blocks | These were cast in the laboratory using a 5mm maximum size aggregate with a cement: sand: aggregate ratio of 1:1 ¹ / ₂ :3 (by weight) using ordinary Portland cement. The blocks were centrally reinforced with a 5mm square section mild steel bar that was tapped to take the 3mm threaded stud bar. | Figure 45 and Figure 37 |



Figure 35: General view of test tank



Figure 36: Loading Frame

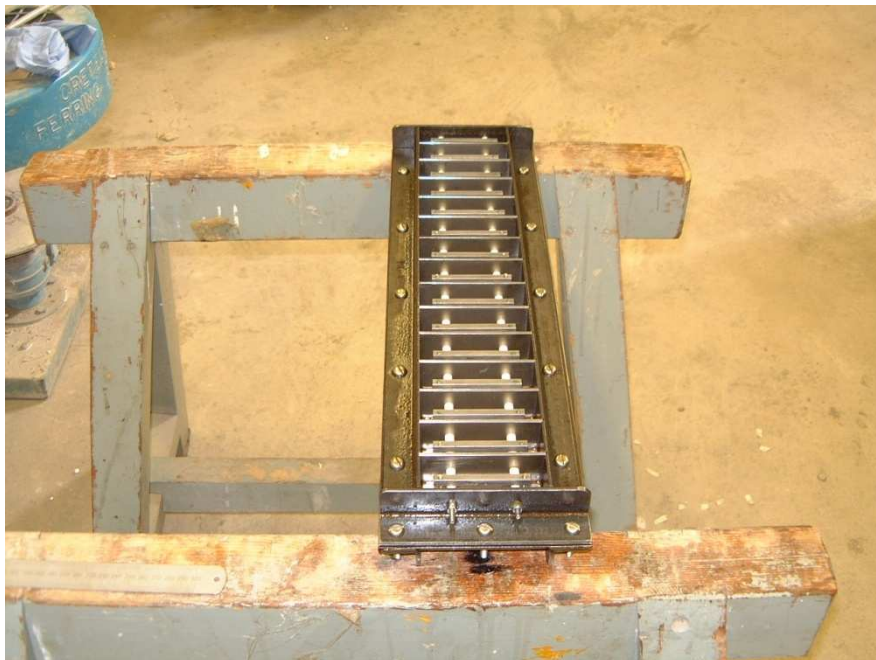


Figure 37: Steel formwork for the model scour protection blocks

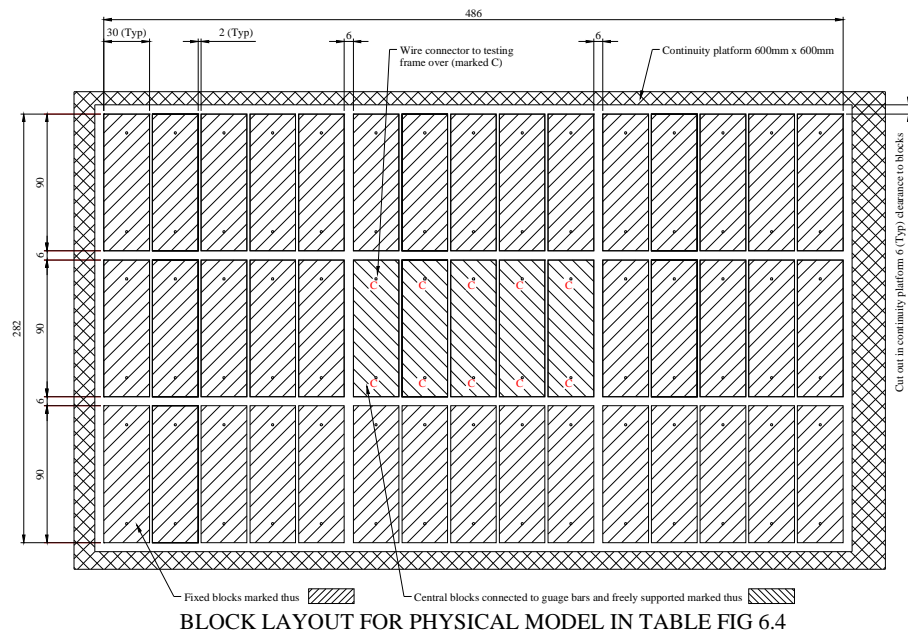


Figure 38 : Drawing of Model Scour Protection



Figure 39: General view of loading frame showing gauge bars



Figure 40: View on bridge amplifier and ‘Pad’ data logger



Figure 41: Pump unit and connection hose



Figure 42: Jet pipe and air feed



Figure 43: Load gauge

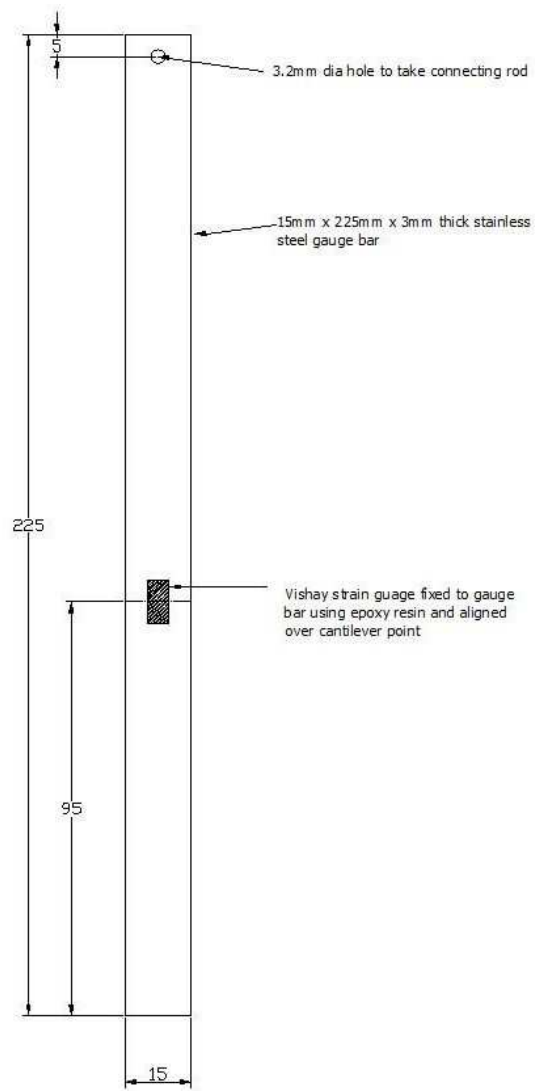


Figure 44: Gauge bar and strain gauge

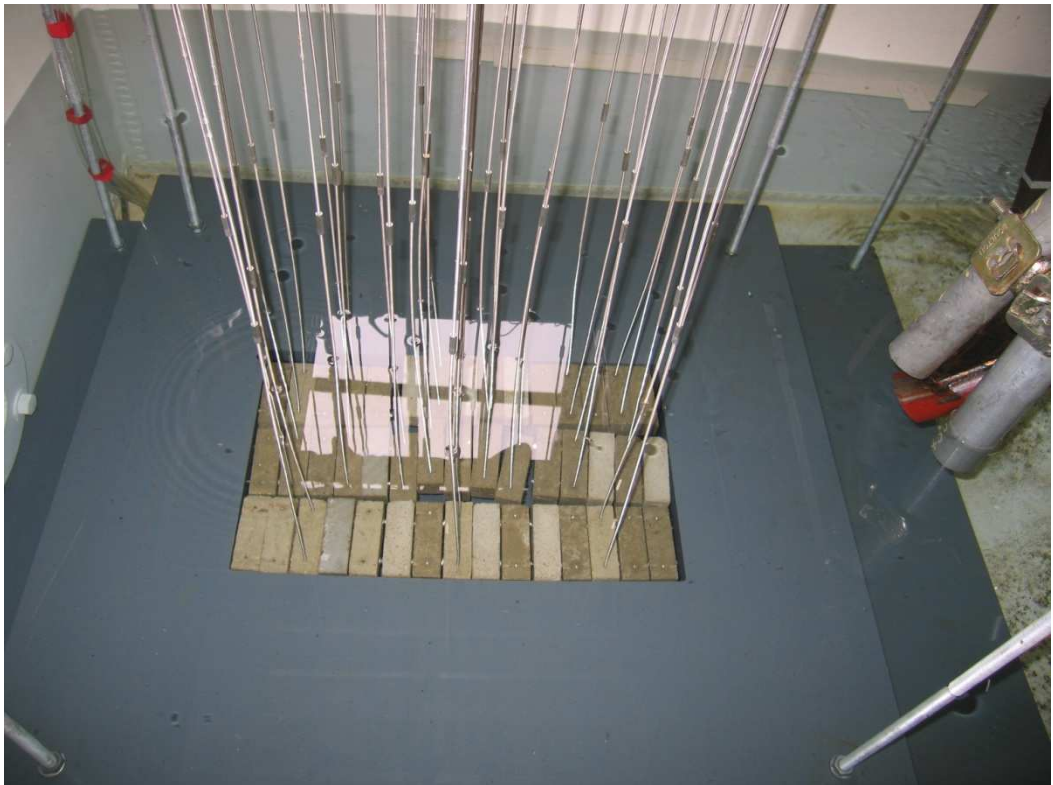


Figure 45: Showing model concrete blocks and connection rods

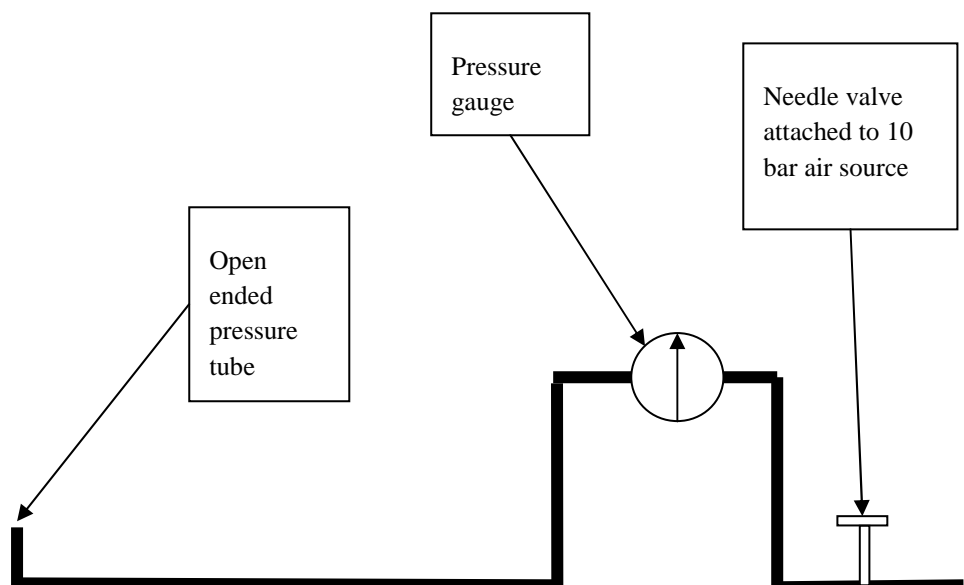


Figure 46: Diagram of static pressure measurement system

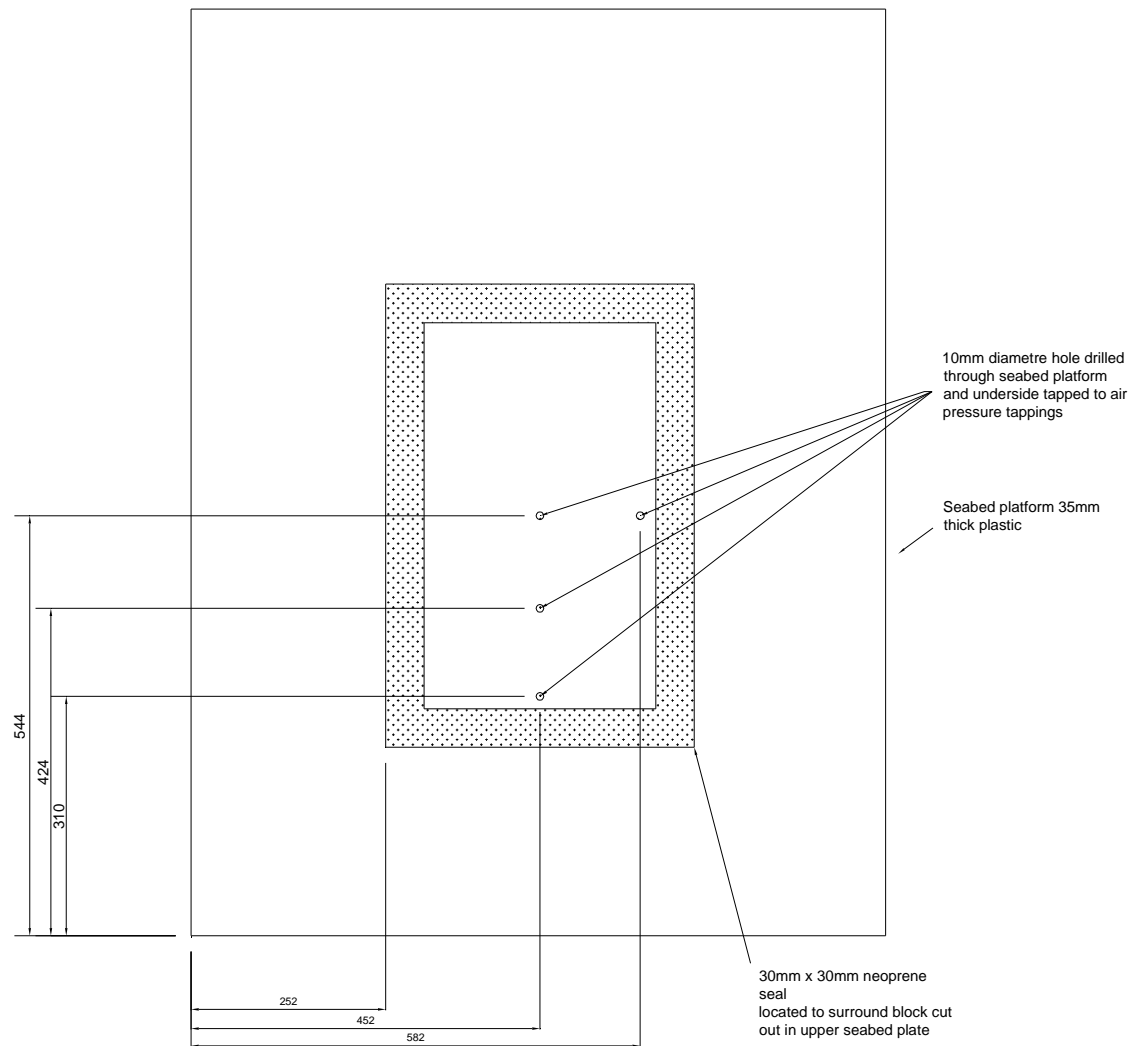


Figure 47: Layout of lower seabed platform and position of static pressure tapings

6.3 Discussion on the model and calibration procedures

Direct load measurement of the jet forces on the model blocks was carried out for several reasons.

- The turbulent flow around the model would have required high speed pressure transducers and logging equipment that were not available.

- It was the forces on the blocks that were of interest and if pressure measurements had been used to derive these the result would have been an approximation based upon an assumed pressure distribution across the block.
- Supporting the blocks on cantilever gauges allowed the elasticity of the supporting soil to be modelled. This meant that structural interaction (i.e. a load sharing system due to shear) of the blocks in the turbulent flow could occur.
- Allowing differential movement of the adjacent blocks allowed the flow environment to change dynamically during the testing as the blocks would deflect according to the imposed loading (Carling et al., 2002)
- Load measurements would reflect the inertial damping of the high frequency pressure transients arising from the turbulent flow.
- The measurement of the forces at either end of the blocks allowed the differential force across the supports to be measured.

Following the experimental work it should be noted that if high speed pressure measurements around the blocks could have been recorded simultaneously then a more complete picture would have been obtained. It is also recognised that the measurement system used could potentially produce significant ‘noise’ due to flow excitation of the rods and gauges bars. For this reason the resonant frequency of individual components was calculated and compared against the load oscillation outputs as part of the data integrity checking.

Load Gauges

Calibration of the load of measuring gauges was carried out by connecting the gauges to the computer via the amplifier and parallel pad device. Each gauge was mounted on the testing frame and loaded with a series of calibrated weights. The weights were added individually in sequence and then removed in the same order. This process allowed for any hysteresis effects to be identified, the unloading figures were found to be a very close match to the loading figures in all cases. Single axis strain gauges were used since only longitudinal bending of the gauge bars needed to be measured

The results from a calibration graph are shown in Figure 48. The results from the calibration procedures were analysed to check for errors and to check that the repeat results were consistent for all the gauges. During this process it was noted that amplifier 'drift' occurred which caused variations in the gauge readings, but this stabilised after 10 minutes. The recorded data during the calibration was analysed and used to establish calibration graphs for each gauge. These calibration graphs were used to analyse the test results. The calibration results and load charts for the gauges are shown in Appendix 3 and reduced versions are included here see Figure 48. The load - voltage were plotted and the function for load against voltage was deduced for each gauge.

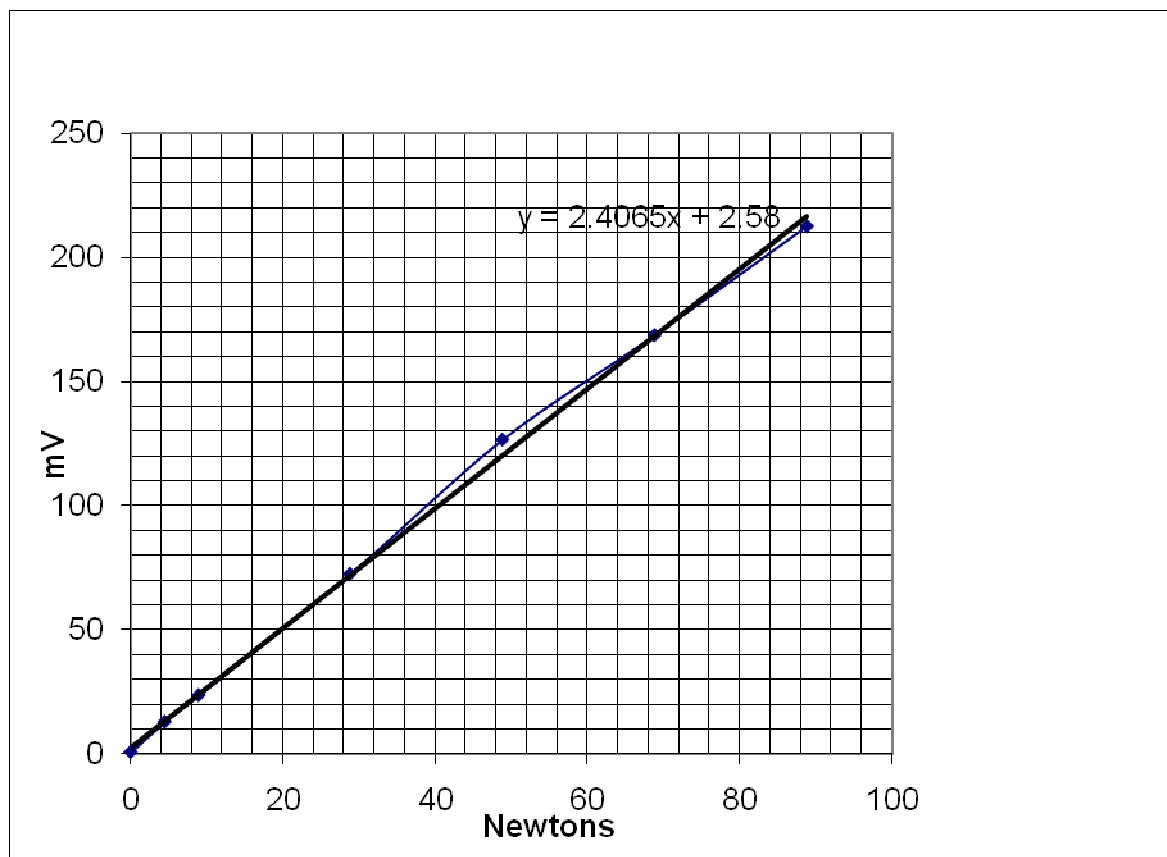


Figure 48: Calibration graph gauge 3

Initially a linear load voltage relationship was used for the gauge – force calculations, the error resulting from the slight lack on linearity was considered acceptable in this case. The theoretical relationship for this measurement system should be linear however there are a few experimental factors that will have affected this:

- The fixed end of the gauge will not have been completely rigid
- The propped support had a finite length
- The connection between the drop rod and the gauge had partial fixity due to the securing nuts

Where the amplifier was not zeroed prior to taking the readings this was found not to affect the calibration curve and only caused an axis shift. This factor was taken into account when analyzing the test results to enable any slight drift in the zero voltage to be taken into account during the post processing.

The natural frequencies of the gauge bars are derived to establish whether excitation of the load measuring system was likely to be influencing the experimental results.

The frequency of an elastic system is given by Timoshenko (1937)

$$f = \frac{1}{2\pi} \sqrt{\frac{g}{\delta_{st}}} \dots\dots\dots\text{Equation 14}$$

And

$$\delta_{st} = \frac{\left(W + \frac{W_i}{4}\right) l^3}{3EI} \dots\dots\dots\text{Equation 15}$$

Where:

f is the fundamental frequency of the cantilever

δ_{st} is the initial displacement at the end of a free cantilever

W is the weight on the end of the cantilever

W_i is the self weight of the cantilever

E is Young's modulus for stainless steel

I is the second moment of area of the cantilever strip

This gives a fundamental frequency of the gauge and block system of 29Hz using the submerged weight of the concrete block. To understand the sensitivity of the system, if the concrete block weight was doubled this would change the natural frequency of the measurement system to 23Hz, this indicates the level of change in the natural frequency of the system that can arise due to the interaction between adjacent model blocks.

When analysed elastically the support system for the model blocks did not indicate that any appreciable load transfer between the supports would occur due to moment resistance from the support rods. This was also verified experimentally by independently loading each support rod in turn and taking deflection readings on both gauges. A typical plot showing the gauge deflection against load is shown in Figure 49. In this case support 1 is being loaded and unloaded and the resulting deflection of gauge 2 is plotted. This revealed that the maximum error of less than 5% on load readings.

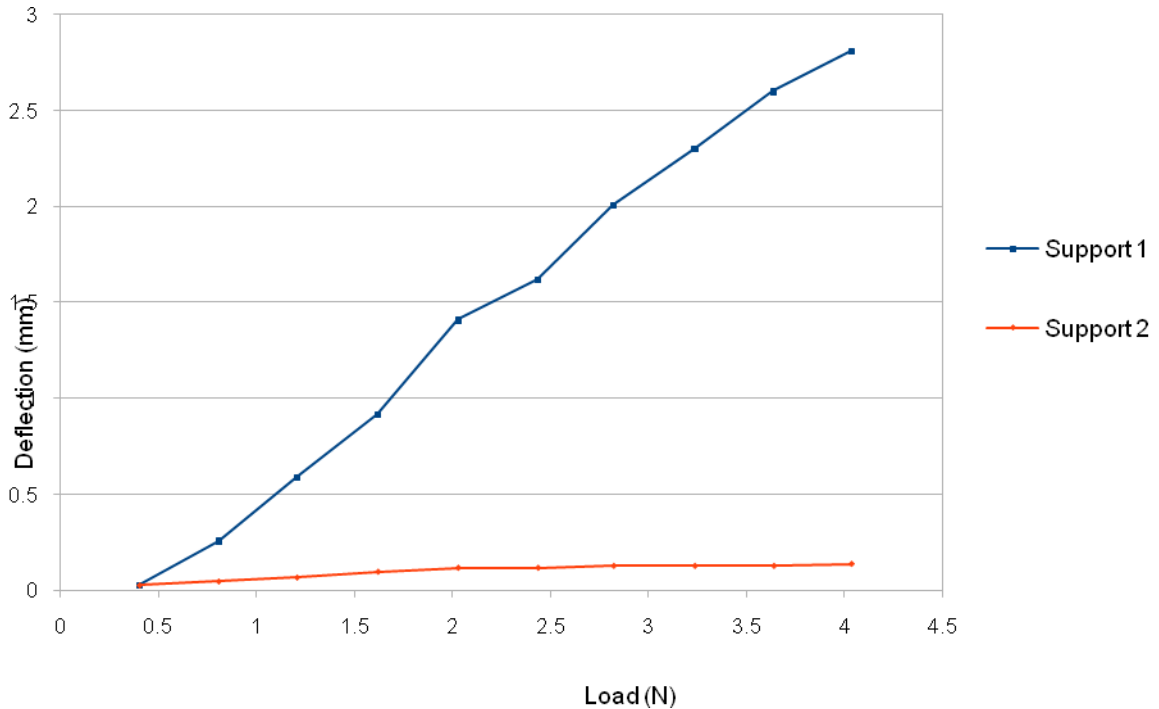


Figure 49: Graph showing the secondary gauge deflections when support 1 only is loaded

The block support system was also compared with the anticipated soil modulus of the seabed at Poole Harbour. The seabed at Poole Harbour can be described as a coarse grained loose sand. This sand strata extend to depth and with respect to the deflection of the armour blocks will be considered as a linear elastic isotropic half-space, in reality the load deflection behaviour of the blocks would not be fully elastic and plastic deflection would occur. For the purposes of experimentation however the plastic deflection will be ignored since this would primarily affect the long term deflection rather than the short term behaviour that is being analysed in this work. On this basis the strata can be modelled as an infinite depth and having constant linear elastic properties. Using Boussinesq formulation it was possible to generate values for the anticipated vertical displacements under the blocks for a given load.

$$\sigma_z = \frac{3Q}{2\pi z^3} \left[\frac{1}{\left(1 + \left(\frac{r}{z}\right)^2\right)^{\frac{5}{2}}} \right] \dots\dots\dots \text{Equation 16}$$

Boussinesq formula for vertical displacement

Where:

σ_z = Vertical displacement

Q = Load

z = depth

r = horizontal distance from load

Jet Impingement Angle

The manoeuvring buckets used on the HSS can deflect the jet across a full range of angles to the seabed. Therefore tests were carried out with the jet at 60° and 40° to the horizontal.

Seabed Permeability

The permeability of the underlying seabed was modelled by adjusting the height of the plastic sheet under the scour blocks. This varied from effectively impermeable when the neoprene seal on the lower section was tight against the upper section to fully permeable when the lower section was dropped clear of the upper section. The permeability was not modelled quantitatively since under the two extremes no major changes were noted to the concrete block forces.

Seabed Clearance

On the prototype the distance between the vessel jet units and the seabed varies with the tide. The range of possible clearances is shown in Figure 25. The prototype clearances (3.6 metres to 4.7 metres) are such that a fully developed jet will be formed

at seabed level for most states of tide. The seabed clearance on the model was 250mm which is 5.0 metres on the prototype. This value was used to ensure a the jet was fully developed, since earlier research suggested that a fully developed jet produced greater pressure transients at seabed level.

6.3 Scale Factors

The scale factors used for the model were;

Table 7: Model Scale Factors

| Type | Prototype | Model |
|--------------------------------|----------------------------------|----------------------------------|
| Geometric | 1 | 1/20 |
| Velocity | 1 | 1/4.46 |
| Force | 1 | 1/20 |
| Reynolds number see Table 3 | Not significant for jet flows | Not significant for jet flows |

Water Jet

The water jet unit was calibrated by recording the time taken for discharge of the tank at a given throttle setting on the pump. During this procedure the head of the jet was maintained at the same height and orientation as for the test runs and the supply and return hoses were maintained in similar positions. In order to eliminate errors due to flow variations during the pump start up phase, the drop in water level of the tank was timed between two set points. These results were then used to give a volume of water

discharged by the jet over a measured time period following each series of tests, providing an average flow rate from the water jet.

The jet pipe calibration gave very consistent results of discharge against throttle setting with a variation in results of no greater than 3% when carrying of successive runs on the same settings.

The likely frequency generation from the water pump was checked by measuring the speed of the pump input shaft using a tachometer; this also allowed the throttle setting on the pump to be directly calibrated to shaft speed while the pump was under constant load. The water pump itself was stripped and checked for any defects. The centrifugal pump was a two port unit which meant that any pulsing of the water jet arising from this source would be at a frequency of twice the shaft speed of the pump.

The flow rates from the jet were calculated by discharging the water from the tank through the jet nozzle and recording the time taken to discharge a given volume of water at a constant pump speed. Whilst the jet pipe was removed from the tank in order to carry out this measurement care was taken to ensure the flow and return pipes to the pump were kept to the same length, configuration and relative head as though used during the experimentation. The results are summarized in Figure 50 below

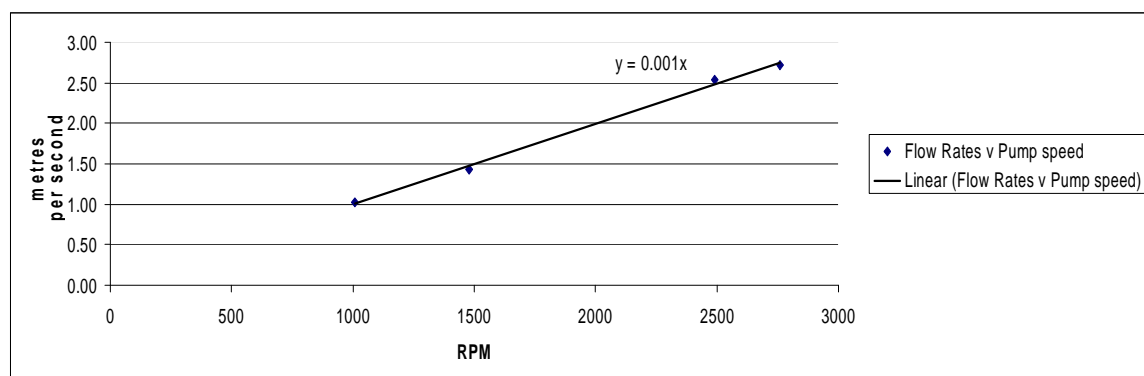


Figure 50: Jet flow versus pump speed

Air Entrainment System

The modelling of air entrainment can lead to either impossibly large models (of around 1:10) or scale effects due to the difficulty obtaining in similitude with respect to the bubble size. (Melo, 2002). The model was also operated using fresh water which has different bubble generation characteristics to the partially saline environment of the prototype (Craig et al., 1993). Notwithstanding these issues, the use of air entrainment in the jet allowed the qualitative effect of air entrainment to be studied.

Calibration procedures carried out for the air entrainment system are set out below. The needle valve supplying the air to the jet was marked at certain settings and the supply air to the needle valve maintained at a constant pressure. The time taken for a given volume of air to be released from the discharge nozzle was then recorded. This then enabled the flow rates to be calculated. The results are shown below in Figure 51.

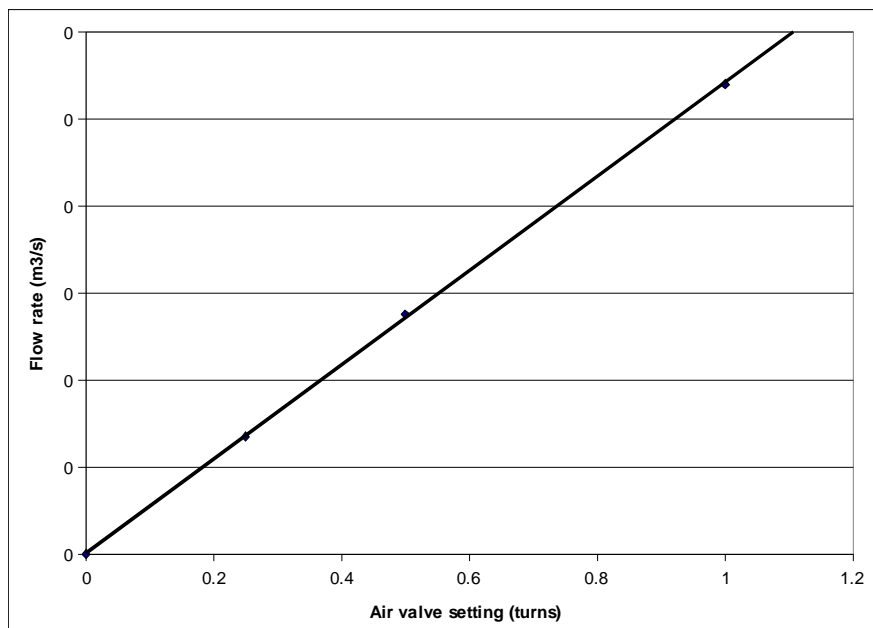


Figure 51: Air valve setting versus air flow rate

The above results have then been converted to provide a figure for percentage of air entrained for a different pump speeds and air valve settings and these are shown below in Figure 52.

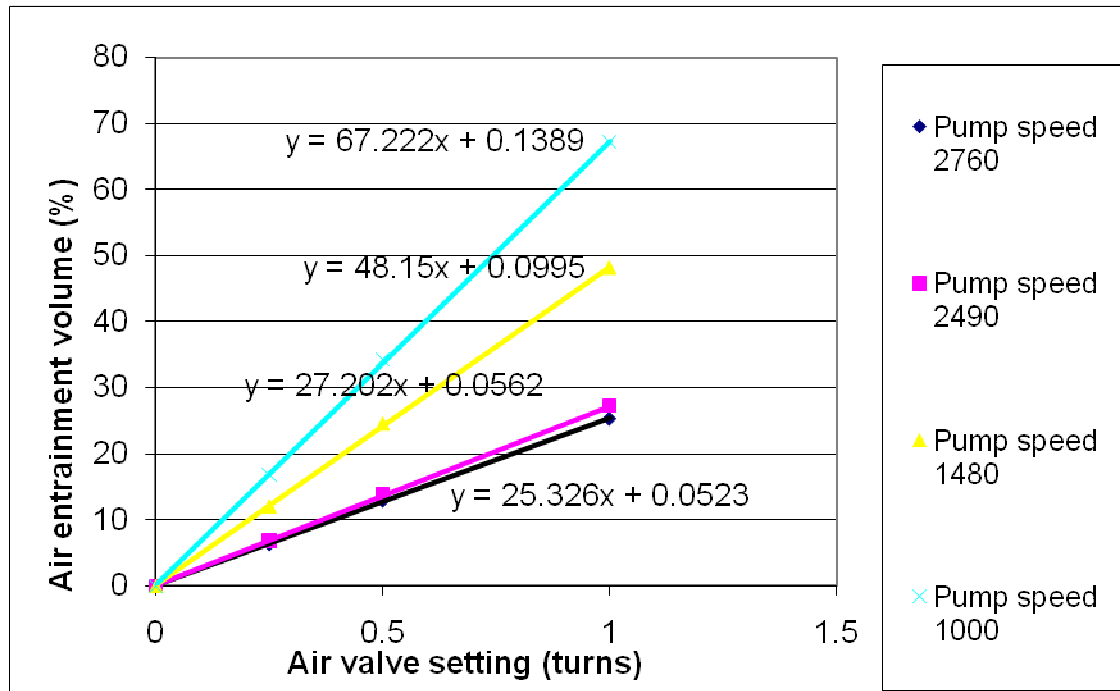


Figure 52: Air valve setting versus air entrainment % by volume for various pump speeds

Static Pressure System

The static pressure take off points on the lower seabed platform were connected to a pressure gauge. This gauge was calibrated against a calibration gauge (Druck DPG). In addition a cross check was carried out as the tank was filled with water to verify that each pressure tapping showed the expected hydrostatic pressure once the tank had been filled. Whilst the system proved adequate for measuring static water pressures the air tubes damped out the high frequency pressure fluctuations and therefore no meaningful measurements of dynamic pressure fluctuations were recorded beneath the blocks

Health and Safety Considerations

A method statement and risk assessment were carried out for the work to ensure the safety of the personnel working on the tank and also to make sure the other users in the laboratory. The following key measures were adopted;

- The petrol driven pump unit was operated in the open air immediately outside the laboratory. This was to reduce noise and avoid the problems of exhaust gases
- A chlorine disinfectant was added to the water in the tank to prevent algae growth and reduce the risk of infection
- All electrical equipment was operated through an RCD (Residual Current Device) and kept at least 1 metre away from the test tank during operation

The jet unit was only operated when securely clamped to a fixed object

Chapter 7

Model Test Results and Data Analysis

7.1 Introduction

The tests carried out involved 38 test runs where the concrete block forces were measured with jet angle varying between 40 and 60 degrees to the horizontal, jet velocities of between 1.00ms^{-1} and 3.00ms^{-1} and air entrained jet flows.

The first set of runs (1 to 20) was on multiple blocks set up to model the arrangement of the seabed protection at Poole Harbour. From the analysis of these runs it was clear that the blocks were being subject to highly oscillating forces from the jet flow. Because of these force oscillations the interaction between adjacent blocks gave rise to a highly complex behaviour on individual blocks, it was therefore decided to carry out a further series of test runs (21 to 38) this time with a single block positioned in the test tank so that it was free to move without touching adjacent blocks. These runs were carried out using similar parameters to those for the initial set of runs.

Following the first set of runs and having identified the force oscillations, a series of test and measurements were taken on all the test equipment to establish whether any of the oscillations were likely to have been generated or excited by the laboratory procedures.

7.2 Data Handling

The data files have been mapped and displayed against the testing regime and this is shown in Table 8.

Table 8: Data file mapping

| Data file ref | Raw file name | Time frame of run | Jet angle | Jet speed (ms ⁻¹) | Seabed location | Air valve setting | Gauge map | Comments |
|---------------|---------------|-------------------|-----------|-------------------------------|-----------------|-------------------|-----------|-----------------|
| Run 1 | Run10 | | 60 | 3.0 | Up | 0 | 1 | Multiple blocks |
| Run 2 | Bloc2931 | 21:27 – 21:30 | 60 | 1.0 | Up | 0 | 1 | Multiple blocks |
| Run 3 | Bloc2931 | 21:29 – 21:36 | 60 | 2.49 | Up | 0 | 1 | Multiple blocks |
| Run 4 | Bloc2931 | 21:35 – 21:40 | 60 | 2.49 | Up | 0.25 | 1 | Multiple blocks |
| Run 5 | Bloc2931 | 21:39 – end | 60 | 2.49 | Up | 0 | 1 | Multiple blocks |
| Run 6 | Bloc2932 | 21:55 – 22:06 | 60 | 1.00 | Down | 0.25 | 1 | Multiple blocks |
| Run 7 | Bloc2932 | 22:05 – 22:07 | 60 | 1.00 | Down | 0 | 1 | Multiple blocks |
| Run 8 | Bloc2932 | 22:06 – 22:10 | 60 | 2.49 | Down | 0 | 1 | Multiple blocks |
| Run 9 | Bloc2932 | 22:09 – 22:15 | 60 | 2.49 | Down | 0.25 | 1 | Multiple blocks |
| Run 10 | SBM20041 | 13:00 – 13:02 | 50 | 1.00 | Down | 0 | 1 | Multiple blocks |
| Run 11 | SBM20041 | 13:01 – 13:05 | 50 | 1.00 | Down | 0 | 1 | Multiple blocks |

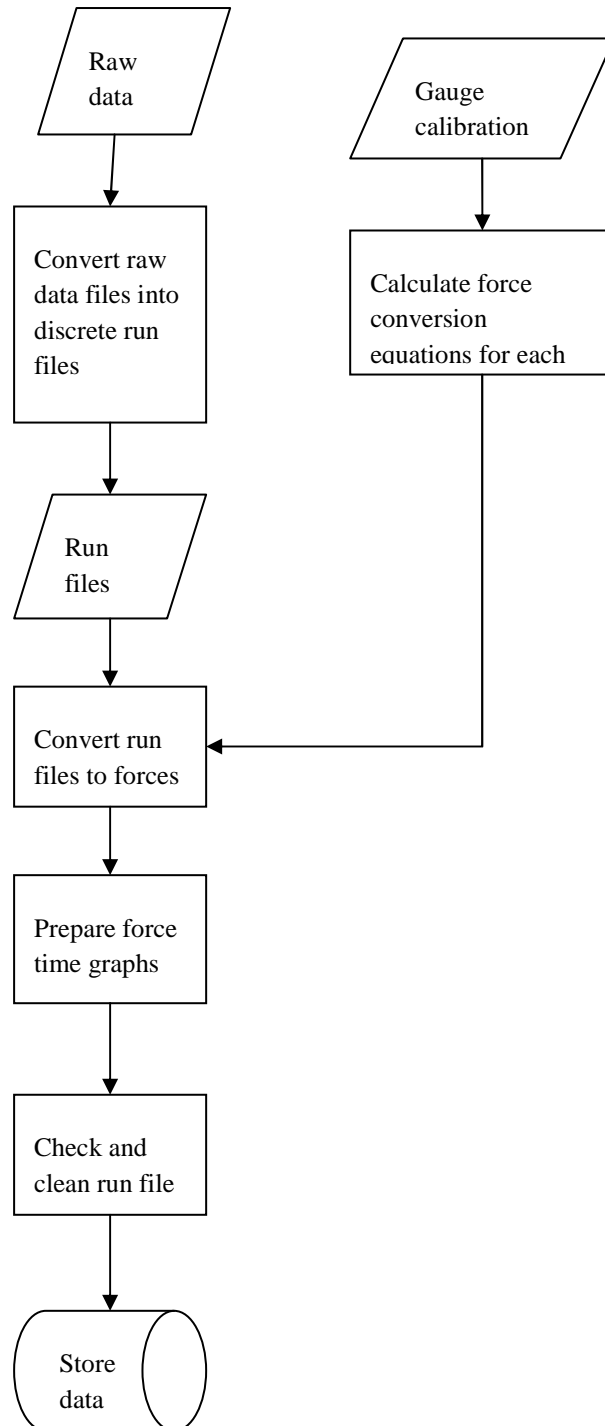
| Data file ref | Raw file name | Time frame of run | Jet angle | Jet speed (ms ⁻¹) | Seabed location | Air valve setting | Gauge map | Comments |
|---------------|---------------|-------------------|-----------|-------------------------------|-----------------|-------------------|-----------|-----------------|
| Run 12 | SBM20041 | 13:04 – 13:09 | 50 | 1.00 | Down | 0.25 | 1 | Multiple blocks |
| Run 13 | SBM20041 | 13:09 – 13:10 | 50 | 1.00 | Down | 0 | 1 | Multiple blocks |
| Run 14 | SBM20041 | 13:10 – end | 50 | 1.00 | Down | 0.25 | 1 | Multiple blocks |
| Run 15 | SBM20042 | 13:30 – 13:32 | 50 | 2.49 | Down | 0 | 1 | Multiple blocks |
| Run 16 | SBM20042 | 13:32 – 13:38 | 50 | 2.49 | Down | 0.25 | 1 | Multiple blocks |
| Run 17 | SBM20042 | 13:37 – 13:44 | 50 | 2.49 | Down | 0 | 1 | Multiple blocks |
| Run 18 | SBM20043 | 13:47 – 13:50 | 50 | 1.00 | Up | 0 | 1 | Multiple blocks |
| Run 19 | SBM20043 | 13:50 – 13:53 | 50 | 100 | Up | 0.25 | 1 | Multiple blocks |
| Run 20 | SBM20043 | 13:53 – 13:55 | 50 | 1.00 | Up | 0 | 1 | Multiple blocks |
| Run 21 | 12912 | 10:40 – 10:43 | 40 | 2.76 | Down | 0 | 2 | Single block |
| Run 22 | 12912 | 10:42 – 10:47 | 40 | 2.00 | Down | 0 | 2 | Single block |
| Run 23 | 22912 | 12:10 – 12:12 | 40 | 2.00 | Down | 0 | 2 | Single block |

| Data file ref | Raw file name | Time frame of run | Jet angle | Jet speed (ms⁻¹) | Seabed location | Air valve setting | Gauge map | Comments |
|----------------------|----------------------|--------------------------|------------------|------------------------------------|------------------------|--------------------------|------------------|-----------------|
| Run 24 | 22912 | 12:11 – 12:15 | 40 | 2.00 | Down | 0.25 | 2 | Single block |
| Run 25 | 22912 | 12:14 – 12:16 | 40 | 2.00 | Down | 0.5 | 2 | Single block |
| Run 26 | 22912 | 12:16 – 12:18 | 40 | 2.00 | Down | 1 | 2 | Single block |
| Run 27 | 22912 | 12:18 – 12:21 | 40 | 2.00 | Down | 0.25 | 2 | Single block |
| Run 28 | 22912 | 12:21 – 12:30 | 40 | 1.46 | Down | 0 | 2 | Single block |
| Run 29 | 22912 | 12:30 – 12:33 | 40 | 1.46 | Down | 0 | 2 | Single block |
| Run 30 | 22912 | 12:33 – 12:36 | 40 | 1.46 | Down | 0.25 | 2 | Single block |
| Run 31 | 22912 | 12:36 – 12:38 | 40 | 1.46 | Down | 0.5 | 2 | Single block |
| Run 32 | 22912 | 12:38 – 12:40 | 40 | 1.46 | Down | 1 | 2 | Single block |
| Run 33 | 22912 | 12:40 – 12:41 | 40 | 1.46 | Down | 0 | 2 | Single block |
| Run 34 | 22912 | 12:41 – 12:45 | 40 | 2.49 | Down | 0 | 2 | Single block |
| Run 35 | 22912 | 12:45 – 12:48 | 40 | 2.49 | Down | 0.25 | 2 | Single block |

| Data file ref | Raw file name | Time frame of run | Jet angle | Jet speed (ms⁻¹) | Seabed location | Air valve setting | Gauge map | Comments |
|----------------------|----------------------|--------------------------|------------------|------------------------------------|------------------------|--------------------------|------------------|-----------------|
| Run 36 | 22912 | 12:47 – 12:53 | 40 | 2.49 | Down | 0.5 | 2 | Single block |
| Run 37 | 22912 | 12:53 – 12:59 | 40 | 2.49 | Down | 1 | 2 | Single block |
| Run 38 | 22912 | 12:59 - end | 40 | 2.49 | Down | 0 | 2 | Single block |

The method used for data handling and processing is shown on Figure 53, Figure 54 and Figure 55 in the form of flow charts. In Figure 53 the process ‘check and clean run file’ involved editing the data file to include output for the time interval of the test run. The raw data file extended from the time of the experimental setup to completion of the proceedings. The extended period of logging allowed checks on signal drift and for calibration checks on the load gauges to be carried out at the end of each period.

7.2 Data Preparation

**Figure 53: Conversion of raw data**

Preliminary data analysis – oscillation frequencies

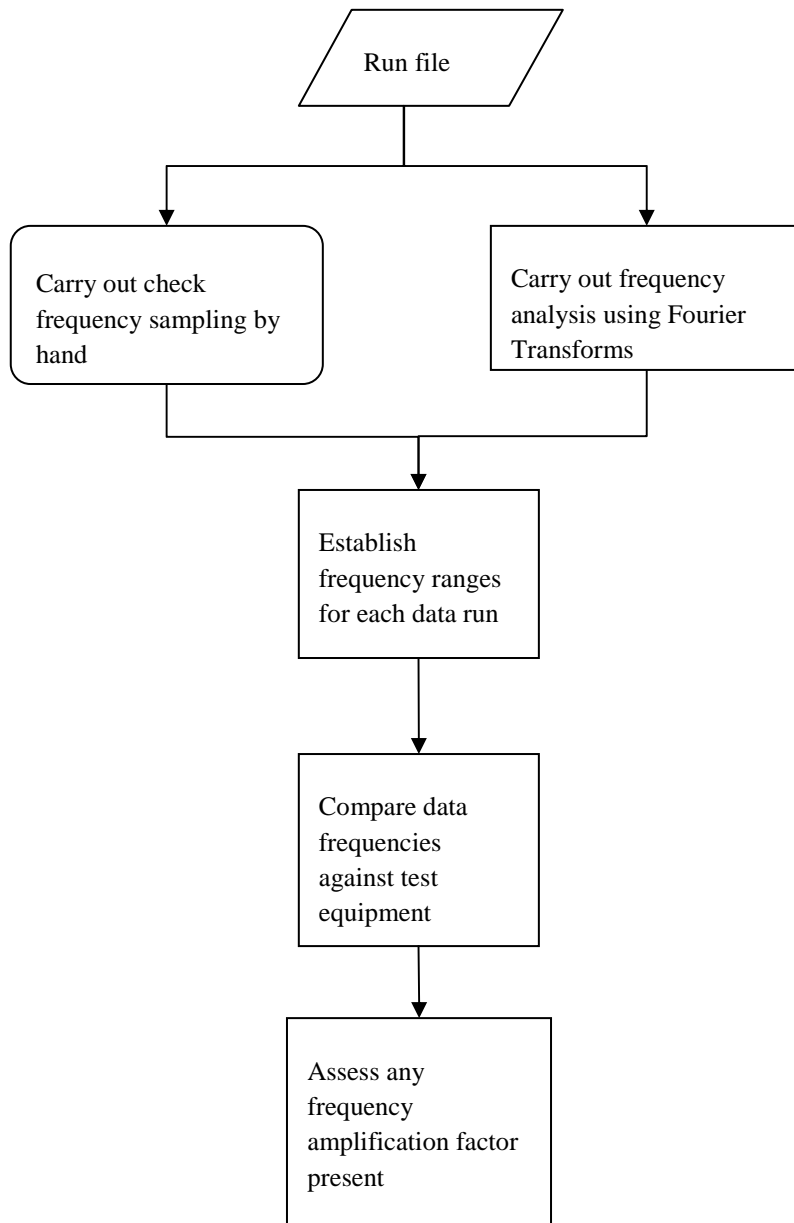


Figure 54: Frequency analysis procedure

Data Analysis – Run files

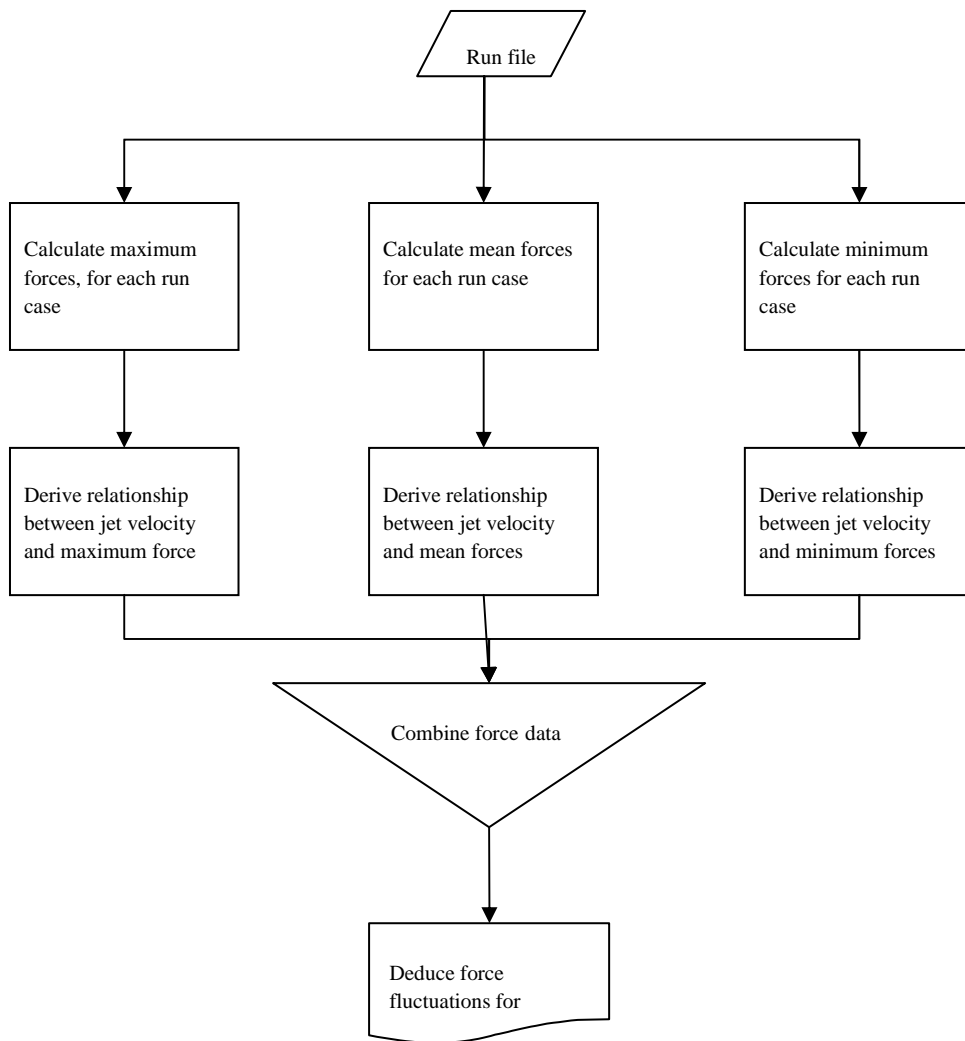


Figure 55: Data analysis carried out on the data for each test run

7.3 Data analysis and integrity checking

The load gauge results were initially converted from the voltages as recorded into load readings using the conversion formula derived from the calibration curves.

The data was then analysed using spreadsheets to process the figures and produce graphs of the test data. Statistical analysis of the figures was carried out to see if the variation of the forces fitted into any of the normal distribution curves. This proved that the oscillations lay outside these parameters with much of the data falling as outliers.

For the data recording system used the Nyquist critical frequency is given by

$$f_c \equiv 1/2\Delta$$

Where Δ is the sampling rate in this case 10Hz for the data logger, therefore $f_c = 5\text{Hz}$.

From this the analysis will not be able to identify any frequencies greater than 5Hz however the data suggests that the frequencies involved are generally less than this figure. The pad data logger was capable of recording at the rate of 10Hz per channel but was a multiplexer device so data from adjacent channels would not be recorded simultaneously as the logger would step through the channels at 100Hz. The frequencies obtained were compared with the natural and harmonic frequencies of the jet pump to check whether these elements are contributing to the oscillations.

Pump Frequencies: the water pump was operated in the range of 1000 to 3000 RPM, it was a two port centrifugal pump, and therefore any pulse frequencies emanating from the pump would be 33Hz to 100Hz

The electrical noise arising from the strain gauges together with the bridge amplifier and the pad data recorder were checked by inputting the signal output through an oscilloscope. This showed that all the signal oscillations were of extremely small amplitude and that where there were oscillations were detected; these were at very high frequencies (in excess of 1000Hz).

The natural frequency of the gauge together with the concrete block weight was calculated as 28Hz therefore all the natural frequencies from the test equipment were above the capability of the data recording system.

7.4 Gauge calibration

The tools available within Excel were used to calculate the maximum, minimum and mean values for the load data and these were stored on a separate worksheet within each data analysis file as shown in Figure 56.

Run 2 Analysis

| | gauge 3 | gauge 9 | gauge 4 | gauge 5 | gauge 10 | gauge 11 | gauge 12 |
|---------------------------|----------------|----------------|----------------|----------------|-----------------|-----------------|-----------------|
| Max load | 0.236 | 0.218 | 1.145 | 0.097 | 0.897 | 1.357 | 1.140 |
| Minimum Load | 0.094 | -0.196 | -0.191 | 0.000 | -0.073 | 0.145 | -0.047 |
| Average load | 0.115 | -0.087 | 0.319 | 0.026 | 0.181 | 0.509 | 0.308 |
| Average frequency | 1.878 | 0.830 | 2.657 | 0.989 | 0.781 | 1.597 | 0.800 |
| Standard Deviation | 0.018 | 0.081 | 0.250 | 0.014 | 0.150 | 0.179 | 0.175 |

Figure 56: Example of Data Analysis Summary

For each run the load time graphs were prepared for each load gauge separately and also for selected load combinations. Where load combinations were analysed the load was calculated by summing the load gauge readings for each time interval. Examples of the load/time graphs are shown in Figure 57 and Figure 58. This approach can be compared with that taken by Bollaert and Schleiss (2001), where they suggest combining pressures falling within different time intervals as providing the worst possible forces. In this instance this is considered to be too conservative since the duration of the manoeuvres of the HSS can be measured in minutes and not in tens of hours as would be the case with a dam spillway.

The selection of (near) simultaneous maxima and minima from the support loads is used since these represent the most credible combinations to give rise to movement of the blocks. Whilst this is not definitive it is a similar approach to that taken by other researchers (Caroni et al., 2002). The force measurements represent support loads at either end of a block, where both these loads are acting in the same direction and are of the highest magnitude then there is the greatest probability that overall movement of the block will occur. Where these are on opposing directions or of very different magnitude then rotation of the block is a more likely outcome.

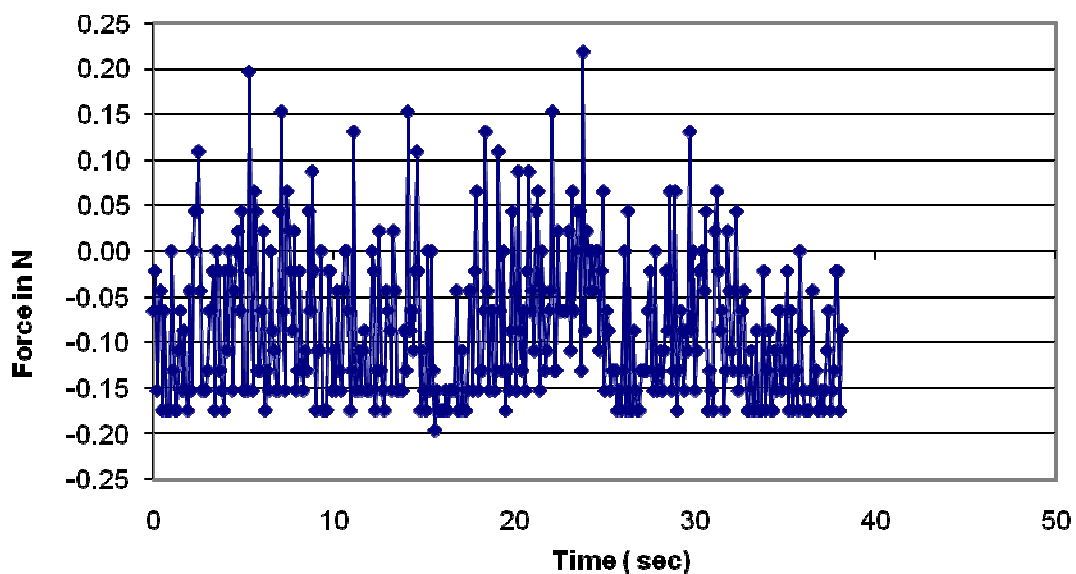


Figure 57: Example of load v time graph for a gauge (Run 2 Load gauge 9)

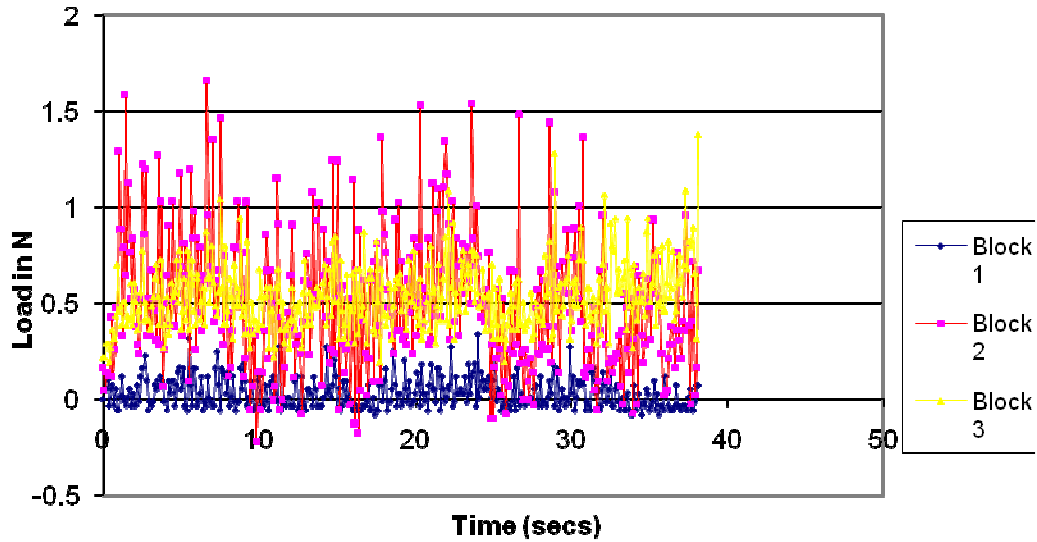


Figure 58: Example of a load v time graph showing total loads on blocks (Run 2 block loads)

The output graphs were examined to see if the data points suggested frequencies beyond the measuring system were predominant. These checks suggested that there were frequencies present that were above the ability of the data recorder but generally there were data points showing a waveform. Examples of the check graphs are shown in Figure 59.

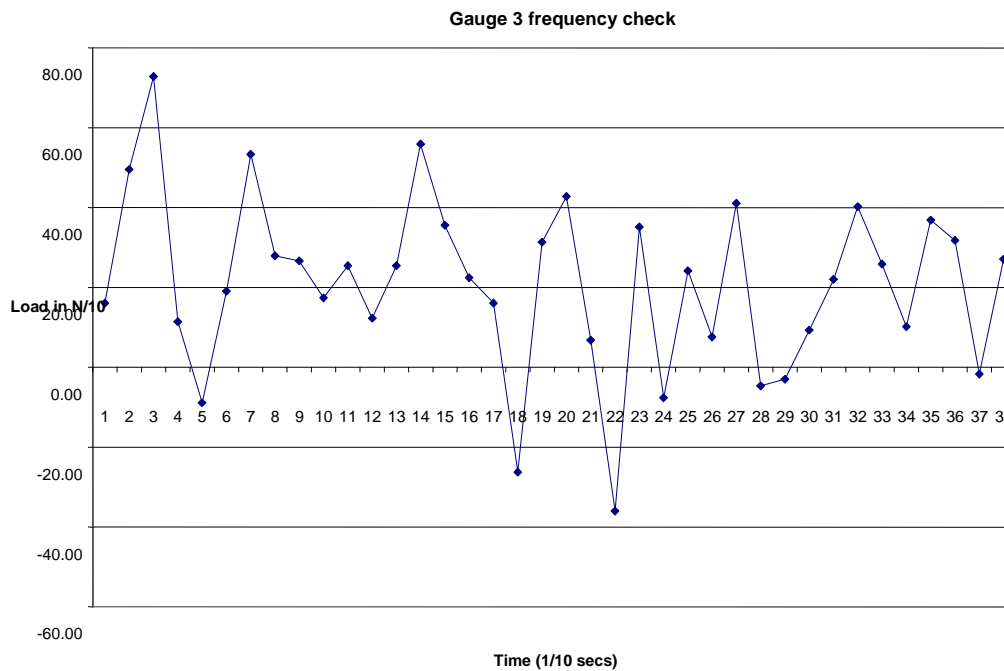


Figure 59: Example of a load time graph used to check frequency analysis

Once all the data from the individual runs had been processed, the data from each run was examined in detail to compare the actual results to those anticipated. This process was used to look for errors or discrepancies within the data sets. For example in the case of the multiple block runs, some of the load gauges appeared to be providing no significant load readings and it was initially thought that an error had occurred with the gauge output. Upon closer study the gauges were found to produce output and the reduced loads were due to the affected block being held against adjacent blocks and the observed readings were correct. Where the full data sets have been appended to this report this not only included the run parameters and the test results but where appropriate a short commentary on any discrepancies noted.

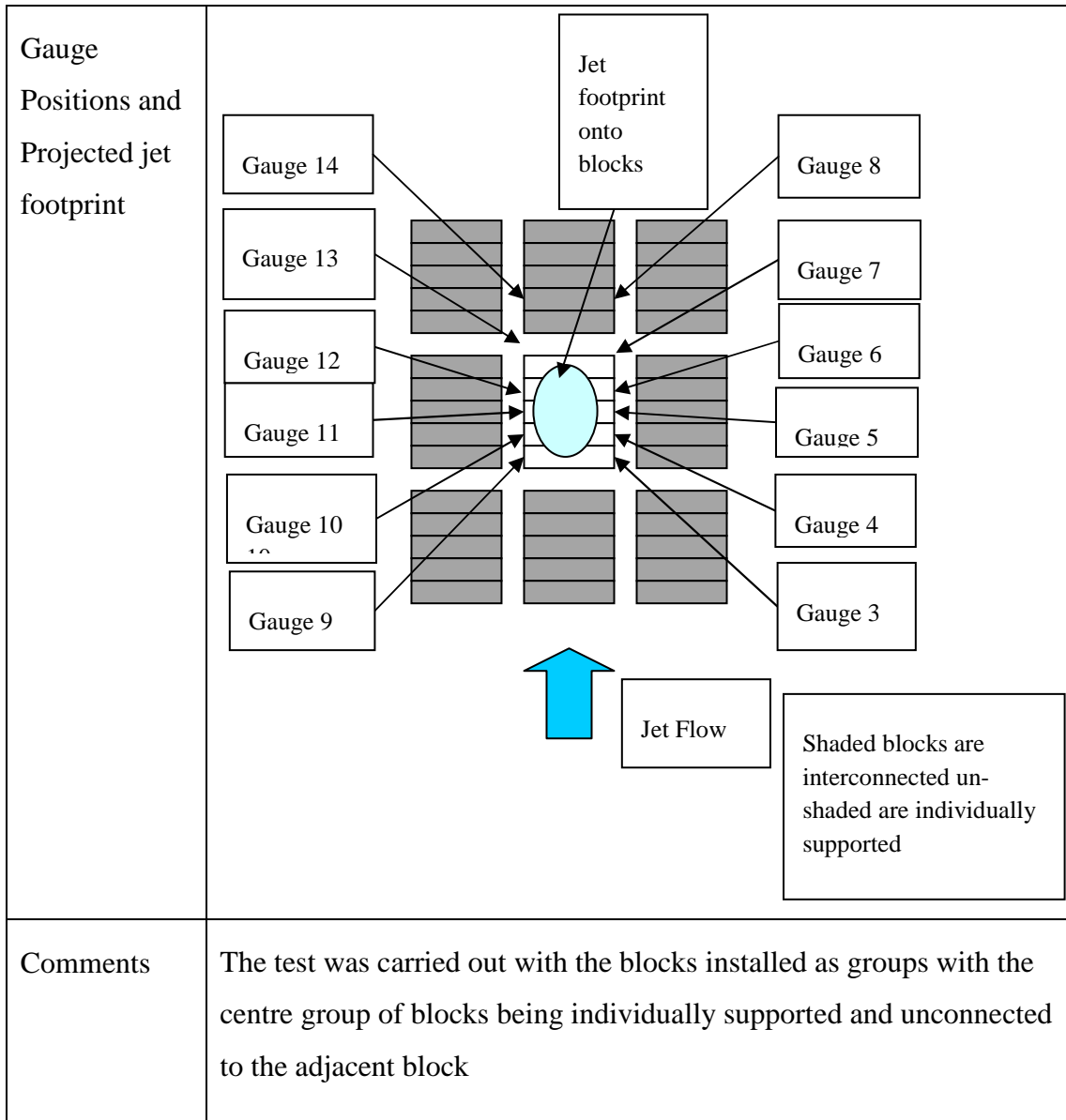
7.6 Example test run commentary

Run 1

This run was carried out primarily as an initial test to check the equipment behaviour. The jet unit was run at higher speed than the subsequent runs and the effects produced proved sufficiently interesting to include this run within the experimental data. The example run parameters are shown in Table 10.

Table 9: Example of parameter summary used for each test run.

| Run No 1 | | |
|-----------------|---|--|
| | | |
| Jet Angle | 60 degrees to horizontal | |
| | | |
| Jet velocity | 3 ms ⁻¹ (prototype 16.29ms ⁻¹) | |
| | | |
| Air Flow | 0 | |
| | | |
| Seabed Location | Up | |
| | | |



The pump was run at high speed for several minutes with the load gauges reading continuously at the rate of 10 times per second. At time reference 200 seconds as illustrated on the graph below (halfway through the test run) the left hand group of blocks, that were not instrumented, were ejected from the cut-out in the upper plate. This left the instrumented blocks with free water on their left hand side. The load time graphs for two of the gauges are shown below and the point of failure is clearly identified by the jump in the load readings at time 200.

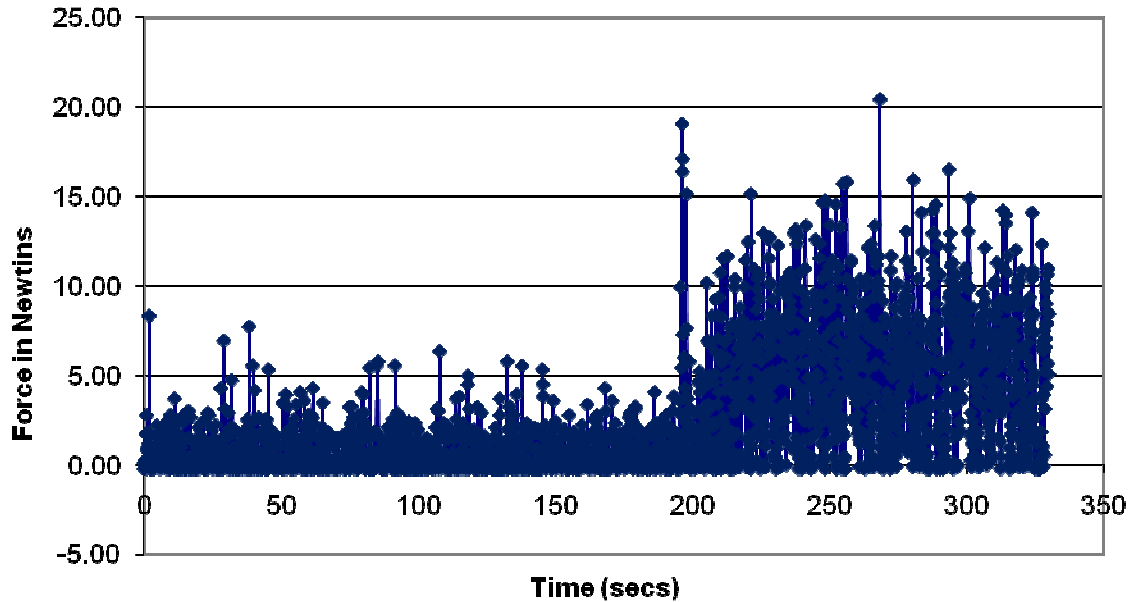


Figure 60: Example of a load v time graph (Run 1 Load gauge 3)

Following the ejection of the adjacent blocks it can be seen there is around a three-fold increase in the forces acting on the remaining blocks. The ejection of the set of blocks was observed as being almost instantaneous, and there were no visual indications that failure was about to occur. Following the run, the tank was drained and the position of the ejected block set is shown in Figure 61.

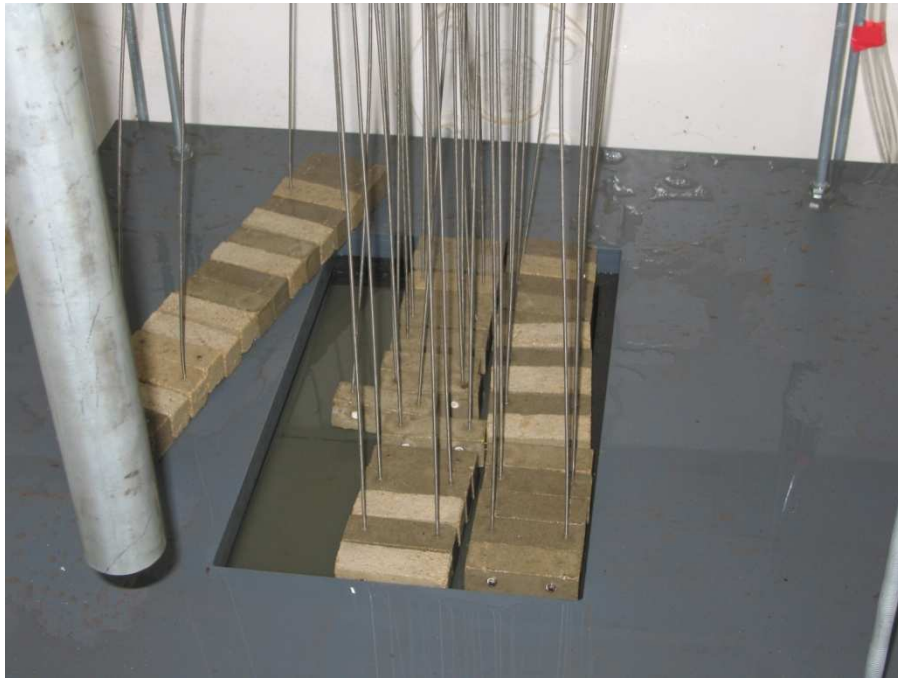


Figure 61: Showing the ejected block set following test run 1

7.5 Static pressure readings

The static pressure readings obtained during the experiments are tabulated below (

Table 10) with the full details included in the appendices. The static pressures were recorded prior to each set of runs and the readings taken again during each run. The table below shows the differential pressure for each run in millibars.

Table 10: Static pressure tube readings

| Run No | Jet speed | Seabed | Air valve | Jet angle | Differential static pressures | | | |
|--------|-----------|--------|-----------|-----------|-------------------------------|---------------|---------------|---------------|
| | | | | | Tube 1 (mbar) | Tube 2 (mbar) | Tube 3 (mbar) | Tube 4 (mbar) |
| 2 | 1000 | Up | 0 | 60 | 0 | 0 | 10 | 40 |
| 3 | 2490 | Up | 0 | 60 | 60 | 50 | 60 | 50 |
| 4 | 2490 | Up | 25 | 60 | 60 | 50 | 30 | 60 |
| 6 | 1000 | Down | 0.25 | 60 | 10 | 10 | 10 | 10 |
| 8 | 2490 | Down | 0 | 60 | 50 | 10 | 90 | 90 |
| 9 | 2490 | Down | 0.25 | 60 | 50 | 10 | 10 | 10 |
| 10 | 1000 | Down | 0 | 50 | 0 | 0 | 0 | 20 |
| 11 | 1000 | Down | 0 | 50 | 0 | 0 | 10 | 10 |
| 12 | 1000 | Down | 0.25 | 50 | 10 | 10 | 0 | 0 |
| 15 | 2490 | Down | 0 | 50 | 30 | 20 | 10 | 10 |
| 16 | 2490 | Down | 0.25 | 50 | 40 | 30 | 10 | 10 |
| 18 | 1000 | Up | 0 | 50 | 0 | 0 | 20 | 50 |
| 19 | 1000 | Up | 0.25 | 50 | 10 | 10 | 10 | 10 |

Chapter 8

Discussion of MODEL TEST Results

8.1 Introduction

The key findings from the model tests are

- Force oscillations
- Jet velocity effect
- Air entrainment effect
- Static pressure effects

Each of these is discussed below.

8.2 Force oscillations

The force oscillations on the model concrete blocks were observed across all the experimental data. The oscillation frequency was in the range of 2 to >5Hz but appeared to be centred around 5 Hz for the single blocks and a lower frequency for the grouped blocks. The range of values recorded was between 2 and 30 times the average force measured on the block. Close examination of the load time graphs for the block groups reveals intermediate values between the maxima and minima point on the graphs. This indicates that there are not predominantly high frequency oscillations occurring beyond the measurement capability of the data recording system, which was 5Hz for the block groups. The single blocks, however, with higher

oscillation frequencies were at the limit of the capability of the test equipment. In both cases the oscillations were clearly visible during all the test runs.

The load gauges were measuring the forces at each end of the model blocks as if they were a simply supported beam, as demonstrated in Figure 49: Graph showing the secondary gauge deflections when support 1 only is loaded, the moment transfer from the support system resulted in an error of less than 10% between two supports. This error would be cancelled out when the support loads are summed. It was also noted that the data logger was a multiplexing device that was operating at 100 Hz (NB only 10 gauges could be recorded at any one time), therefore the gauge forces will have been recorded within 0.01 seconds of each other in the best case (and 0.09 at worst).

The load measurement system itself will have had a distorting effect on oscillations of the blocks and therefore the frequencies measured are not necessarily representative of block oscillations in a fully unconstrained system.

The load measuring system was capable of measuring uplift forces. As the bridge amplifier was adjusted to zero at the start of each run, there was effectively a preload of the submerged weight of the block and its connecting rods already on the gauge. This meant that the 3mm diameter connecting rod between the concrete block and the gauge bar would not go into compression until the submerged weight of the block and its connection rods had been exceeded by the uplift force. In many of the test runs this was actually the case and the connecting rod proved capable of transferring the, relatively small, compressive loads into the gauge and the readings remained valid. The threaded connecting rods had been secured to the gauge bars using nuts on either side of the steel plate and it was noted during the longer runs that these nuts had a tendency to slacken off due to the vibration. This was prevented by using a 'Loctite' compound on the threads of the connecting rod.

Examples of the force oscillations are shown on the Figure 62 and Figure 63.

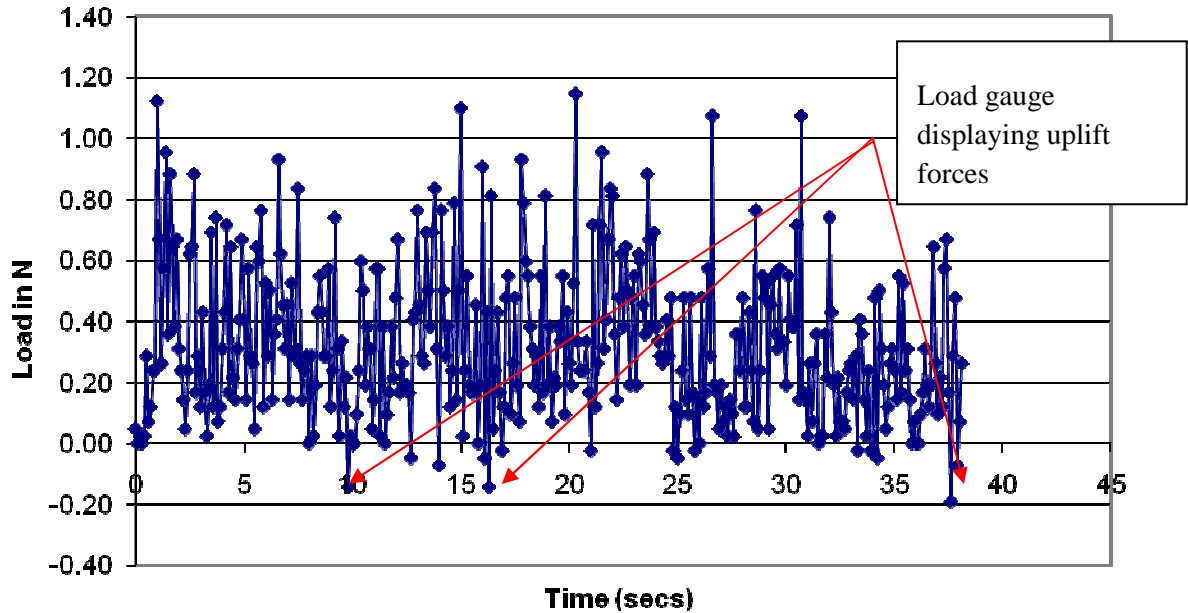


Figure 62: Single load gauge reading on block 2 Run 2 Load gauge 4)

Figure 62 shows the readings from a single load gauge which is supporting half of block 2. In Figure 63, which is for the same run, the total block loads are shown, in this case the simultaneous readings from both load gauges have been summed to give the total block load at a particular instant. This shows that the same block experiences an uplift force during several instances during the run. However this is very small and does not approach the submerged weight of the block.

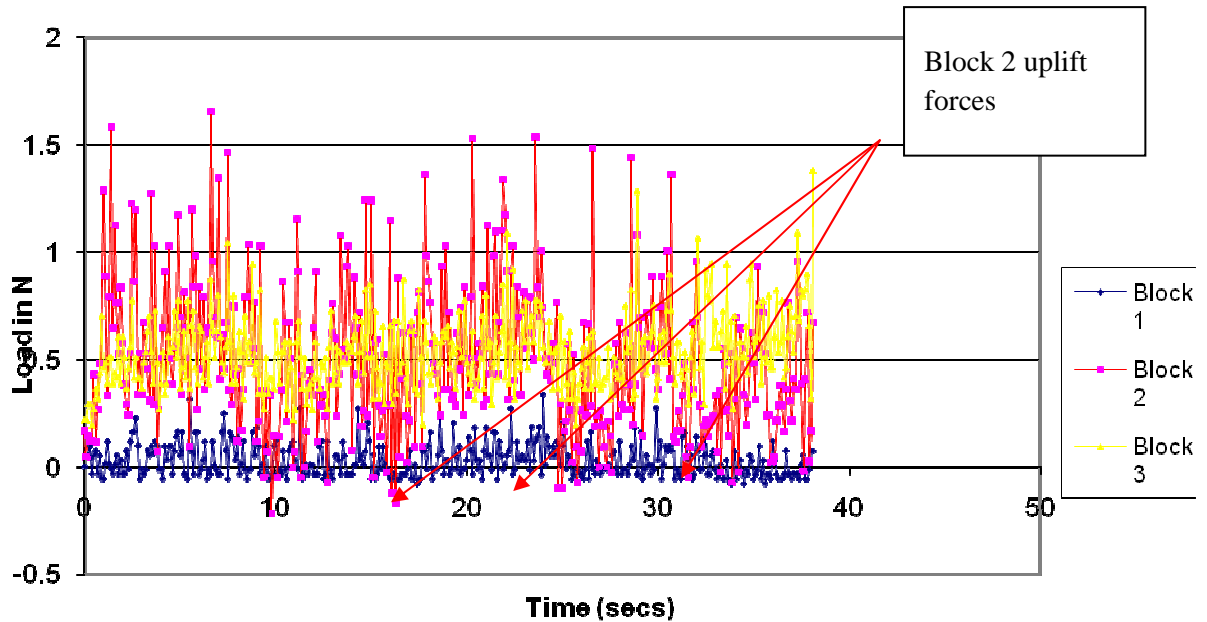


Figure 63: Block loads v time for multiple blocks (Run 2 Block Loads)

In Figure 64 the same scenario is illustrated, although this time as the load gauges on a single block. Here it is clear that the uplift forces are sufficient to cause ejection of the block. The graph also illustrates that while the high frequency oscillations that are occurring on the individual load gauges are not in phase and do not show any significant correlation, this is not the case with the secondary frequencies which are occurring and these are discussed below.

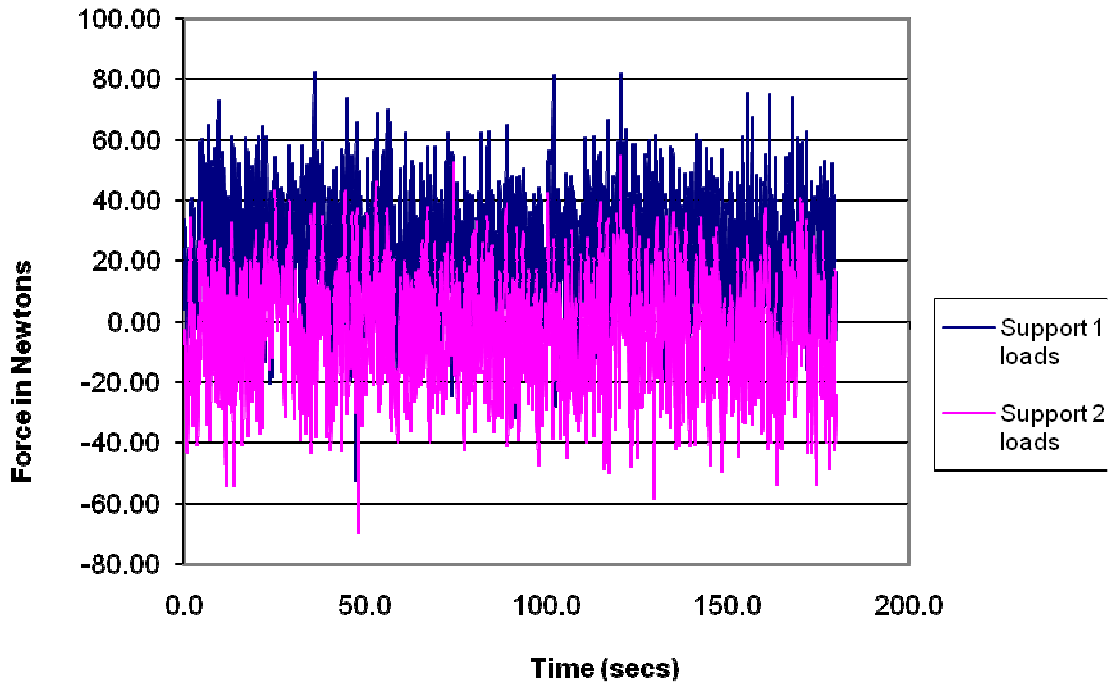


Figure 64: Gauge loads v time single block (Run 22)

In addition to the 2-6Hz frequencies noted on the blocks it is clear from the graphs that there are lower secondary frequency oscillations occurring to the blocks. This effect has been illustrated on some of the output by analysing the data using rolling averages. An example is shown in Figure 65. This is more evident in the multiple blocks but can also be observed on the single block examples and is more noticeable on the higher jet flows. These low frequency oscillations have a period of oscillation of between 12 and 20 seconds and are not present on all the test runs. The most probable cause is pressure fluctuations in the body of water underneath the blocks.

To verify this hypothesis requires more data than is currently available from this set of tests. It would require better instrumentation for the pressure recording and continuous logging of these pressures.

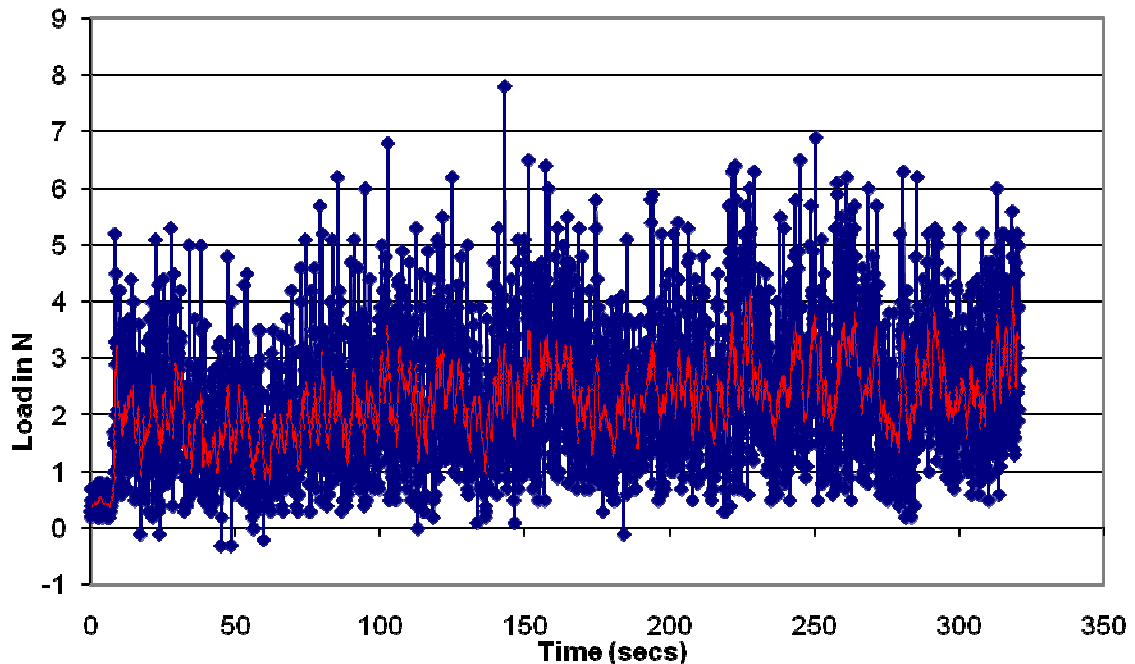


Figure 65: Illustration of secondary graph oscillations for a load v time (Run 3 gauge 5 including a 10 period moving average)

When the model blocks are put in close proximity, even though not physically connected to each other, the oscillating forces are greatly reduced. The experiments show the maximum forces are around 5% to 10% of those occurring on an isolated block which is much greater than can be explained by just the shielding effect that adjacent blocks will have on the jet flows. The force reduction is most probably due to two effects:

1. The close proximity of the blocks will limit the volume of jet flow penetrating beneath the layer and hence the dynamic pressures on the underside of the blocks will be reduced.
2. The horizontal component of the jet flow will impose a lateral force on the top of the blocks due to boundary layer forces and from direct impact on the sides of any blocks that are raised above adjacent ones (Carling et al., 2002). This will generate an effective prestress force between the individual block units and allow shear transfer between the blocks creating a load shearing system into the model blocks ‘down stream’ of the flow (see Figure 66) . This is illustrated during some of the runs where there are almost no load

oscillations recorded on certain blocks. In the model test carried out this allowed load transfer into sets of block and the seabed platform that were not instrumented.

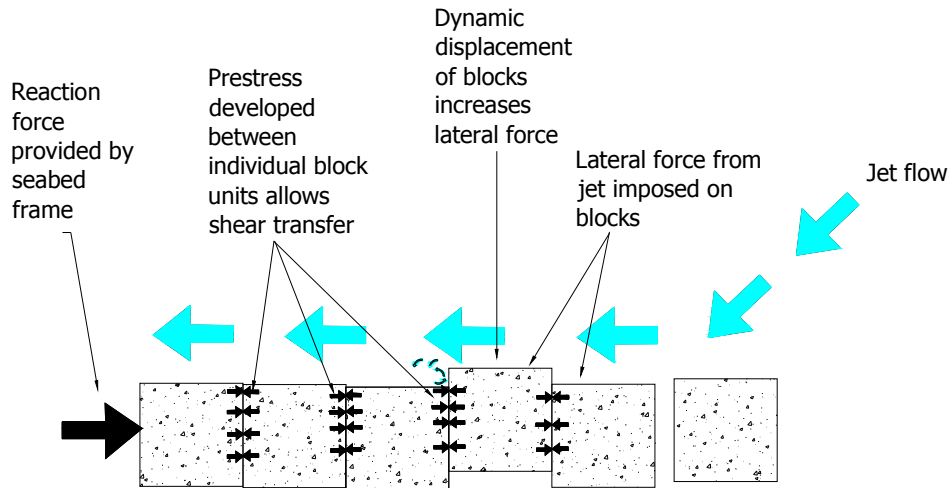


Figure 66: Load transfer mechanism between blocks

8.3 Jet velocity

As would be expected, the force on the blocks increased as the jet velocity increased. The minimum forces mirrored that of the maximum force.

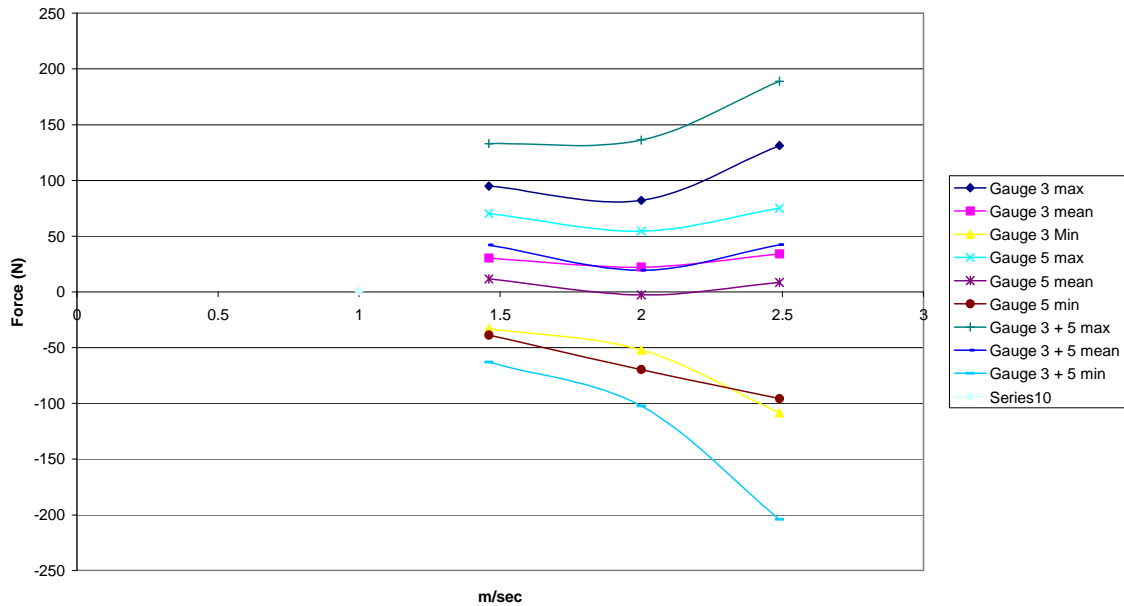


Figure 67: Block Force vs. jet velocity

The maximum, mean and minimum forces for both the individual support loads and the total support loads for the block have been plotted. This approach of using maximum figures from the apparently ‘noisy’ signal from the load gauges is similar to that used by other researchers ((Bollaert & Schleiss, 2001), (Caroni et al., 2002) (Melo, 2002)). The maximum and minimum values of each support have similar trends with the mean value of the force remaining relatively constant. The forces varied considerably across the length of the blocks with adjacent gauges having notably different readings at any instant in time. In this regard it is apparent from the visual observations during the tests, that the flow regime in the area of the block was highly turbulent and as a consequence the forces and oscillation frequencies on either end of the block were different. This is to be expected in the highly turbulent flow regime that is present. The results show that the increased flow rate on the jet is significantly increasing the force fluctuations around the blocks whilst the mean force value is not varying appreciably, which again would be expected for a highly turbulent flow.

The previous work on scour has concentrated on the prediction of the potential scour hole that would develop as a result of an applied flow (from fluvial currents, acceleration effects or dam spillway jets). In this case the displacing flows have been occurring on relatively small and numerous particles where the behaviour is more like a dense viscous fluid. In this work the concern is to identify the free body forces occurring on the large, relatively discrete, scour protection blocks. Therefore it is not considered appropriate to follow the same approach as the previous researchers on scour affects from current flows. The work carried out on tailwater jets from dam spillways are more representative of the mechanisms involved in this work and have been used as a basis for this work. It should be recognised that the spillway jet velocities are considerably greater than those modelled for this study, typically 10ms^{-1} to 30ms^{-1} (model velocities).

An examination of the problem from first principles would suggest that there are potentially two primary effects that are potentially acting on an individual block.

- Drag
- Pressure variations under and around the block which result from the jet flow penetrating between and under the armour layer.

The influence of each of the above will vary greatly for a given block depending on its location relative to the jet stream and the proximity of the adjacent blocks. In this case, with the very high Reynolds numbers associated with these flows, it is likely the form drag is virtually zero and that the pressure drag coefficient is less than unity. The small variation in mean force acting on the model block as shown in Figure 67 also suggests that drag forces are very low.

In all cases the principle of energy conservation can be applied, which means the jet energy cannot be lost and has to be absorbed or redirected by the scour protection system and the underlying seabed.

8.4 Air entrainment

When air was introduced into the flow at low jet speed this reduced the block forces by around 20% to 30%, until the percentage of air entrained reached 20%. At this figure, there was little change in block forces even when more air was introduced. As the jet velocities increased the effect of the air entrainment diminished. However the threshold, at which the air entrainment ceased to affect the flow, increased and at the highest flows the initial introduction of air gave a slight increase in the maximum block loads, but more importantly gave a reduction in the negative (or uplift forces) on the blocks.

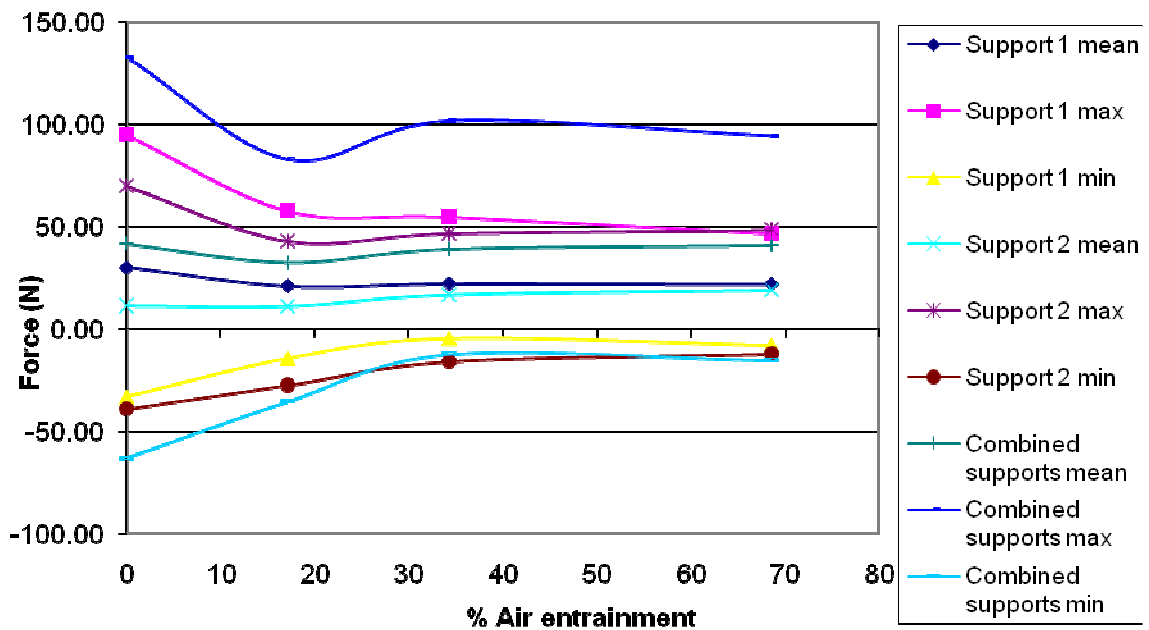


Figure 68: Air entrainment v force for 1.46 m/s jet flow

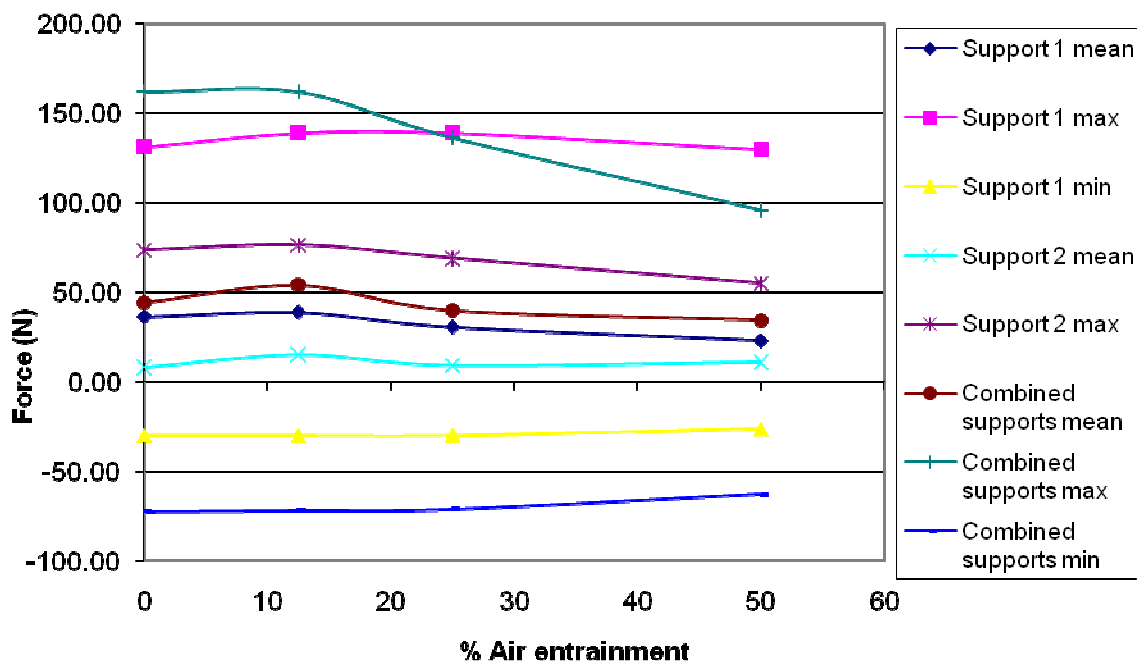


Figure 69: Air entrainment v force for 2.00 ms⁻¹ jet flow

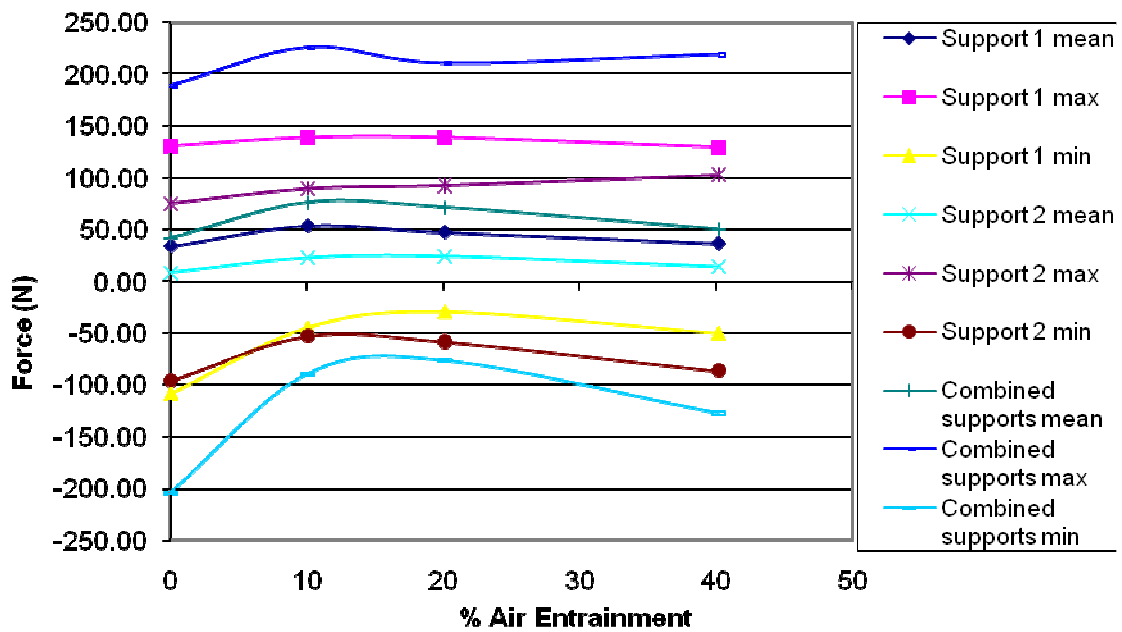


Figure 70: Air entrainment v force for 2.49 m/s jet flow

If the same data is analysed in terms of the range of force oscillations (where the range is the difference between the maximum and minimum force for each gauge or gauge combination) the effects of the air entrainment are more uniform. These are illustrated in

Figure 71, Figure 72 and Figure 73. The use of the force range is useful as it more clearly displays the jet energy acting on the blocks, and other researchers have used pressure range for the same reason (Bollaert, 2002).

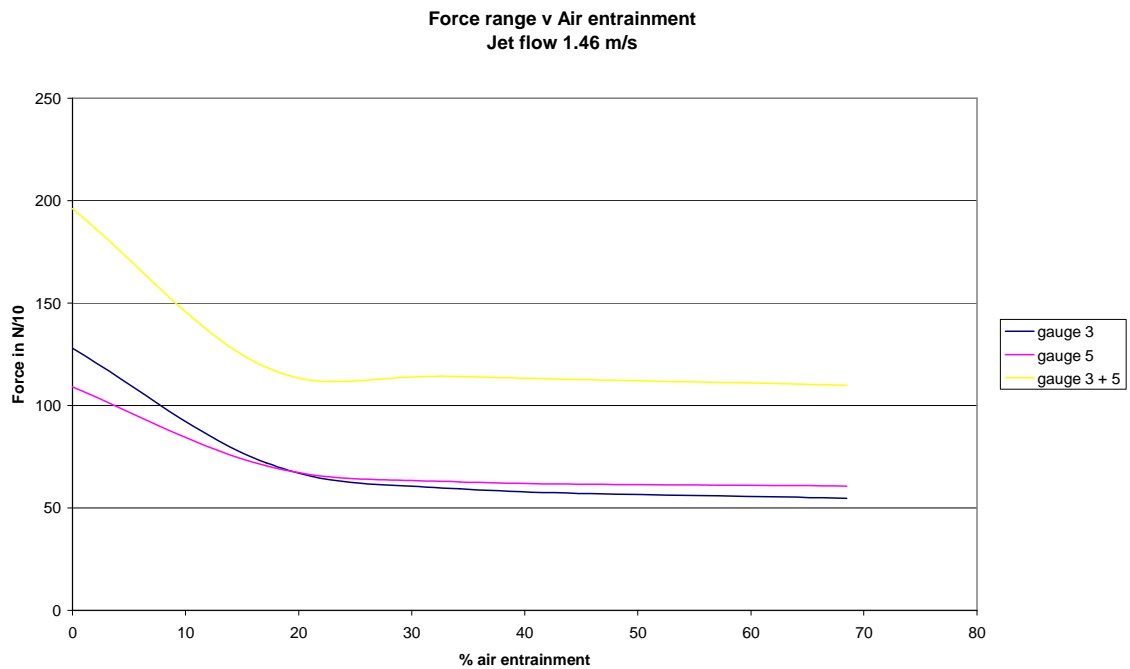


Figure 71: Air entrainment v force range for 1.46 m/s jet flow

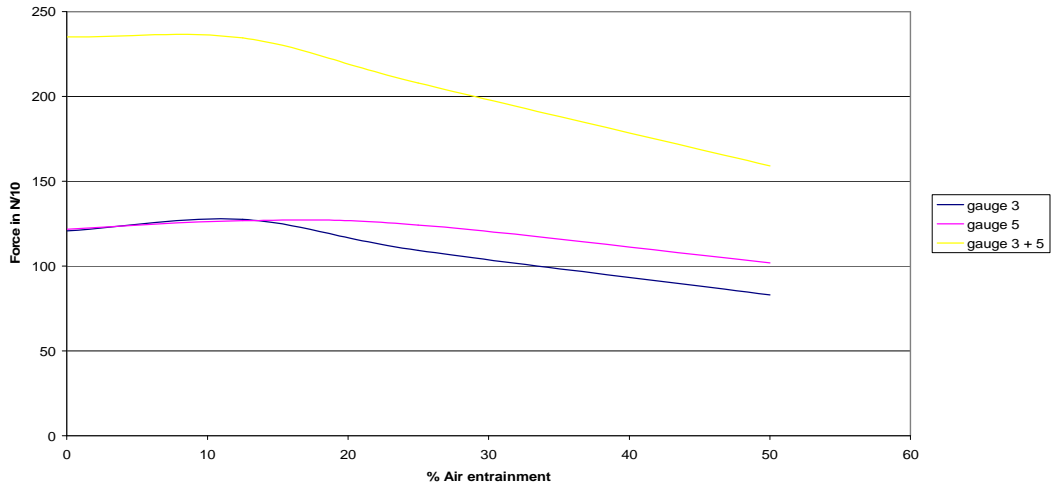


Figure 72: Air entrainment v force range for 2.00 m/s jet flow

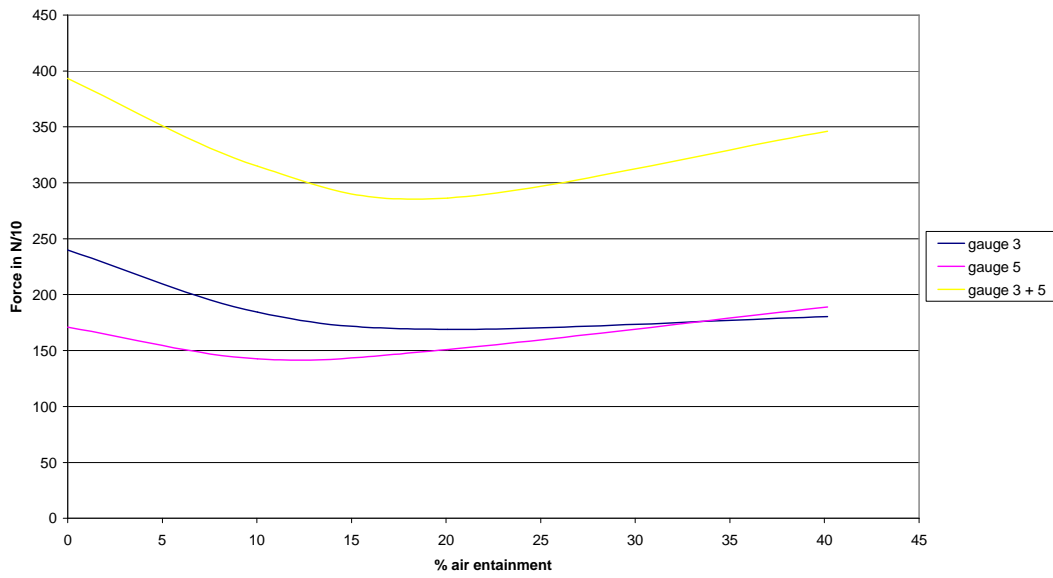


Figure 73: Air entrainment v force range for 2.49 m/s jet flow

8.5 Static Pressures

A particular problem highlighted from this work is the measurement of high frequency oscillations (particularly underwater). The use of air tubes for measuring pressure variations is only effective for static or very low frequencies since the air column between the end of the pressure pipe and the pressure will attenuate any high frequency oscillations. It is clear that more expensive diaphragm pressure sensors are required to measure these effects.

The pressure readings obtained during the experimentation are included in the appendices, and the position of the pressure intake is shown in Figure 47. The results showed a pressure increase beneath the blocks of 20 – 40 millibars with the higher jet flows. This pressure varied according to the position of the pitot tube although there was a noticeable pressure increase in the tube located immediately in front of the neoprene strip used as the seal between the two plates.

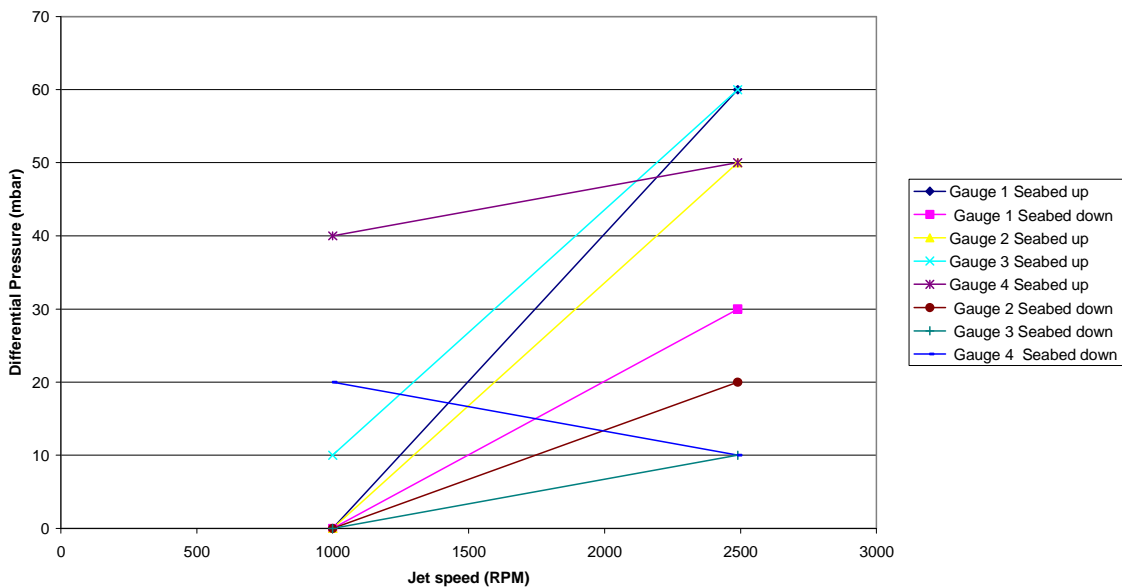


Figure 74: Static pressure reading v jet flow with no air entrainment

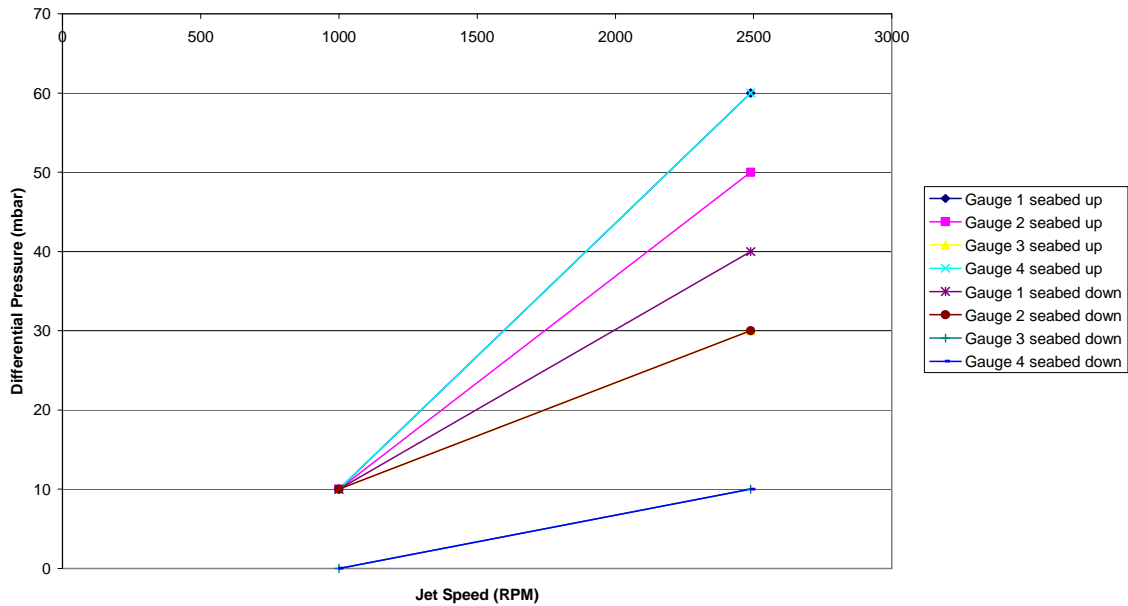


Figure 75: Static pressure readings v jet flow with air entrainment

Following the initial set of tests where the occurrence of high frequency oscillation of the blocks was found, further literature searches were carried out to review whether there was equipment available to measure high frequency pressure variations along with the water velocity and how these were undertaken underwater. This problem has been identified in wind tunnel experimentation. Gauges have had to be produced so that a multi-faceted pressure transducer can be mounted directly in the airflow in order to enable direct pressure measurements to be undertaken and the air velocity to be directly computed. At the time of this work, these miniature gauges were not available for use underwater, and the only gauges available were too large to use in this work. In any further work it is recommended that high frequency pressure transducers are used for any pressure measurements.

Chapter 9

DISCUSSION ON THE SCOUR PROTECTION SYSTEM

9.1 Introduction

The model test data and the full scale prototype at Poole Harbour have demonstrated the potential failure mechanisms of the scour protection system. The combination of the full scale testing and model testing has provided a unique insight into potential modes of failure.

At the outset of the project it was anticipated that given the ability to predict the stability of the blocks under a given jet velocity would enable a prescribed solution for the size and spacing of the armour blocks. The work has identified the modes of potential failure and a critical long term effect that may have a direct impact on the future design of quay walls.

The following failure modes for the scour protection system have been identified:

- Block ejection
- Block migration
- Fatigue failure of the block connections
- Fretting failure of the filter membrane

With regard to the work at Poole Harbour, a review of the survey results showed that the scour protection system became buried beneath the original founding level and it is likely that the mechanism for burial was partial liquefaction of the seabed due to raised pore pressures in the sand. If this is proved to be the case then the design criteria for sheet pile walls subject to propeller or jet scour may have to be revised.

9.2 Block ejection

There are two type of failure due to block ejection that can occur,

- Ejection of an individual block within the impingement area of the jet. (see Figure 10 for the jet dispersion zone)
- Ejection of blocks from outside the jet impingement zone

Individual block ejection (jet impingement area)

From the model testing the forces on the blocks caused by the pressure variations in the turbulent flow have the potential to cause instant or progressive ejection of individual blocks. The use of a continuous interconnected blanket of shaped blocks reduces the transient forces on the individual blocks by between 10 and 50 times compared to those experienced by a loose laid protection system.

The use of the interconnecting cables on the groups of blocks (as used at Poole harbour) is essential to prevent block displacement and ejection, but these cables need to be designed to resist greater forces than originally envisaged and to cope with fretting and cyclic loading. The cyclic loading requirement will involve reducing the design stresses in the cables to around 50% of that normally used and the cable will also have to sustain the block loads when acting as a catenary support over seabed depressions or soft spots. Consideration will also be required to incorporating some pre-stress into the connecting cables to limit any block displacement and to provide shear transfer between blocks.

Block Ejection (outside jet impingement area)

Where the jet flows impinge on the seabed there will be some flow between the blocks to the seabed. This flow will be dependent on the voids between the blocks, the jet velocity and the extent of voiding present under the blocks and the seabed permeability. The seabed beneath the scour system will be undulating as shown in the diagram and so the nature and extent of any voids is unpredictable.

If there is sufficient dispersion and venting of this flow then it will not result in a significant pressure increase beneath the block. However if the flows are not adequately dispersed there is the potential for an increase in pressure between the seabed and the underside of the blocks. This mechanism can be considered to be similar to an open ended pitot tube being placed in a jet flow. If the pitot tube is sealed the air will enter the tube until pressure in the tube matches the dynamic pressure of the flow. If the tube has a small hole then there will be a pressure increase in the tube until dynamic equilibrium is achieved and the inflow matches the outflow. In the case of the prototype this effect is shown schematically in Figure 76 and a more detailed diagram of the model failure is shown in Figure 78

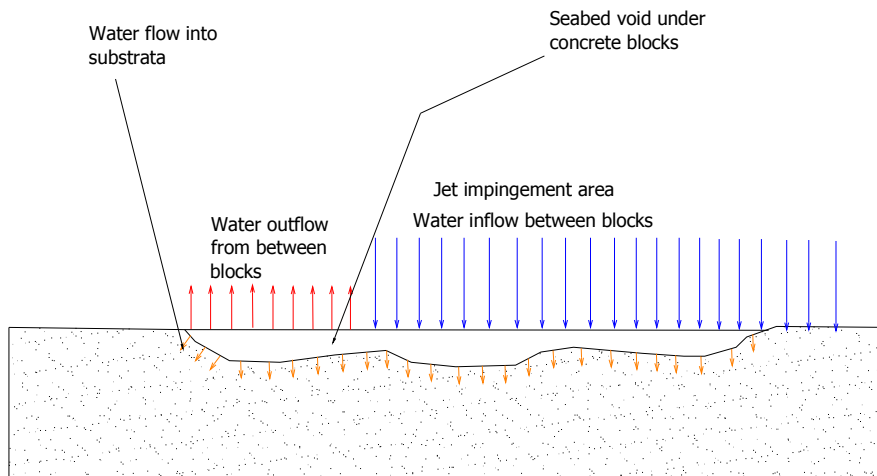


Figure 76: Schematic diagram showing mechanism for potential pressure increase beneath concrete blocks

Where the scour protection is subject to the jet impingement then the overall force from the jet on the block groups will be greater than any uplift pressure generated under the blocks. Where blocks lie outside the impingement area, this is not the case and the potential for ejection of blocks due to this pressure arises.

It is believed that this mechanism was the cause of the failure of the scour protection system used at Portsmouth ferry Port.

During the first phase of the experimentation (Run 1) the jet speed was modelled at the rate of 15.6 ms^{-1} (Prototype velocity) and this caused catastrophic failure of the multiple block set to the side of the model outside the jet impingement area (the full description of the event is given in the detailed run results which are appended). Of particular interest was the instantaneous nature of the failure and the subsequent effect on the adjacent blocks. The graph showing the block loads against time is shown in Figure 77. The occurrence of raised pressures under the blocks was confirmed by the pitot tube readings. These also showed that a variation of these pressures occurred around the point of jet impact although there was insufficient data to plot pressure contours.

This was the only occurrence during the whole test procedure where the failure of the blocks occurred. With the experimental setup used, physical failure during the testing was not expected due to the restraint being provided by the load measurement and block support system and sufficient force was generated during the test run to not only overcome the submerged weight of the test blocks but also the weight and buckling load of the support rods. It should be noted that the tests carried out on the single blocks were such that this mode of failure could not sensibly occur as the block being measured was unconstrained and was not located within a group of blocks from which it could be ejected.

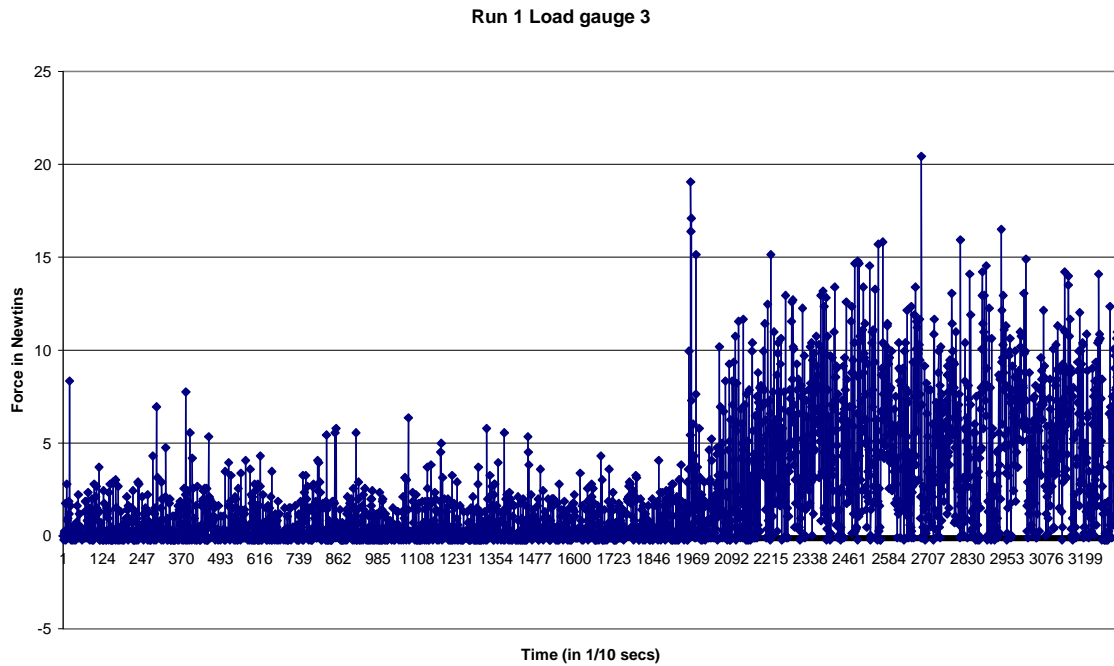


Figure 77: Showing the load gauge readings before and after the ejection of an adjacent block set

In the case of run 1, a complete set of blocks was ejected from the test model. These blocks lay outside the jet footprint and the cause of their failure resulted from raised pressures and accompanying water flows as a result of the jet infiltrating under the blocks. The process is illustrated in Figure 78

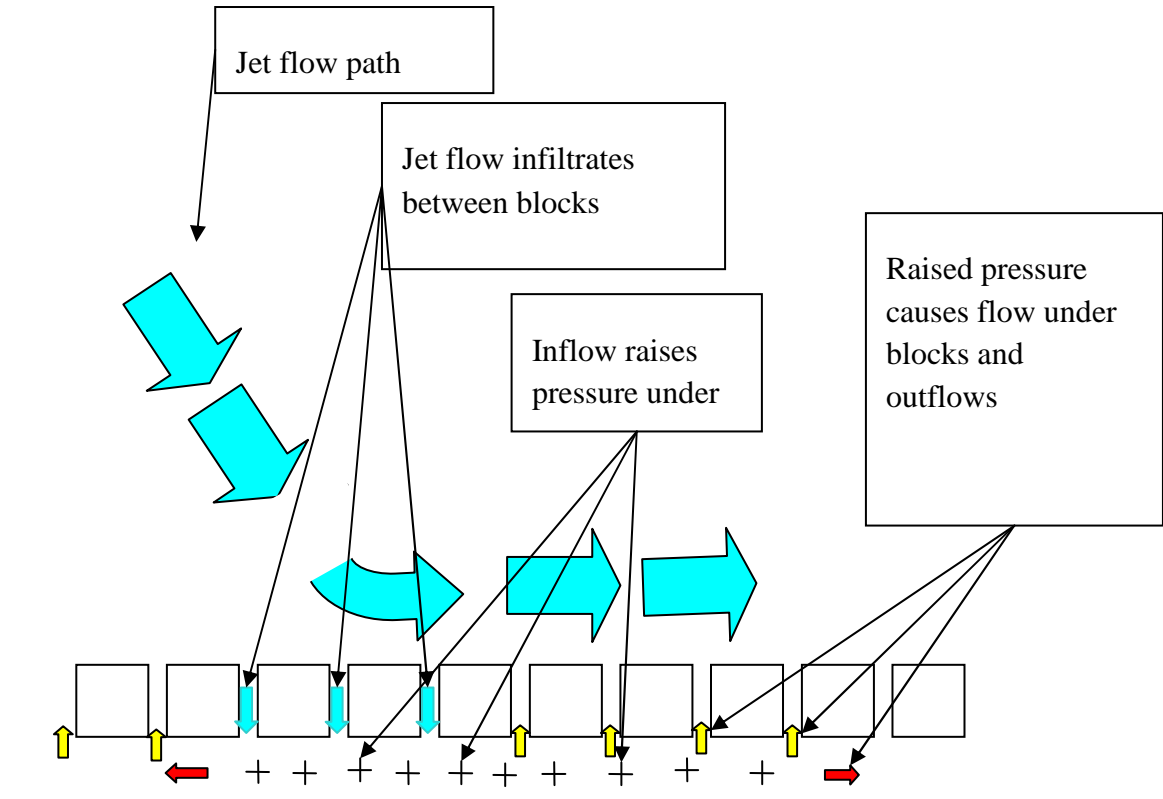


Figure 78: Illustrating mechanism for uplift pressures on blocks

It is to be anticipated that the infiltration flows will be accompanied by water flows beneath the blocks and exfiltration flow which would reduce the pressure. In the case of no exfiltration occurring, the uplift pressure generated by the jet flow is not reduced and it is therefore possible to calculate the maximum possible value. The dynamic pressure from the jet is given by:

$$P_d = \frac{1}{2} \rho_w v^2 \dots\dots\dots \text{Equation 17}$$

Where:

P_d = dynamic pressure

ρ_w = density of water

v = jet velocity

Using equation 17, the maximum potential pressures from this mechanism are shown in Figure 79. Also included are the minimum pressures required to cause uplift of the model block for various thicknesses. Potential failure (i.e. when uplift pressure equals the block weight) cannot occur below these values. For 20mm thick blocks a jet flow of greater than 0.75ms^{-1} and above would be required for failure, whilst for the 30mm thick blocks flows of greater than 0.9ms^{-1} would be required. From the test, the blocks were shown to be stable up to flows of 2.49ms^{-1} which shows that the outflow of water from beneath the blocks was (as expected) reducing the pressure.

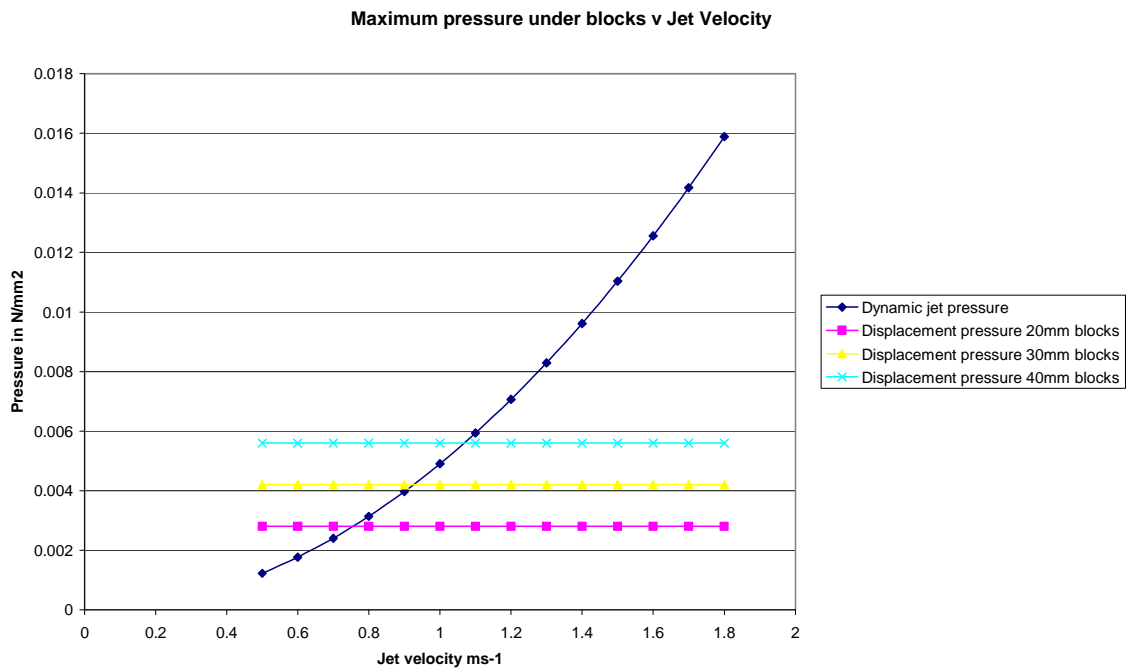


Figure 79: Showing maximum pressure under blocks as a result of jet flow

From this it is possible to develop an equation relating the jet velocity to the concrete block depth required for stability against block ejection. If the pressure beneath the blocks is given by:

$$P_{ub} = R_p \left(\frac{1}{2} \rho_w v^2 \right) \dots\dots\dots \text{Equation 18}$$

Where

P_{ub} = Pressure beneath the blocks

R_p = Pressure reduction coefficient which is a function of (Exfiltration Rate/ Infiltration rate)

And for stability the following must be true:

$$P_{ub} < (\rho_c - \rho_w)gh \dots\dots\dots \text{Equation 19}$$

Where:

ρ_c = Density of the concrete blocks

Therefore:

$$R_p \left(\frac{1}{2} \rho_w v^2 \right) < (\rho_c - \rho_w)gh$$

So this can be rewritten as:

$$v < \sqrt{\frac{(\rho_c - \rho_w)gh}{0.5 \rho_w R_p}} \dots\dots\dots \text{Equation 20}$$

The minimum theoretical failure pressure of the blocks (from Figure 79) was 0.004N/mm² and the jet pressure at a model speed of 3.0 ms⁻¹ was 0.045Nmm⁻² The model blocks were stable during all other jet runs with jet speeds of up to 2.47 ms⁻¹ (Jet pressure of 0.030Nmm⁻²)

Taking these values and using equation 20 gives values for R_p of 0.091 at the failure (run 2, model test failure criteria) and 0.133 for the maximum jet flows used in the model where failure did not occur (model test suggested criteria).

From the prototype test at Poole Harbour the 600mm deep blocks are known to be stable under jet flows of 10 ms^{-1} (which would equate to a model jet flow of 2.24 ms^{-1} and an equivalent model jet pressure of 0.025 Nmm^{-2}). This gives an R_p of 0.16. Therefore taking these values for R_p , jet flows can be plotted against block thickness to show the conditions from the model tests and these compared with the blocks used at Poole Harbour (Figure 80).

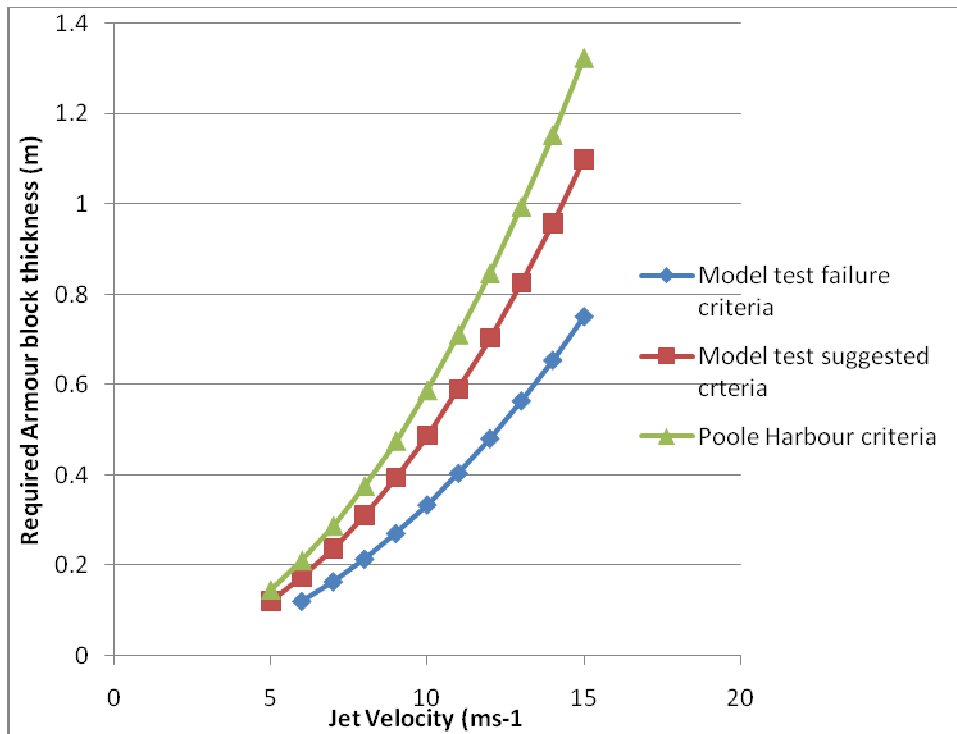


Figure 80: Required concrete block thicknesses for a given jet flow (Prototype)

It can be seen from Figure 80 that the stable conditions in both the model and prototype are similar and that the block thicknesses used at Poole Harbour would appear to provide a sensible factor of safety against failure.

It should be noted that this approach would only be valid for high jet flows where the Reynolds number is high and where the coefficient of drag is dominated by pressure drag and not profile drag.

The above formula could be modified to take into account air entrainment. This would involve the substitution of ρ_w by ρ_{we} which would be the equivalent density of the air

entrained water. The percentage of air in the water jet is likely to have changed considerably from the time it left the jet nozzle to when it is dispersed beneath the blocks so this modification was considered inappropriate without further data.

The above discussion does not take into account the filter layer used in scour protection works but it is clear that if this layer is of low permeability and becomes damaged in the area of jet impingement then jet flows penetrating under this layer could cause uplift of the concrete blocks due to restricting the outflow.

9.3 Block migration and movement

Movement of the concrete blocks across the seabed was noted at Poole Harbour. The likely mechanism for this movement is described below.

The water jet from the ferries impacts the seabed at between 40 and 60 degrees to the horizontal. A jet will therefore have both a vertical and horizontal component. If the blocks were laid in a uniform horizontal plane the jet flow would only generate small horizontal force on the blocks, however the seabed will be uneven and this will allow adjacent blocks to be at varying levels. At Poole the worst case recorded was a 150mm high projecting face. Jet impingement on the projecting face will cause a lateral force to be imparted to the block (Carling et al., 2002). This process may also occur dynamically as the fluctuating vertical force on the blocks causes them to move vertically relative to the adjacent blocks.

This lateral load will be resisted by the friction between the block and the filter layer and by the interaction with the adjacent blocks. In addition the friction force between the blocks and the filter layer will vary due to the vertical force fluctuations affecting the normal contact force. In the case of Poole Harbour it was found that there were gaps between the blocks and the interconnection wires were in some cases sufficiently slack to allow small movements of individual blocks to occur. This would allow the block migration to occur by a shuffling movement of the individual blocks. The situation would become significantly worse if the seabed was sloping.

The jet flows will also cause local changes to the pore pressure in the seabed strata, and an increase in soil pore pressures will reduce soil strength and may give rise to lateral movement of the filter layer along with the block.

It is therefore of interest to deduce the forces required to initiate the failure and to examine the forces required to displace a single block, even if it is restrained from ejection. The oscillating loads on the blocks mean that any forces are transitory, therefore single block forces must be considered in combination with the time of application of the load. This approach is a crude analysis using the equations of motion based upon constant force which is clearly not true in this case but they do provide indicative figures. Whilst these could be modified by integrating the force over the time period being measured at this stage this was not considered appropriate, however this might be a useful approach in the future if the forces were being numerically modelled using CFD methods. These curves are shown in Figure 81.

For a block initially at rest, it is required to be lifted to the height of the adjacent block for ejection to occur, therefore assuming constant acceleration:

$$s = ut + \frac{at^2}{2}$$

Where

s = Height of adjacent blocks

u = Initial velocity (zero in this case)

t = time of application of the ejection force

a = acceleration of the block

In combination with the equation

$$F = ma$$

F = net uplift force on block

m = mass of block

This can be rewritten as;

$$s = \frac{Ft^2}{2m}$$

Therefore in the case of the model blocks

$s = 0.03$ metres

$m = 194$ grams

F = total uplift force - submerged weight of block

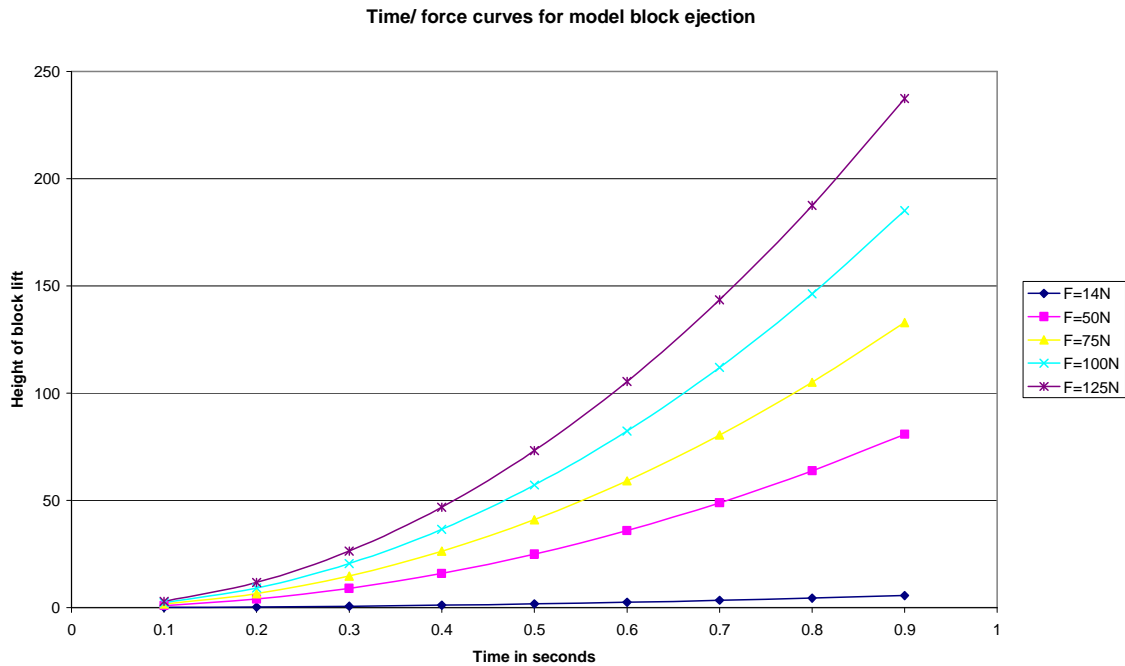


Figure 81: Time v force to achieve ejection of block

Figure 81 shows that for the model to achieve complete ejection of the blocks a force of 50N would have to be sustained for 0.6 seconds or 100N for 0.4 seconds. This demonstrates that the system can sustain very high transient loads for brief periods without failure. Based on the experimental data where the typical load frequencies on the blocks were around 5Hz this would suggest that a transient load of 50N at this frequency would only lift the block 8mm. However when considered in conjunction with the work by (Carling et al., 2002) where the block would be held in its new position by the lateral loads from the jet, it can be seen that progressive ejection of individual blocks can occur. It is interesting to note that this mode of failure is also likely to be occurring on the dam spillway erosion where the transient frequencies of pressure are very high (around 20 – 100Hz) so the energy during each transient is insufficient to cause complete ejection of a large rock, but successive events will cause failure.

Where the block experiences an upward movement it will lose contact with the geotextile and therefore have no resistance to lateral movement. In addition, the

movement will cause fretting against the geotextile and dynamic loading of the block connection wire. It is not considered economic to provide blocks that have sufficient mass to resist all movement but this does provide some data to calculate the number of load cycles that are likely to occur within the connection wire and fretting cycles for the geotextile. In addition with the energy provided by the jet compared to that required to eject a single block, it clearly indicates the high risk of failure if unconnected blocks are used.

Examination of the load time graphs suggests that a negative load event sufficient to cause upward movement of half the block is occurring once every 15 to 25 seconds. The likely number of fretting and fatigue cycles for the connection wire and geotextile are:

Number of vessel movements per day = 2

Duration of jet operations during berthing operations = 10 minutes

Number of operations per year = $2 \times 240 = 480$

Frequency of model block movement = 4 per minute

Therefore time scaling according to Froude gives a prototype block movement of 4.472 which equate to 0.9 movements per minute

For a 10 year design life total number of cycles

$480 \times 10 \times 10 \times 0.9 = 43200$

Therefore a design requirement of 50,000 cycles for the fretting of the geotextile would appear appropriate and a similar figure could be adopted for the connection wire.

9.4 Fatigue failure of the filter membrane

Following the model testing the full scale trial at Poole Harbour was inspected and the appreciation of the force oscillations that were present meant that a detailed inspection of the geotextile membrane was carried out to check for fretting. This was found to be present in a number of locations and can now be considered to be a failure mechanism that needs to be addressed in any design solution. Not only will the geotextile be subject to abrasion by the oscillation of the concrete blocks but it will itself be subject to fatigue due to oscillating movement of the geotextile where it is not trapped between the seabed and block. This condition will occur in many areas both between and under blocks due to slight undulations in the seabed.

The likely number of cycles required from the geotextile is calculated below

$$\text{Number of vessel movements per day} = 2$$

$$\text{Duration of jet operations during berthing operations} = 10 \text{ minutes}$$

$$\text{Number of operations per year} = 2 \times 240 = 480$$

$$\text{Frequency of oscillation of fabric} = (5/4.472) \text{ Hz}$$

For a 10 year design life total number of cycles

$$480 \times 10 \times 10 \times 60 \times 1.1 = 3.22 \text{ million}$$

Chapter 10

CONCLUSIONS

10.1 General comments

The review of current literature and the results from the works at Poole Harbour clearly show that current design approaches for scour protection systems are not appropriate when dealing with manoeuvring areas for High Speed Ships. It should be noted that scour protection will normally be required on existing berths that are being adopted to take high speed ferries.

The works at Poole have shown that a loose laid rock scour protection system is inappropriate for High Speed Ships. The existing design formulae for Rip Rap protection are not appropriate for the design flows associated with the water jets from high speed ferries, and unless the natural strata is competent rock then scour protection will be required around vulnerable structures. This also needs to be considered where HSS are berthing adjacent to open piled structures for both the potential affect on the piles and the possible scour of any revetment slope under the structure

The model tests have shown that the jet flows cause a highly oscillating force on the blocks with isolated peak force events that mean any system designed on the basis of isolated blocks is either going to be extremely expensive or have a high probability failure.

During the initial phases and monitoring at Poole Harbour an instance was recorded, during a single berthing operation, where the jets from the HSS caused a 5 metre deep hole to be formed in an unprotected area of seabed, in this case the scour area was distant from the quay wall and was rapidly refilled by sand accretion. The event

illustrated the potential both for catastrophic failure and for the potential long term instability of a quay wall that could arise from a number of smaller scour events. The design of cantilever sheet piled walls relies on the passive soil pressure on the seaward side of the wall. Where undisturbed soil is present the design parameter for passive earth pressure will be used. In the event of a scour hole forming and being refilled this factor is no longer valid and the coefficient for active earth pressure would be more appropriate which would reduce the beneficial effect of the earth pressure by a factor of between 6 and 10 (see Table 1)

The effect of the water jet on the seabed strata has not been investigated as part of this work however some of the movement recorded at Poole Harbour suggests that the water jet has caused short term highly elevated soil pore pressures, which has allowed burial of the scour armour layer. The implications of this may prove serious for the long term stability of quay walls. This is discussed in greater detail in Chapter 2.

The most appropriate scour protection will be a two layer system comprising, a filter blanket protected by an armour layer. Typically the filter layer will be a geotextile which, for a given natural strata, is relatively easy to design and construct.

10.2 Filter Layer

The requirements of the filter layer are

- It should prevent migration of the natural strata
- Have sufficient porosity to prevent build up of differential pressures.
- Have sufficient abrasion resistance to particle entrained water flows from the jets
- Have sufficient abrasion resistance against fretting movement from the armour blocks
- Provide an appropriate coefficient of friction to prevent sliding of the armour blocks

- Due to the high frequency oscillations in flows that will occur in the vicinity of the membrane it will need to have a high resistance to fatigue failure resulting from cyclic movement

10.3 Armour layer

At the outset of this project it was clear that the forces generated on the seabed by water jets were not catered for by current design practice and that this was giving rise to failures of scour protection systems. The model tests have shown that the resultant forces on the scour protection system is a highly variable oscillating flow.

The linked concrete block system that was used as the armour layer at Poole Harbour has been capable of sustaining the jet flows from the HSS but the subsequent checks carried out on the system have highlighted a number of deficiencies.

The critical failure mode for the connected armour blocks is ejection of the block group. This is caused by raised water pressure beneath the blocks due to the pressure and volume of water from the jet which penetrates between the blocks. This effect is dependent on a number of variables but for the case within Poole Harbour, where the seabed is a non cohesive sand, a formula has been proposed to determine the minimum thickness of the concrete blocks for a given jet flow. The tentative relationship between block thickness and jet flow is derived in chapter 8 and shown in Figure 80, which is reproduced here as Figure 82.

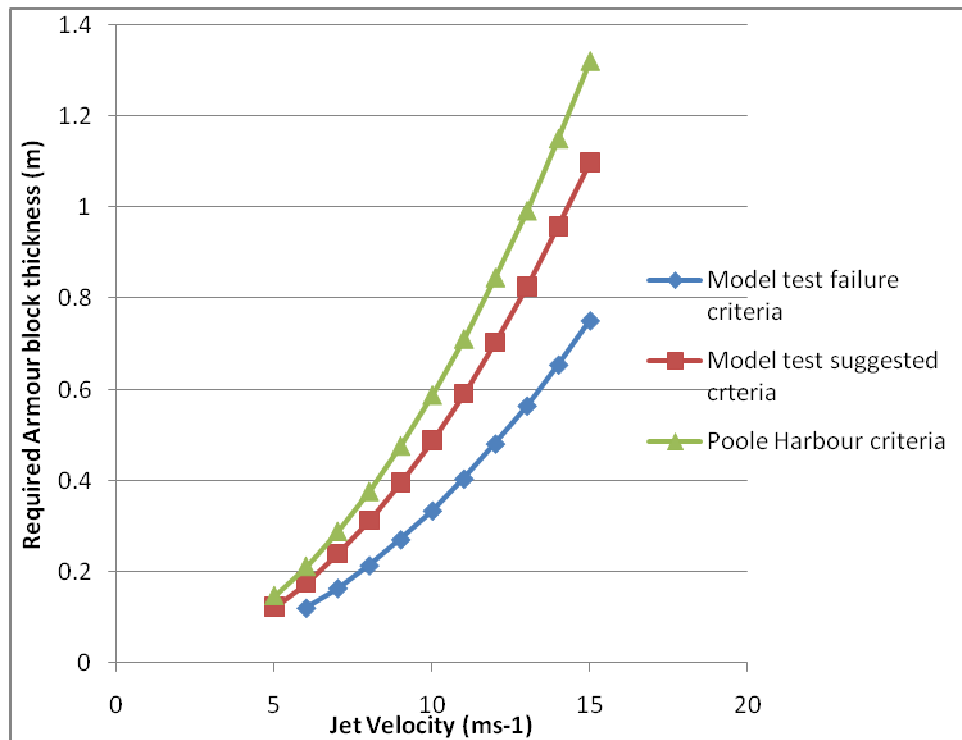


Figure 82: Required concrete block thicknesses for a given jet flow

The curves on the graph represent the design criteria used at Poole Harbour, where the protection blocks have been in place for 7 years, the stable flow state from the model testing and the model failure line. It is not appropriate to use this curve for design since considerably more testing and verification would be required to gain confidence in the figures. It does however provide an indication of the expected criteria for a stable armour layer.

A number of secondary problems were encountered with the armour blocks used at Poole Harbour:

- The block oscillations caused fretting and failure of the cables connecting the armour blocks
- The interface between the quay wall and the blocks failed on a number of occasions and had to be reconstructed.
- From the model testing it is clear that the connecting cables for the armour blocks should be designed to sustain catenary loads from the block group.

Chapter 11

FUTURE WORK

This work has been undertaken without the benefit of previous research and although a much greater understanding of the subject has been gained there is still a need for further work to be carried out to develop a more complete understanding.

The work to date has identified the potential modes of failure of the armour layer and a further series of tests and investigations could now be undertaken to fully investigate each mode of failure.

The area of particular concern encountered during this work was the potential for the water jets to raise the pore pressure within the seabed strata. This is an area that requires urgent investigation. The results from this work may have a significant impact on both the design and appraisal of quay walls. The primary requirement is to establish the depth and extent of pore pressure changes within non cohesive strata subject to jet impingement.

The model testing as carried out to date needs to be repeated using a range of block thicknesses, varying jet speeds and jet angles to verify the failure criteria. The use of high frequency data logging for both the loads and pressures is essential, and recording pressure variations to correlate with the force variations is desirable. For more advanced work the armour layer needs to be modelled in the vicinity of the quay wall.

Ideally remote logging equipment could be built into some of the prototype blocks used at Poole Harbour in order to gain numerical data to provide a comparison with the model test results.

References

WORKS CITED

- Agershoo, H., 2004. *Planning and Design of Ports and Marine Terminals*. Thomas Telford.
- Akagi, S., 1991. Synthetic Aspects of Transport; Economy and transport vehicle performance with reference to high speed marine vehicles FAST 91. Trondheim, 1991.
- Angus, N.M. & Moore, R.L., 1982. Scour Repair methods in the Southern North Sea. In *14th Annual Offshore Technology Conference*. Houston, Texas, 1982.
- Annadale, G.W., 1995. Erodibility. *Journal of Hydraulic Research*, Vol 33(No 4), pp.471-94.
- Annadale, G.W., Wittler, R.J., Ruff, J. & Lewis, T.M., 1998. Prototype validation of erodibility index for scor in fractured rock media. In *Proceedings of the 1998 International Water Resources Engineering conference*. Memphis, Tennessee, USA, 1998.
- Baird, A. & Martin, 1998. Fast Freight Ferries as an Instrument of Modal Shift from Road to Sea R.I.N.A. Conference, Fast Freight transportation by sea. London, 1998. RINA.
- Batani, S.M., Jeng, D. & Melville, B.W., 2007. Bayesian neural networks for the prediction of equilibrium and time dependant scour depth around bridge piers. *Advances in Engineering Software*, 38, pp.102 - 111.
- Berg, H. & Cederwall, K., 1981. *Propellor Erosion in Harbours*. Stockholm: Hydraulics Laboratory, Royal Institute of Technology Sweden.
- Bollaert, E., 2002. Transient water pressures in joints and formation of rock scour due to high velocity jet impact. *Communcation No 13 of the Laboratory of Hydraulic Constructions*, (EPFL Lausanne).
- Bollaert, E., 2004. *A Comprehensive Model to evaluate scour formation in plunge pools*.
- Bollaert, E. & Schleiss, A., 2001. Scour of rock due to high velocity plunging jets; Part 1: A state of the art review. *Journal of Hydraulic Research IAHR*.
- Bollaert, E. & Schleiss, A., 2001. *Scour of rock due to high velocity plunging jets; Part 1; A state of the art review*. Delft, Netherlands: IAHR Journal of Hydraulic research.
- Bollaert, E. & Schleiss, A., 2001. Scour of Rock due to High velocity plunging jets; Part 2; Experimental results of dynamic pressures at pool bottoms and in one and two dimensional closed rock ends. *Journal of Hydraulic research IAHR, Delft, The Netherlands*.
- Breusers, H.N.C. & Raudkivi, A.J., 1991. Scouring. In *Hydraulic Structures Design Manual*. Rotterdam: Balkema.
- Brewster, P.B. & Hamill, G.A., 1997. CFD Model of a marine propeller wash. In *Proceedings International Offshore and Polar Engineering Conference*., 1997.
- British Standards Institute, 1984. *BS 6349 - 1; Code of Practice for Maritime Structures, Part 1, General Criteria*. London.

-
- Carling, P.A., Hoffman, M. & Blatter, A.S., 2002. Initial motion of boulders in bedrock channels. In K. House, ed. *Ancient Floods, Modern Hazards: Principles and Applications of Paleoflood Hydrology*. Water Science and Applications Vol 5 American Geophysical Union. pp.147-60.
- Caroni, E., Fiorotto, V. & Belicchi, M., 2002. Slab stability in hydraulic jump and stilling basins. In *Rock Scour due to falling high velocity jets*. Lausanne Switzerland: A A Balkema. pp.43 - 54.
- Craig, V.S.J., Ninham, B.W. & Pashley, R.M., 1993. The effect of electrolytes on bubble coalescence in water. *J Phys. Chem*, 97, pp.10192 - 10197.
- Dargahi, B., 2003. Three dimensional modelling of ship induced flow and erosion. *Proceedings of the Institution of Civil Engineers Water and Maritime Engineering*, pp.193 - 204.
- Douglas, J.F., Gasiorek, J.M., Swaffield, J.A. & Jack, L.B., 2005. *Fluid Mechanics*. 5th ed. London: Pearson.
- Ervine, D.A., 1998. Air Entrainment in Hydraulic Structures. *Proceedings of the Institution of Civil Engineers, Water, Maritime and Energy*. Vol 130, pp.142-53.
- Ervine, D.A. & Falvey, H.T., 1987. Behaviour of turbulent jets in the atmosphere and in plunge pools. *Proceedings of the Institution of Civil Engineers Part 2*, 83, pp.295-314.
- Ervine, D.A., Falvey, H.T. & Withers, W., 1997. Pressure Fluctuations on Plunge Pool Floors. *Journal of Hydraulic Research*, 35(2), pp.257-79.
- Fotherby, L.M., 1995. *Concrete Armour Units in Rivers; Dissertation; Colorado State University*.
- Fotherby, L.M. & Ruff, J., 1998. Concrete Armour units in Rivers.
- Fuehrer, M. & Pohl, H.a.R.K., 1987. *Propellor Jet erosion and Stability Criteria for Bottom Protection of Various Construction*. Bulletin No 58. PIANC.
- Fuehrer, M. & Romisch, K., 1977. Effects of Modern Ship traffic on inland- and ocean-waterways and their Structures. In *24th International Navigational Congress*. Leningrad, 1977. Permanent International Association of Navigational Congresses (PIANC).
- Ghodsian, M., Melville, B. & Tajkarimi, D., 2006. Local scour due to free overfall jet. *Proceedings of the Institution of Civil Engineers Water Management*, (Dec).
- Hamill, G., 1988. *The Scouring Action of the Propellor Jet*.
- Hamill, G.A. & al, e., 1998. Method for estimating the bed velocities produced by a ships propeller wash influenced by rudder. In *Coastal Engineering Conference*. Copenhagen, 1998.
- Hamill, G.A., Johnston, H.T. & Stewart, D.P., 1999. Propellor wash scour near quay walls. *Waterway, Port, Coastal and Ocean Engineering ASCE*, 125(4), pp.170-75.
- Hamill, G.A. & McGarvey, J.A., 1997. Influence of Ships rudder on the scouring action of a propeller wash. *Proceedings of Offshore and Polar Engineering Conference*, pp.754 - 757.
- Hamill, G.A. & McGarvey, J.A., 1997. The influence of a Ship's rudder on the scouring action of propellor wash. In *Seventh International Offshore and Polar Engineering Conference*. Honolulu USA, 1997.

-
- Hamill, G.A., McGarvey, J.A. & Mackinnon, P.A., 1998. A Method for estimating Bed velocities produced by a ships propellor wash influenced by rudder. In *26th International Conference on Coastal Engineering*. Copenhagen, Denmark, 1998.
- Hamill, G.A. & McGarvey, J.A., 1996. Designing for propellor actions in harbours. In *25th International Conference on Coastal Engineering*. Orlando, Florida, 1996.
- Heibaum, M.H., 2000. Scour Countermeasures using Geosynthetics and Partially grouted rip rap; Transportation Reseach Record. *Journal of the Transportation Research Board*, 1696(Volume 1696/2000), pp.244 - 250.
- Hoffmans, G.J.C.M. & Verheij, 1997. *Scour Manual*. Rotterdam: A A Balkema.
- Karayannis, T., Papnikolavo & Molland, A., 2000. The Introduction of High Speed Ferries into the Mediterranean. In *Proceedings of the International Congress of International Maritime Association (IMAM)*. Ischia, Italy, 2000.
- Lam, W.R. et al., 2006. Simulations of a ships propeller was. In *Proceedings of the Sixteenth International Offshore and Polar Engineering Conference.*, 2006.
- Lewis, E.V., 1988. Principles of Naval Architecture Vol II Resistance, Propulsion and Vibration.
- Liang, D., Cheng, L. & Yeow, L., 2005. Numerical study of the Reynolds number dependance of two dimensional scour beneath offshore pipelines in steady currents. *Ocean Engineering*, 32, pp.1590 - 1607.
- Madsen, O.S., 1978. Wave induced pore pressures and effective stresses in a porous bed. *Geotechnique*, 28, pp.377-93.
- Maeno, S. & Nago, H., 1988. Settlement of a concrete block into a sand bed under water pressure variation. In K.e. al, ed. *Modelling soil structure Interactions*. Balkema. pp.67-76.
- Mason, P.J., 1989. Effects of Air Entrainment on plunge pool scour. In *Journal of Hydraulic Engineering 115 (3)*., 1989.
- Mason, P.J. & Arumugam, K., 1985. Free jet scour below dams and flip buckets. *Journal of Hydraulic Engineering ASCE*, 111 No 2, pp.220-35.
- McDougal, W.G. & Sollitt, C.K., 1984. Geotextile stabalisation of Seabed : theory. In *Engineering Structures Vol 6*. pp.211-16.
- Melo, J.F., 2002. Reduction of plunge pool floor dynamic pressure due to jet air entrainment. In A.J. Schleiss & E. Bollaert, eds. *Rock Scour due to falling High velocity jets*. Lisse: A ABalkema. pp.125-35.
- Melville, B.W. & Coleman, S.E., 2000. In *Bridge Scour*. Water Resources Publications.
- National Ports and Waterways Institute Lousiana State University, 2000. *High Speed Ferries and coastwise Vessels; Evaluation of parameters and Markets for Application*.
- Peiqing, L. & Aihua, L., 2007. *Fluctuating uplift acting on rock blocks at the bottom of the river bed and estimation of limiting scour depth*. Madrid: International Association of Hydraulic Engineering Research.

-
- Perng, A.T.G. & Caoart, H., 2008. Underwater and sand bed erosion and internal jump formation by travelling plane jets. *Journal of Fluid Mechanics*, 595, pp.1 - 43.
- PIANC, 1987. *Guidelines for the design and construction of flexible revetments incorporating geotextiles for inland waterways*. PIANC.
- PIANC, 1997. *Guidelines for the design of armoured slopes under open piled quay walls*. PIANC.
- PIANC, 2003. *Guidelines for managing wake wash from high speed vessels*. PIANC.
- Quarrain, 1994. *Influence of the seabed geometry and berth geometry on the hydrodynamics of the wash from a ships propellor*.
- Rajaratnam, 1981. *Erosion by plain turbulent jets*.
- Rajaratnam, N. & Berry, B., 1977. Erosion by circular turbulent Wall Jaets. *Journal of Hydraulics research*, pp.277 - 289.
- Report of the working group 22, 1997. *Guidelines for Design of Armoured Slopes under Open Piled Quay Walls*. Supplement to Bulletin No 96. PIANC.
- Robakiewicz, W., 1987. *Bottom Erosion as an Effect of Propellor Action near the Harbour Quays*. Bulletin No 58. PIANC.
- Ryan, D., Hamill, G.A. & Hughes, D., 1999. Designing for protection against propellor scour in harbours. In *Fifth International Conference on Coastal and Port Engineering in Developing Countries*. Cape Town, South Africa, 1999.
- Sakai, T. & Gotoh, H.a.Y., 1994. Block Subsidence under pressure and flow. In *24th Conference on Coastal Engineering*. Kobe, Japan, 1994.
- Sakai, T., Hatanaka, K. & Mase, H., 1992. Wave induced stress in seabed and its mometary liquifaction. *Waterway, Port , Coastal and Ocean Engineering*, Vol 118 No 2, pp.202-06.
- Schleiss, A.J., 2002. Scour Evaluation in space and time. In Schleiss, A.J. & Bollaert, E., eds. *Proceedings of the International Workshop on Rock Scour due to High Velocity Jets*. Lausanne, Switzerland, 2002. Balkema.
- Shields, A., 1936. Anwedug der Aehnlichkeitsmechanic und der Turbulenzforschung auf die Geschiebewegung. *Mitteilungen Wasserbau und Schiffbau Nr 6*.
- Simpson, B. & Driscoll, R., 1998. *Eurocode 7 A commentary*. London: Construction Research Communications Ltd.
- Standing Committee on Structural Safety, 1994. *Tenth Report July 1992 to June 1994*. London: Institution of Structural Engineers.
- Stewart, D.P.J., Hamill, G.A. & Johnston, H.T., 1991. Velocities in a ships propeller wash. *Environmental Hydraulics*, pp.651 - 656.
- Sumer, B.M., Cokgor, S. & Fredsoe, J., 2001. Suction of sediment between armour blocks. *Hydraulic Engineering*, Vol 127 No 4, pp.293-306.

-
- Sumer, B.M. & Fredsoe, J., 2002. *The Mechanics of Scour in a Marine Environment*. Singapore: Utopia Press Ptc Ltd.
- Sunday Herald, 2001. Marine motorways are the future. *Sunday Herald*.
- Sutherland, J. & Whitehouse, R., 1998. *Scale effects in the Physical modelling of seabed scour*. H R Wallingford Report TR64.
- Terzaghi, K., 1948. *Theoretical Soil Mechanics*. London: Chapman and Hall.
- Thomson, D.M., 2006. The role of Vortex Shedding in the scour of pools. *Advance in Water Resources*, 29, pp.121 - 129.
- Timoshenko, S., 1937. *Vibration Problems in Engineering*. Second Edition, Fifth Printing ed. New York: D Van Nostrand Company Inc.
- Tomlinson, M.J. & R, B., 2001. *Foundation Design and Construction*. 7th ed. Pearson Education Ltd.
- U S Army Corps of Engineers, 2001. *Coastal Engineering Manual. Scour and Scour Protection*. Washington D. C.
- Verhey, H.J., 1983. *The Stability of Bottom and Banks subject to the velocities in the propellor jet behind ships*. D H Publication No 303.
- Vino, G. & Watkins, S., 2004. A thirteen hole probe for measurements in bluff body wakes. In *Fifth International Collouium on the bluff body aerodynamics and applications*. Ottawa, Canada, 2004.
- Vino, G. et al., 2005. Flow structures in the near woke of the Ahmed model. *Journal of Fluids and Structures*, 20(5), pp.673 - 695.
- Wartsila, 2003. Heavy Fuel Oil an economical option for the high speed transportation market. *Marine News*.
- Wellin, Xo, Jon & Deng, 2004. Experimental Investigation on the influence of aeration on plane jet scour. In *Journal of Hydraulic Engineering; Feb.*, 2004.
- Whitehouse, R., 1998. *Scour at Marine Structures*. London: Thomas Telford.
- Wood, W.A., 2000. Speed Ferry Issues for Operators and Designers; *Marine Technology; Vol37; pp230- 237.*, 2000.
- Yuksel, A. & Celikoglu, Y., 2005. Jet scour around vertical piles and pile groups. *Ocean Engineering*, 32, pp.349 - 362.
- Zen, K. & Yamakazi, H., 1993. Wave-induced liquefaction in a permeable seabed. *Report of the Port and Harbout Institute, Japan*, 6, pp.155 - 192.

Appendix 1

Model Test Details and Run Analyses

Contents

| | |
|-------------------|-----|
| INTRODUCTION..... | 3 |
| RUN 01..... | 3 |
| RUN 02..... | 6 |
| RUN 03..... | 10 |
| RUN 04..... | 15 |
| RUN 05..... | 19 |
| RUN 06..... | 22 |
| RUN 07..... | 25 |
| RUN 08..... | 28 |
| RUN 09..... | 31 |
| RUN 10..... | 35 |
| RUN 11..... | 38 |
| RUN 12..... | 41 |
| RUN 13..... | 44 |
| RUN 14..... | 47 |
| RUN 15..... | 50 |
| RUN 16..... | 53 |
| RUN 17..... | 56 |
| RUN 18..... | 59 |
| RUN 19..... | 62 |
| RUN 20..... | 65 |
| RUN 21..... | 68 |
| RUN 22..... | 71 |
| RUN 23..... | 74 |
| RUN 24..... | 77 |
| RUN 25..... | 80 |
| RUN 26..... | 83 |
| RUN 27..... | 86 |
| RUN 28..... | 89 |
| RUN 29..... | 92 |
| RUN 30..... | 95 |
| RUN 31..... | 98 |
| RUN 32..... | 101 |
| RUN 33..... | 104 |
| RUN 34..... | 107 |
| RUN 35..... | 110 |
| RUN 36..... | 113 |
| RUN 37..... | 116 |
| RUN 38..... | 119 |

INTRODUCTION

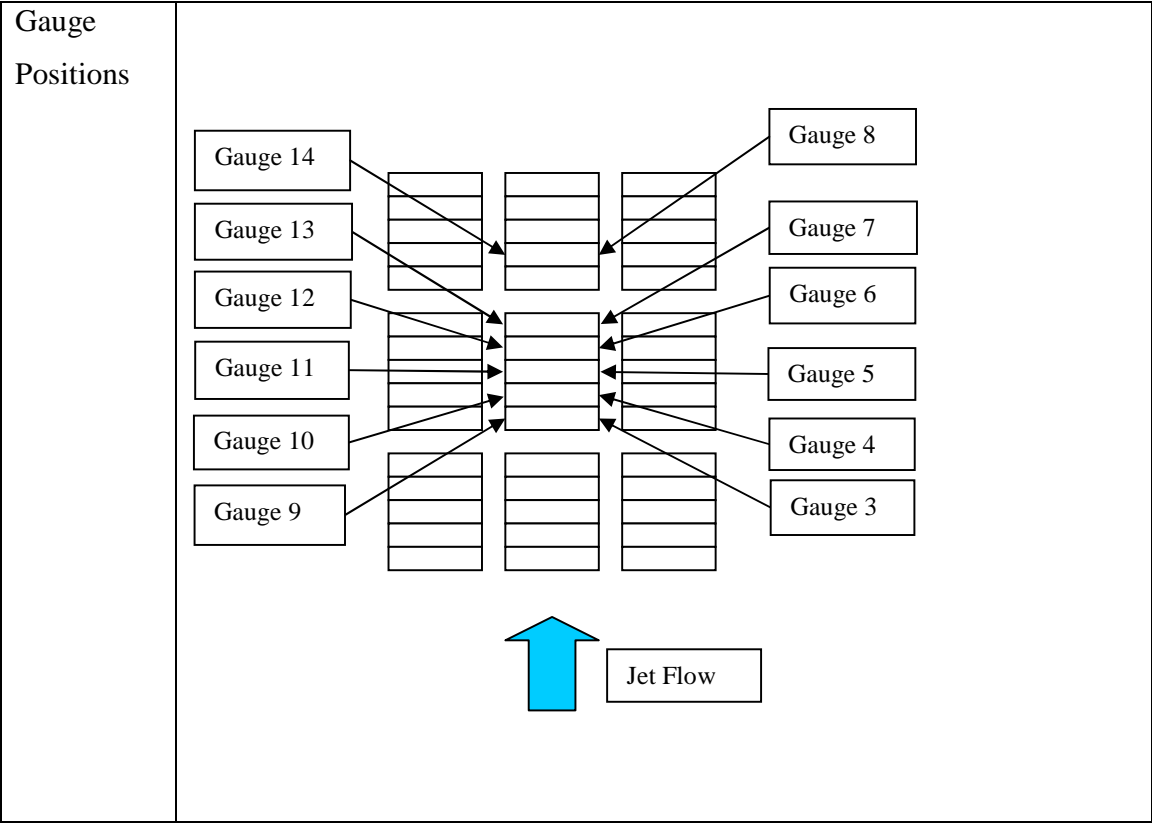
The parameters of each test run are shown in tabulated form in this appendix and a brief commentary is included on each run where appropriate mentioning any pertinent observations made during the test run

TEST RESULTS

RUN 01

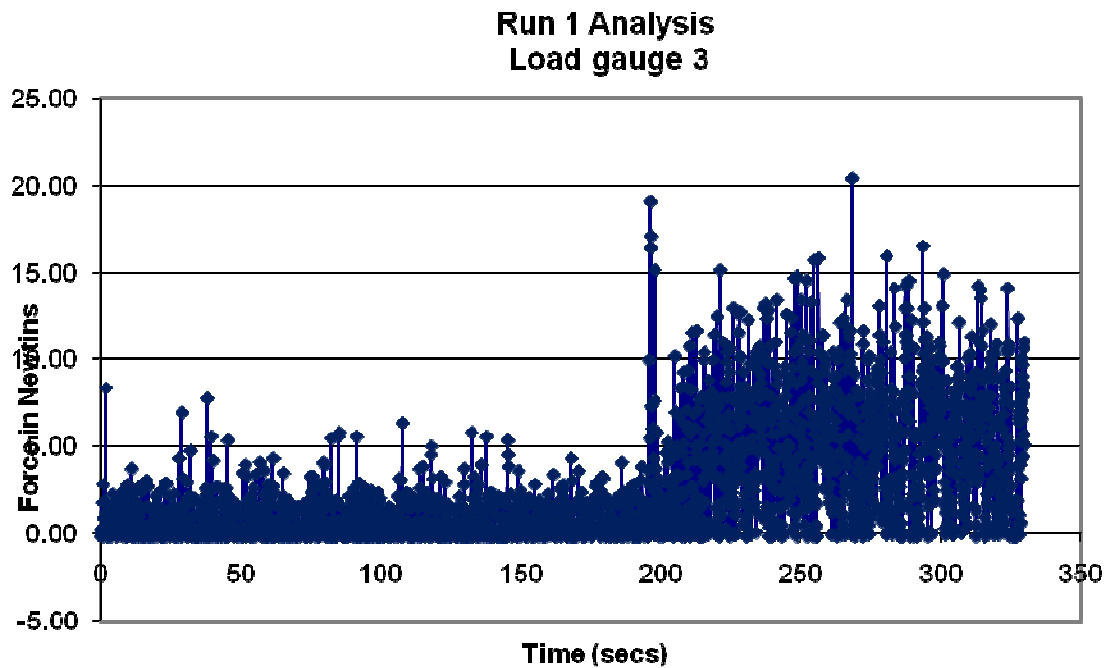
This run was carried out primarily as an initial test to check the equipment behaviour. The jet unit was run at higher speed than the subsequent runs and the effects produced proved sufficiently interesting to include this run within the experimental data. The run parameters are tabulated below.

| Run No 1 | | |
|-----------------|---|--|
| | | |
| Jet Angle | 60 degrees to horizontal | |
| | | |
| Jet velocity | 3 ms ⁻¹ (prototype 16.29ms ⁻¹) | |
| | | |
| Air Flow | 0 | |
| | | |
| Seabed Location | Up | |

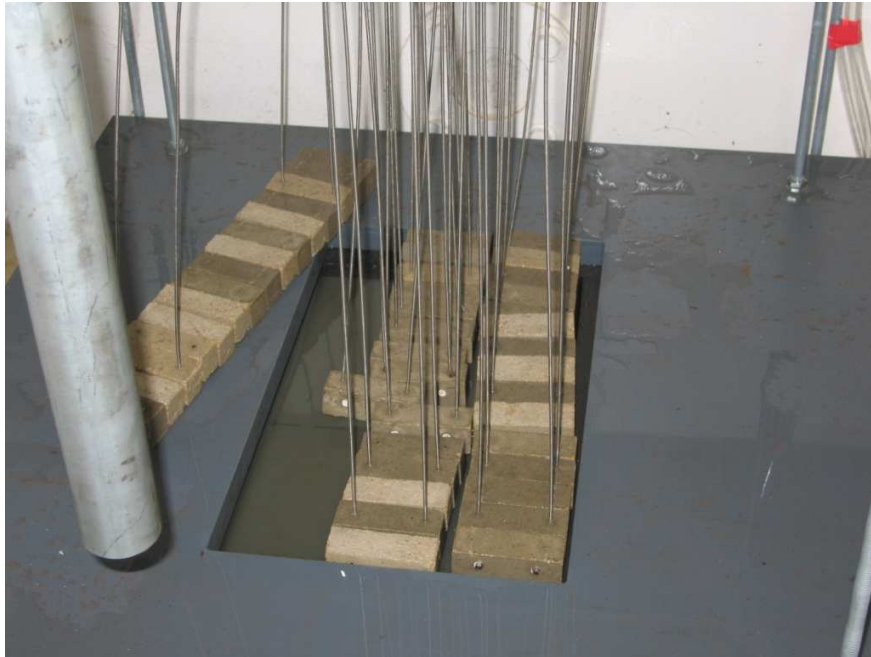


| | |
|----------------------|---|
| <p>Jet footprint</p> | <p>The diagram shows a 3x3 grid of blocks. The central block is unshaded and contains a cyan oval labeled 'Jet footprint onto blocks'. The surrounding eight blocks are shaded. A blue arrow labeled 'Jet Flow' points upwards towards the central block. A text box to the left of the arrow states: 'Shaded blocks are interconnected unshaded are individually supported'.</p> |
| <p>Comments</p> | <p>The test was carried out with the blocks installed as groups with the centre group of blocks being individually supported and unconnected to the adjacent block</p> |

The pump was run at high speed for several minutes with the load gauges reading continuously at the rate of 10 times per second. At time reference 1969 as illustrated on the graph below (halfway through the test run) the left hand group of blocks that were not instrumented were ejected from the cutout in the upper plate. This left the instrumented blocks with free water on their left hand side. The load time graphs for two of the gauges are shown below and the point of failure is clearly identified by the jump in the load readings at time 200 secs.



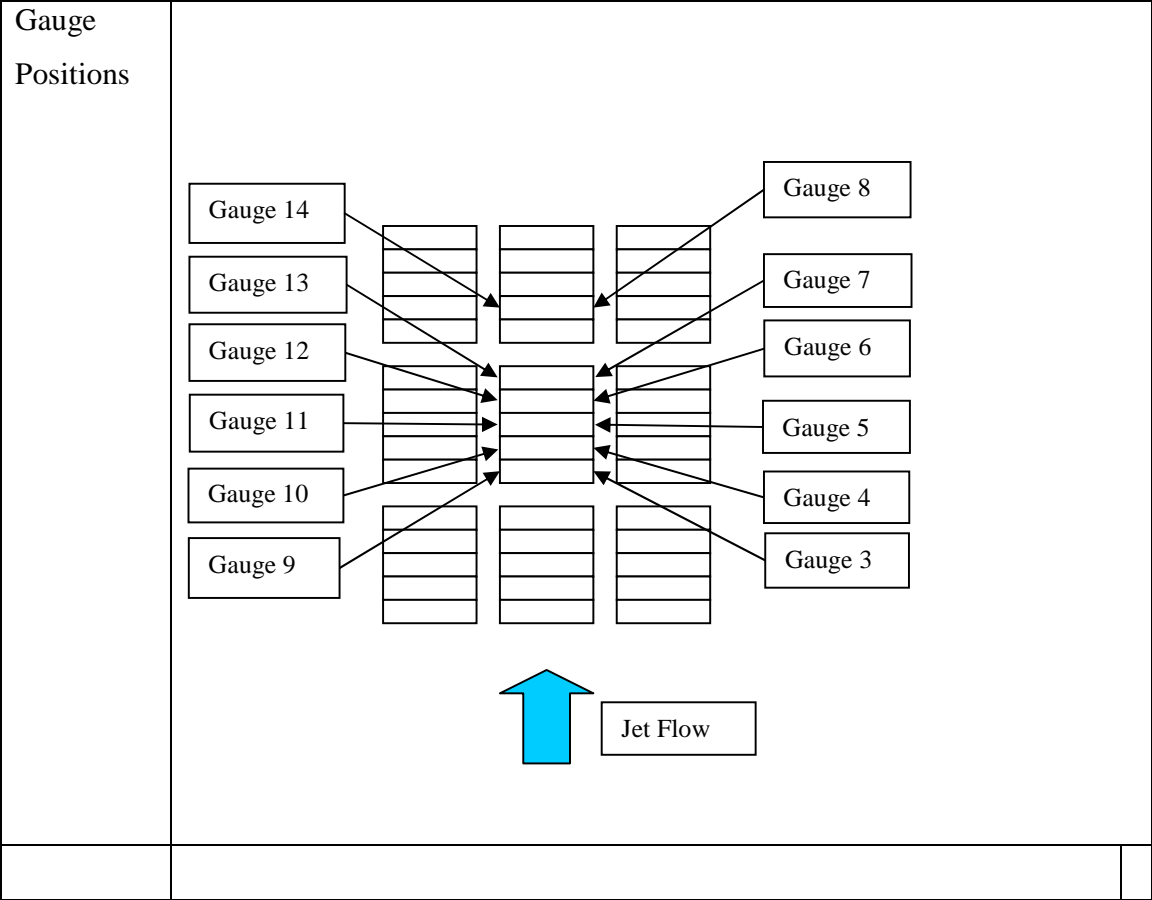
Following the ejection of the adjacent blocks it can be seen there is around a three fold increase in the forces acting on the remaining blocks. The ejection of the set of blocks was observed as being almost instantaneous, and there were no visual indications that failure was about to occur. Following the run the tank was drained and the position of the ejected block set photographed as shown below

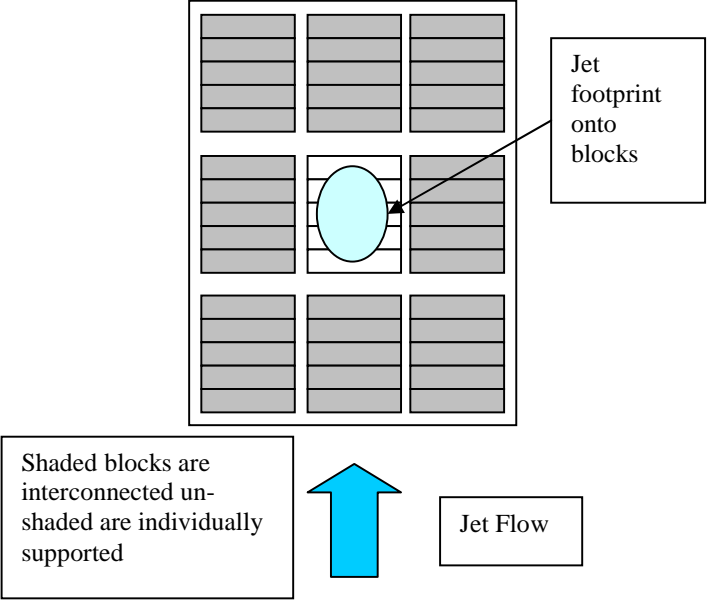


Photograph showing the ejected block set following test run 1

RUN 02

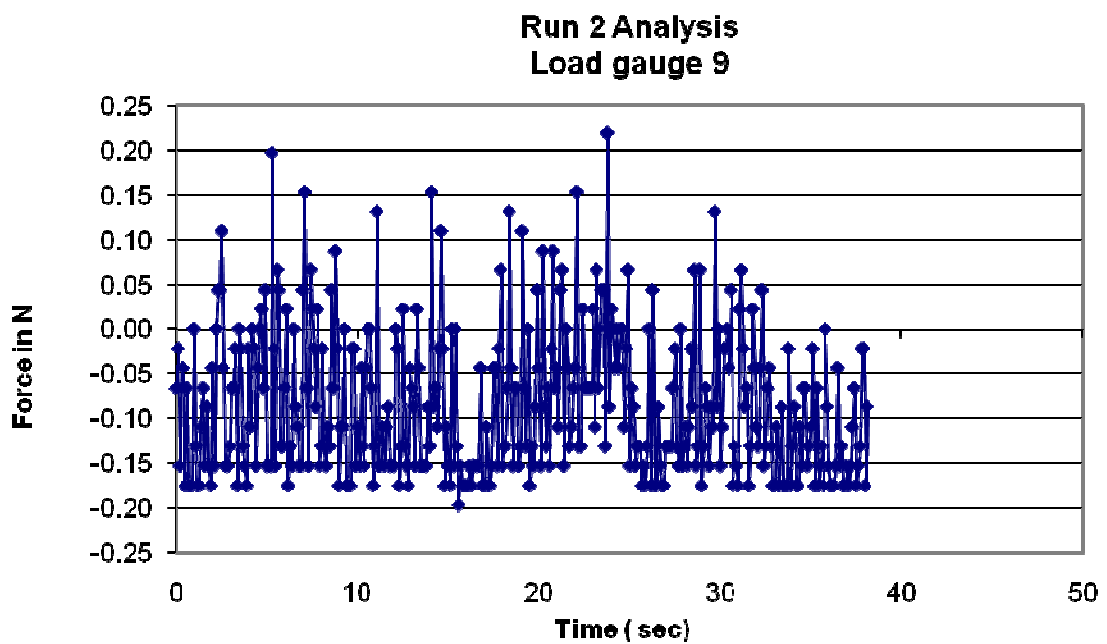
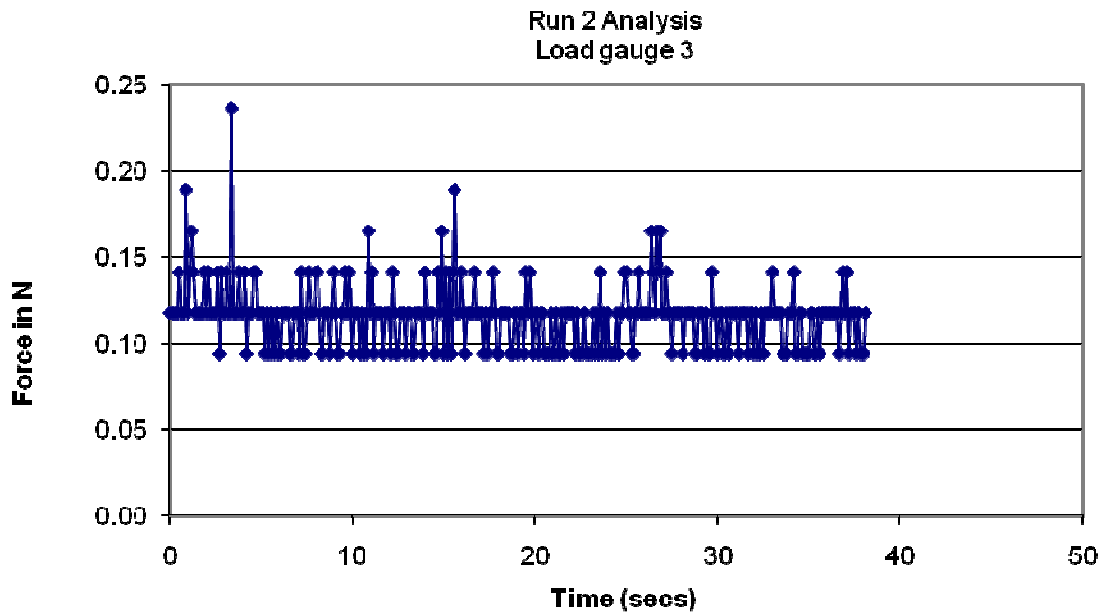
| Run No 2 | | |
|-----------------|---|--|
| | | |
| Jet Angle | 60 degrees to horizontal | |
| | | |
| Jet velocity | 1 ms ⁻¹ (prototype 4.46 ms ⁻¹) | |
| | | |
| Air Flow | 0 | |
| | | |
| Seabed Location | Up | |
| | | |



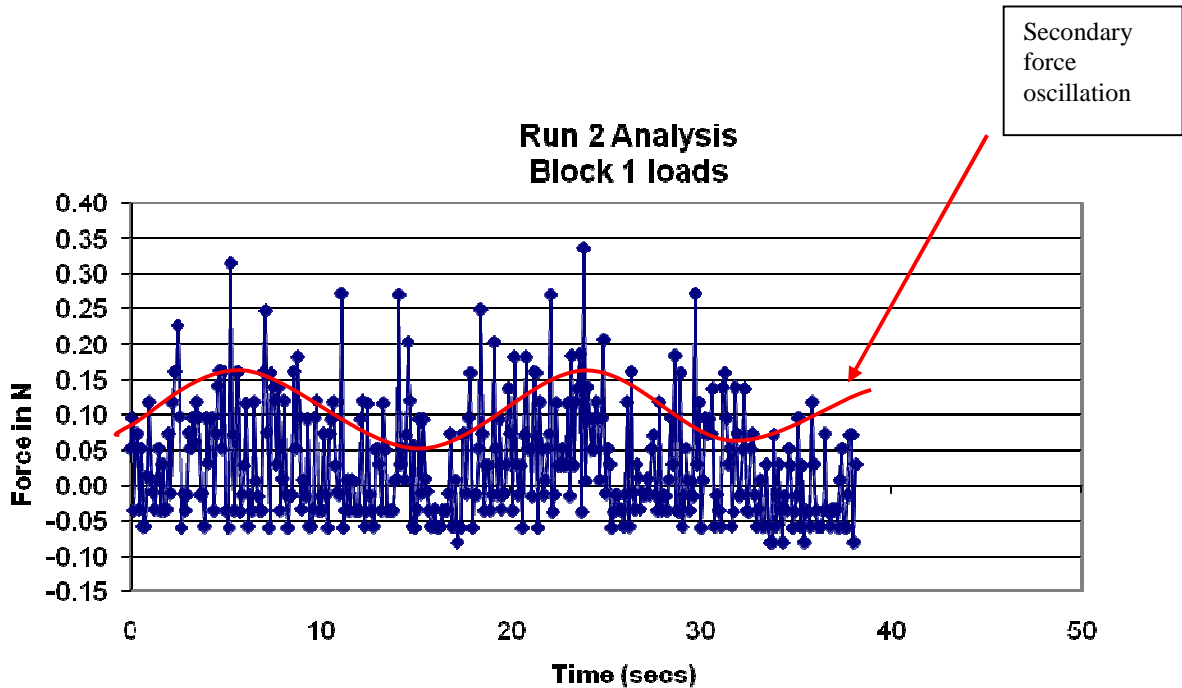
| | |
|----------------------|---|
| <p>Jet footprint</p> |  |
| <p>Comments</p> | <p>The test was carried out with the blocks installed as groups with the centre group of blocks being individually supported and unconnected to the adjacent blocks After start up the pump was run for several minutes to allow entrained air to be ejected from the pump system</p> |

The forces measured on the blocks with this level of jet flow were found to be very small on block 1 (which was only subject to a small area footprint from the jet) although the maximum loads were found to be considerably larger than the mean. At these low flows the block appeared to stay in contact with each other for most of the time but comparison between the graphs for gauges 3 and 9 shows how the right hand end of the block is undergoing significantly more movement than the left hand end which probably reflects

the contact points of this block onto the adjacent block is primarily at the left hand side. It is also apparent that the areas outside and upstream of the jet footprint are subject to very little force. The load time graph for gauges 3 and 9 are shown below



The net force on the block can be illustrated by adding the readings from gauges 3 and 9 for each identical time period. When the global forces on the block is examined the range of force does not change significantly from that on gauge 9 but the maximum downward force on the block shows a slight increase. The graph of this is shown below



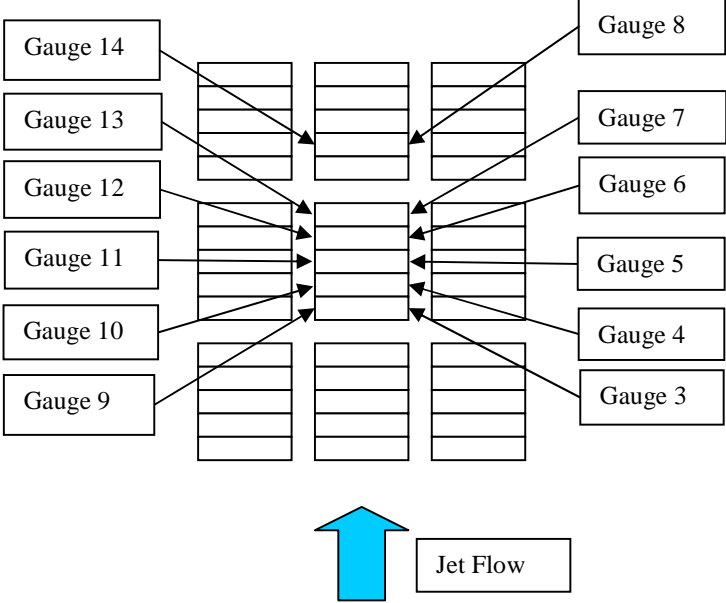
When a similar process is carried out on all the gauges then a comparative load time plot can be made on adjacent blocks. This shows that blocks 2 and 3 are subject to the main loads from the jet and they have a high frequency force variation of around 1- 3 Hz but also there appears to be a secondary much slower oscillation occurring, this has been highlighted in red on the load time plot. The adjacent blocks are also displaying this secondary oscillation and are all in phase with one another this is shown on the graph below.

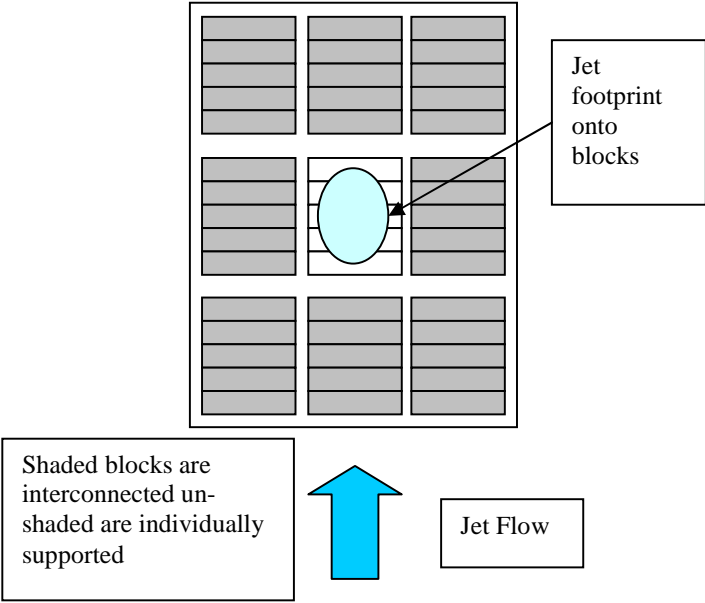


RUN 03

Run 3 was a sequential part of a run that included test runs 2-5. In this case, the jet speed has been increased to model the normal jet speed output by the high-speed catamaran during berthing operations.

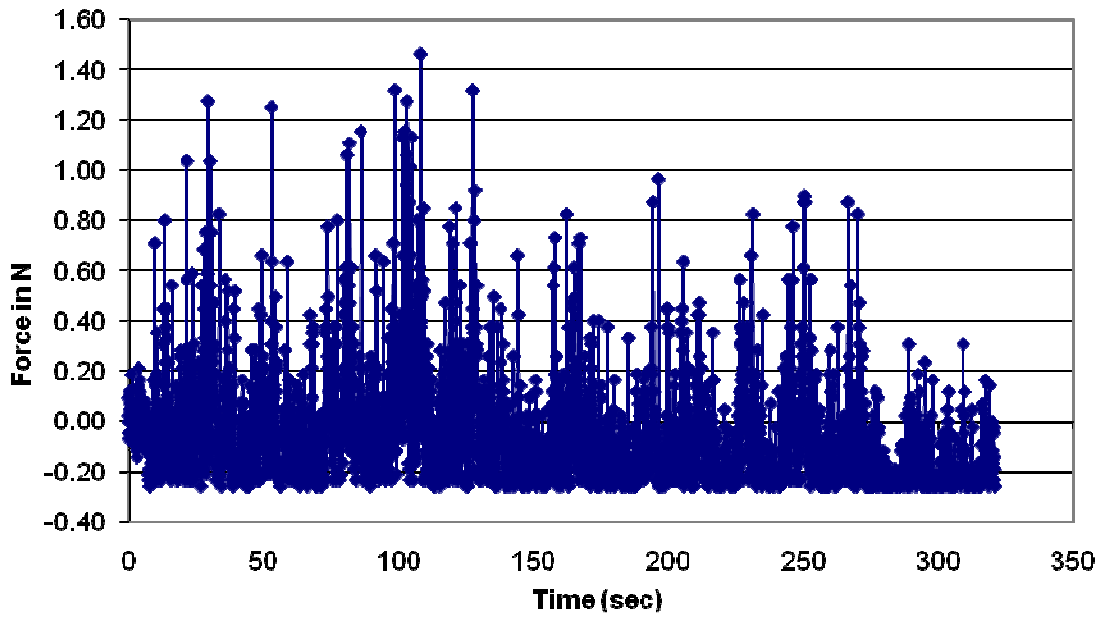
| Run No 3 | | |
|-----------------|--|--|
| | | |
| Jet Angle | 60 degrees to horizontal | |
| | | |
| Jet velocity | 2.49 ms ⁻¹ (prototype 11.31ms ⁻¹) | |
| | | |
| Air Flow | 0 | |

| | | |
|-----------------|--|--|
| | | |
| Seabed Location | Up | |
| Gauge Positions |  <p>The diagram shows a central vertical column of five rectangular gauges, labeled Gauge 9 at the bottom to Gauge 14 at the top. To the left of this column are three more vertical columns of five gauges each, labeled Gauge 10, 11, 12, 13, and 14 from bottom to top. To the right of the central column are three more vertical columns of five gauges each, labeled Gauge 3, 4, 5, 6, 7, and 8 from bottom to top. A blue arrow labeled 'Jet Flow' points upwards from the bottom center towards the central gauges. Arrows from each gauge label point to its corresponding gauge in the diagram.</p> | |
| | | |

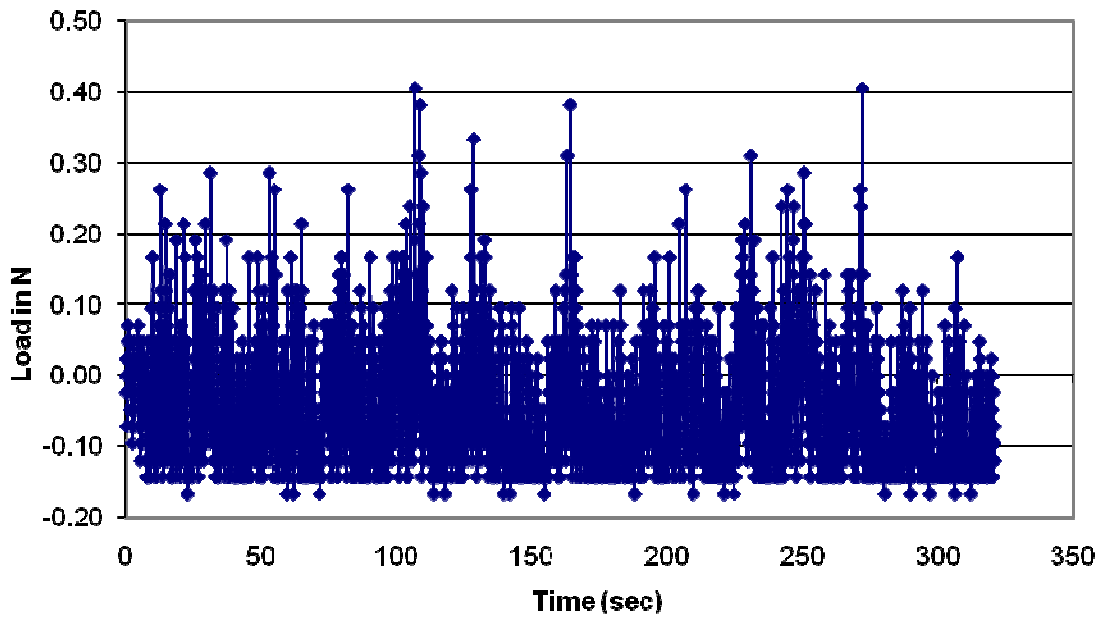
| | |
|----------------------|---|
| <p>Jet footprint</p> |  |
| <p>Comments</p> | <p>The test was carried out with the blocks installed as groups with the centre group of blocks being individually supported and unconnected to the adjacent blocks This is one in a sequence of tests on runs 2-5 Some of the load gauges failed to respond at the start of this run and these have been omitted from the output data.</p> |

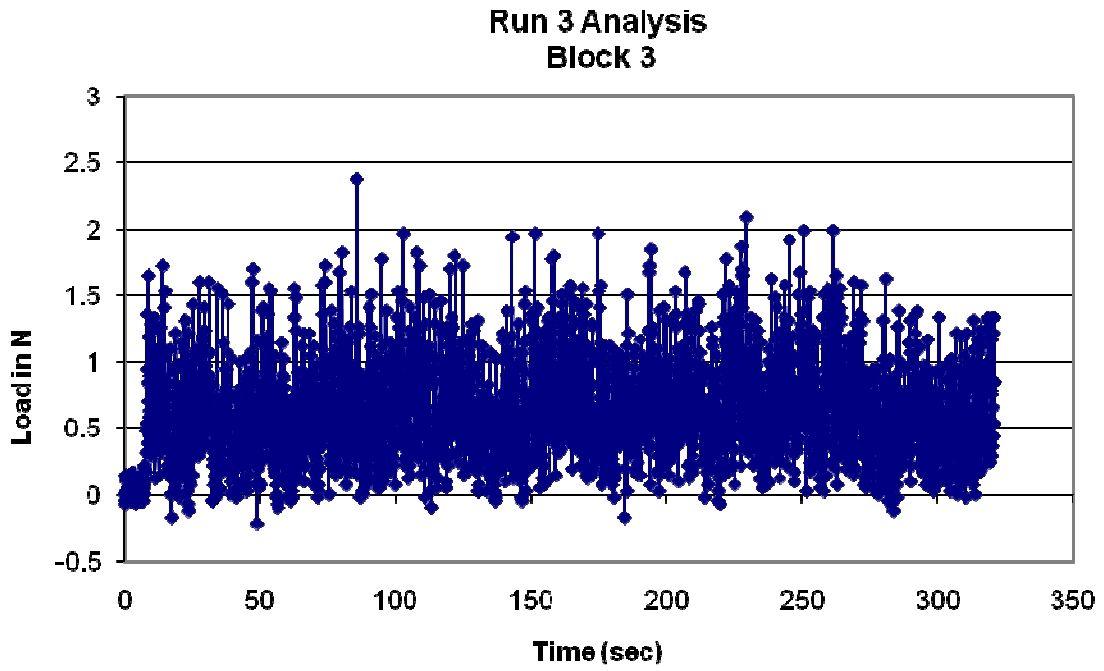
Since some of the gauges did not respond during this run there is a limited data set available. Therefore load gauge 3 and load gauge 4 data has been examined in isolation for blocks 1 and 2, as with the previous runs it can be seen that there is a secondary force oscillation occurring on the blocks and these are similar for all the blocks. Of further interest is the magnitude of the peak forces which are at least three times greater than the 'normal forces'

Run 3 Analysis Gauge 3



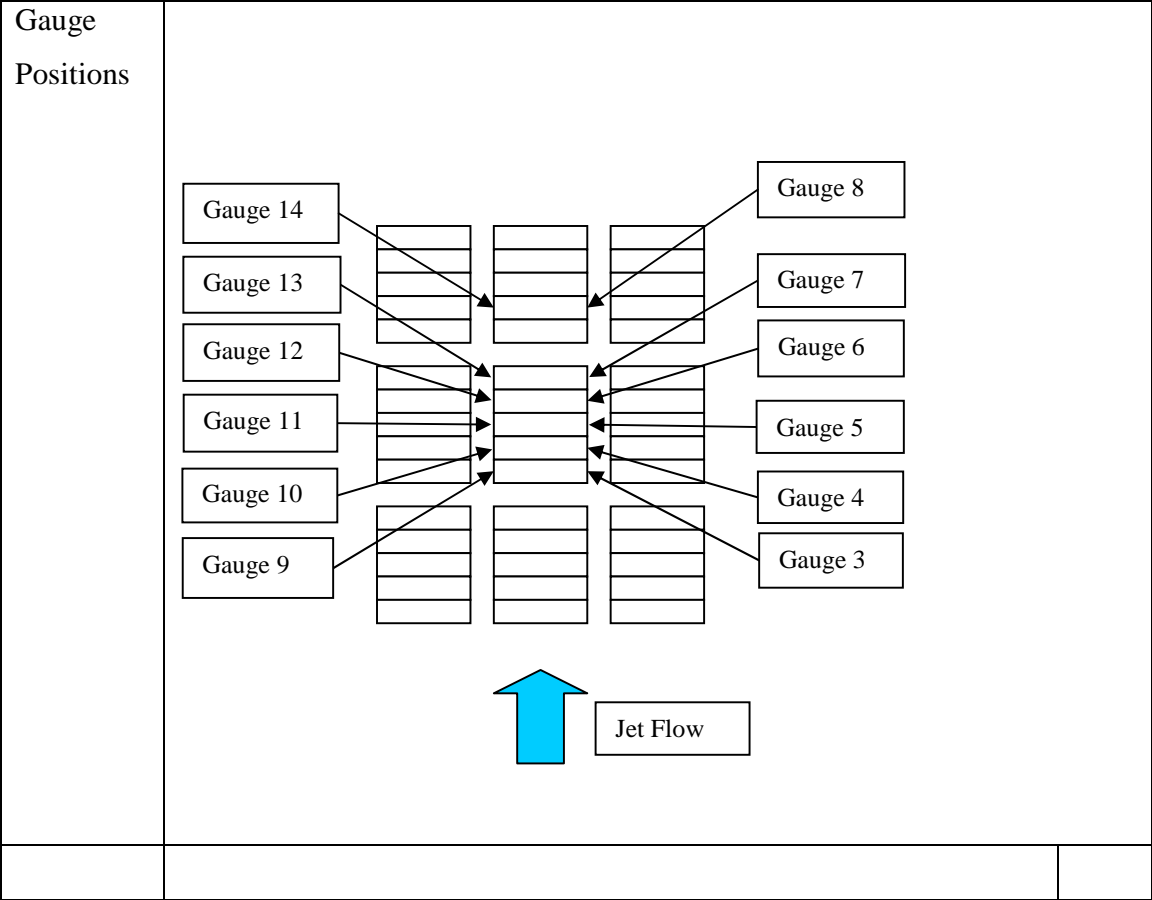
Run 3 Analysis Gauge 4

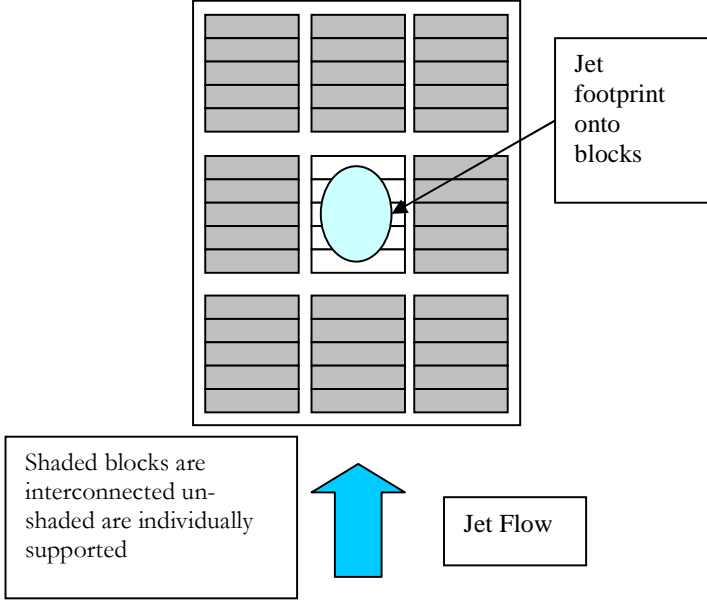




RUN 04

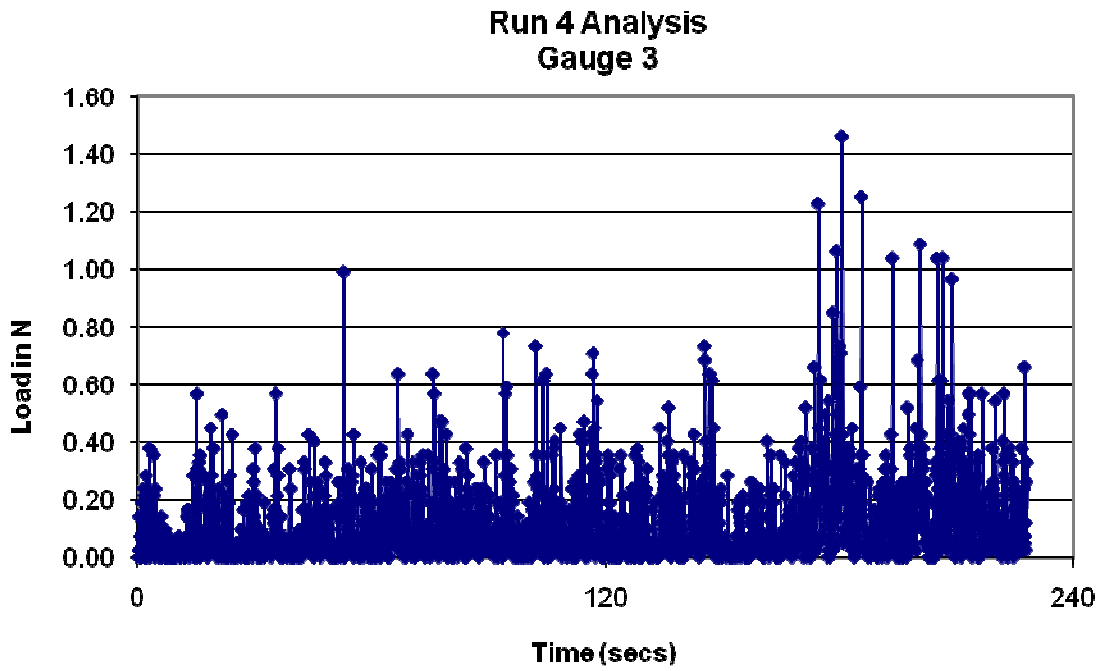
| Run No 4 | | |
|-----------------|--|--|
| | | |
| Jet Angle | 60 degrees to horizontal | |
| | | |
| Jet velocity | 2.49 ms ⁻¹ (prototype 11.31ms ⁻¹) | |
| | | |
| Air Flow | 7% | |
| | | |
| Seabed Location | Up | |
| | | |

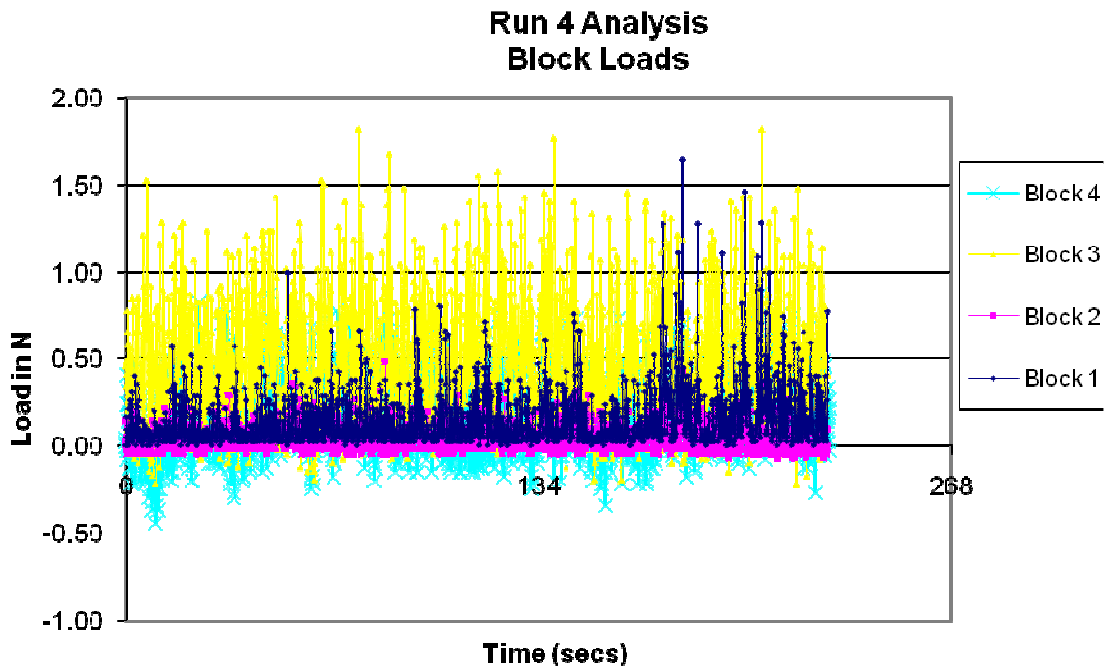
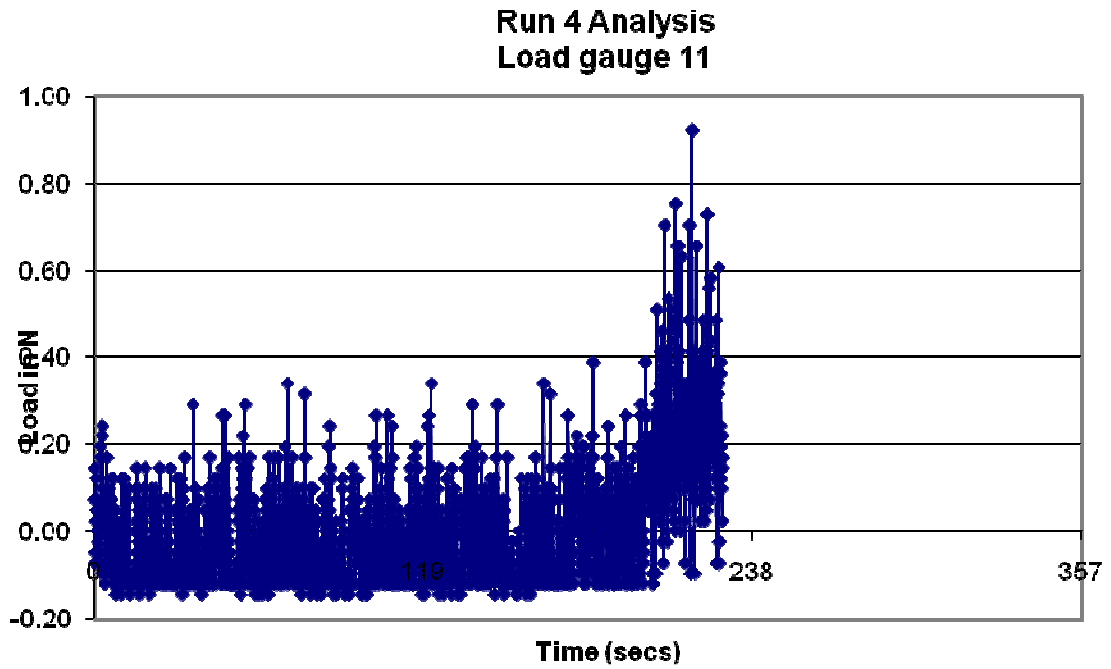


| | |
|----------------------|--|
| <p>Jet footprint</p> |  <p>Shaded blocks are interconnected unshaded are individually supported</p> <p>Jet Flow</p> <p>Jet footprint onto blocks</p> |
| <p>Comments</p> | <p>The test was carried out with the blocks installed as groups with the centre group of blocks being individually supported and unconnected to the adjacent blocks This is one in a sequence of tests on runs 2-5. The air valve in this case was opened to create an air entrained jet flow.</p> |

During this run there was very little load variation noted on gauge 3 which can be explained from the visual observations where this block was seen to be touching the adjacent blocks on the right hand side. Despite this readings were still being obtained from gauge 9 at the left hand end of the block, both gauges did not provide the usual negative (or uplift force) oscillation that was observed in all the other runs. It is therefore suspected that this block was being restrained in uplift during this run which has reduced the apparent forces being displayed for this block. This can be readily seen on both the load gauge and block load graphs below. The load gauges 5 and 11 which were both on block 3 were not providing any significant output and this problem continued for the

remainder of the test runs and was found to be due to a failure of the bridge amplifier. These gauges did however continue to give a reading of noise through the system and therefore their output has been included as a control check on the active gauges.



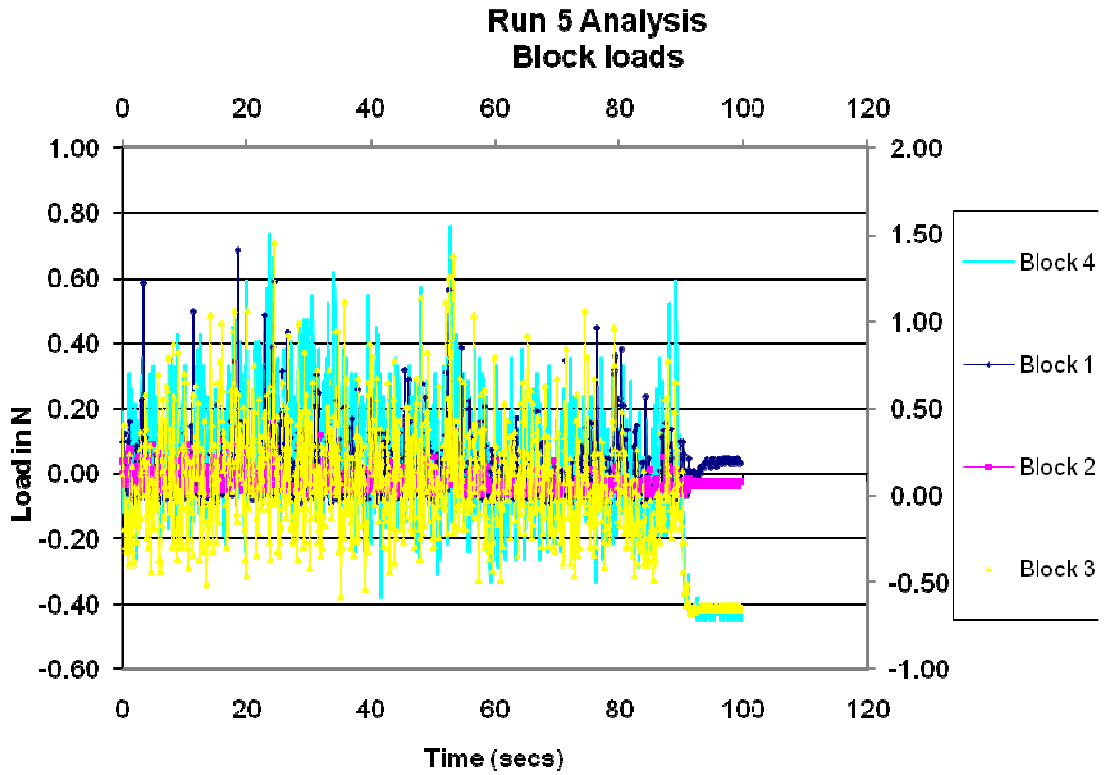


RUN 05

| Run No 5 | | |
|-----------------|--|--|
| Jet Angle | 60 degrees to horizontal | |
| Jet velocity | 2.49 ms ⁻¹ (prototype 11.31ms ⁻¹) | |
| Air Flow | 0 | |
| Seabed Location | Up | |
| Gauge Positions | | |

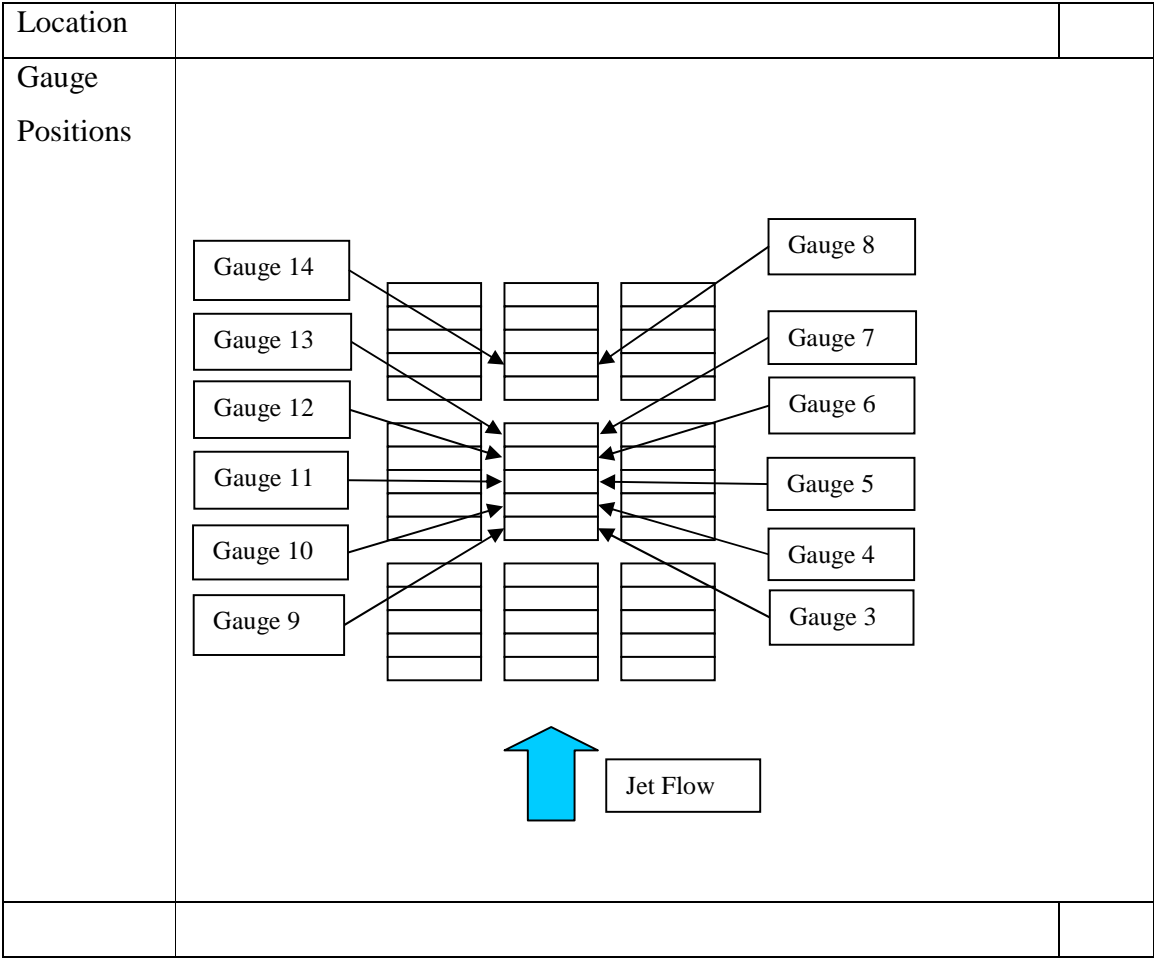
| | |
|----------------------|---|
| <p>Jet footprint</p> | <p>Shaded blocks are interconnected unshaded are individually supported</p> <p>Jet Flow</p> <p>Jet footprint onto blocks</p> |
| <p>Comments</p> | <p>The test was carried out with the blocks installed as groups with the centre group of blocks being individually supported and unconnected to the adjacent blocks This is one in a sequence of tests on runs 2-5.</p> |

As for the preceding runs the gauges to block 1 (gauges 3 and 9) both appear not to be displaying any uplift forces. The reasoning is the same as explained previously, gauges 10 and 4 behaved as expected. The block load forces are shown below with block 1 forces being much lower than expected. Block 3 is showing no force probably due to the block being held against the adjacent blocks but the results are interesting in so far as they show the level of background noise is very low.



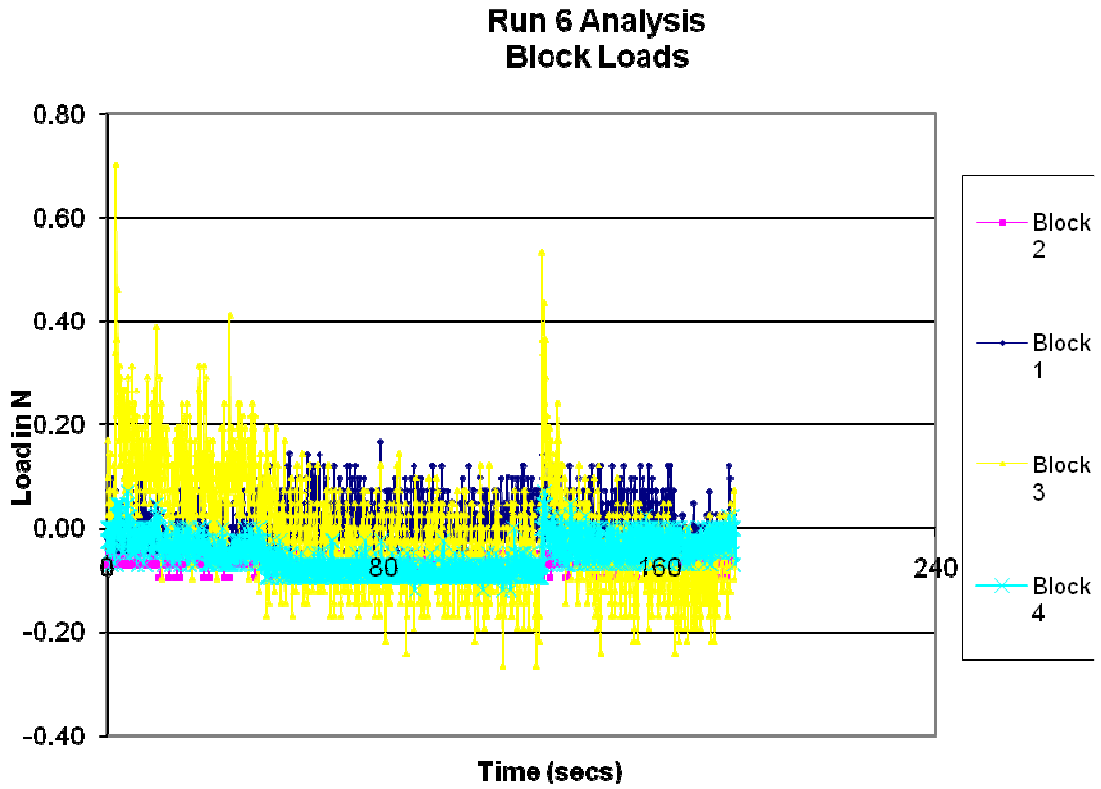
RUN 06

| Run No 6 | | |
|--------------|---|--|
| Jet Angle | 60 degrees to horizontal | |
| Jet velocity | 1 ms ⁻¹ (prototype 4.46 ms ⁻¹) | |
| Air Flow | 17% | |
| Seabed | Down | |



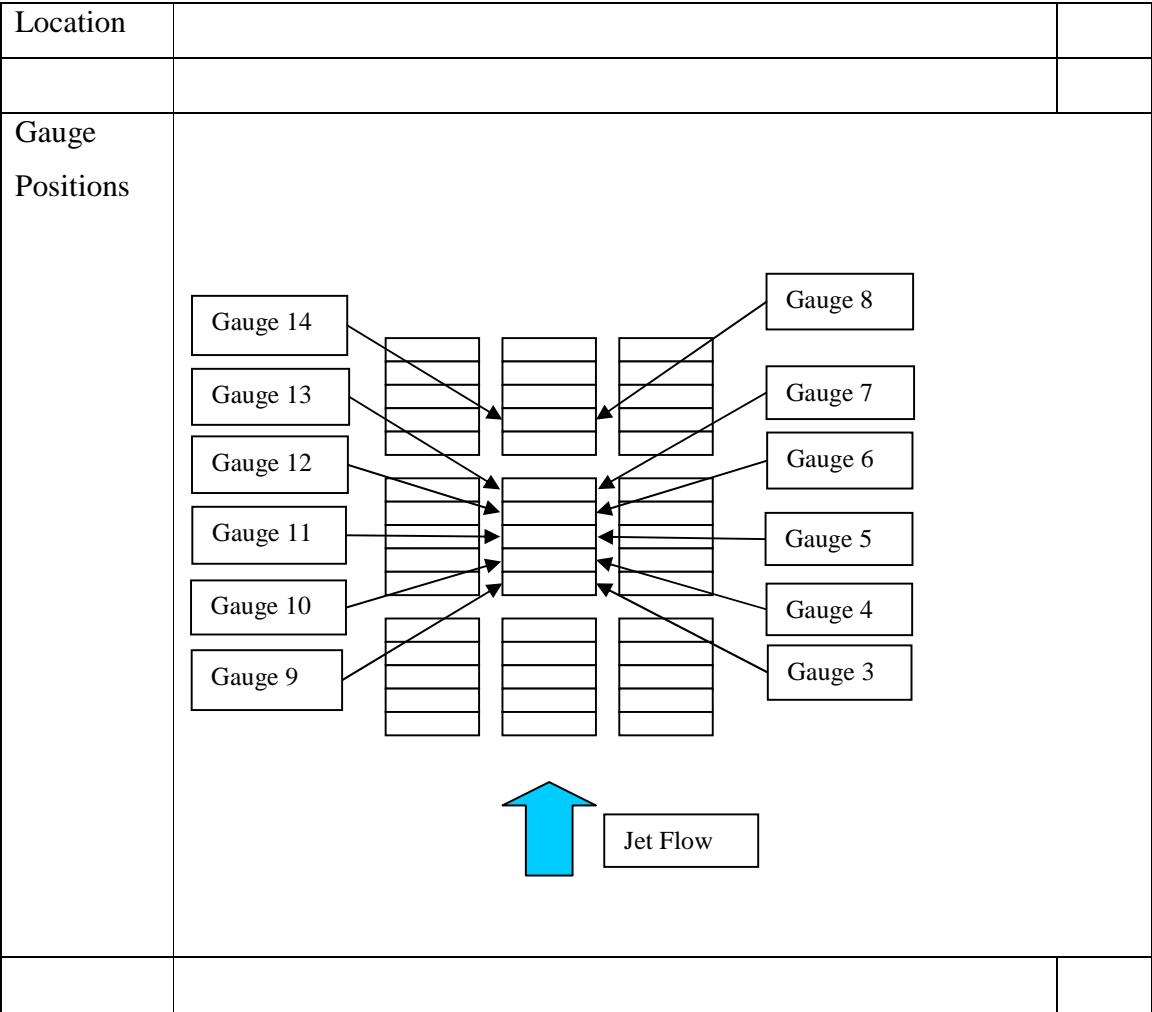
| | |
|----------------------|---|
| <p>Jet footprint</p> | <p>Shaded blocks are interconnected unshaded are individually supported</p> <p>Jet footprint onto blocks</p> <p>Jet Flow</p> |
| <p>Comments</p> | <p>The test was carried out with the blocks installed as groups with the centre group of blocks being individually supported and unconnected to the adjacent blocks This is one in a sequence of tests on runs 2-5.</p> |

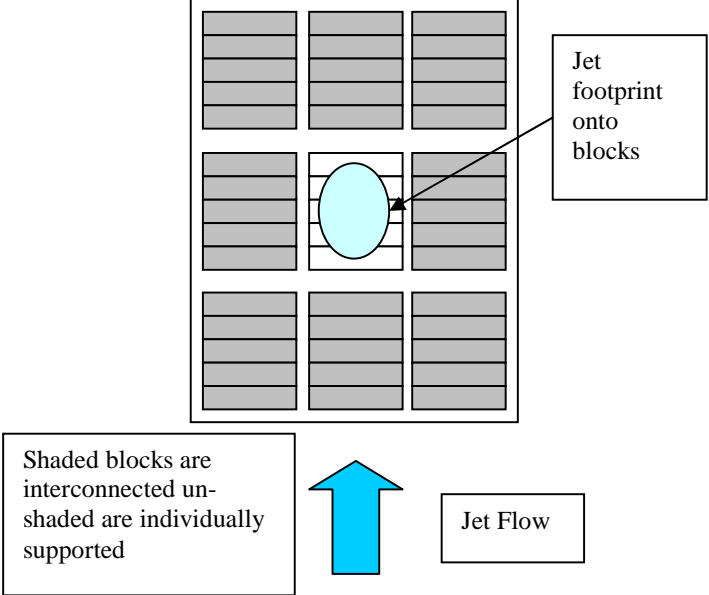
In this run there were no significant force recorded on blocks 1 and 3 and block 2 shows the representative behaviour. With the low power of the pump on idle these results are not unexpected and the block load graph shows the small block forces generated. The shift in the block load shown around two thirds of the way through the run is repeated on the individual gauge plots for this block and is most likely due to the block suddenly moving position relative to the adjacent blocks because following this the range of forces involved does not vary greatly.



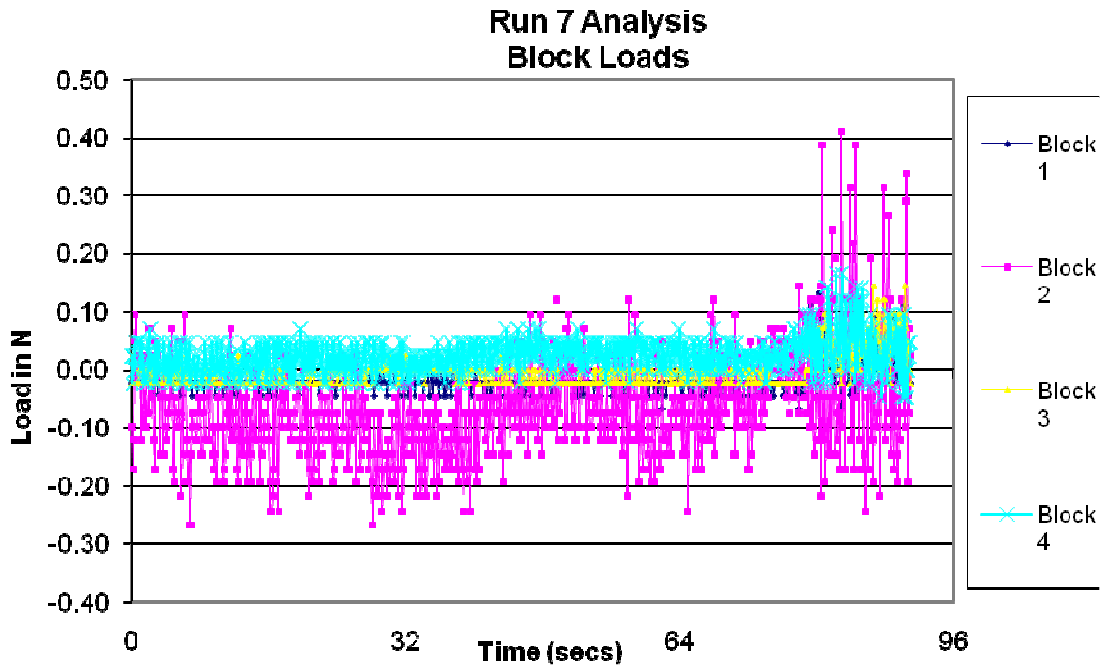
RUN 07

| Run No 7 | | |
|--------------|---|--|
| | | |
| Jet Angle | 60 degrees to horizontal | |
| | | |
| Jet velocity | 1 ms ⁻¹ (prototype 4.46 ms ⁻¹) | |
| | | |
| Air Flow | 0 | |
| | | |
| Seabed | Down | |



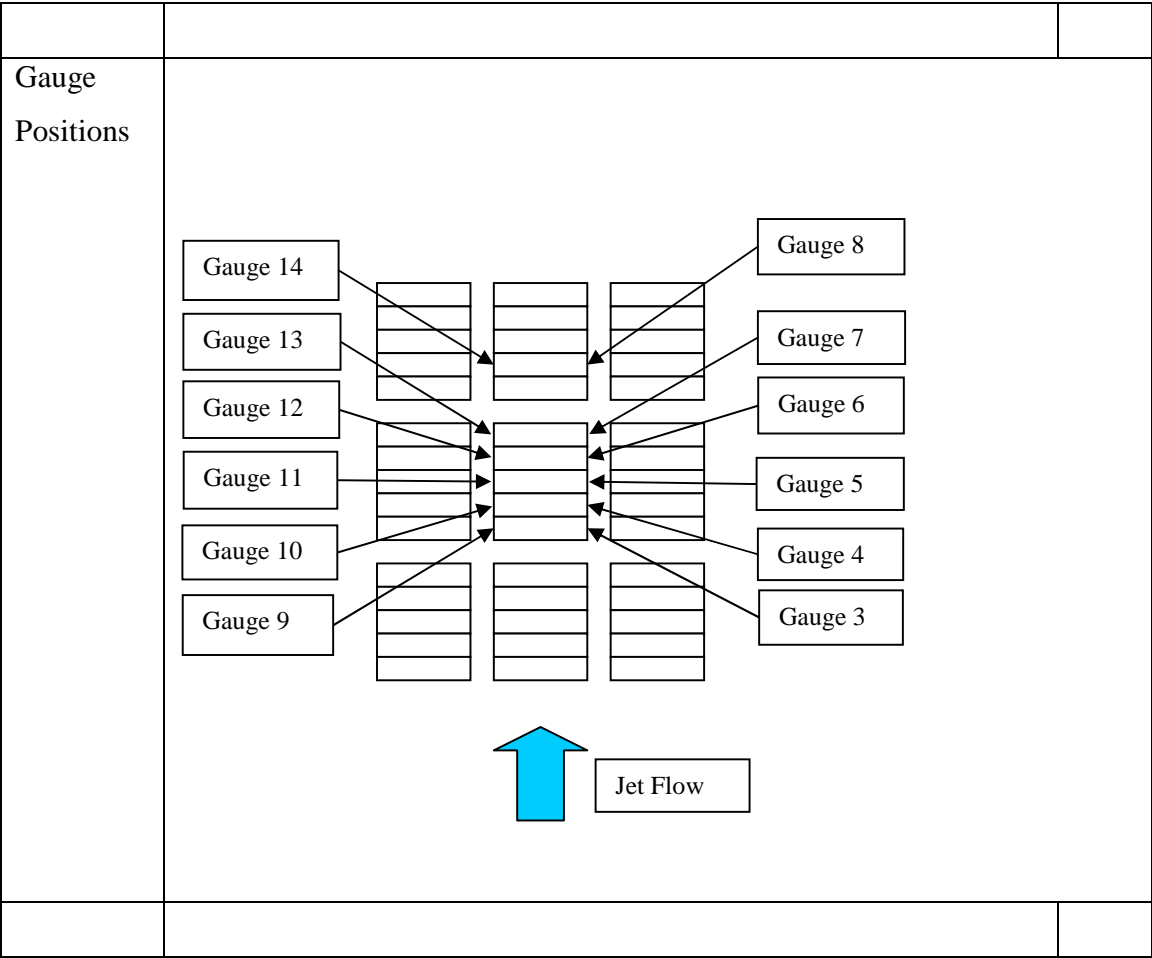
| | |
|----------------------|---|
| <p>Jet footprint</p> |  |
| <p>Comments</p> | <p>The test was carried out with the blocks installed as groups with the centre group of blocks being individually supported and unconnected to the adjacent blocks This is one in a sequence of tests on runs 6-9.</p> |

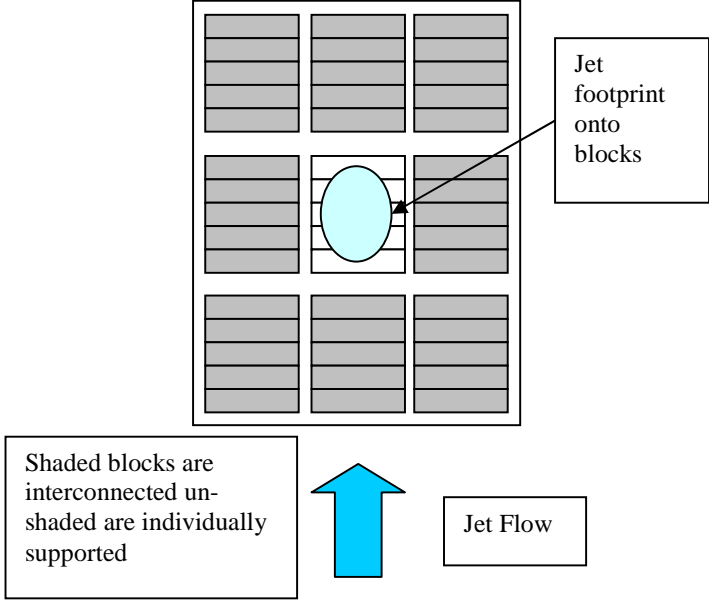
As with previous runs there was very little response from the load gauges on block 1 and the load gauges on block 3 were similarly unresponsive. Block 2 showed the main response o the flows with very notable peak loads compared to the other blocks. As noted in previous runs the secondary load oscillation frequency was also observed



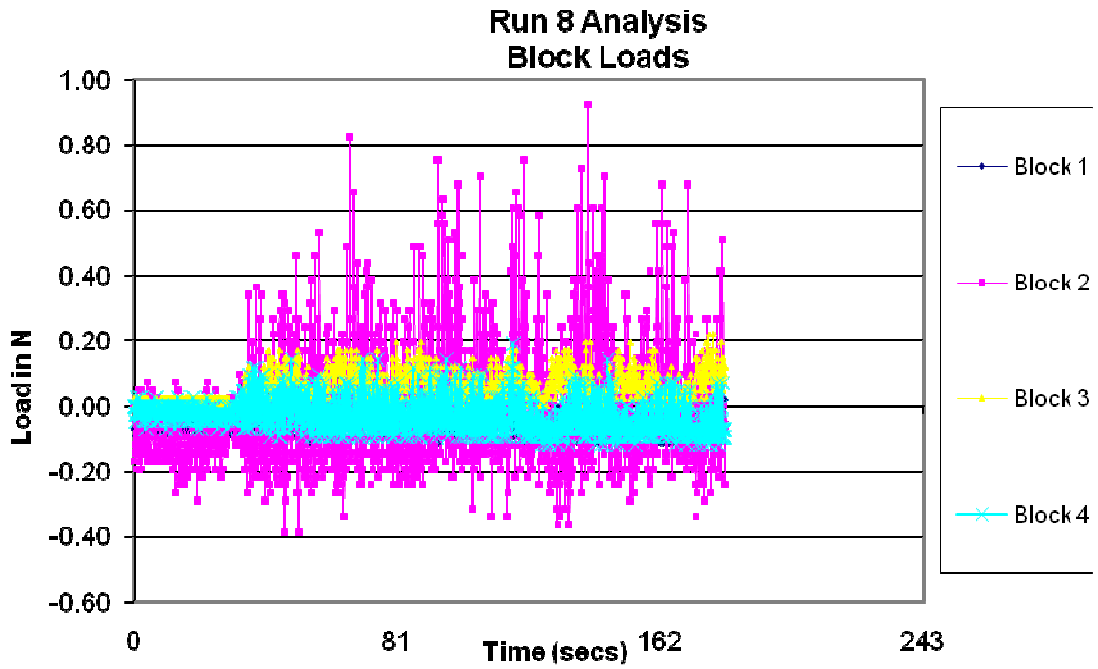
RUN 08

| Run No 8 | | |
|-----------------|--|--|
| Jet Angle | 60 degrees to horizontal | |
| Jet velocity | 2.49 ms ⁻¹ (prototype 11.31ms ⁻¹) | |
| Air Flow | 0 | |
| Seabed Location | Down | |



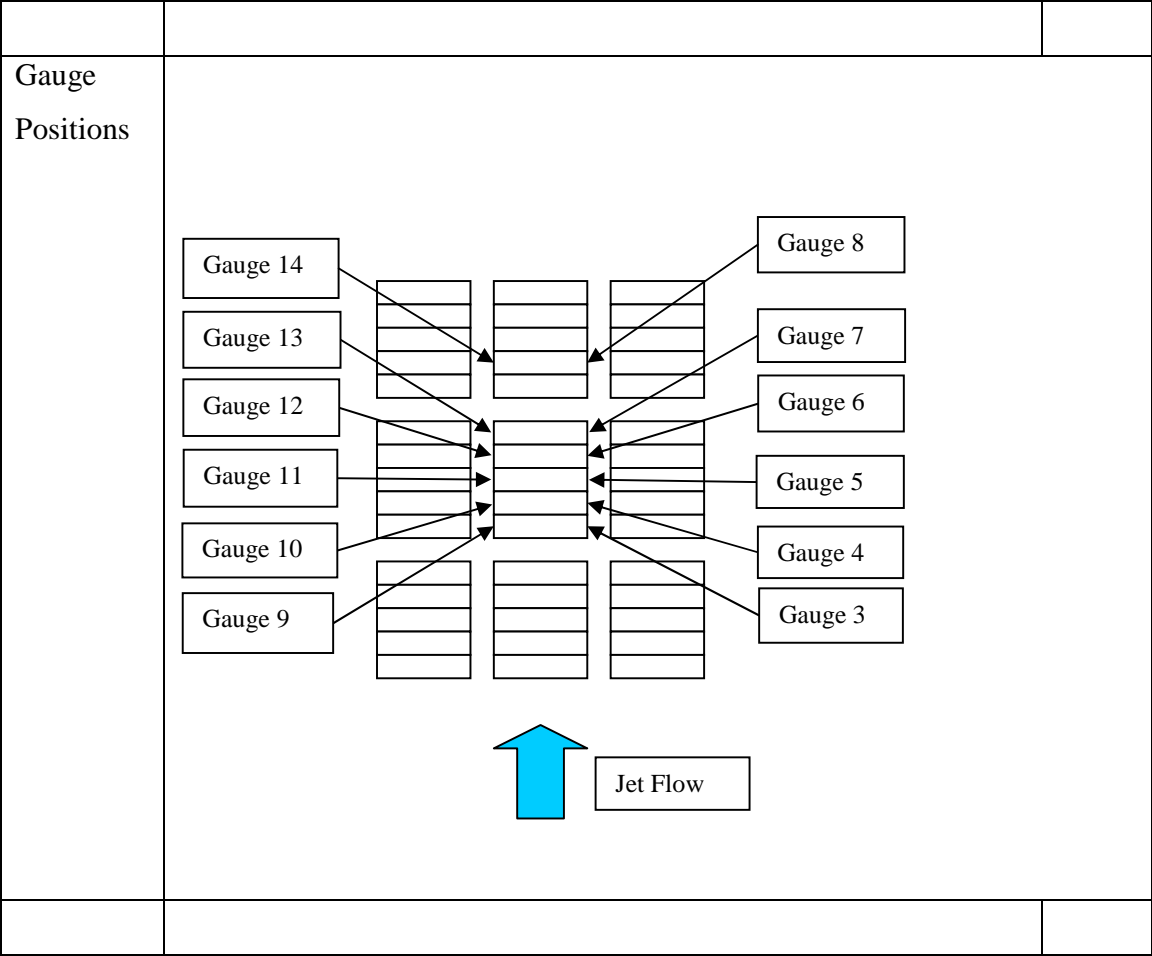
| | |
|----------------------|---|
| <p>Jet footprint</p> |  |
| <p>Comments</p> | <p>The test was carried out with the blocks installed as groups with the centre group of blocks being individually supported and unconnected to the adjacent blocks This is one in a sequence of tests on runs 6-9.</p> |

In this run with the greater flow there was some response from load gauge 3 on Block 1 but little from load gauge 9 on the same block. The loads recorded on block 2 were around eight times greater than block 1. On Blocks 1 and 3 again there was very little in the way of uplift loads.



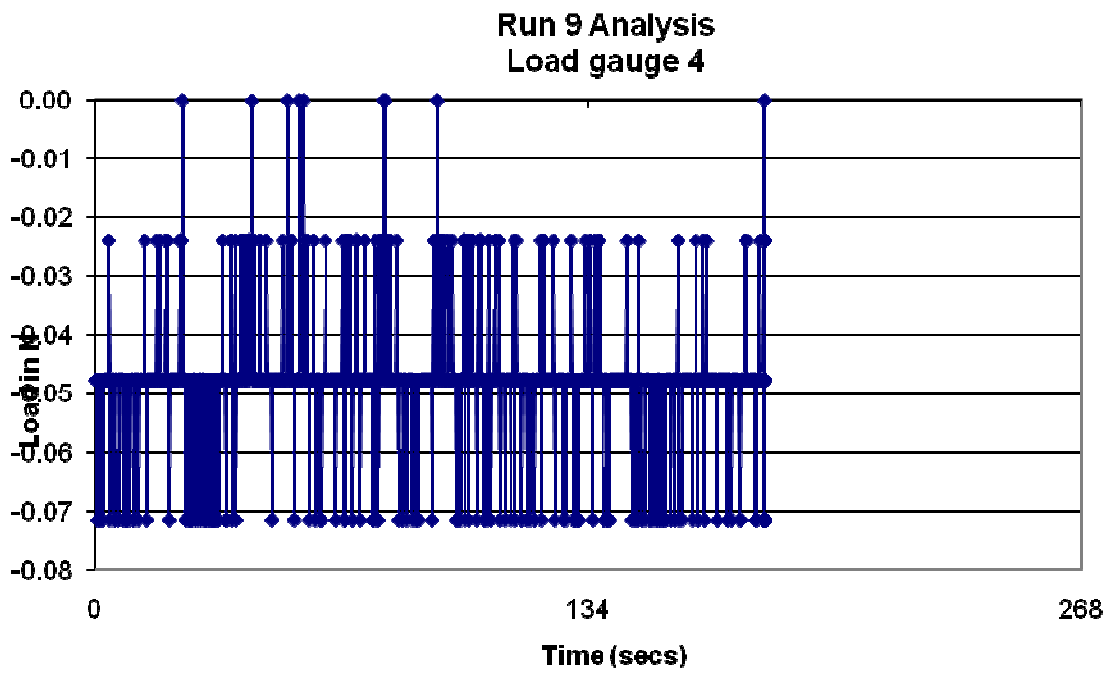
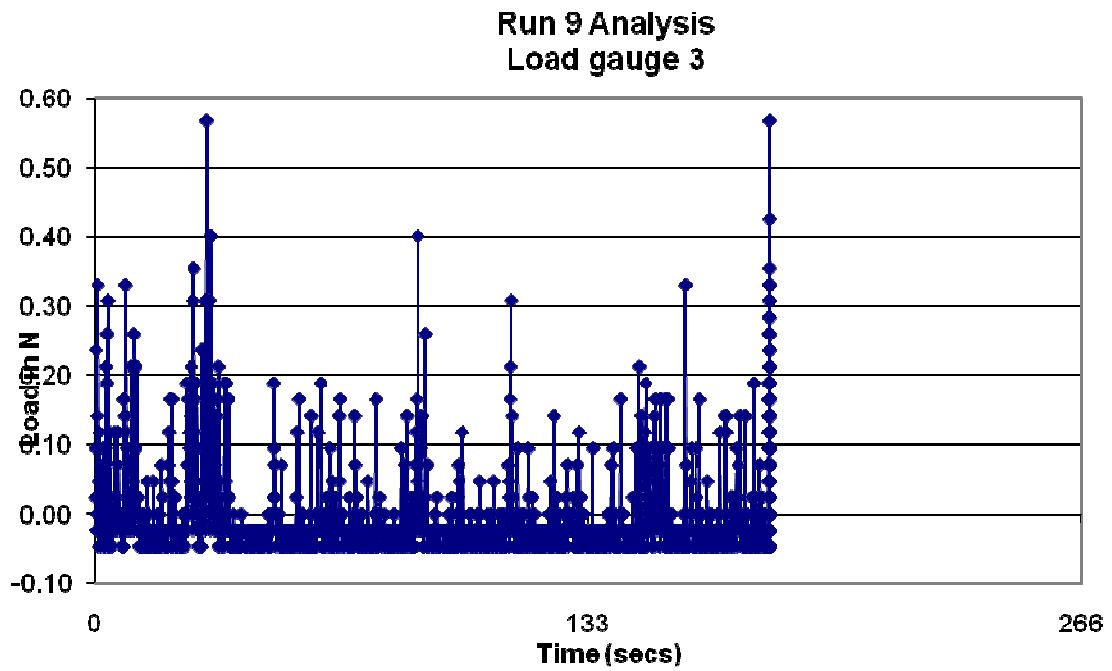
RUN 09

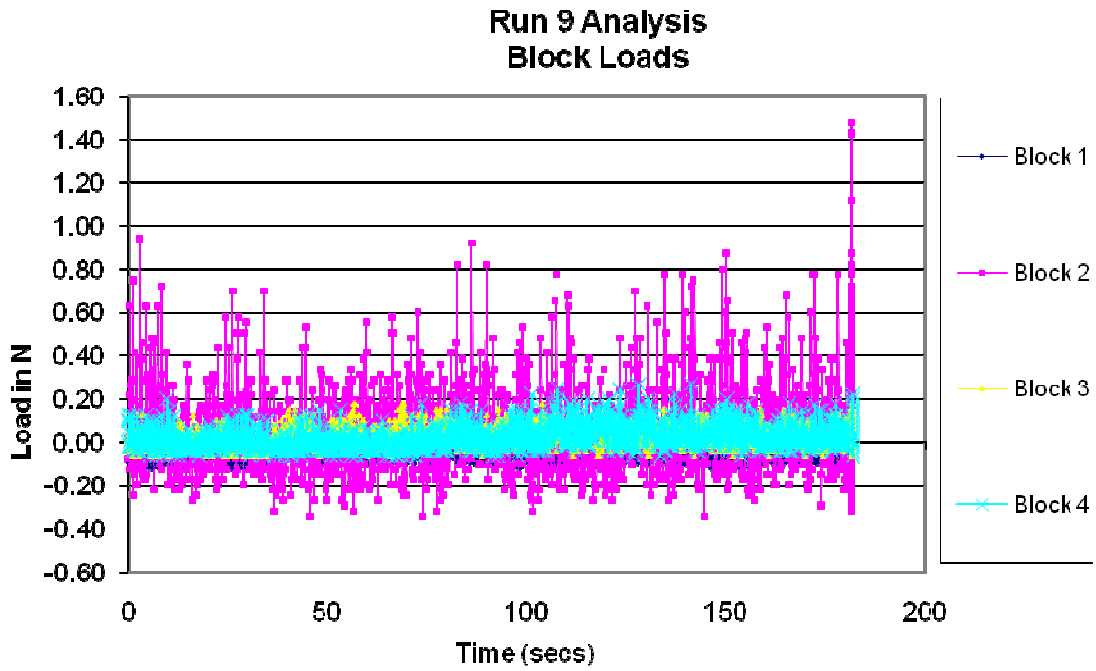
| Run No 9 | | |
|-----------------|--|--|
| Jet Angle | 50 degrees to horizontal | |
| Jet velocity | 2.49 ms ⁻¹ (prototype 11.31ms ⁻¹) | |
| Air Flow | 7% | |
| Seabed Location | Down | |



| | |
|----------------------|---|
| <p>Jet footprint</p> | <p>Shaded blocks are interconnected unshaded are individually supported</p> <p>Jet Flow</p> <p>Jet footprint onto blocks</p> |
| <p>Comments</p> | <p>The test was carried out with the blocks installed as groups with the centre group of blocks being individually supported and unconnected to the adjacent blocks This is one in a sequence of tests on runs 6-9.</p> |

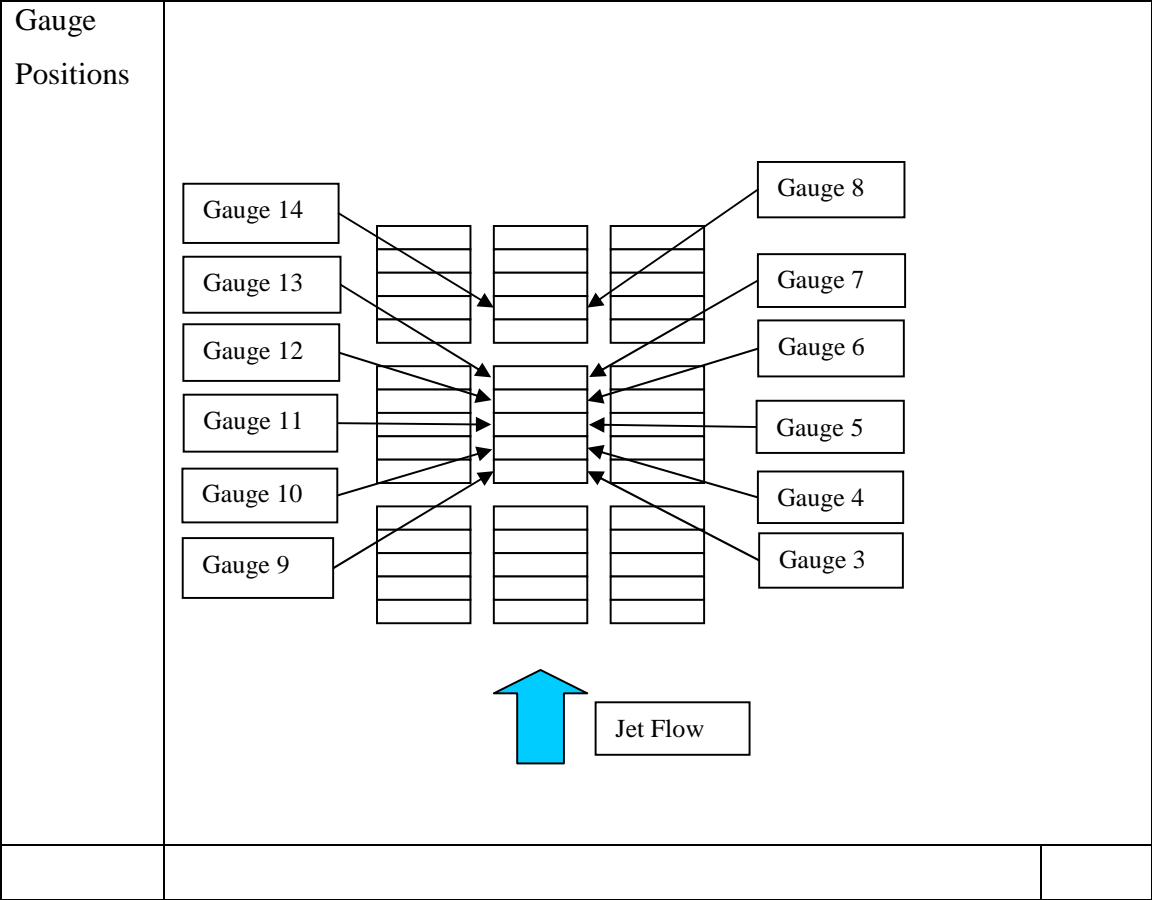
The increased jet flow on this run gave rise to a greater response from blocks 1 and 3 although as previously noted these were very much less than those experienced by block 2. The individual load gauges for blocks 1 and 3 again gave the impression that the load oscillation was restrained.

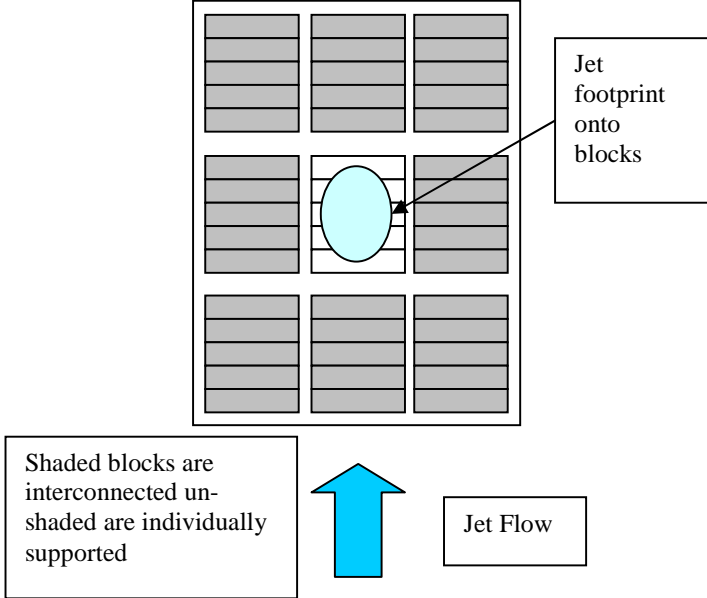




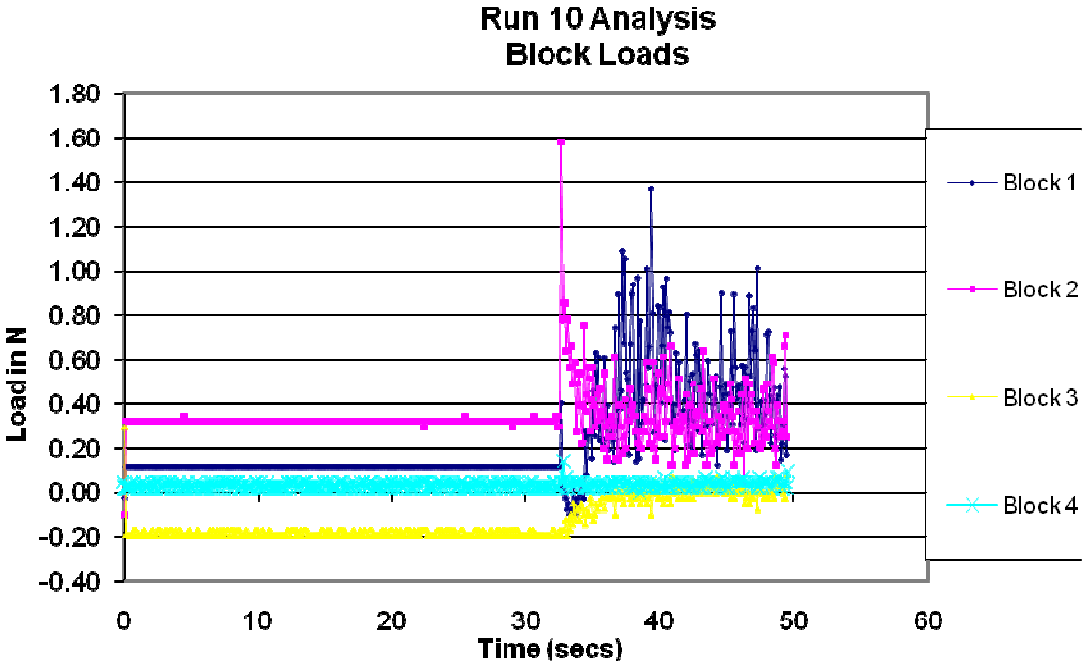
RUN 10

| Run No 10 | | |
|------------------|---|--|
| | | |
| Jet Angle | 50 degrees to horizontal | |
| | | |
| Jet velocity | 1.0 ms ⁻¹ (prototype 11.31ms ⁻¹) | |
| | | |
| Air Flow | 0 | |
| | | |
| Seabed Location | Down | |
| | | |



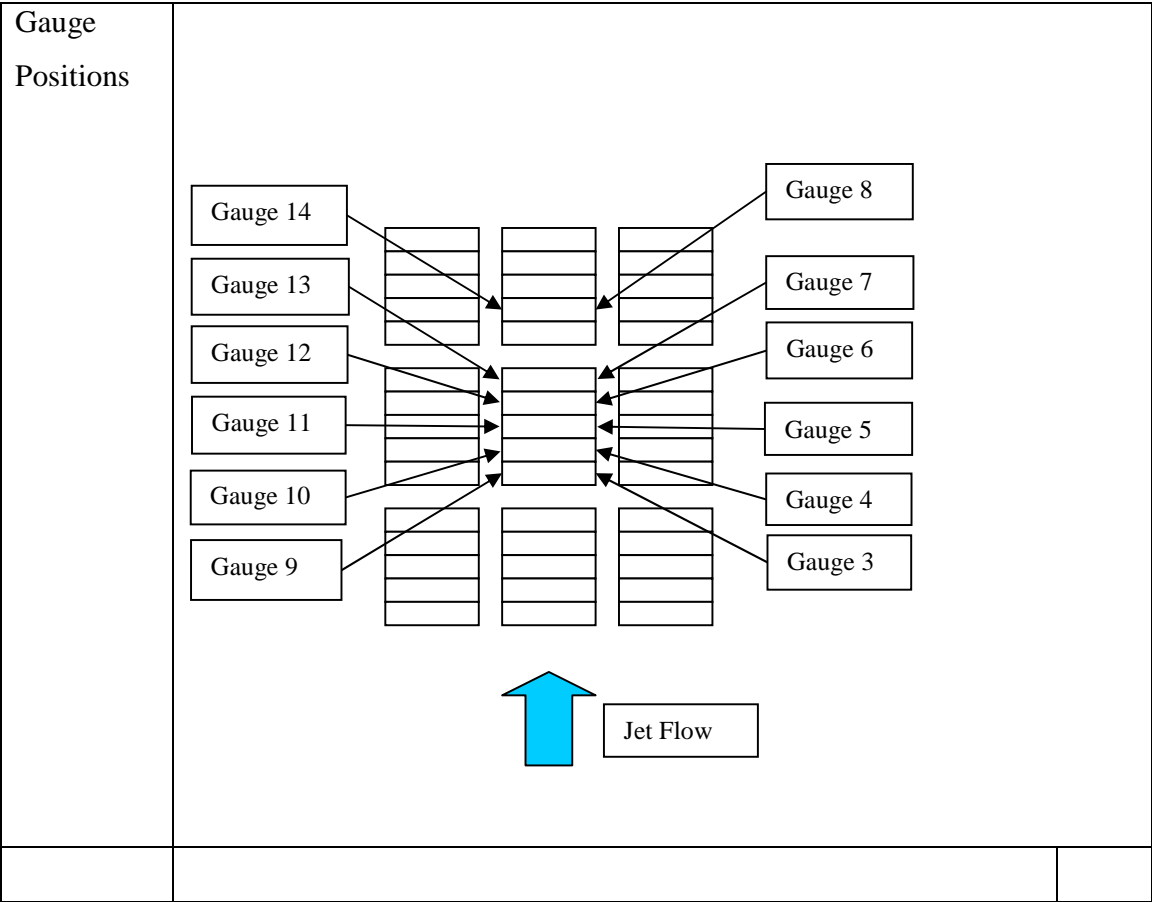
| | |
|----------------------|---|
| <p>Jet footprint</p> |  <p>Shaded blocks are interconnected unshaded are individually supported</p> <p>Jet Flow</p> <p>Jet footprint onto blocks</p> |
| <p>Comments</p> | <p>The test was carried out with the blocks installed as groups with the centre group of blocks being individually supported and unconnected to the adjacent blocks This is one in a sequence of tests on runs 10 - 14.</p> |

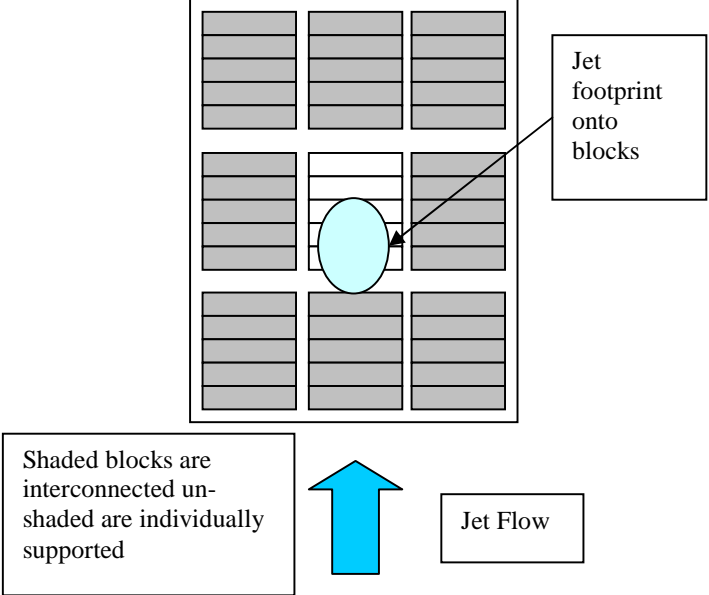
On this run the usable data set is fairly limited with only around 15 seconds of data showing a load response to the jet flow. The static data does however serve to illustrate the stability of the load measurement system when not exposed to flows. The individual load gauges to blocks 1 and 3 appeared to be heavily damped as noted in previous runs. However the load range imposed on block 1 was greater than that on block 2 if the start up jump at time 324 is ignored.



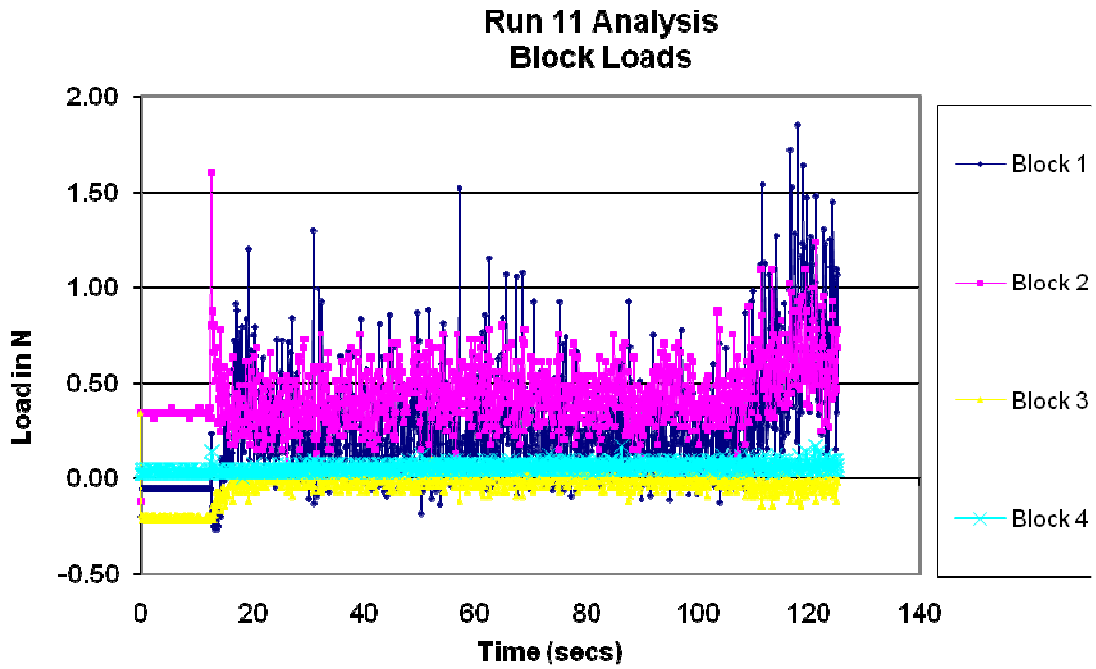
RUN 11

| Run No 11 | | |
|-----------------|---|--|
| | | |
| Jet Angle | 50 degrees to horizontal | |
| | | |
| Jet velocity | 1 ms ⁻¹ (prototype 4.46 ms ⁻¹) | |
| | | |
| Air Flow | 0 | |
| | | |
| Seabed Location | Down | |
| | | |



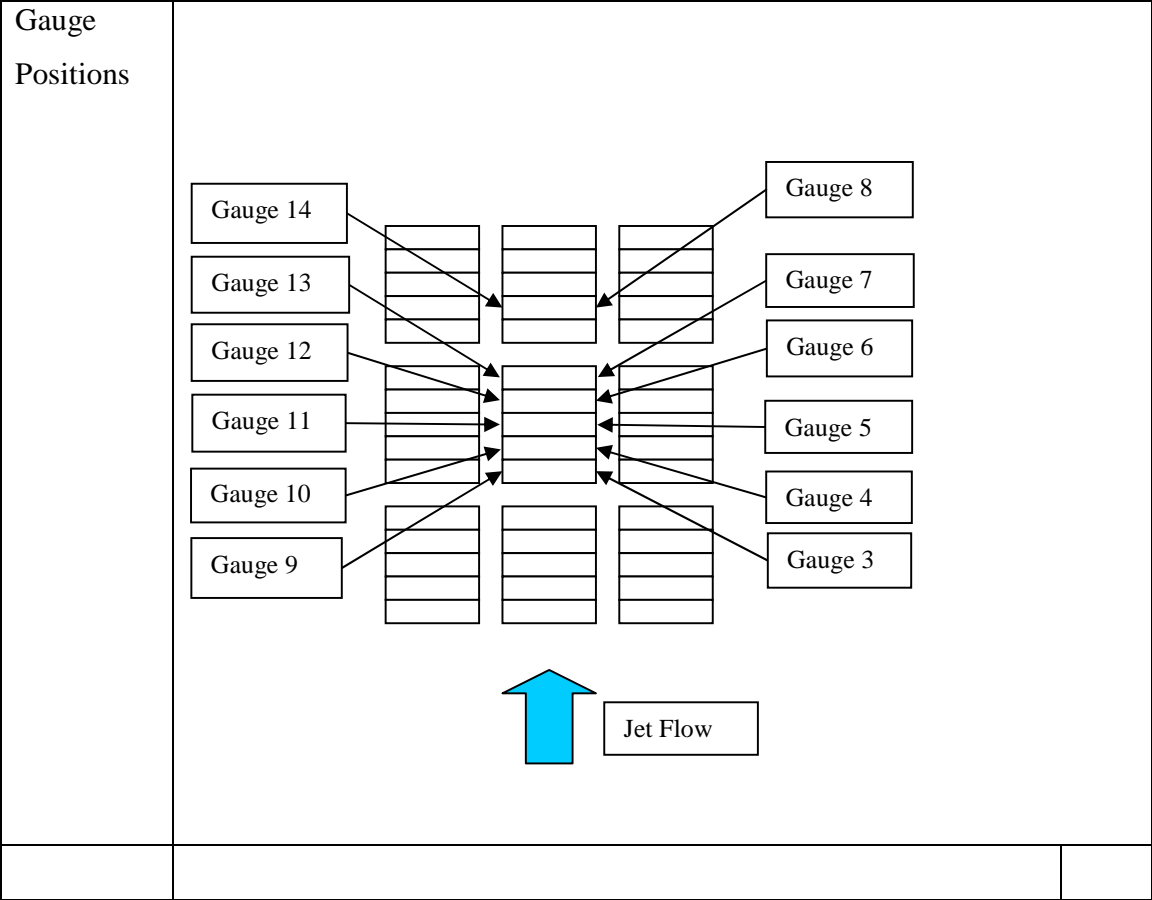
| | |
|----------------------|---|
| <p>Jet footprint</p> |  <p>Shaded blocks are interconnected unshaded are individually supported</p> <p>Jet footprint onto blocks</p> <p>Jet Flow</p> |
| <p>Comments</p> | <p>The test was carried out with the blocks installed as groups with the centre group of blocks being individually supported and unconnected to the adjacent blocks This is one in a sequence of tests on runs 10 - 14.</p> |

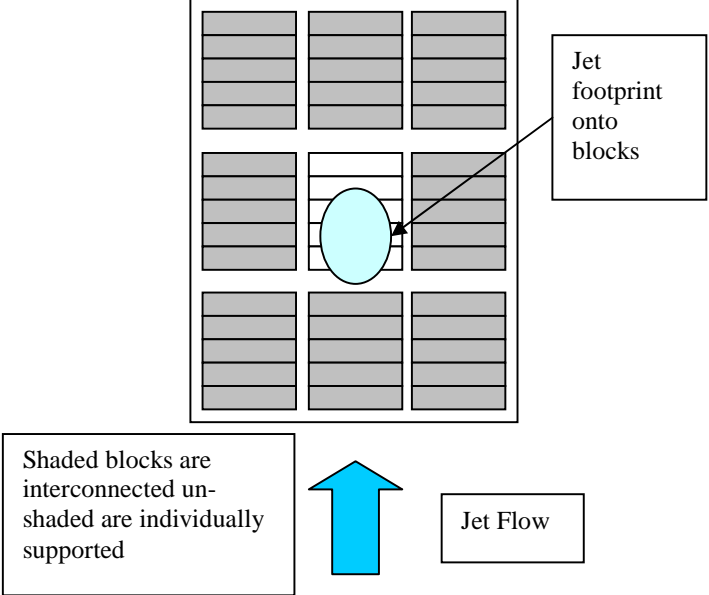
Blocks 1 and 2 show far greater loads than the other blocks and towards the end of the run there is a noticeable increase in the loads on both these blocks



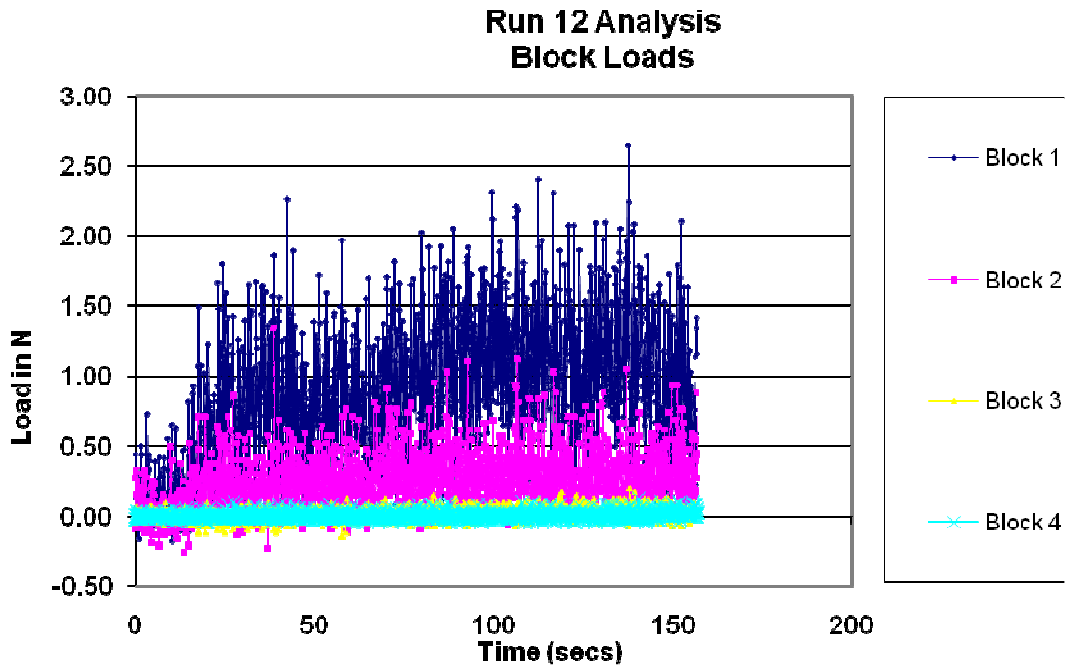
RUN 12

| Run No 12 | | |
|-----------------|---|--|
| | | |
| Jet Angle | 50 degrees to horizontal | |
| | | |
| Jet velocity | 1.00 ms ⁻¹ (prototype 4.46ms ⁻¹) | |
| | | |
| Air Flow | 17% | |
| | | |
| Seabed Location | Down | |
| | | |



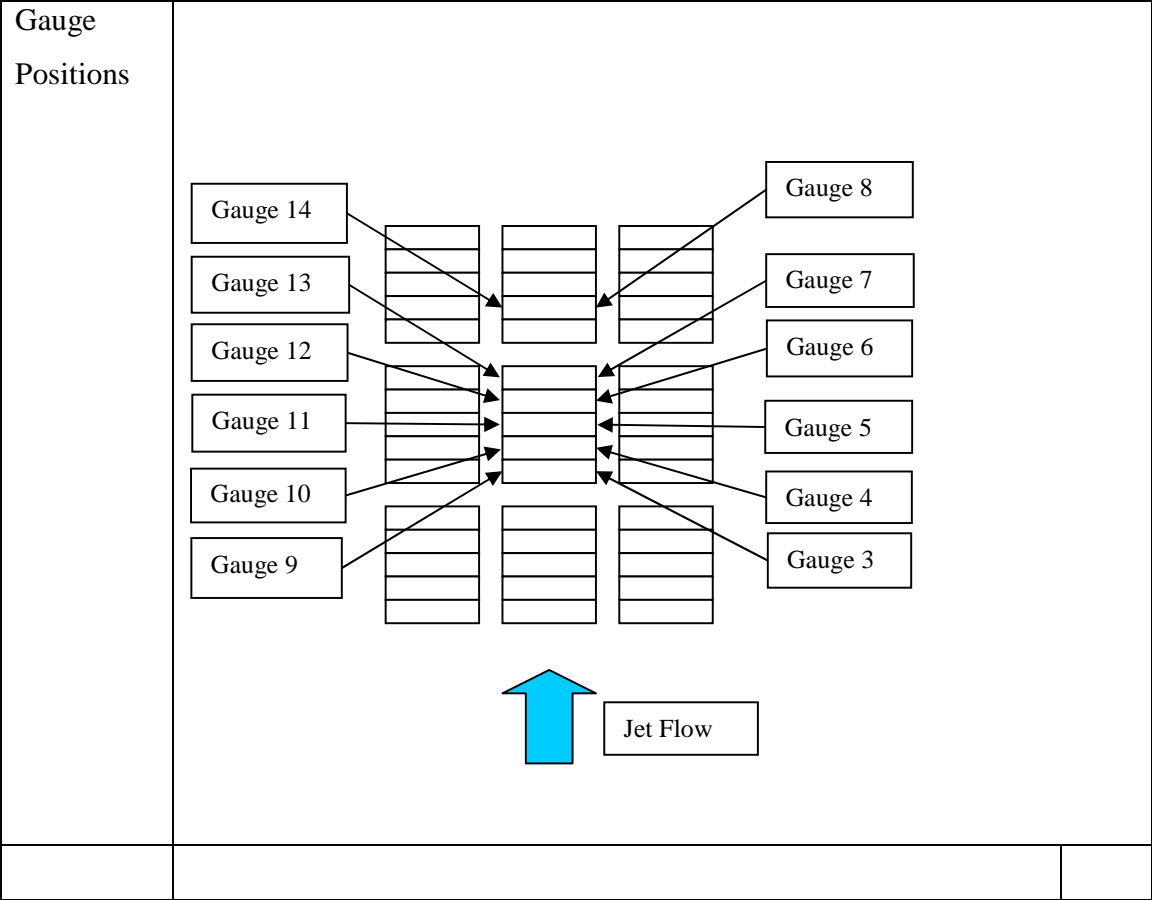
| | |
|----------------------|---|
| <p>Jet footprint</p> |  <p>Shaded blocks are interconnected unshaded are individually supported</p> <p>Jet footprint onto blocks</p> <p>Jet Flow</p> |
| <p>Comments</p> | <p>The test was carried out with the blocks installed as groups with the centre group of blocks being individually supported and unconnected to the adjacent blocks This is one in a sequence of tests on runs 10-14.</p> |

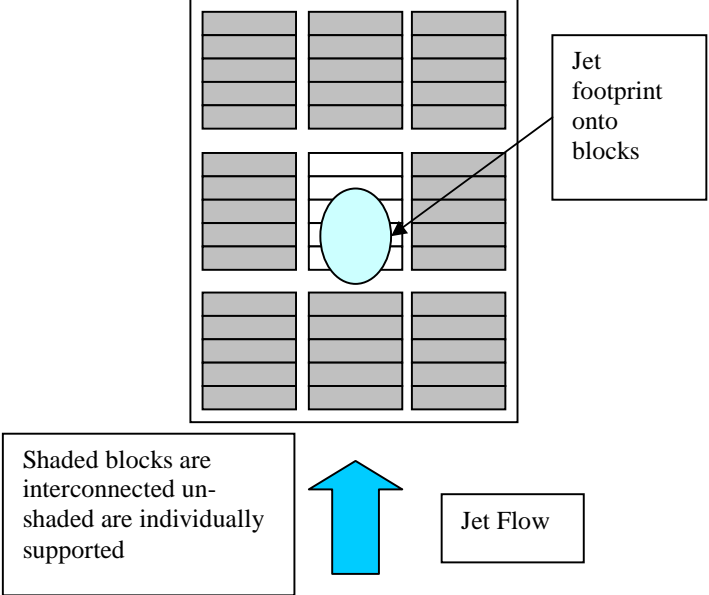
In this run the loads on block 1 were noticeably higher than on the other blocks and the introduction of air into the jet has cause an increase in load on this block whereas on the adjacent blocks the load has decrease compared to the case where there is no air entrainment



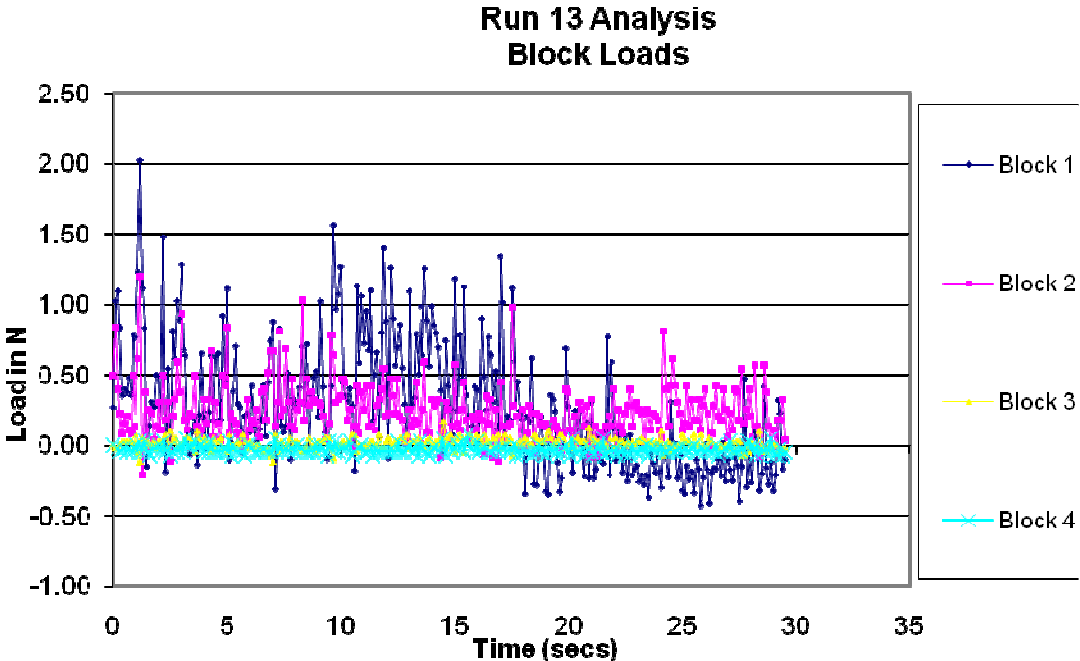
RUN 13

| Run No 13 | | |
|-----------------|---|--|
| | | |
| Jet Angle | 50 degrees to horizontal | |
| Jet velocity | 1.00 ms ⁻¹ (prototype 4.46ms ⁻¹) | |
| Air Flow | 0 | |
| Seabed Location | Down | |
| | | |



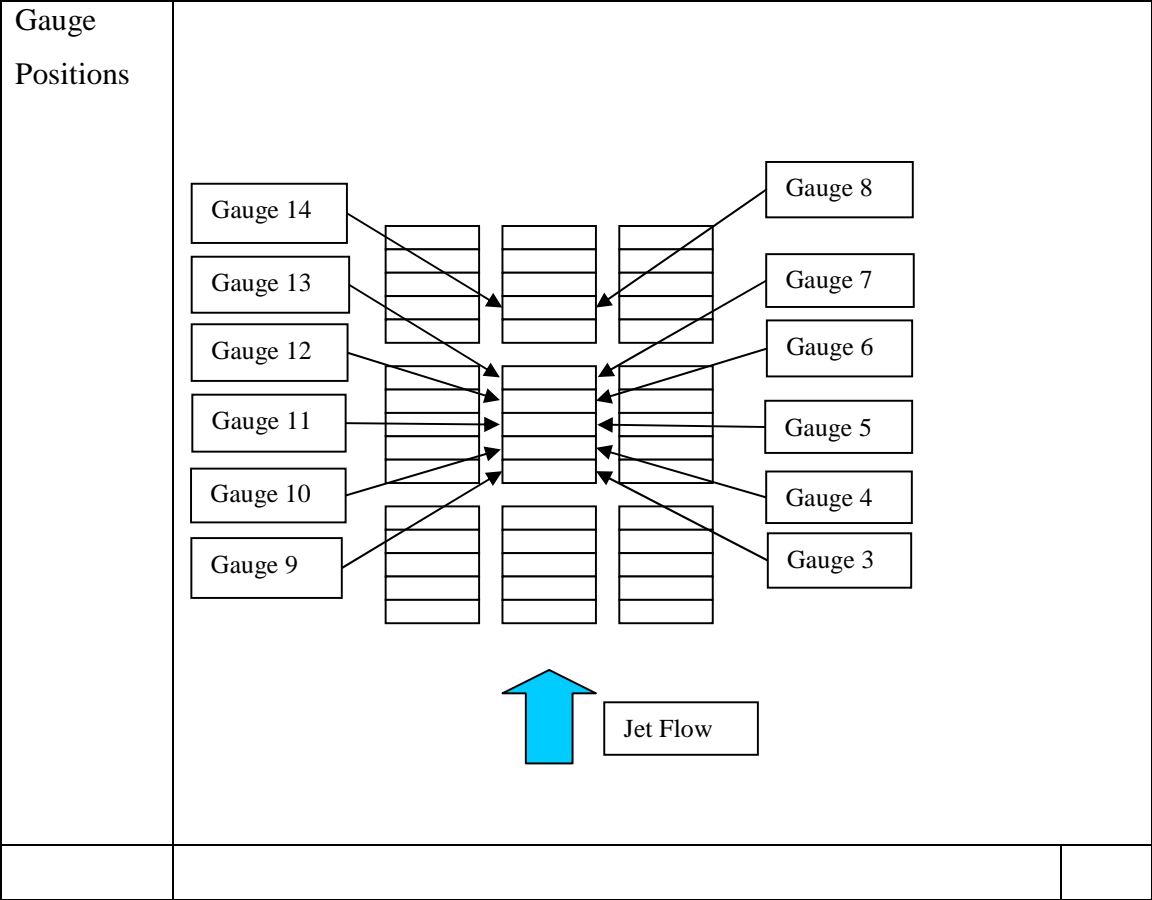
| | |
|----------------------|---|
| <p>Jet footprint</p> |  <p>Shaded blocks are interconnected unshaded are individually supported</p> <p>Jet footprint onto blocks</p> <p>Jet Flow</p> |
| <p>Comments</p> | <p>The test was carried out with the blocks installed as groups with the centre group of blocks being individually supported and unconnected to the adjacent blocks This is one in a sequence of tests on runs 10-14.</p> |

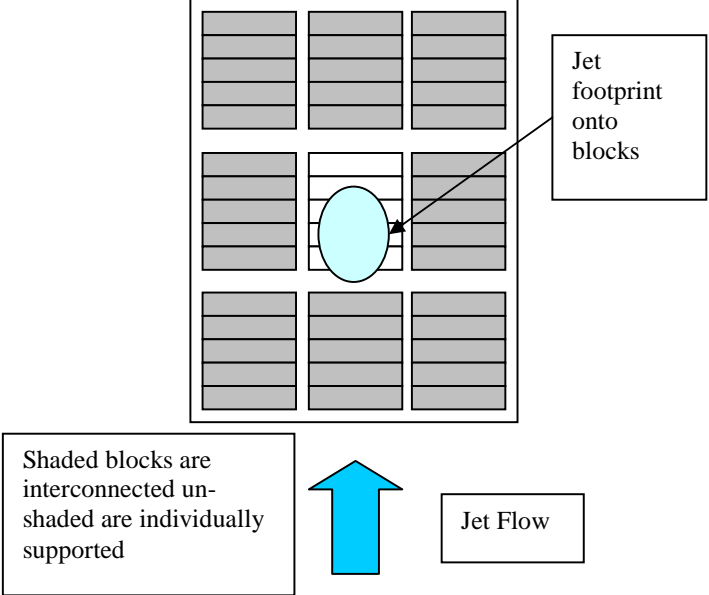
The loads on blocks 1 and 2 are similar with block 1 being slightly greater on average although the peak load on block one is nearly twice that of block 2. Again very little load is shown on blocks 3 and 4



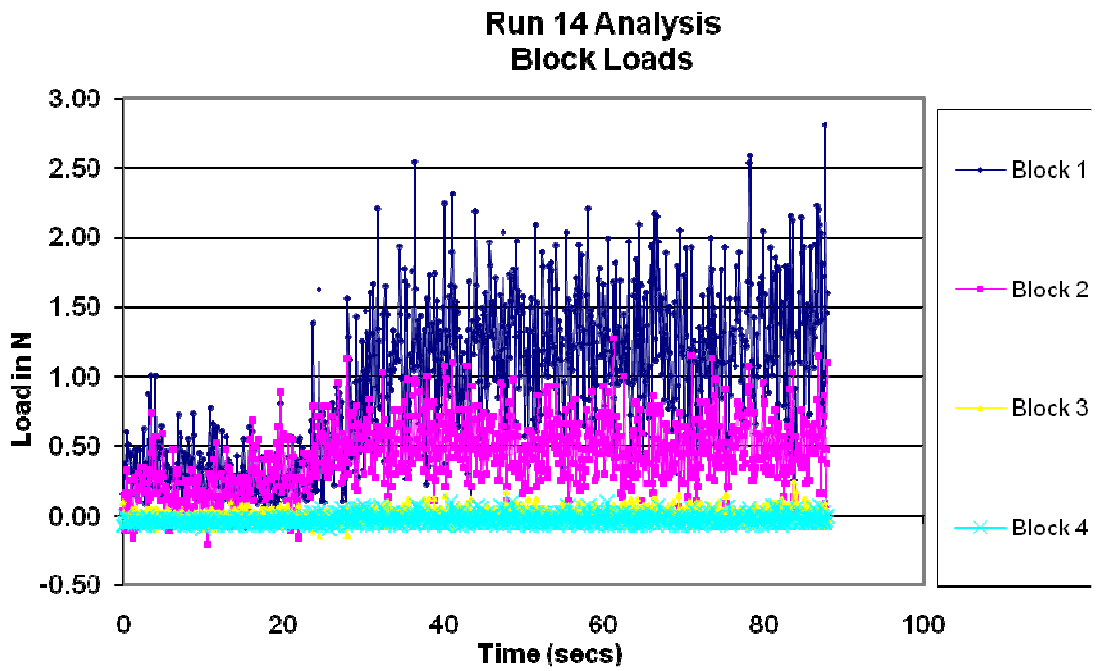
RUN 14

| Run No 14 | | |
|------------------|---|--|
| | | |
| Jet Angle | 50 degrees to horizontal | |
| | | |
| Jet velocity | 1.00 ms ⁻¹ (prototype 4.46ms ⁻¹) | |
| | | |
| Air Flow | 17% | |
| | | |
| Seabed Location | Down | |
| | | |



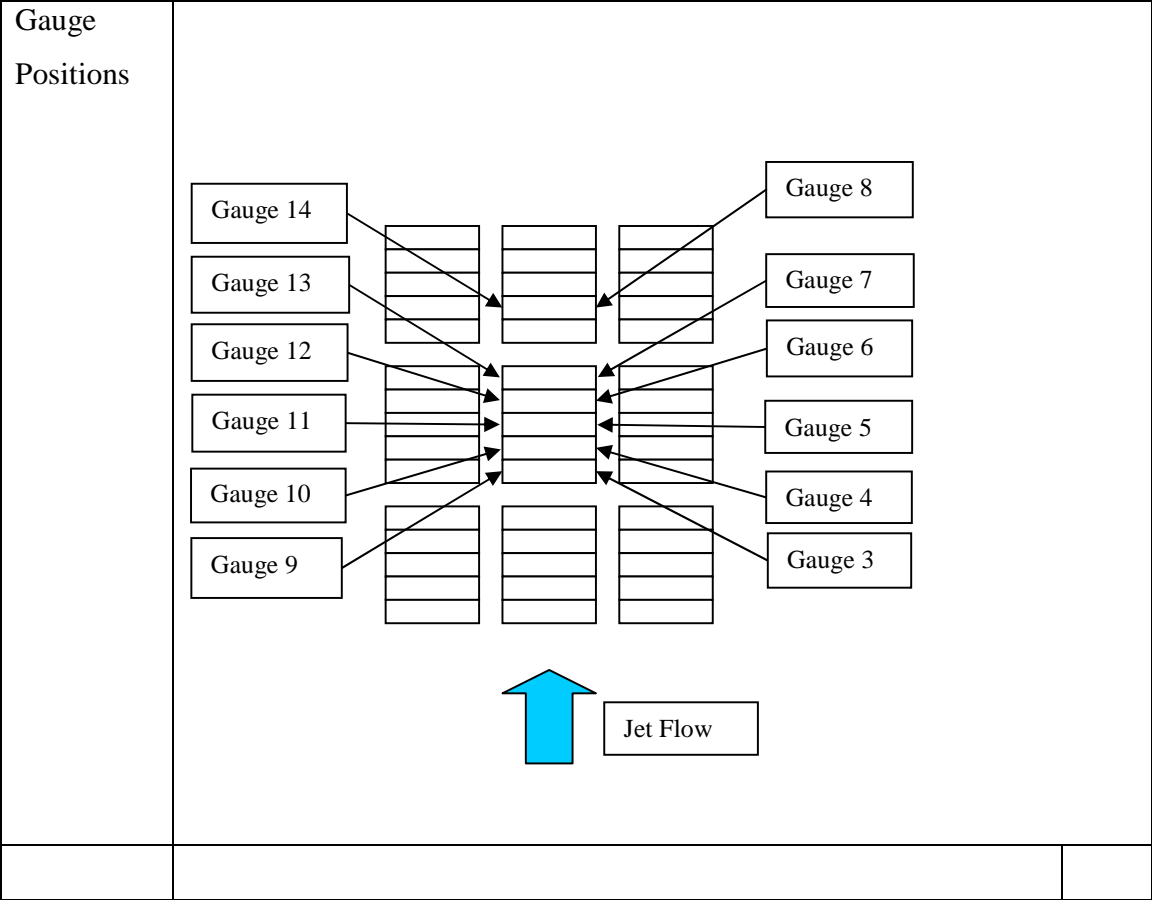
| | |
|----------------------|---|
| <p>Jet footprint</p> |  <p>Shaded blocks are interconnected unshaded are individually supported</p> <p>Jet footprint onto blocks</p> <p>Jet Flow</p> |
| <p>Comments</p> | <p>The test was carried out with the blocks installed as groups with the centre group of blocks being individually supported and unconnected to the adjacent blocks This is one in a sequence of tests on runs 10-14.</p> |

Blocks 1 and 3 both showed significant loads and in this run block 2 had very little recorded load



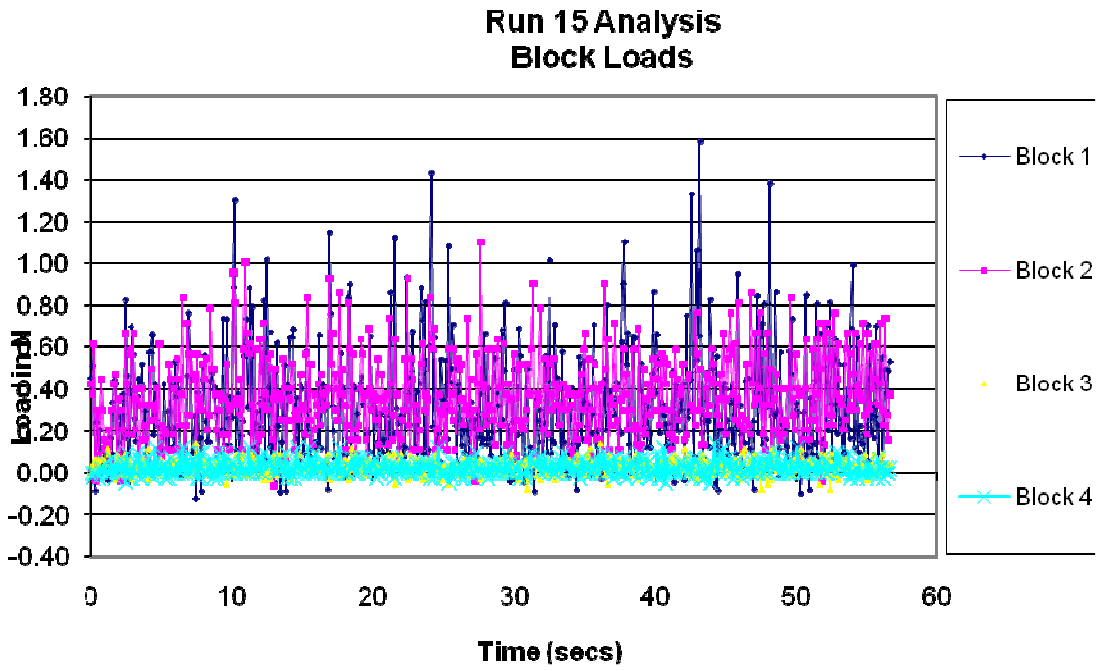
RUN 15

| Run No 15 | | |
|------------------|--|--|
| | | |
| Jet Angle | 50 degrees to horizontal | |
| | | |
| Jet velocity | 2.49 ms ⁻¹ (prototype 11.31ms ⁻¹) | |
| | | |
| Air Flow | 0 | |
| | | |
| Seabed Location | Down | |
| | | |



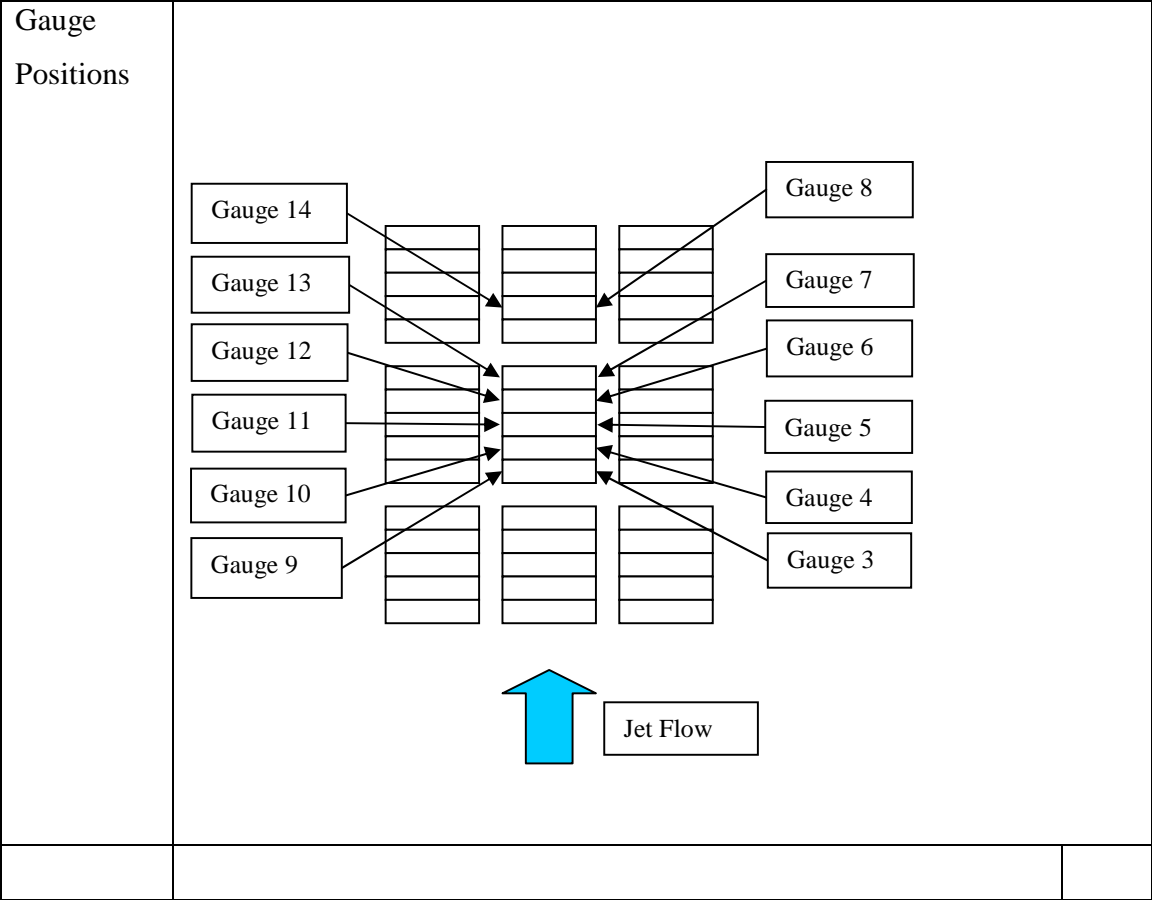
| | |
|----------------------|---|
| <p>Jet footprint</p> | <p>Shaded blocks are interconnected unshaded are individually supported</p> <p>Jet footprint onto blocks</p> <p>Jet Flow</p> |
| <p>Comments</p> | <p>The test was carried out with the blocks installed as groups with the centre group of blocks being individually supported and unconnected to the adjacent blocks This is one in a sequence of tests on runs 15-17.</p> |

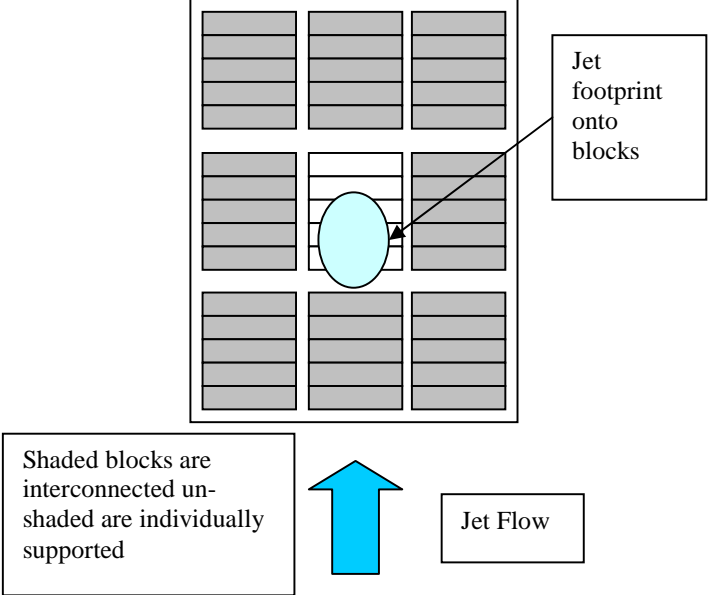
The maximum loads on block1 is about 50% greater than on the previous run, this is to be expected due to the increase in jet speed. In this case it is also accompanied by much more load oscillation



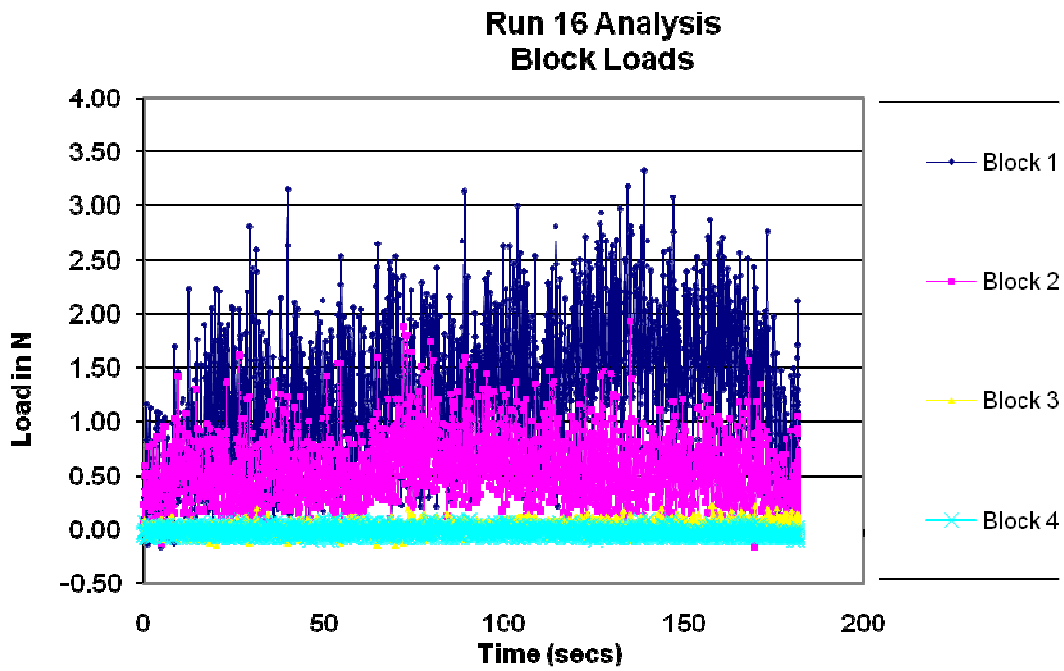
RUN 16

| Run No 16 | | |
|------------------|--|--|
| | | |
| Jet Angle | 50 degrees to horizontal | |
| | | |
| Jet velocity | 2.49 ms ⁻¹ (prototype 11.31ms ⁻¹) | |
| | | |
| Air Flow | 7% | |
| | | |
| Seabed Location | Down | |
| | | |



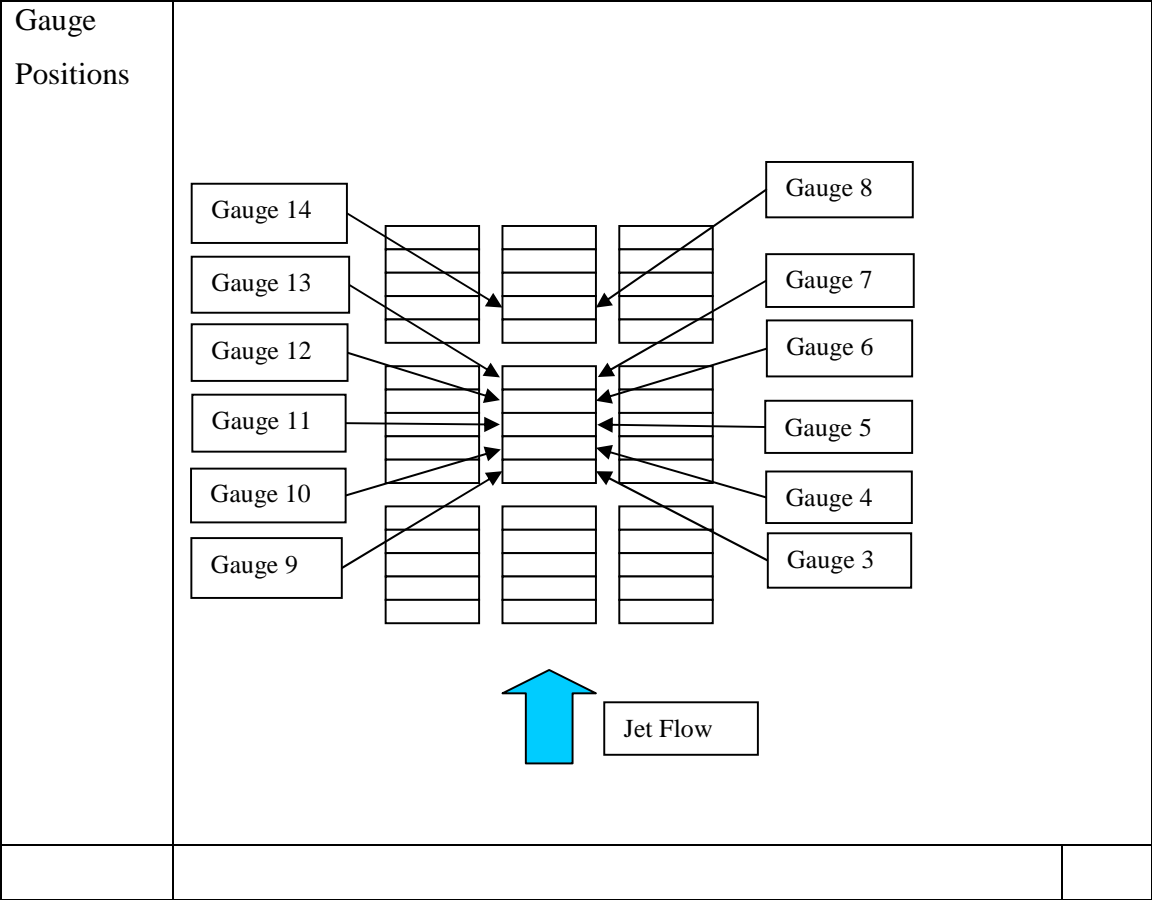
| | |
|----------------------|---|
| <p>Jet footprint</p> |  <p>Shaded blocks are interconnected unshaded are individually supported</p> <p>Jet Flow</p> <p>Jet footprint onto blocks</p> |
| <p>Comments</p> | <p>The test was carried out with the blocks installed as groups with the centre group of blocks being individually supported and unconnected to the adjacent blocks This is one in a sequence of tests on runs 15-17.</p> |

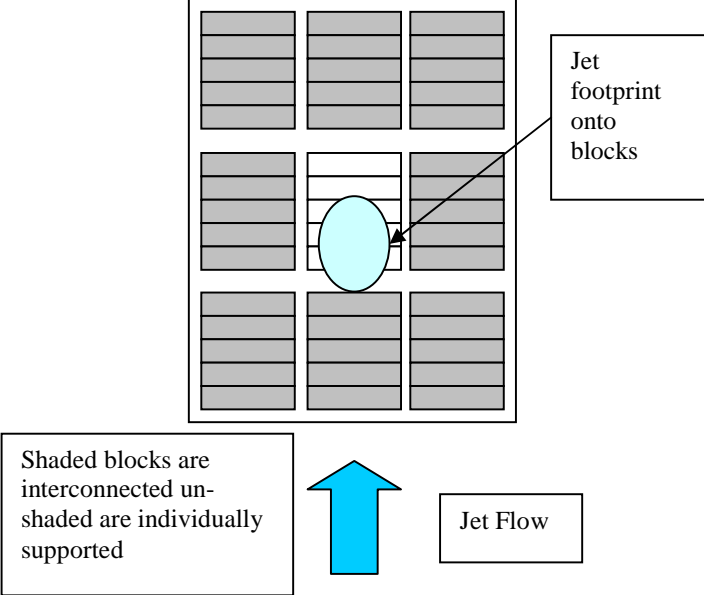
Blocks 1 and 3 experienced considerably more load than blocks 2 and 4 in particular block 1 showed a much greater load range than any of the other blocks



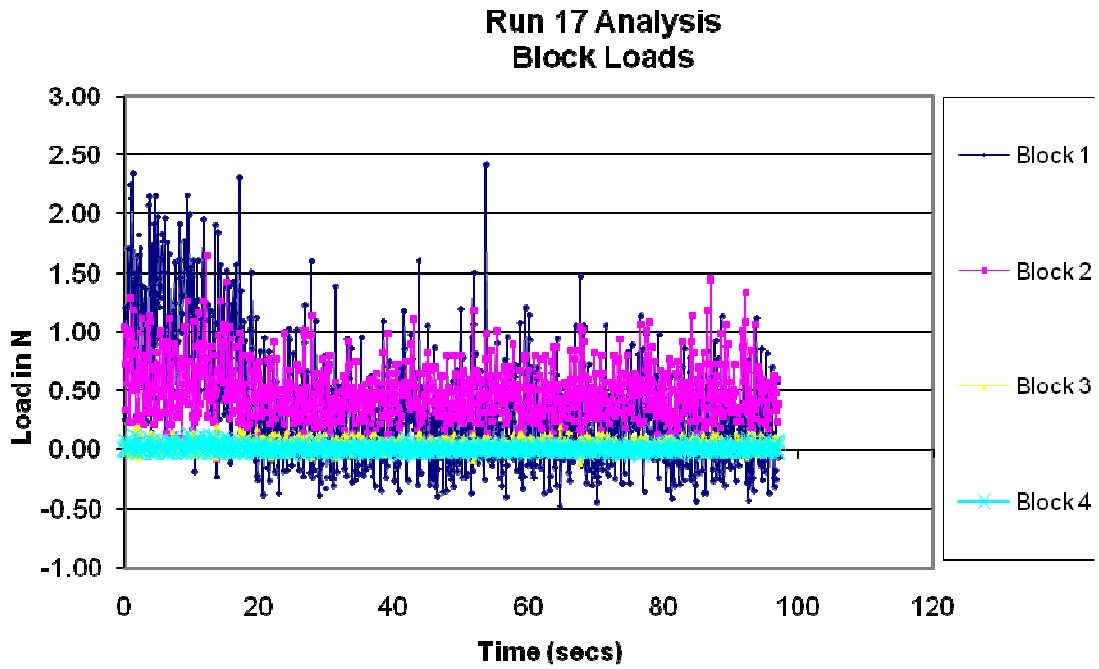
RUN 17

| Run No 17 | | |
|-----------------|--|--|
| | | |
| Jet Angle | 50 degrees to horizontal | |
| | | |
| Jet velocity | 2.49 ms ⁻¹ (prototype 11.31ms ⁻¹) | |
| | | |
| Air Flow | 0 | |
| | | |
| Seabed Location | Down | |
| | | |



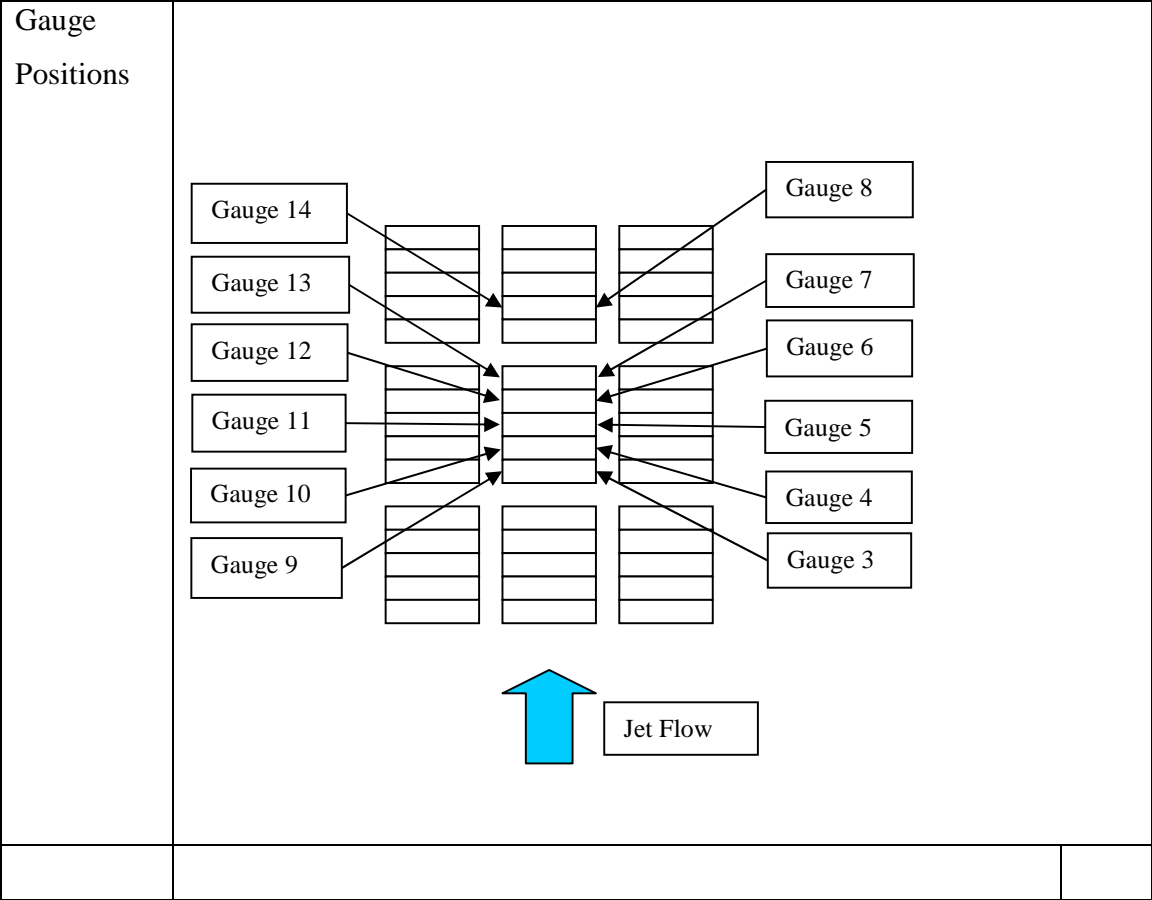
| | |
|----------------------|---|
| <p>Jet footprint</p> |  <p>Shaded blocks are interconnected unshaded are individually supported</p> <p>Jet Flow</p> <p>Jet footprint onto blocks</p> |
| <p>Comments</p> | <p>The test was carried out with the blocks installed as groups with the centre group of blocks being individually supported and unconnected to the adjacent blocks This is one in a sequence of tests on runs 15-17.</p> |

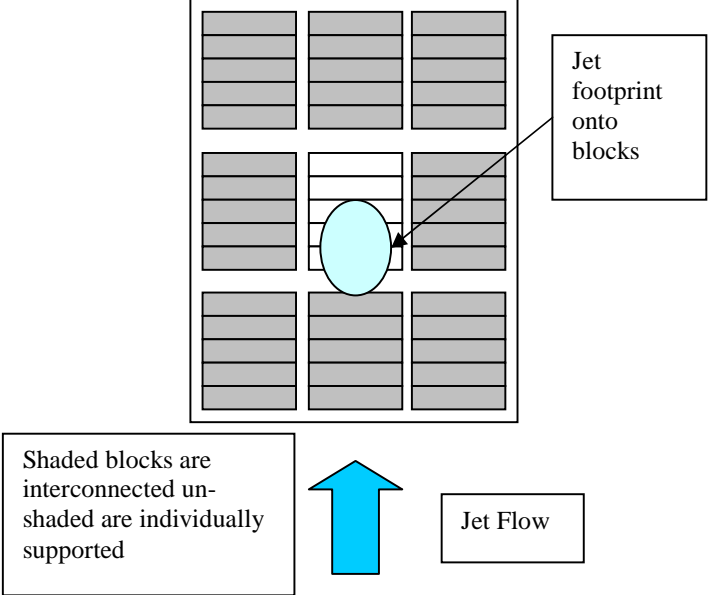
The blocks had fairly high loading at the commencement of the run and then the loads dropped markedly from the observations during the test run the blocks appeared to interlock with the adjacent blocks



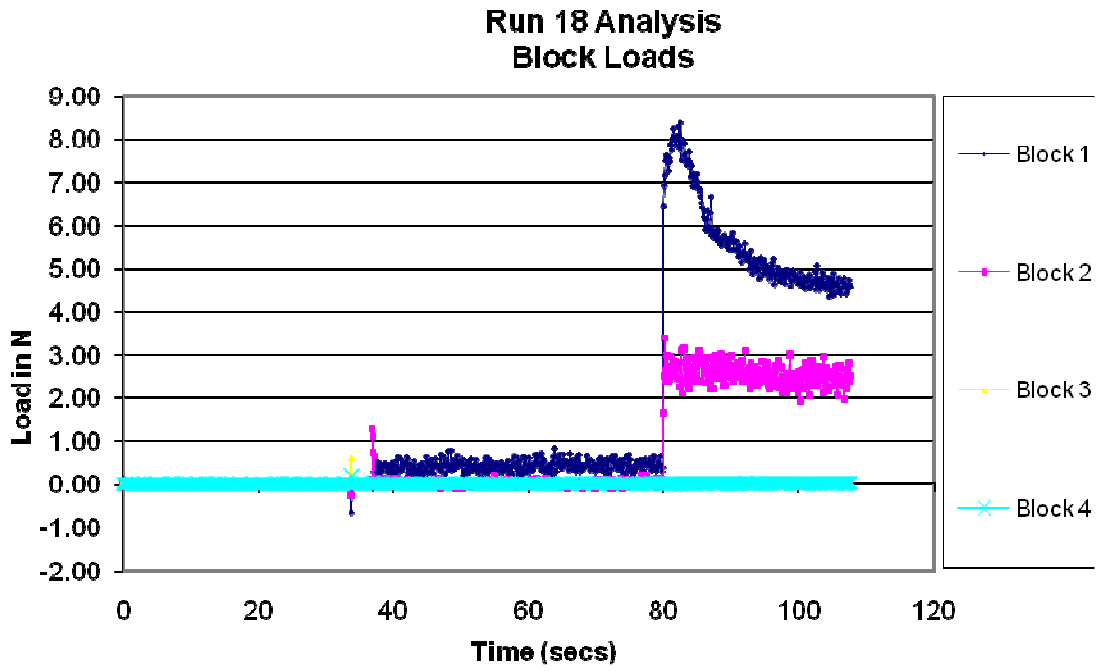
RUN 18

| Run No 18 | | |
|------------------|---|--|
| | | |
| Jet Angle | 50 degrees to horizontal | |
| | | |
| Jet velocity | 1.00 ms ⁻¹ (prototype 4.46ms ⁻¹) | |
| | | |
| Air Flow | 0 | |
| | | |
| Seabed Location | Up | |
| | | |



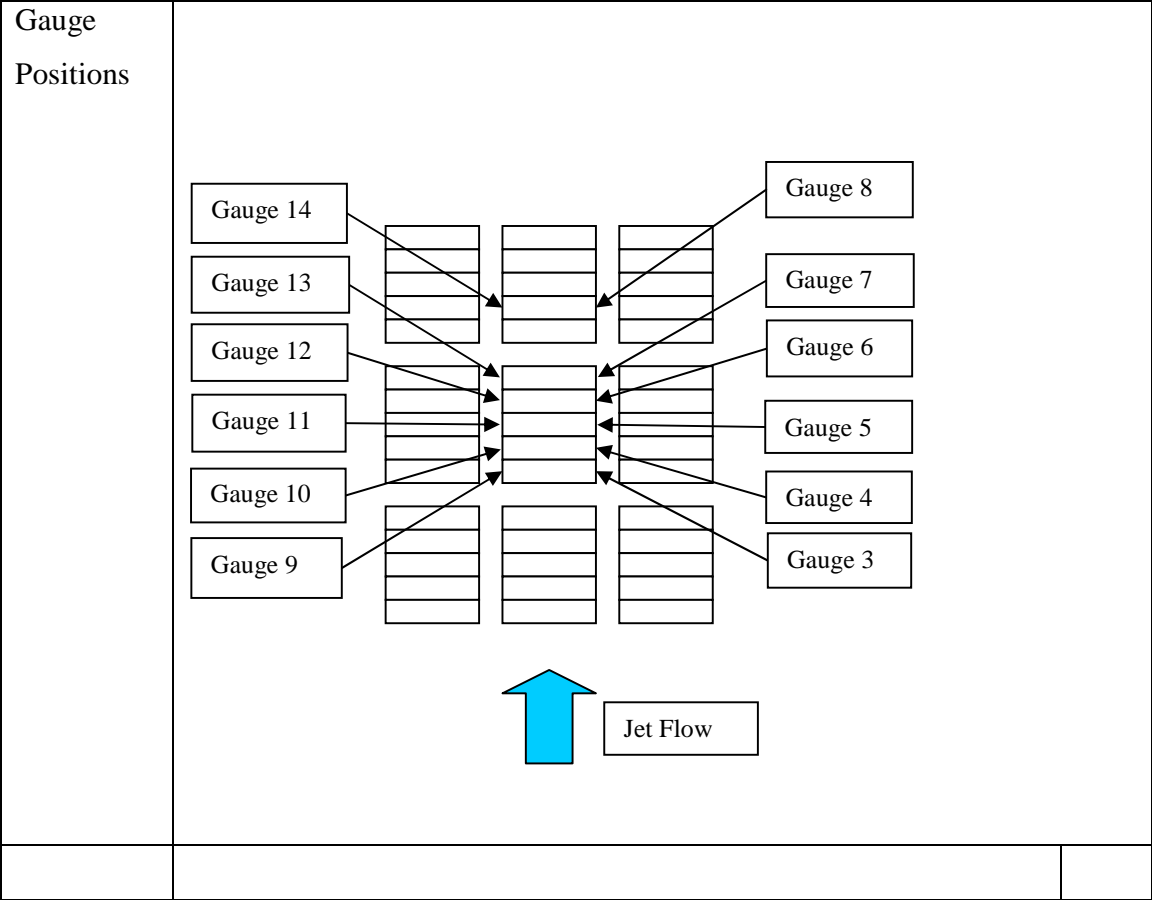
| | |
|----------------------|---|
| <p>Jet footprint</p> |  <p>Shaded blocks are interconnected unshaded are individually supported</p> <p>Jet footprint onto blocks</p> <p>Jet Flow</p> |
| <p>Comments</p> | <p>The test was carried out with the blocks installed as groups with the centre group of blocks being individually supported and unconnected to the adjacent blocks This is one in a sequence of tests on runs 18-20.</p> |

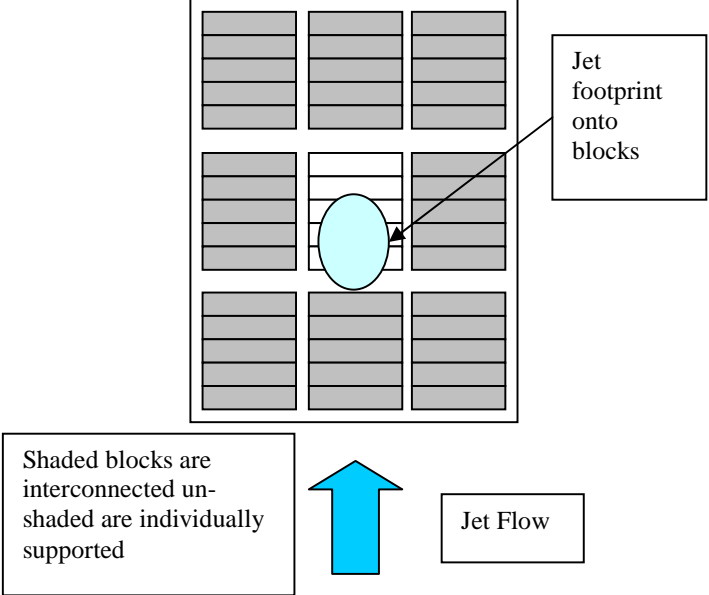
The peak loads that appeared on this run could not be explained from the visual observations but from the graph can be seen to be a single event and are not combined with any increase in load range or oscillation. The peak results from this have therefore been disregarded as anomalous.



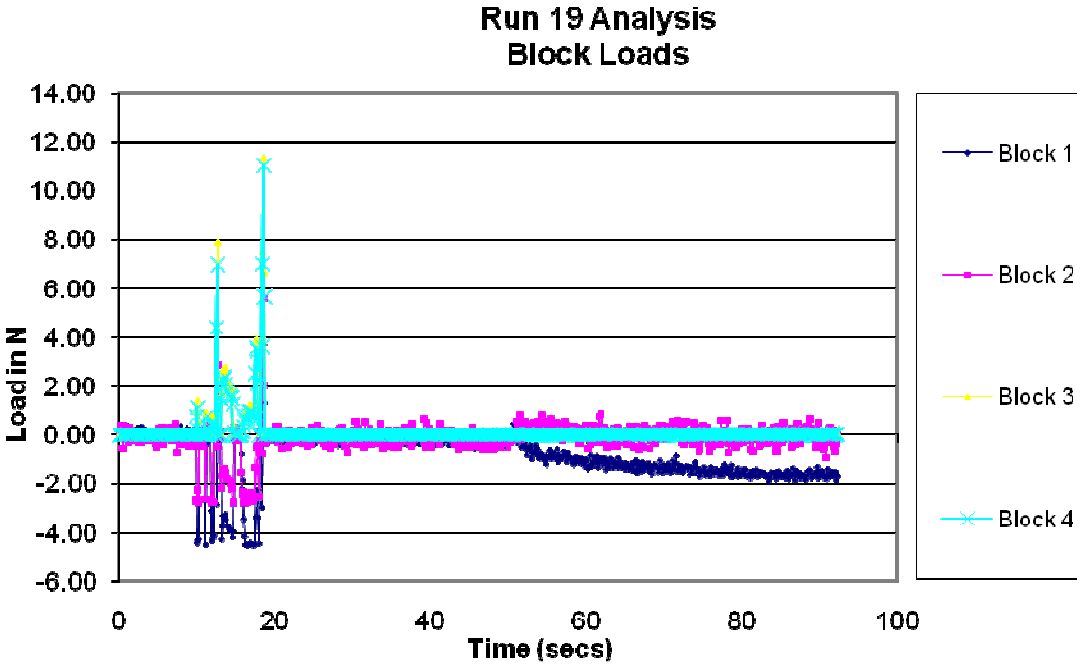
RUN 19

| Run No 19 | | |
|-----------------|---|--|
| | | |
| Jet Angle | 50 degrees to horizontal | |
| | | |
| Jet velocity | 1.00 ms ⁻¹ (prototype 4.46ms ⁻¹) | |
| | | |
| Air Flow | 17% | |
| | | |
| Seabed Location | Up | |
| | | |



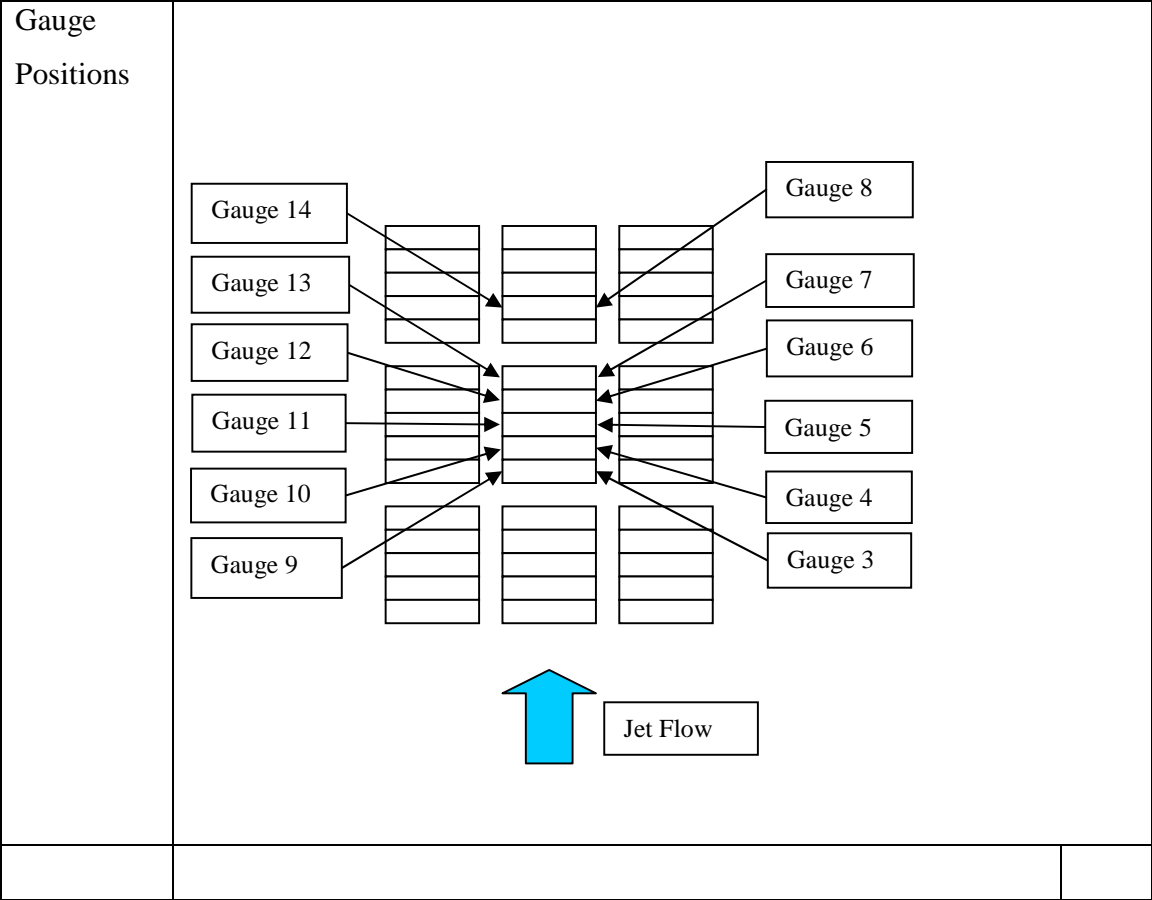
| | |
|----------------------|---|
| <p>Jet footprint</p> |  <p>Shaded blocks are interconnected unshaded are individually supported</p> <p>Jet footprint onto blocks</p> <p>Jet Flow</p> |
| <p>Comments</p> | <p>The test was carried out with the blocks installed as groups with the centre group of blocks being individually supported and unconnected to the adjacent blocks This is one in a sequence of tests on runs 18-20.</p> |

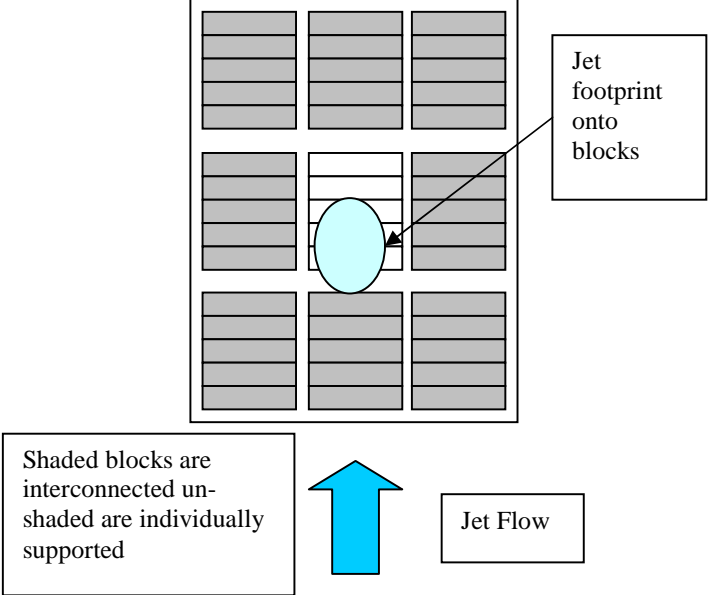
It appears that the blocks have moved relative to each other and the negative block loads are balancing the positive loads. It is believed that this demonstrates the 'ratchet' effect of the blocks moving relative to each other.



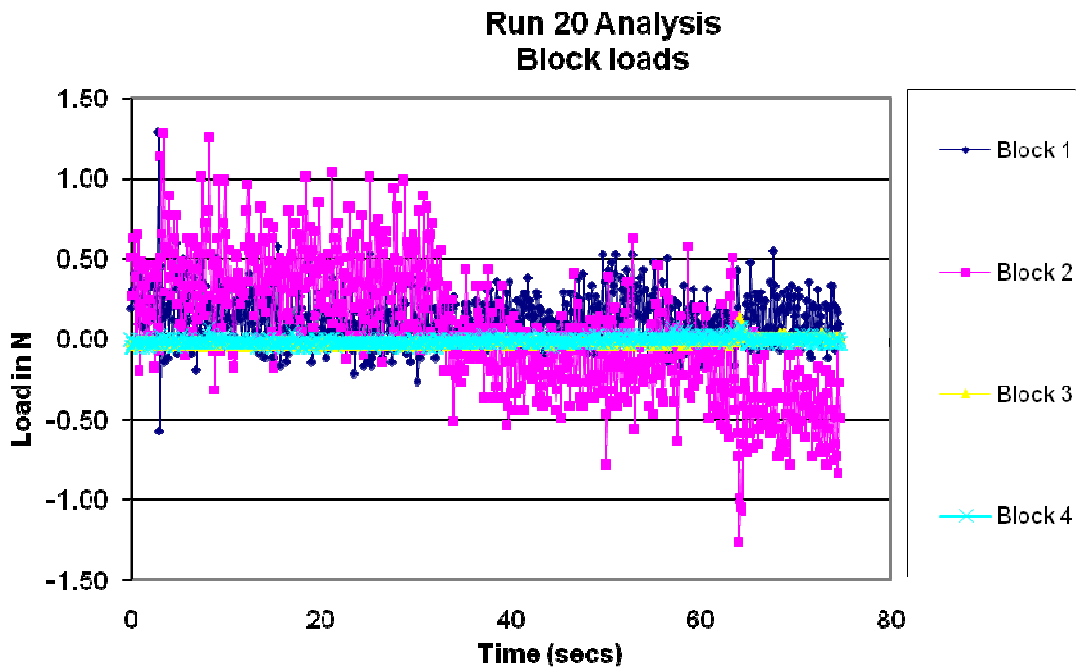
RUN 20

| Run No 20 | | |
|-----------------|---|--|
| | | |
| Jet Angle | 50 degrees to horizontal | |
| | | |
| Jet velocity | 1.00 ms ⁻¹ (prototype 4.46ms ⁻¹) | |
| | | |
| Air Flow | 0 | |
| | | |
| Seabed Location | Up | |
| | | |



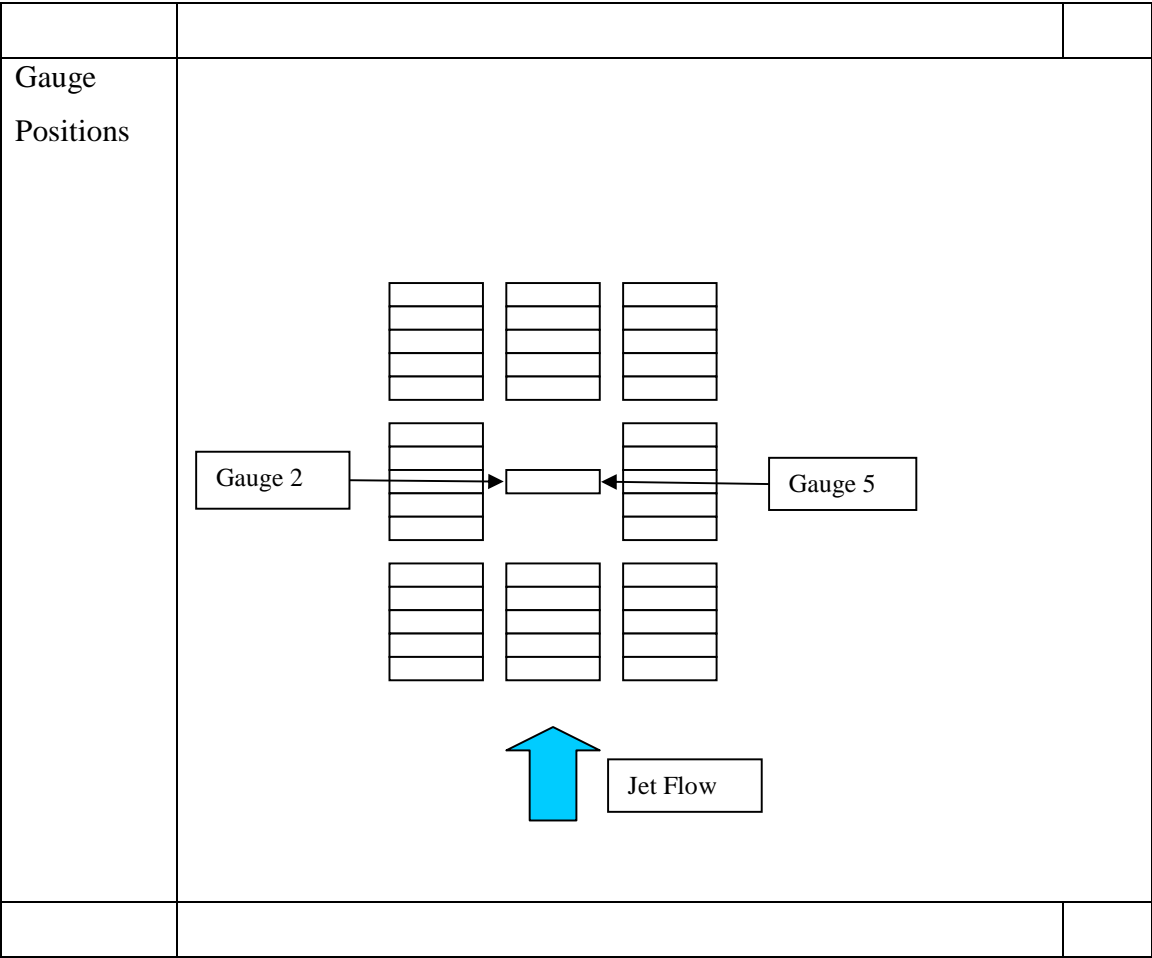
| | |
|----------------------|---|
| <p>Jet footprint</p> |  <p>Shaded blocks are interconnected unshaded are individually supported</p> <p>Jet footprint onto blocks</p> <p>Jet Flow</p> |
| <p>Comments</p> | <p>The test was carried out with the blocks installed as groups with the centre group of blocks being individually supported and unconnected to the adjacent blocks This is one in a sequence of tests on runs 18-20.</p> |

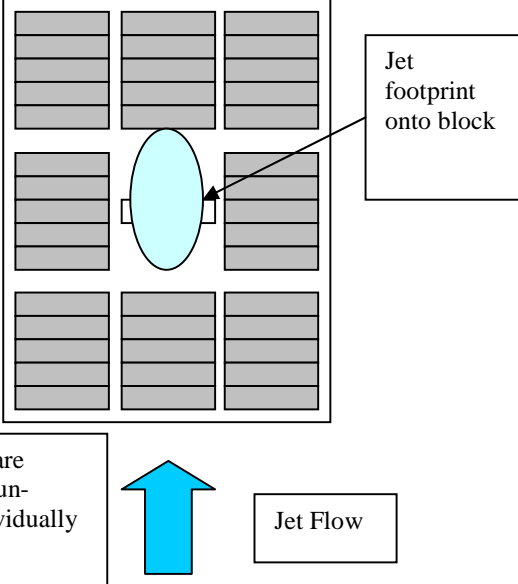
Block 1 displayed a significant load over a very short time frame during this run. Both gauges on the same block showed this load simultaneously which is believed to result from a block ratchet effect as previously described.



RUN 21

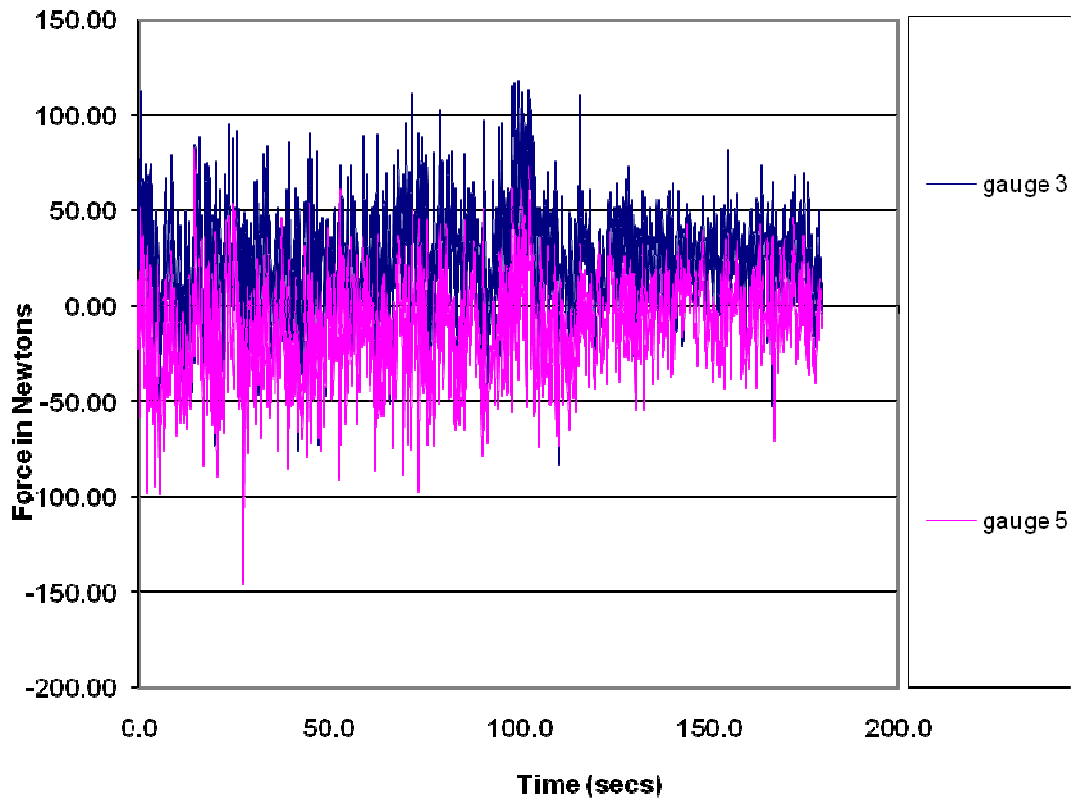
| Run No 21 | | |
|------------------|--|--|
| | | |
| Jet Angle | 40 degrees to horizontal | |
| | | |
| Jet velocity | 2.76 ms ⁻¹ (prototype 12.31ms ⁻¹) | |
| | | |
| Air Flow | 0 | |
| | | |
| Seabed Location | Down | |



| | |
|----------------------|--|
| <p>Jet footprint</p> |  |
| <p>Comments</p> | <p>The test was carried out with the blocks installed as groups with the centre group of blocks being individually supported and unconnected to the adjacent blocks.</p> |

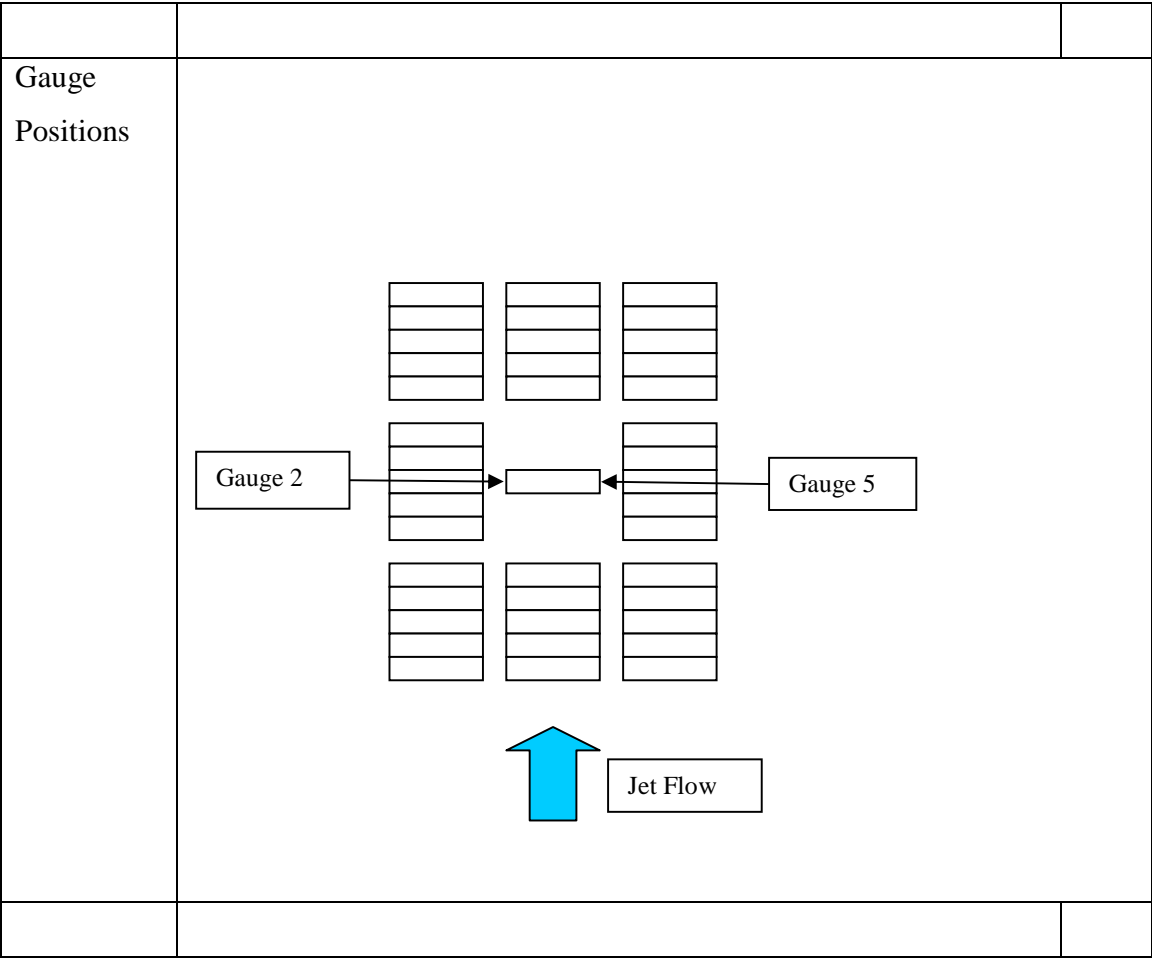
This was the first run using a single block that was positioned so that it did not contact the adjacent blocks. This freedom of movement provided a much clearer view on the block behaviour, since the applied loads were not masked by load transfer to other blocks. The forces measured on the single block were at least ten times more than with the multiple blocks. The load oscillations were similar

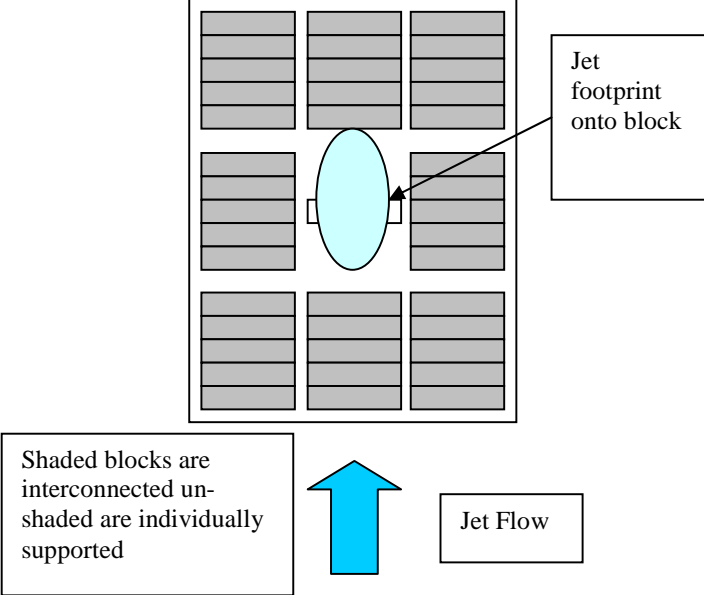
Run 21 Analysis



RUN 22

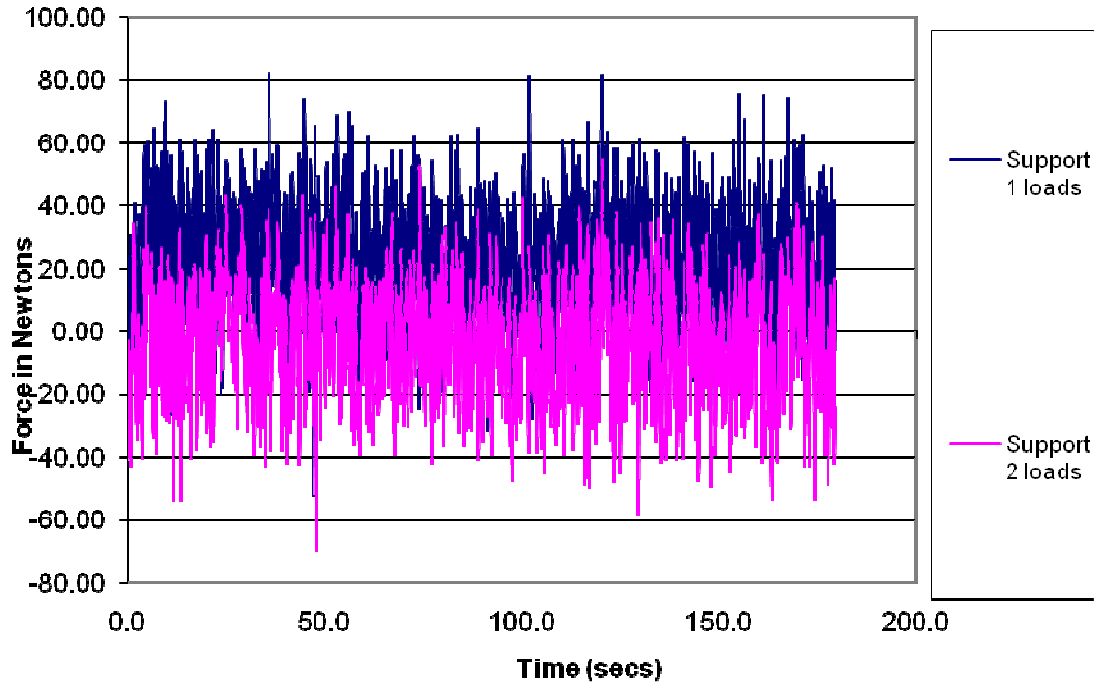
| Run No 22 | | |
|------------------|---|--|
| | | |
| Jet Angle | 40 degrees to horizontal | |
| Jet velocity | 2.00 ms ⁻¹ (prototype 8.92ms ⁻¹) | |
| Air Flow | 0 | |
| Seabed Location | Down | |



| | |
|----------------------|---|
| <p>Jet footprint</p> |  <p>Shaded blocks are interconnected unshaded are individually supported</p> <p>Jet footprint onto block</p> <p>Jet Flow</p> |
| <p>Comments</p> | <p>The test was carried out with the blocks installed as groups with the centre group of blocks being individually supported and unconnected to the adjacent blocks.</p> |

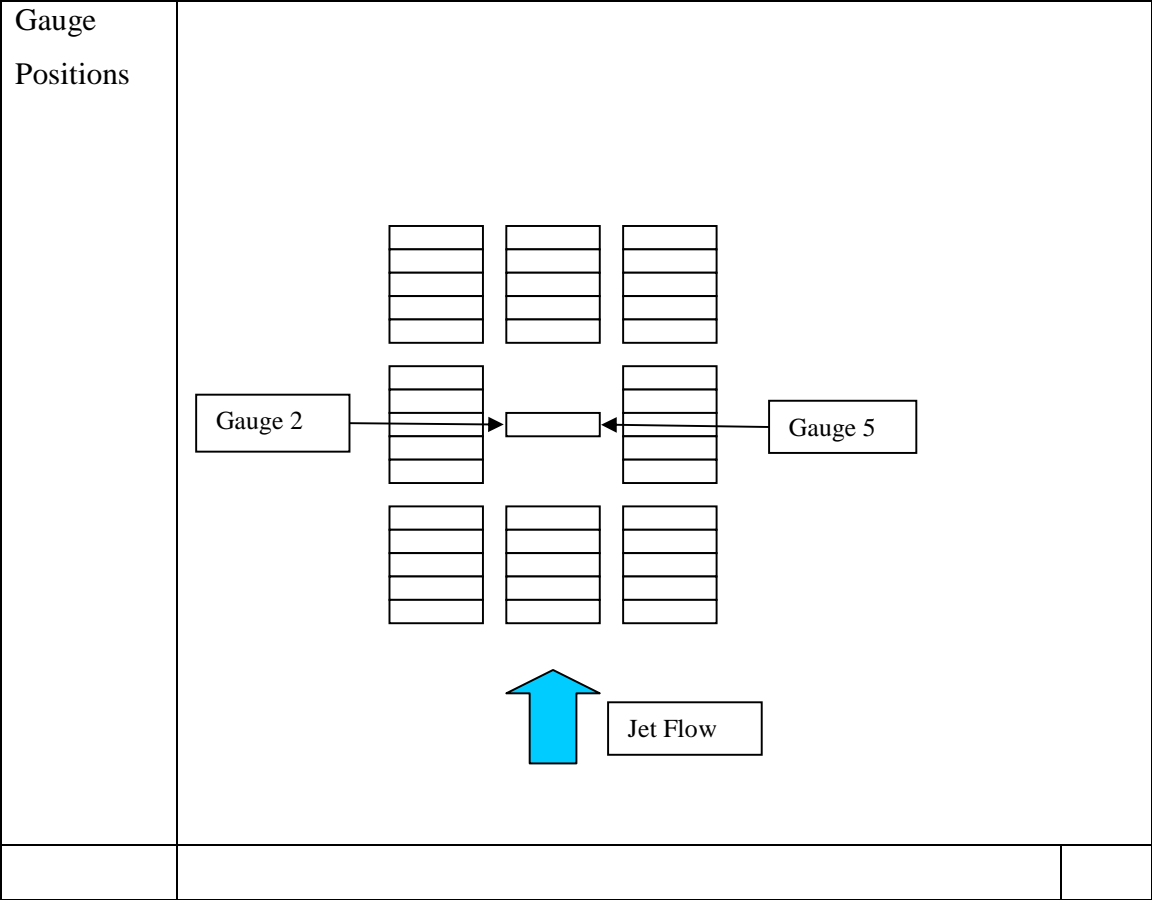
The reduction in jet velocity on this run showed a proportionate decrease in block loads and no significant change in oscillation frequency

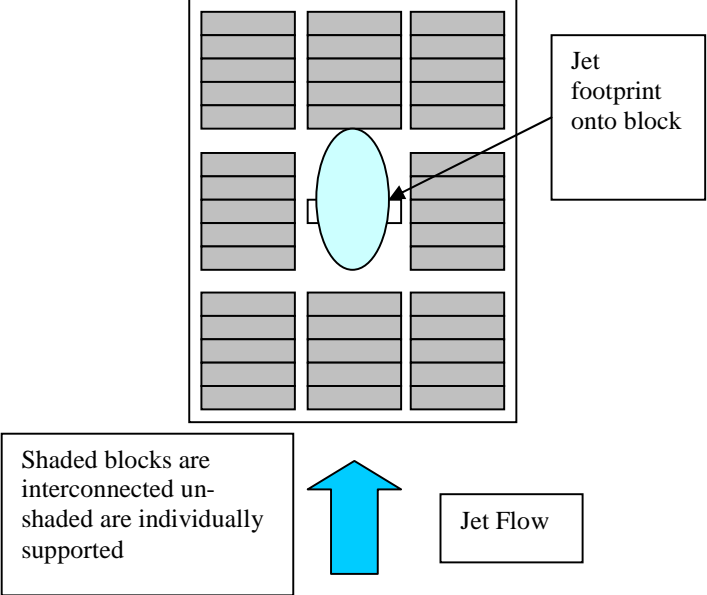
**Run 22 Analysis
Block Loads**



RUN 23

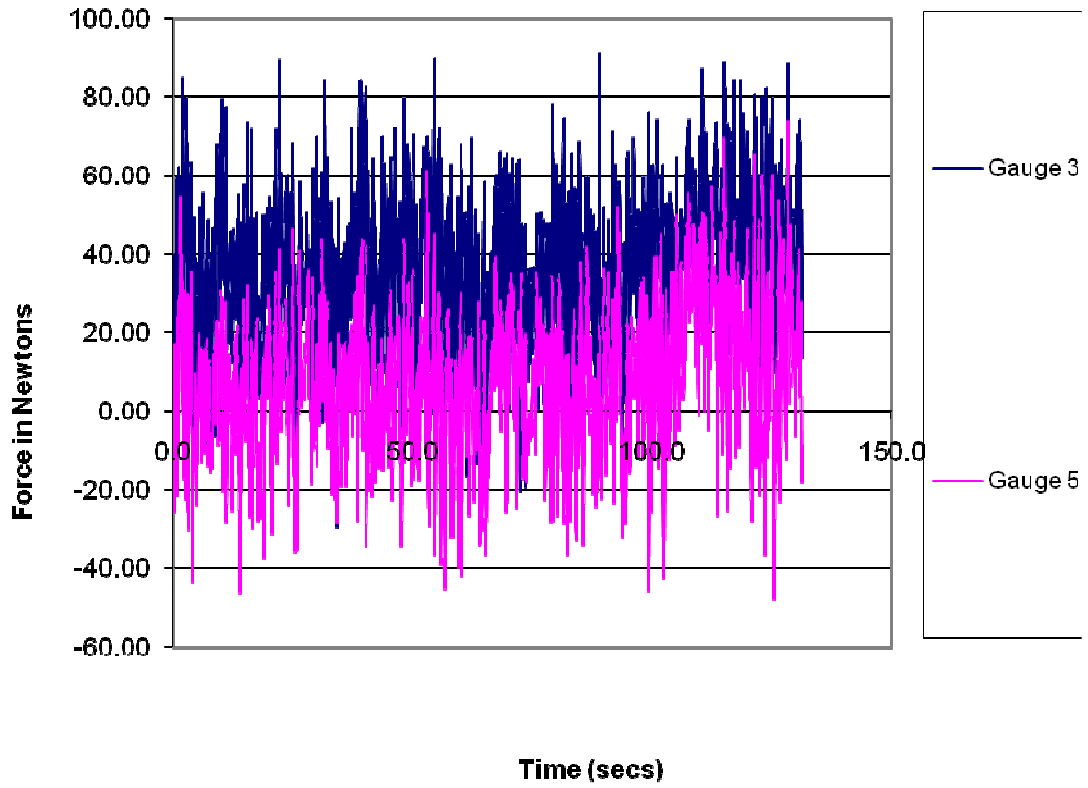
| Run No 23 | | |
|-----------------|---|--|
| Jet Angle | 40 degrees to horizontal | |
| Jet velocity | 2.00 ms ⁻¹ (prototype 8.92ms ⁻¹) | |
| Air Flow | 0 | |
| Seabed Location | Down | |
| | | |



| | |
|----------------------|---|
| <p>Jet footprint</p> |  <p>Shaded blocks are interconnected unshaded are individually supported</p> <p>Jet footprint onto block</p> <p>Jet Flow</p> |
| <p>Comments</p> | <p>The test was carried out with the blocks installed as groups with the centre group of blocks being individually supported and unconnected to the adjacent blocks.</p> |

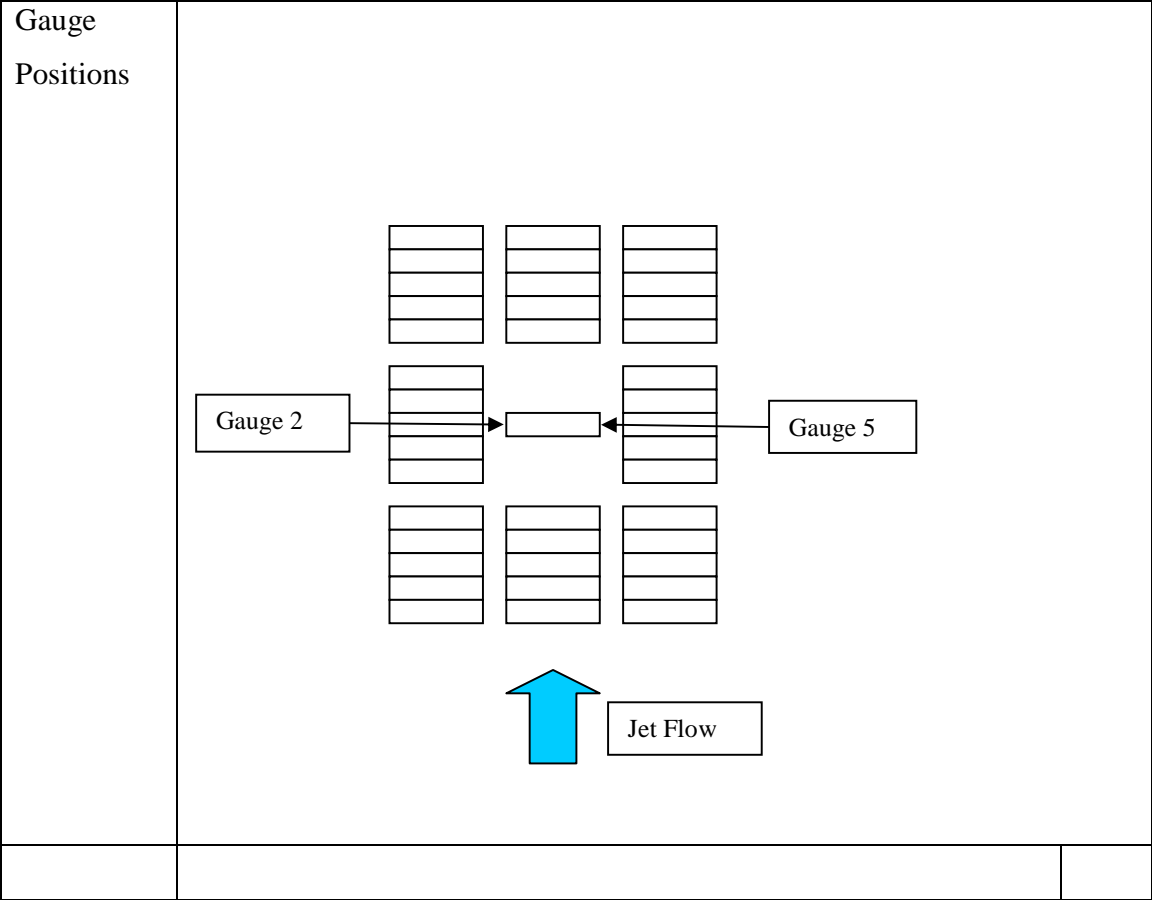
This run was similar to the previous one and used as a repeatability check. The results were very similar.

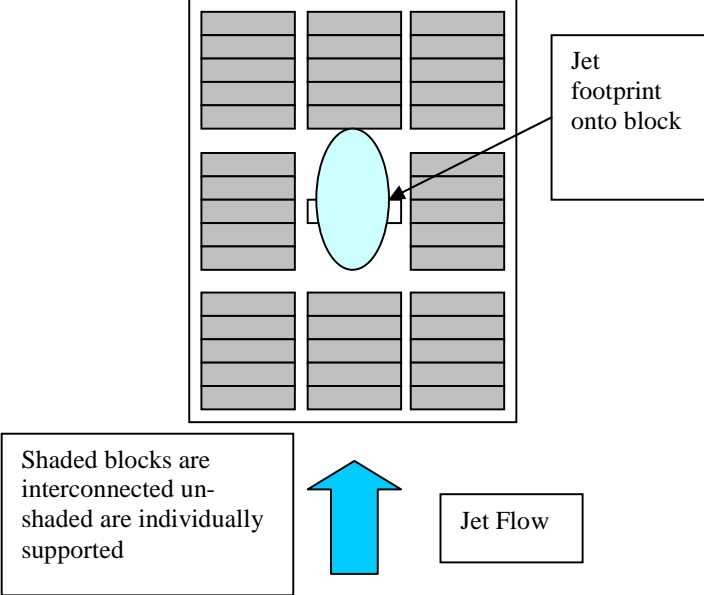
Run 23 Analysis



RUN 24

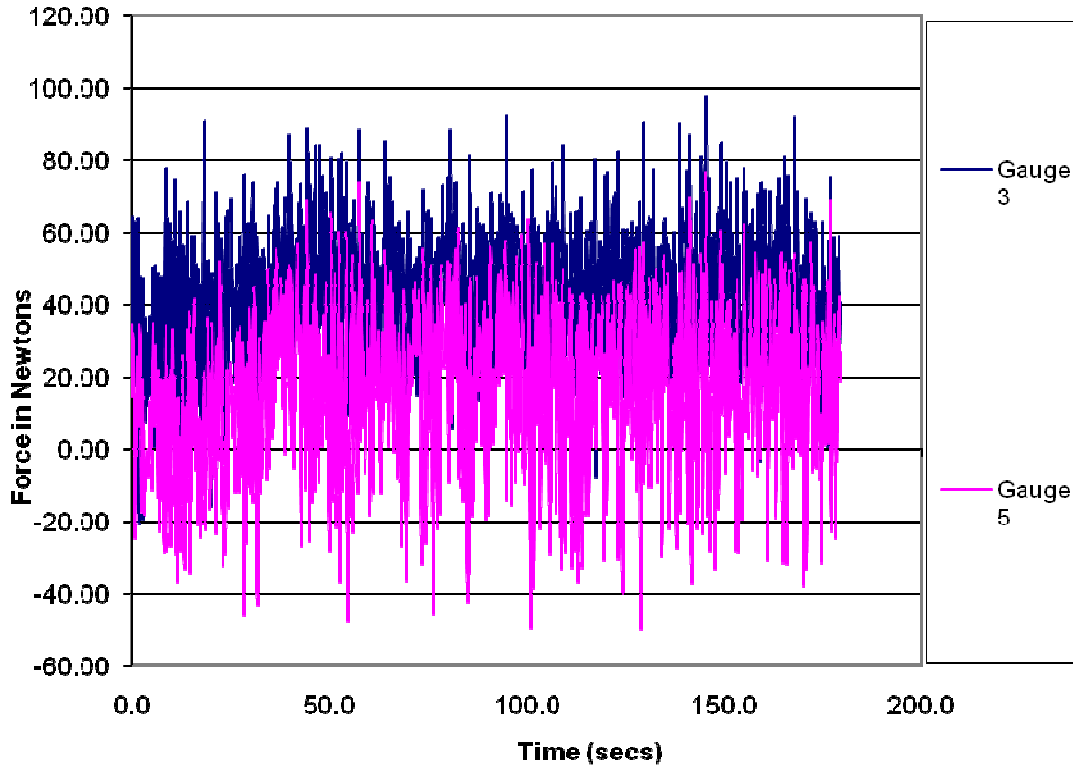
| Run No 24 | | |
|------------------|---|--|
| Jet Angle | 40 degrees to horizontal | |
| Jet velocity | 2.00 ms ⁻¹ (prototype 8.92ms ⁻¹) | |
| Air Flow | 9% | |
| Seabed Location | Down | |
| | | |



| | |
|----------------------|---|
| <p>Jet footprint</p> |  <p>Shaded blocks are interconnected unshaded are individually supported</p> <p>Jet footprint onto block</p> <p>Jet Flow</p> |
| <p>Comments</p> | <p>The test was carried out with the blocks installed as groups with the centre group of blocks being individually supported and unconnected to the adjacent blocks.</p> |

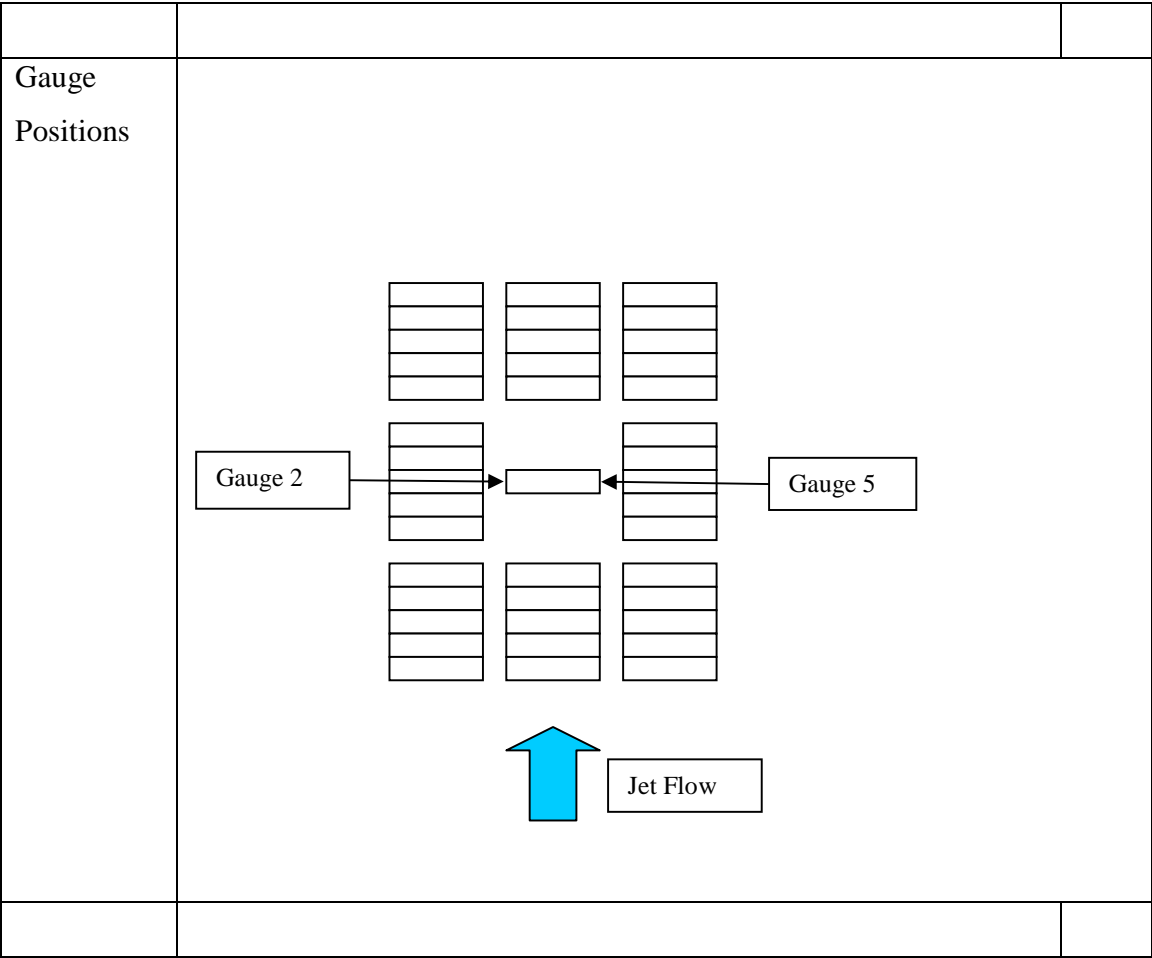
This run was the same as 23 except for a 9% air entrainment in the jet flow. In this case this gave a slightly higher maximum force reading

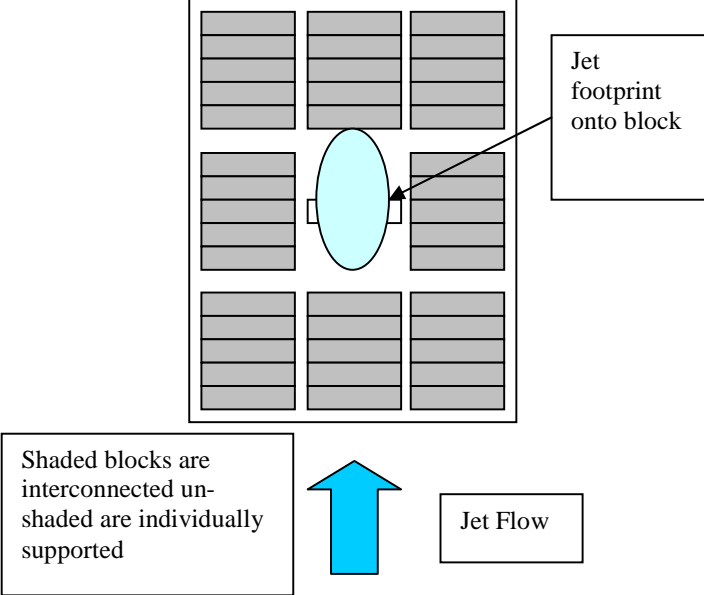
Run 24 Analysis



RUN 25

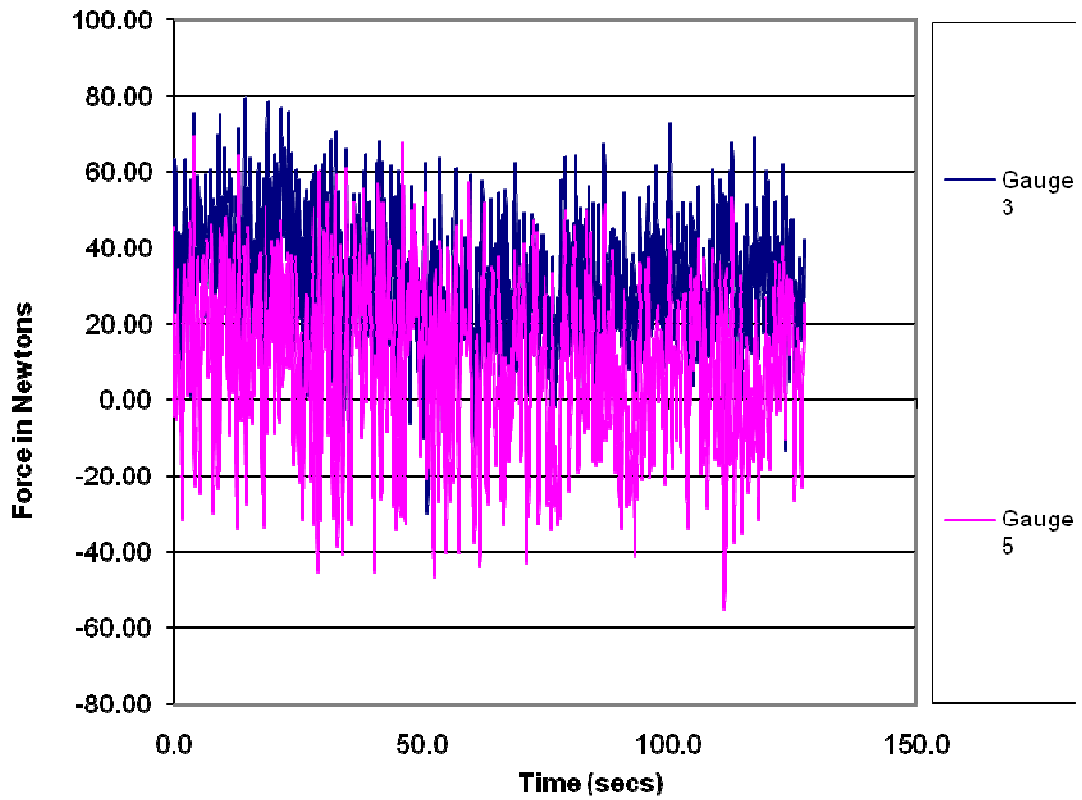
| Run No 25 | | |
|-----------------|---|--|
| Jet Angle | 40 degrees to horizontal | |
| Jet velocity | 2.00 ms ⁻¹ (prototype 8.92ms ⁻¹) | |
| Air Flow | 18% | |
| Seabed Location | Down | |



| | |
|----------------------|---|
| <p>Jet footprint</p> |  <p>Shaded blocks are interconnected unshaded are individually supported</p> <p>Jet footprint onto block</p> <p>Jet Flow</p> |
| <p>Comments</p> | <p>The test was carried out with the blocks installed as groups with the centre group of blocks being individually supported and unconnected to the adjacent blocks.</p> |

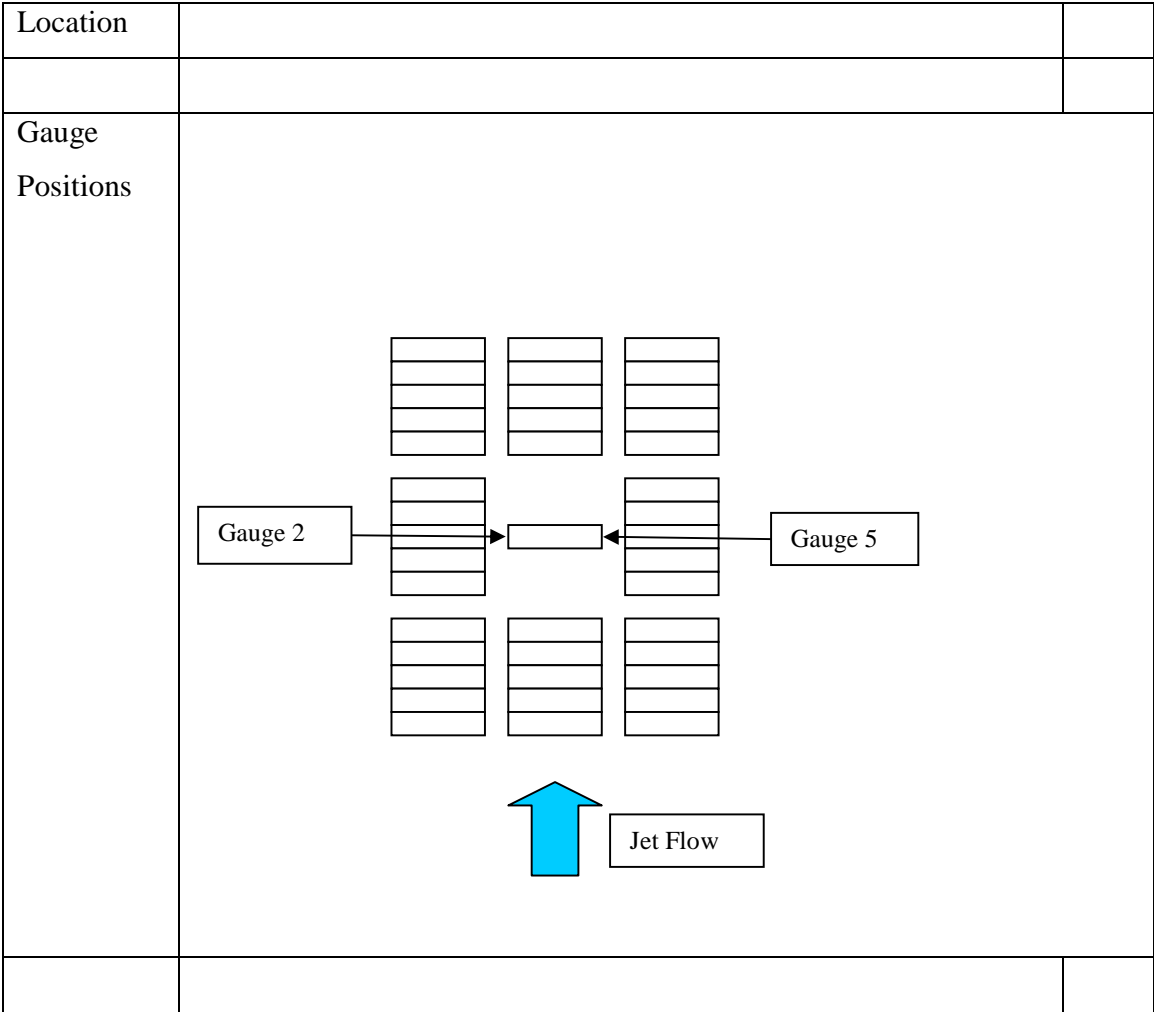
The increase in the airflow gave a noticeable decrease in the maximum forces from the jet on this run

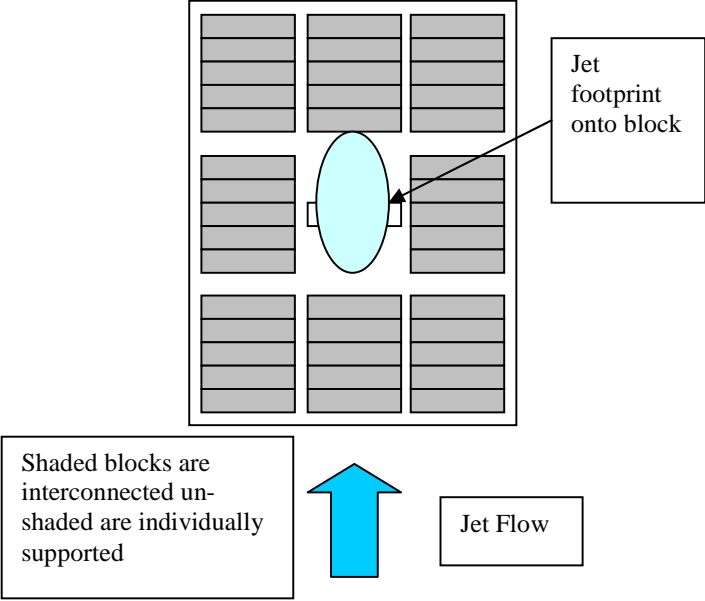
Run 25 Analysis



RUN 26

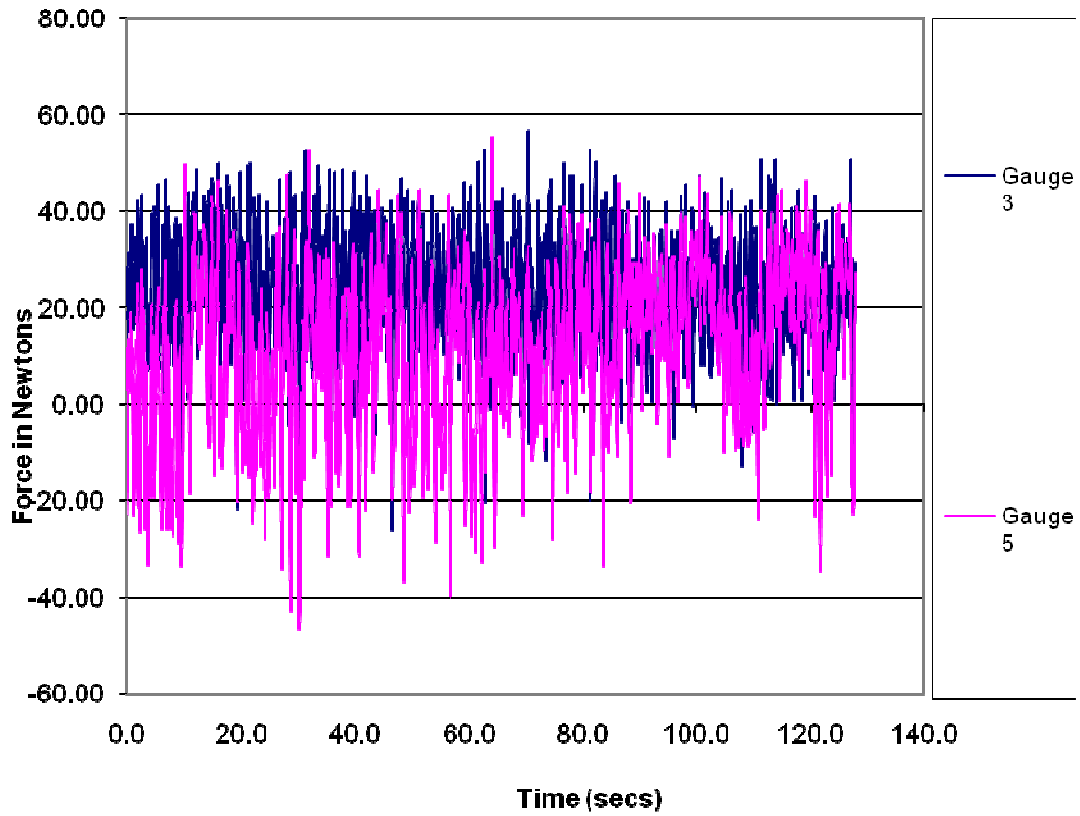
| Run No 26 | | |
|--------------|---|--|
| Jet Angle | 40 degrees to horizontal | |
| Jet velocity | 2.00 ms ⁻¹ (prototype 8.92ms ⁻¹) | |
| Air Flow | 0 | |
| Seabed | Down | |



| | |
|----------------------|---|
| <p>Jet footprint</p> |  <p>Shaded blocks are interconnected unshaded are individually supported</p> <p>Jet footprint onto block</p> <p>Jet Flow</p> |
| <p>Comments</p> | <p>The test was carried out with the blocks installed as groups with the centre group of blocks being individually supported and unconnected to the adjacent blocks.</p> |

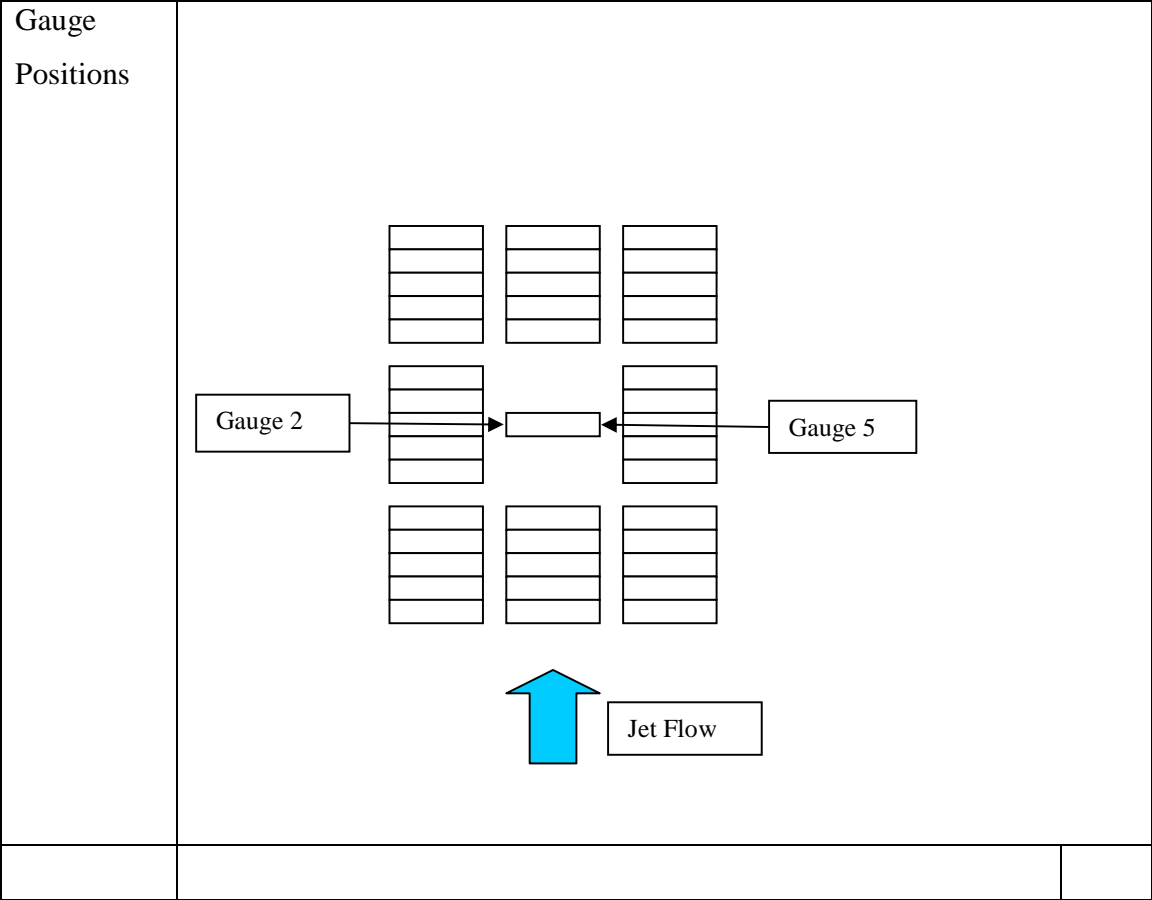
The further increase of air entrainment brought the maximum force of the jet down by almost 40% compared to the same flow with no air entrainment

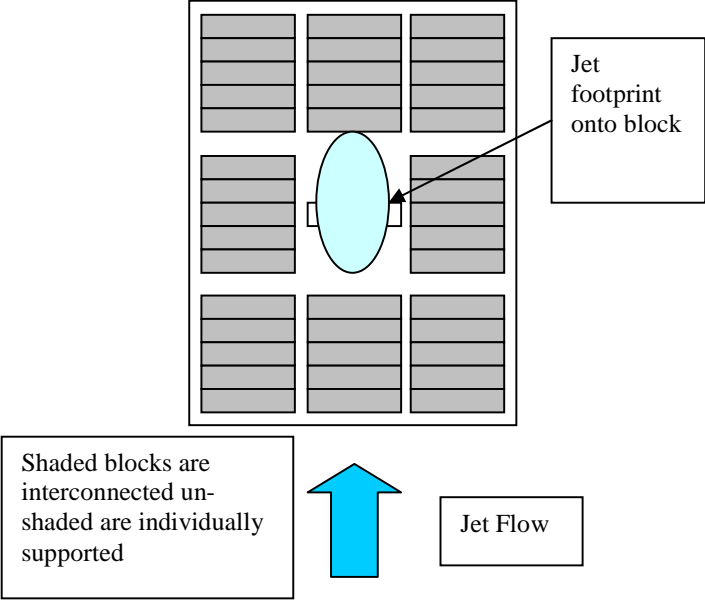
Run 26 Analysis



RUN 27

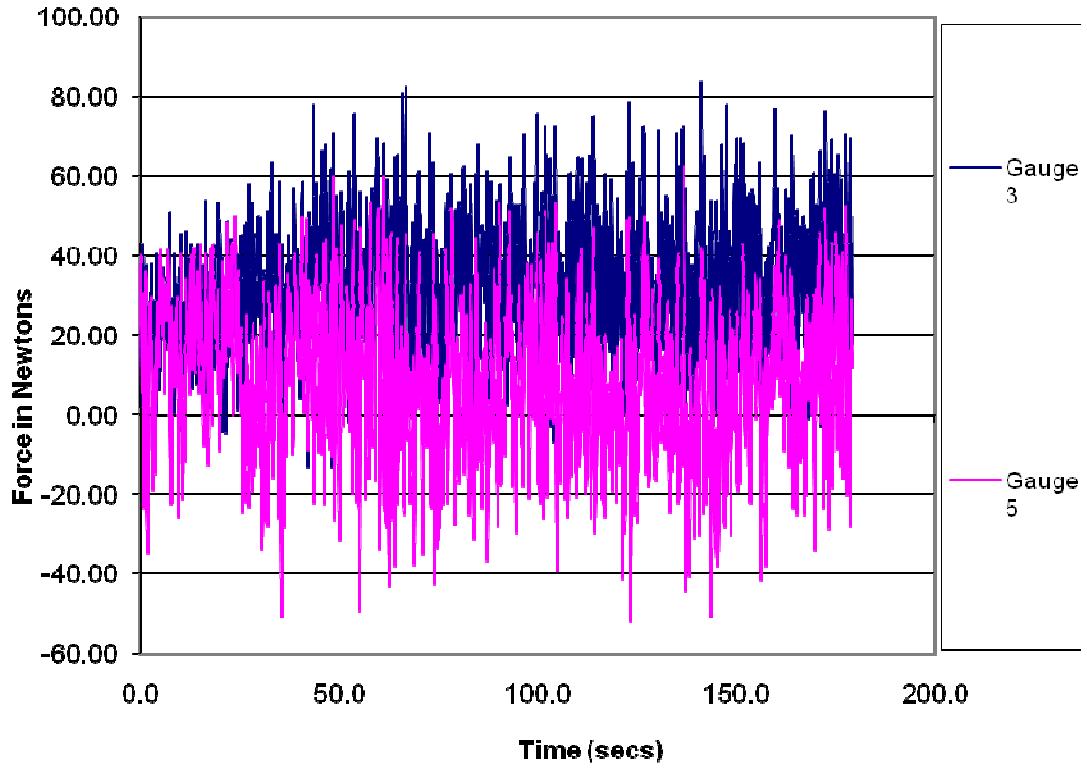
| Run No 27 | | |
|-----------------|---|--|
| Jet Angle | 40 degrees to horizontal | |
| Jet velocity | 2.00 ms ⁻¹ (prototype 8.92ms ⁻¹) | |
| Air Flow | 9% | |
| Seabed Location | Down | |



| | |
|----------------------|---|
| <p>Jet footprint</p> |  <p>Shaded blocks are interconnected unshaded are individually supported</p> <p>Jet footprint onto block</p> <p>Jet Flow</p> |
| <p>Comments</p> | <p>The test was carried out with the blocks installed as groups with the centre group of blocks being individually supported and unconnected to the adjacent blocks.</p> |

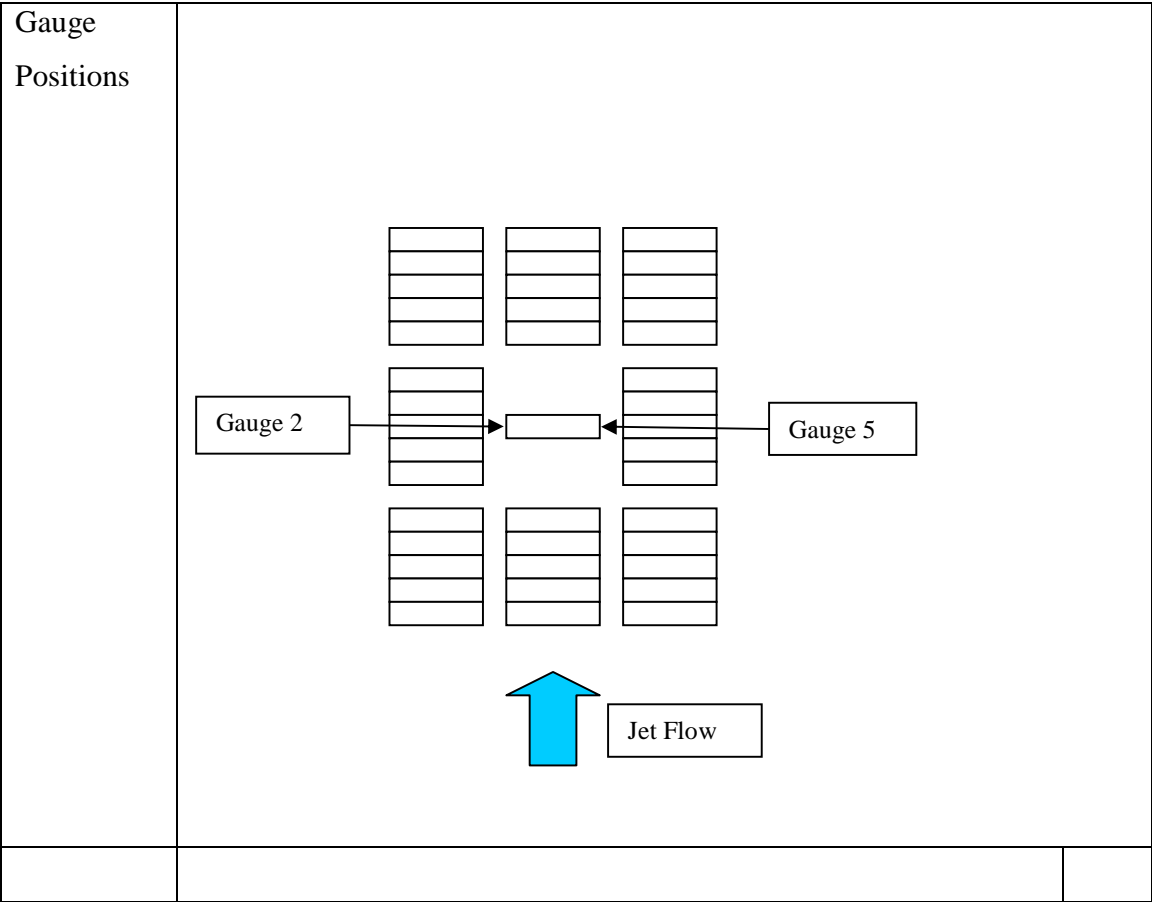
This run is to the same parameters as run 24 and has fairly similar results

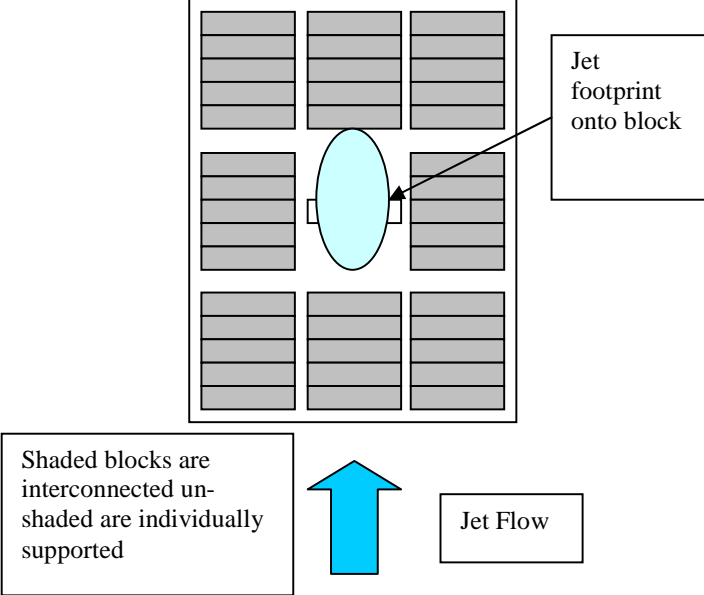
Run 27 Analysis



RUN 28

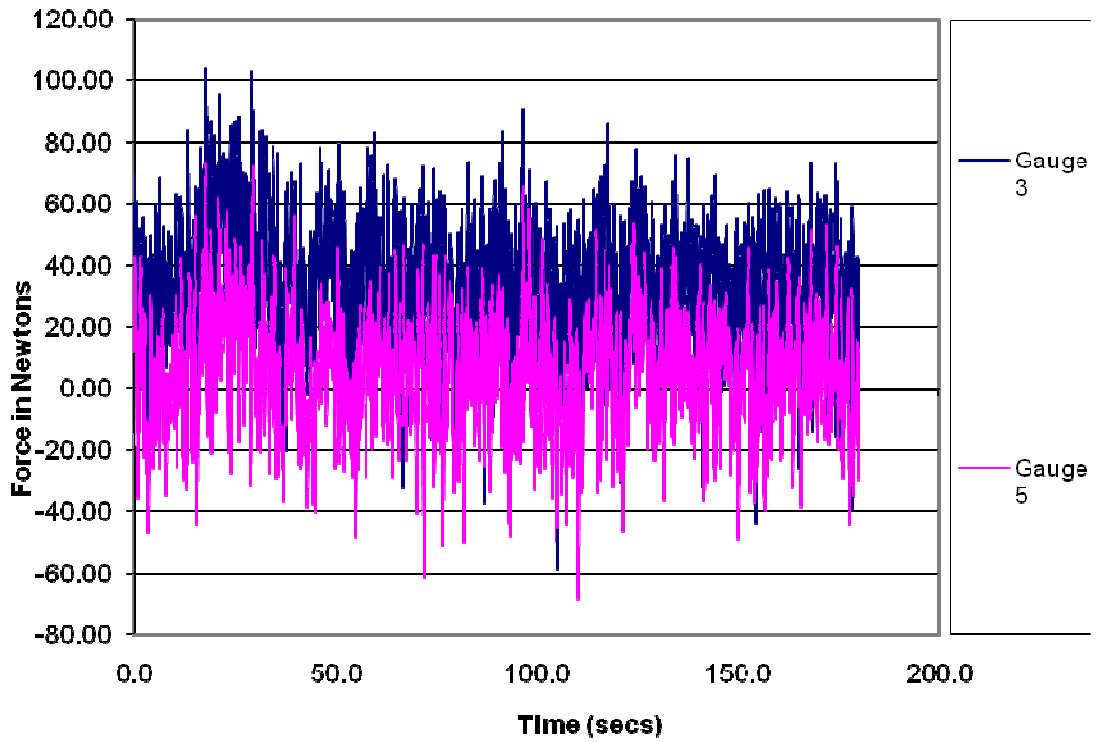
| Run No 28 | | |
|-----------------|--|--|
| Jet Angle | 40 degrees to horizontal | |
| Jet velocity | 1.46 ms ⁻¹ (prototype 11.31ms ⁻¹) | |
| Air Flow | 0 | |
| Seabed Location | Down | |
| | | |



| | |
|----------------------|---|
| <p>Jet footprint</p> |  <p>Shaded blocks are interconnected unshaded are individually supported</p> <p>Jet footprint onto block</p> <p>Jet Flow</p> |
| <p>Comments</p> | <p>The test was carried out with the blocks installed as groups with the centre group of blocks being individually supported and unconnected to the adjacent blocks.</p> |

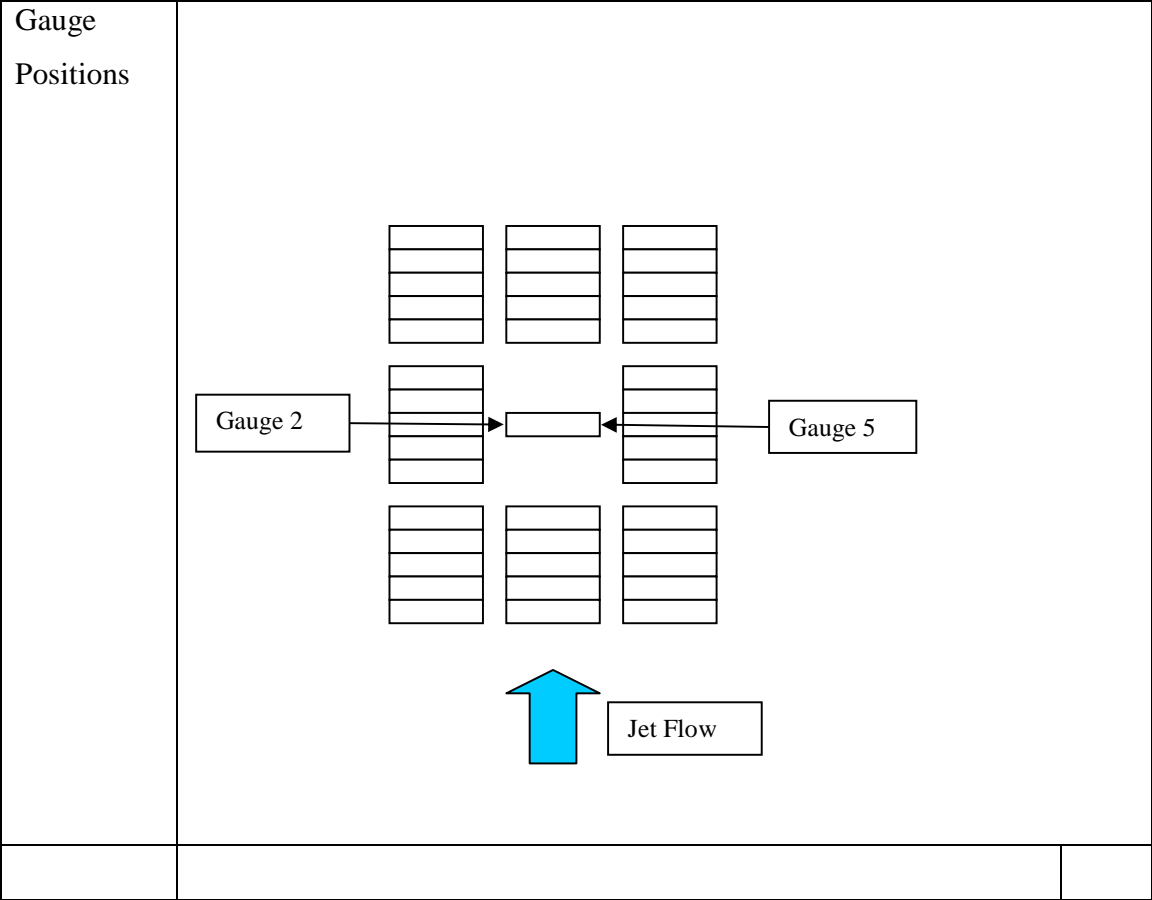
T the beginning of the run there is a noticeable secondary oscillation that gives very high peak values for the forces on the blocks. After this oscillation the forces decrease by about 20%

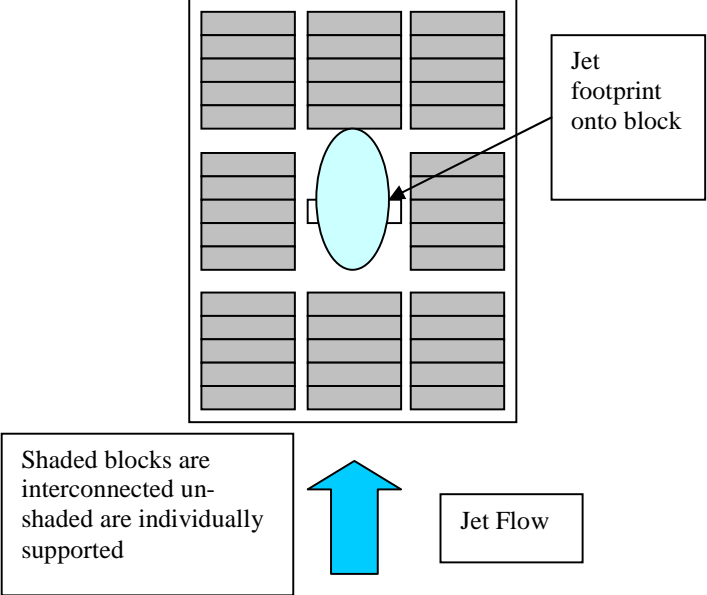
Run 28 Analysis



RUN 29

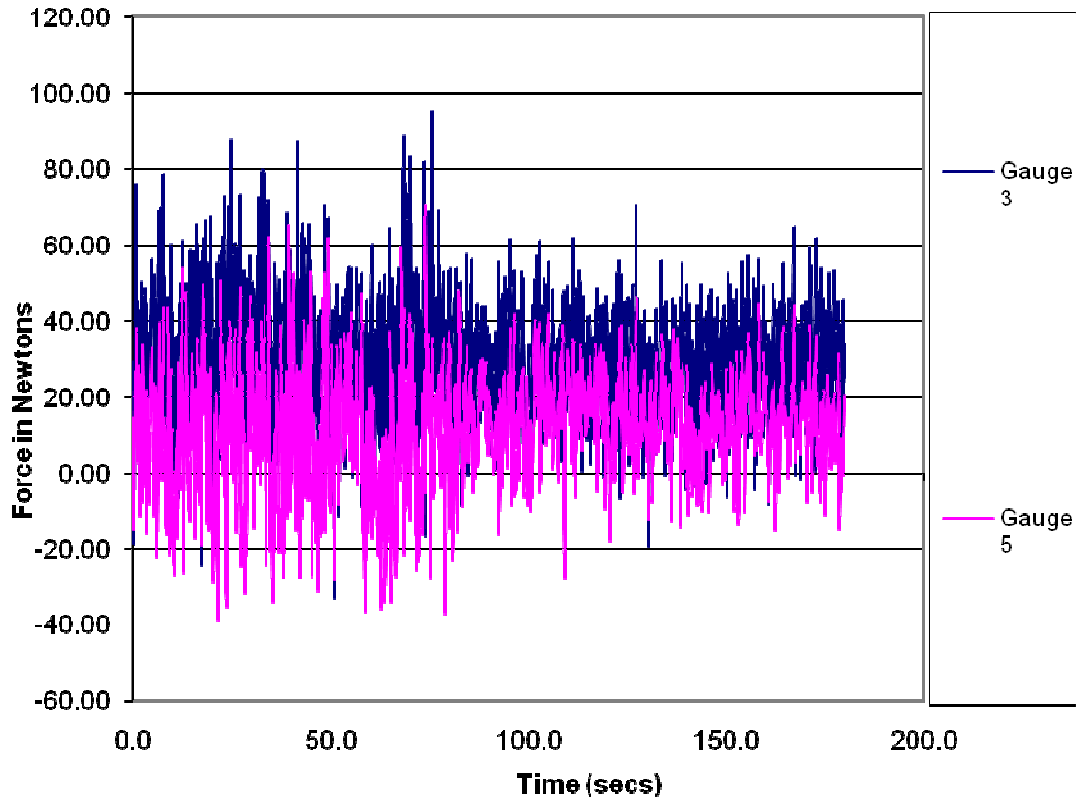
| Run No 29 | | |
|-----------------|---|--|
| Jet Angle | 60 degrees to horizontal | |
| Jet velocity | 1.46 ms ⁻¹ (prototype 6.51ms ⁻¹) | |
| Air Flow | 0 | |
| Seabed Location | Down | |
| | | |



| | |
|----------------------|---|
| <p>Jet footprint</p> |  <p>Shaded blocks are interconnected unshaded are individually supported</p> <p>Jet footprint onto block</p> <p>Jet Flow</p> |
| <p>Comments</p> | <p>The test was carried out with the blocks installed as groups with the centre group of blocks being individually supported and unconnected to the adjacent blocks.</p> |

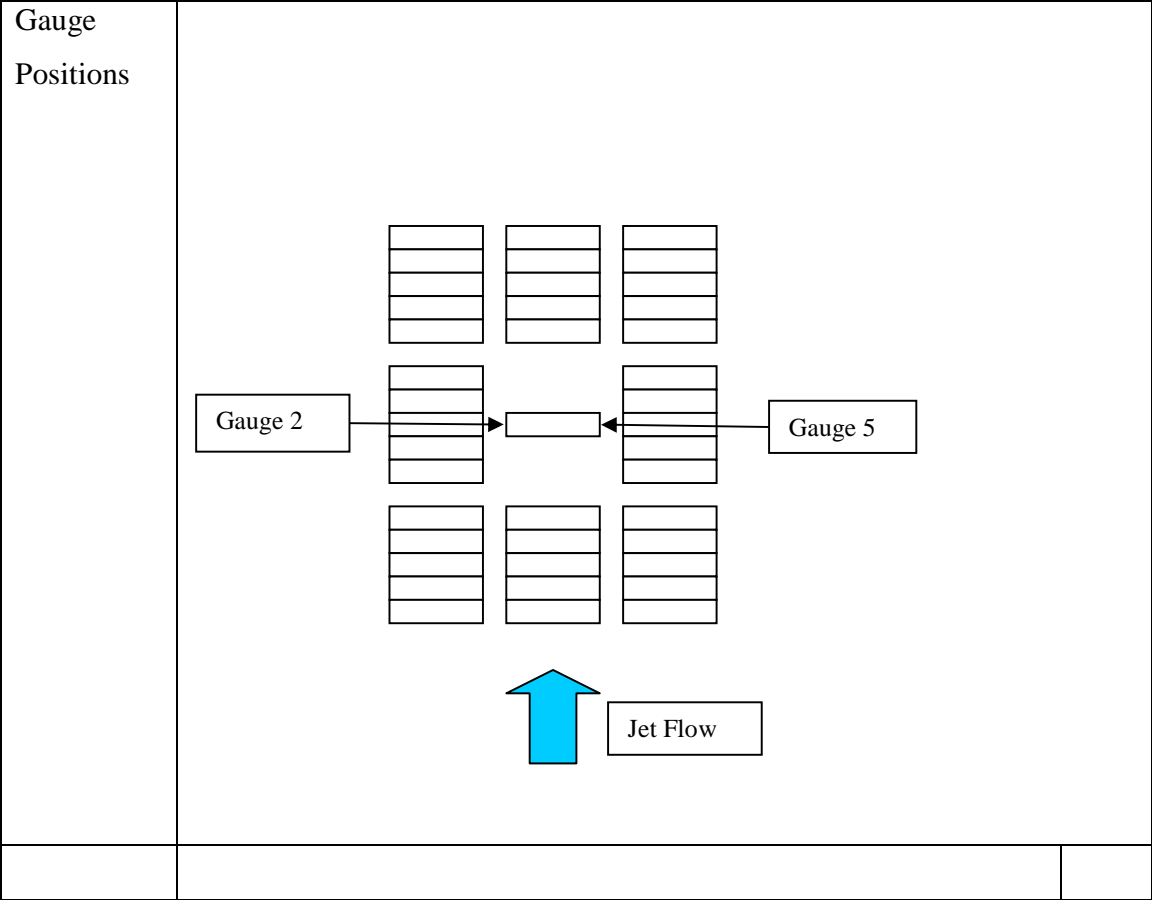
This run is to the same parameters as the previous run. The forces reduce noticeably halfway through the run and this is due to the block moving to the edge of the open area and touching an adjacent block.

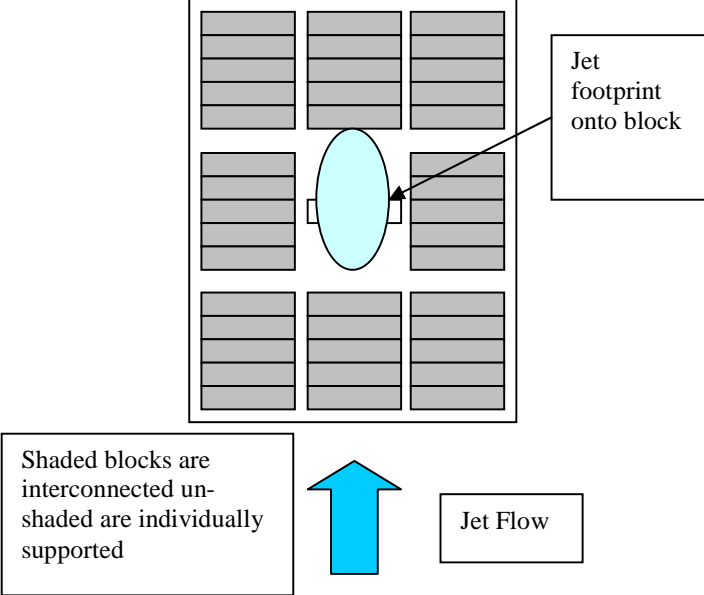
Run 29 Analysis



RUN 30

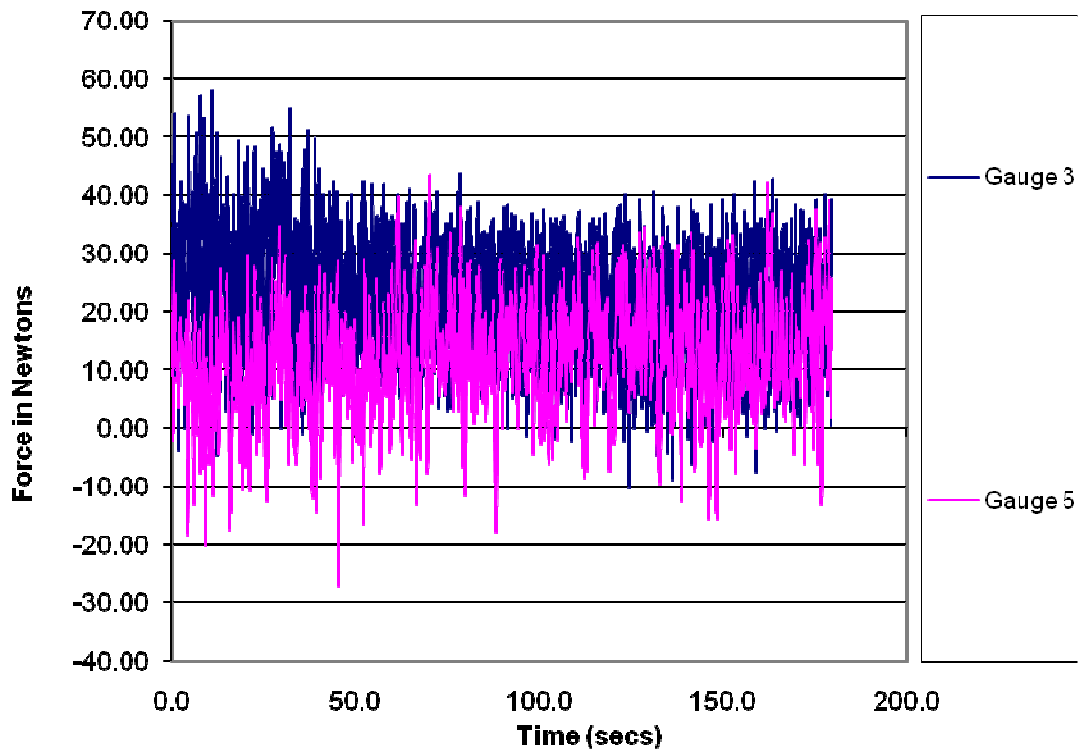
| Run No 30 | | |
|-----------------|---|--|
| Jet Angle | 40 degrees to horizontal | |
| Jet velocity | 1.46 ms ⁻¹ (prototype 6.51ms ⁻¹) | |
| Air Flow | 12% | |
| Seabed Location | Down | |
| | | |



| | |
|----------------------|---|
| <p>Jet footprint</p> |  <p>Shaded blocks are interconnected unshaded are individually supported</p> <p>Jet footprint onto block</p> <p>Jet Flow</p> |
| <p>Comments</p> | <p>The test was carried out with the blocks installed as groups with the centre group of blocks being individually supported and unconnected to the adjacent blocks.</p> |

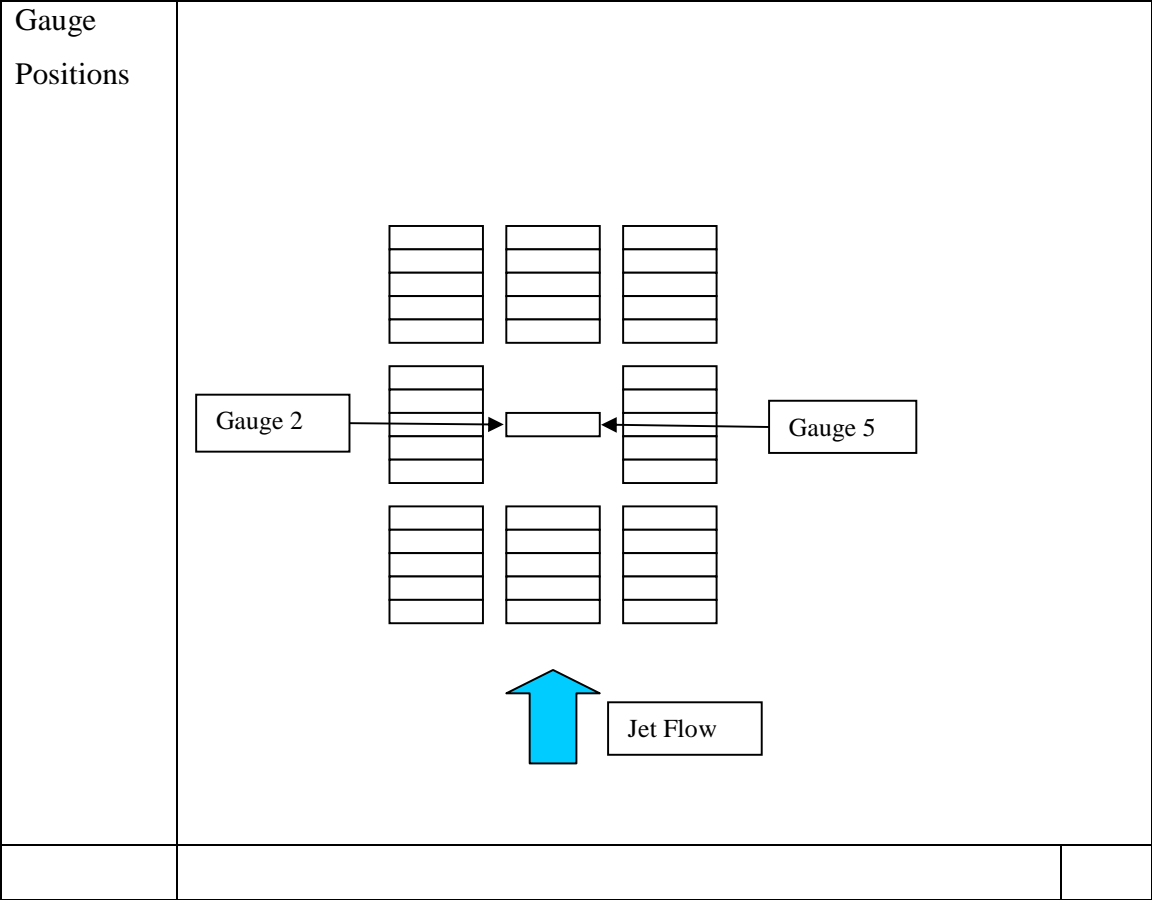
The first 25% of the run showed significantly higher block forces than the remainder (approximately 25%)

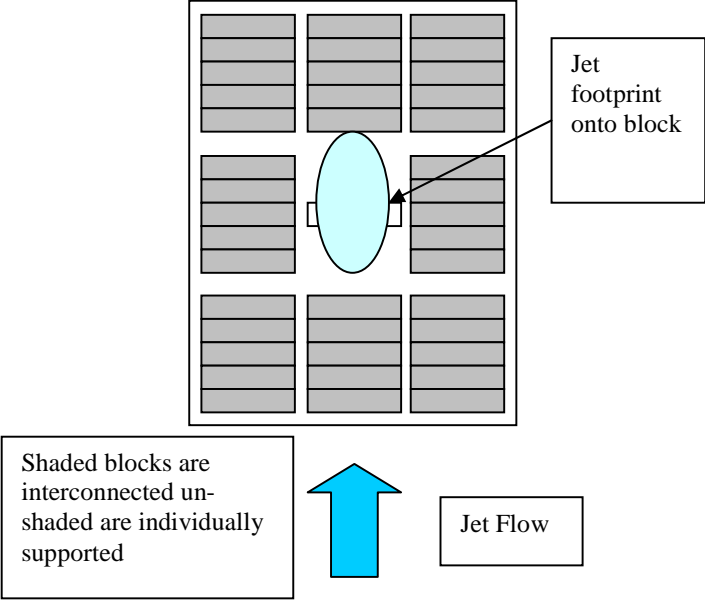
Run 30 Analysis



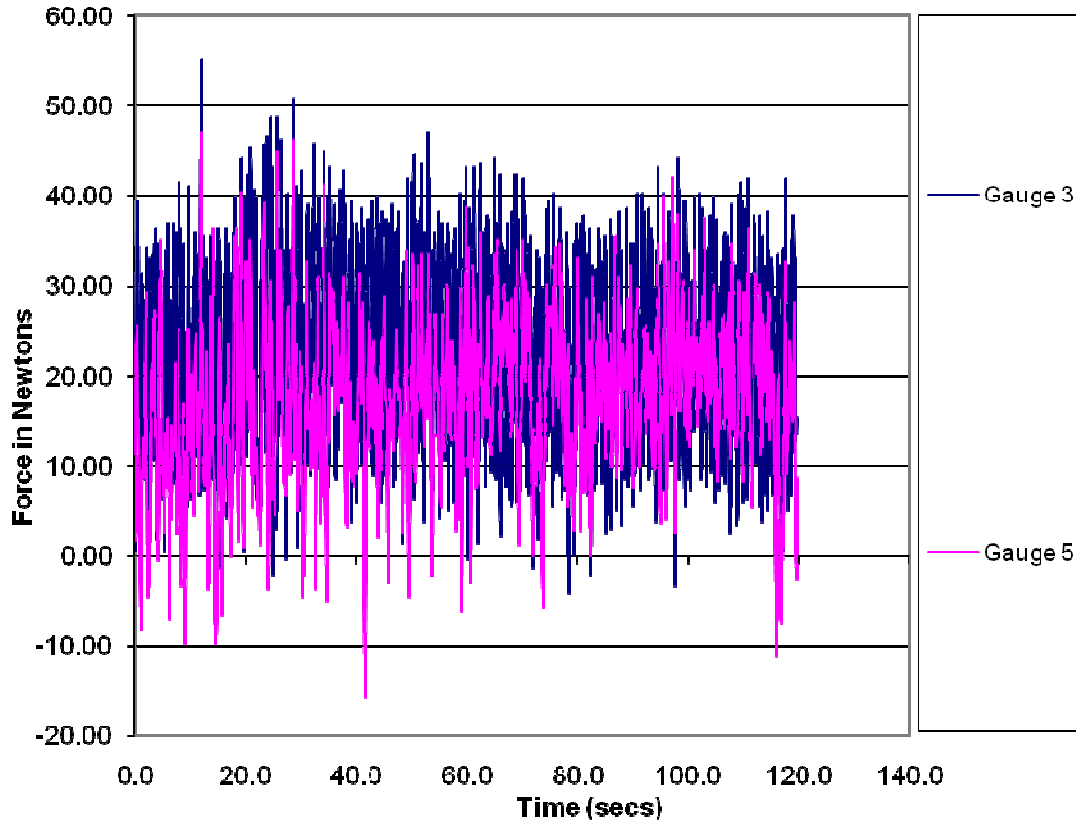
RUN 31

| Run No 31 | | |
|-----------------|---|--|
| Jet Angle | 40 degrees to horizontal | |
| Jet velocity | 1.46 ms ⁻¹ (prototype 6.51ms ⁻¹) | |
| Air Flow | 25% | |
| Seabed Location | Down | |



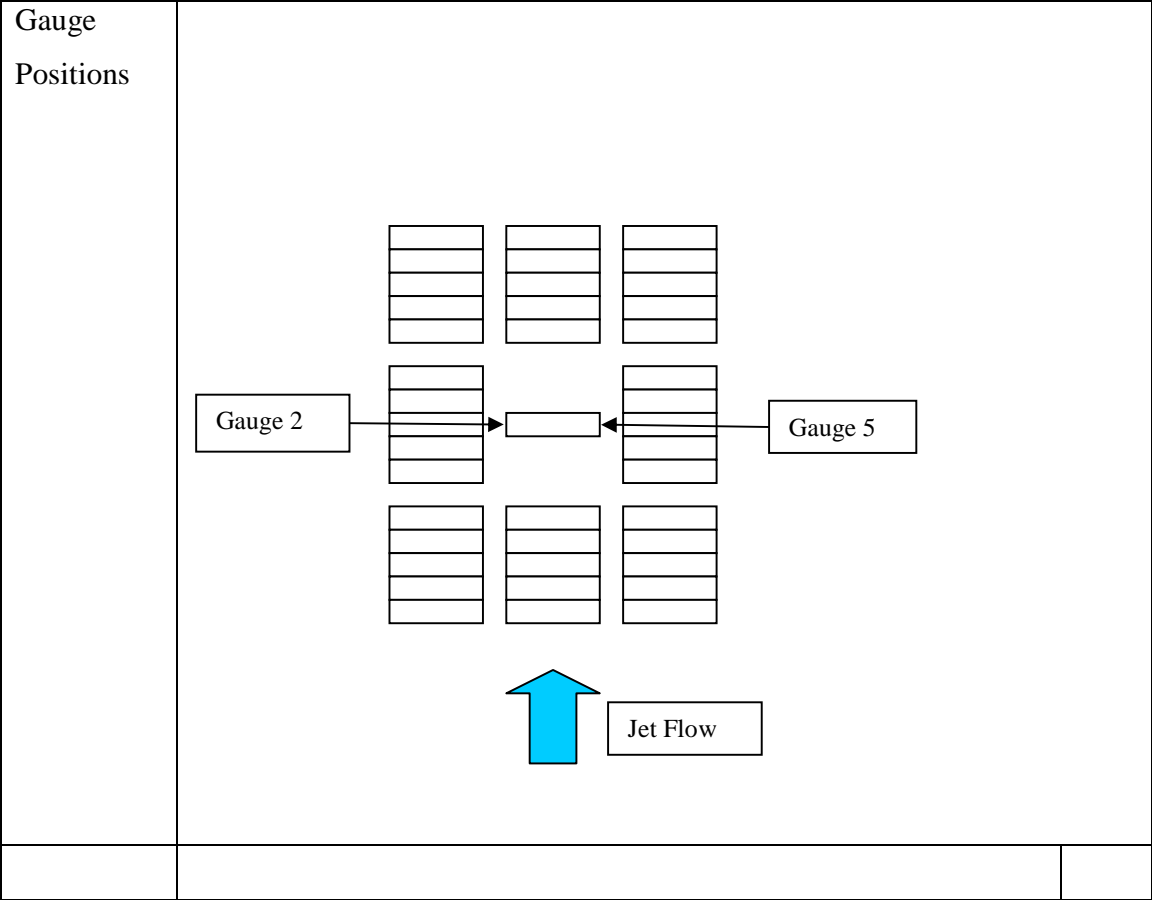
| | |
|----------------------|---|
| <p>Jet footprint</p> |  <p>Shaded blocks are interconnected unshaded are individually supported</p> <p>Jet footprint onto block</p> <p>Jet Flow</p> |
| <p>Comments</p> | <p>The test was carried out with the blocks installed as groups with the centre group of blocks being individually supported and unconnected to the adjacent blocks.</p> |

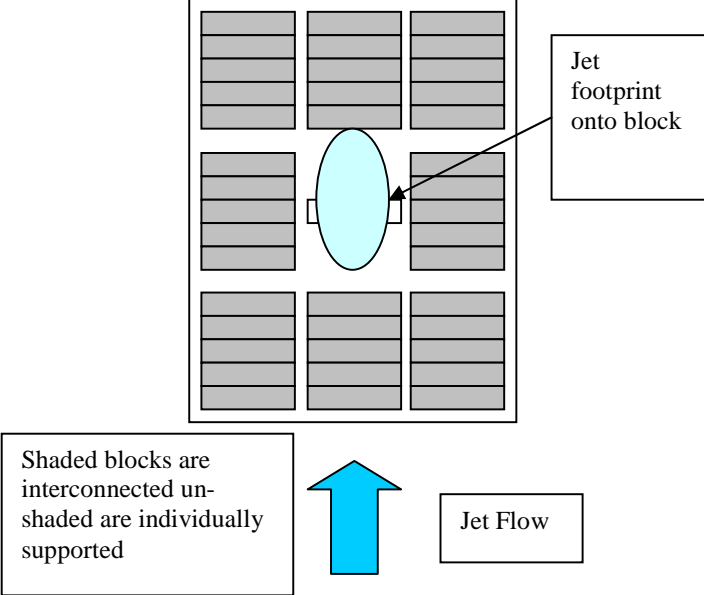
Run 31 Analysis



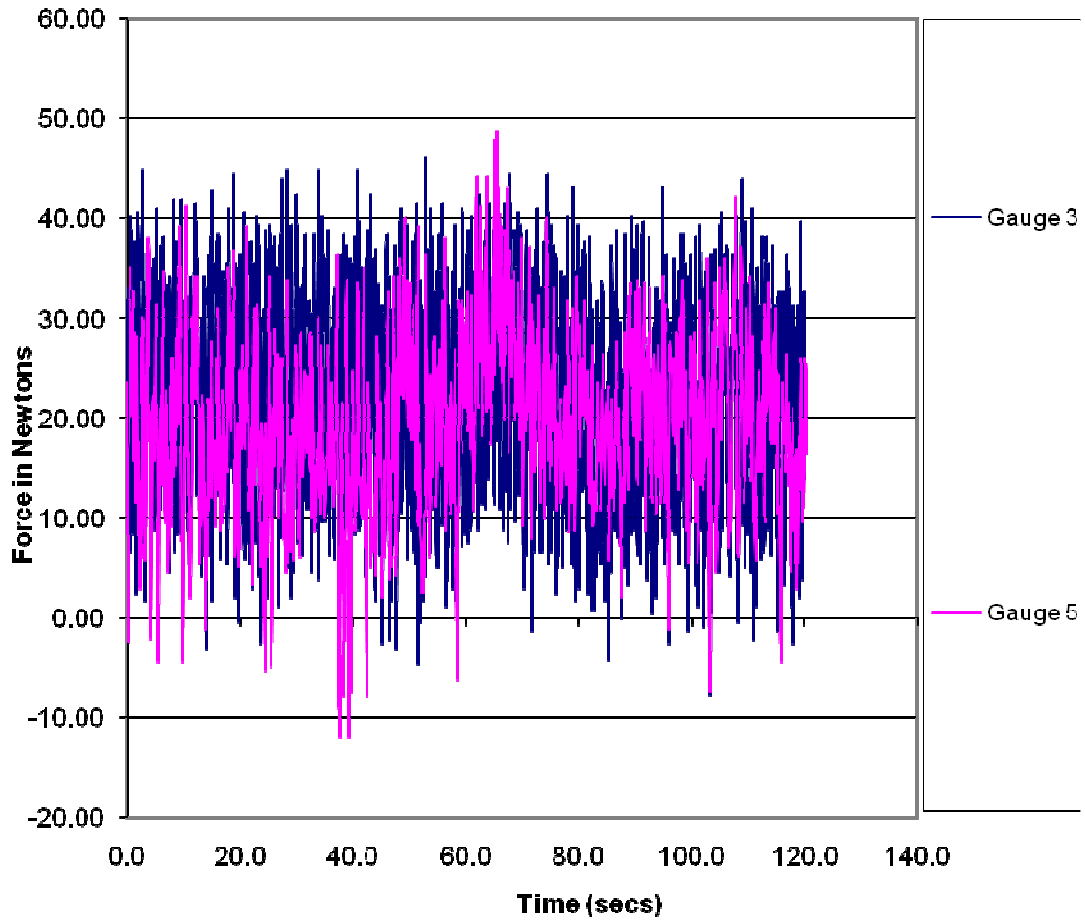
RUN 32

| Run No 32 | | |
|-----------------|---|--|
| Jet Angle | 40 degrees to horizontal | |
| Jet velocity | 1.46 ms ⁻¹ (prototype 6.51ms ⁻¹) | |
| Air Flow | 48% | |
| Seabed Location | Down | |
| | | |



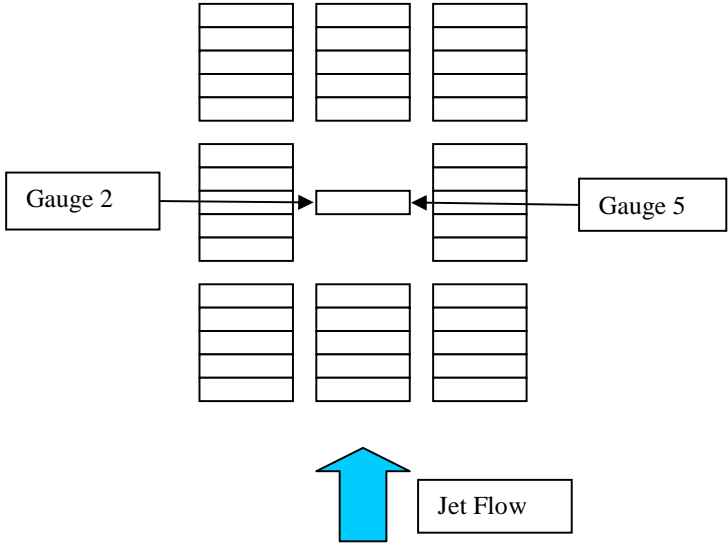
| | |
|----------------------|---|
| <p>Jet footprint</p> |  <p>Shaded blocks are interconnected unshaded are individually supported</p> <p>Jet footprint onto block</p> <p>Jet Flow</p> |
| <p>Comments</p> | <p>The test was carried out with the blocks installed as groups with the centre group of blocks being individually supported and unconnected to the adjacent blocks.</p> |

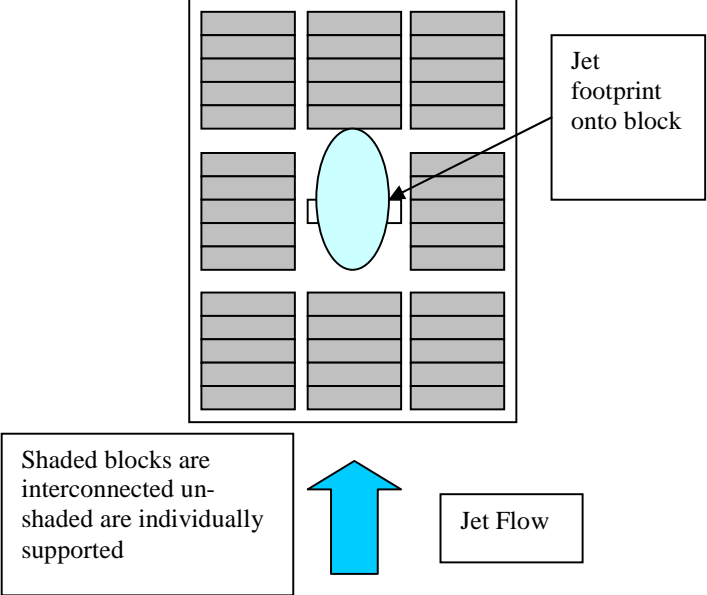
Run 32 Analysis



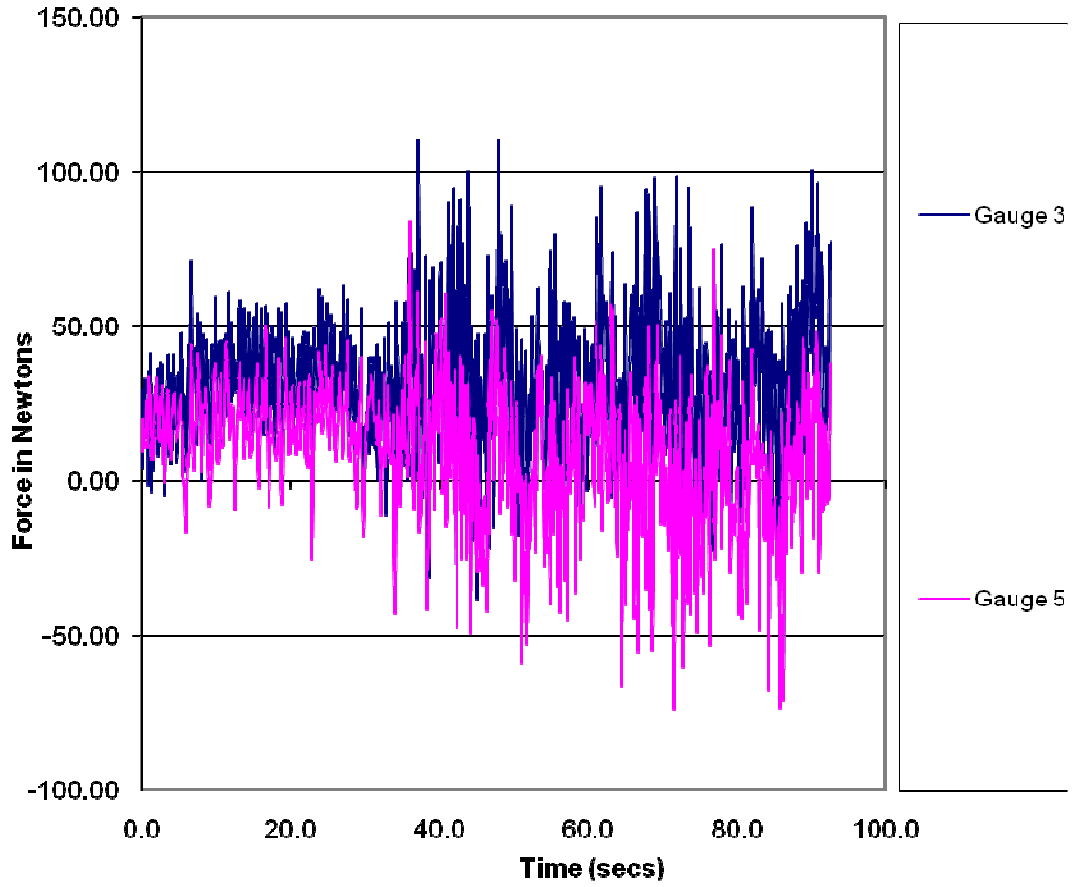
RUN 33

| Run No 33 | | |
|--------------|---|--|
| Jet Angle | 40 degrees to horizontal | |
| Jet velocity | 1.46 ms ⁻¹ (prototype 6.51ms ⁻¹) | |
| Air Flow | 0 | |

| | | |
|-----------------|---|--|
| Seabed Location | Down | |
| | | |
| Gauge Positions |  <p>The diagram shows a central arrangement of gauges. At the bottom center, a blue arrow labeled 'Jet Flow' points upwards. Above it, there are three vertical columns of gauges. The middle column contains a single gauge, while the left and right columns each contain three gauges. Two boxes labeled 'Gauge 2' and 'Gauge 5' are positioned to the left and right of the central gauge, respectively. Arrows point from these boxes towards the central gauge, indicating measurement points.</p> | |
| | | |

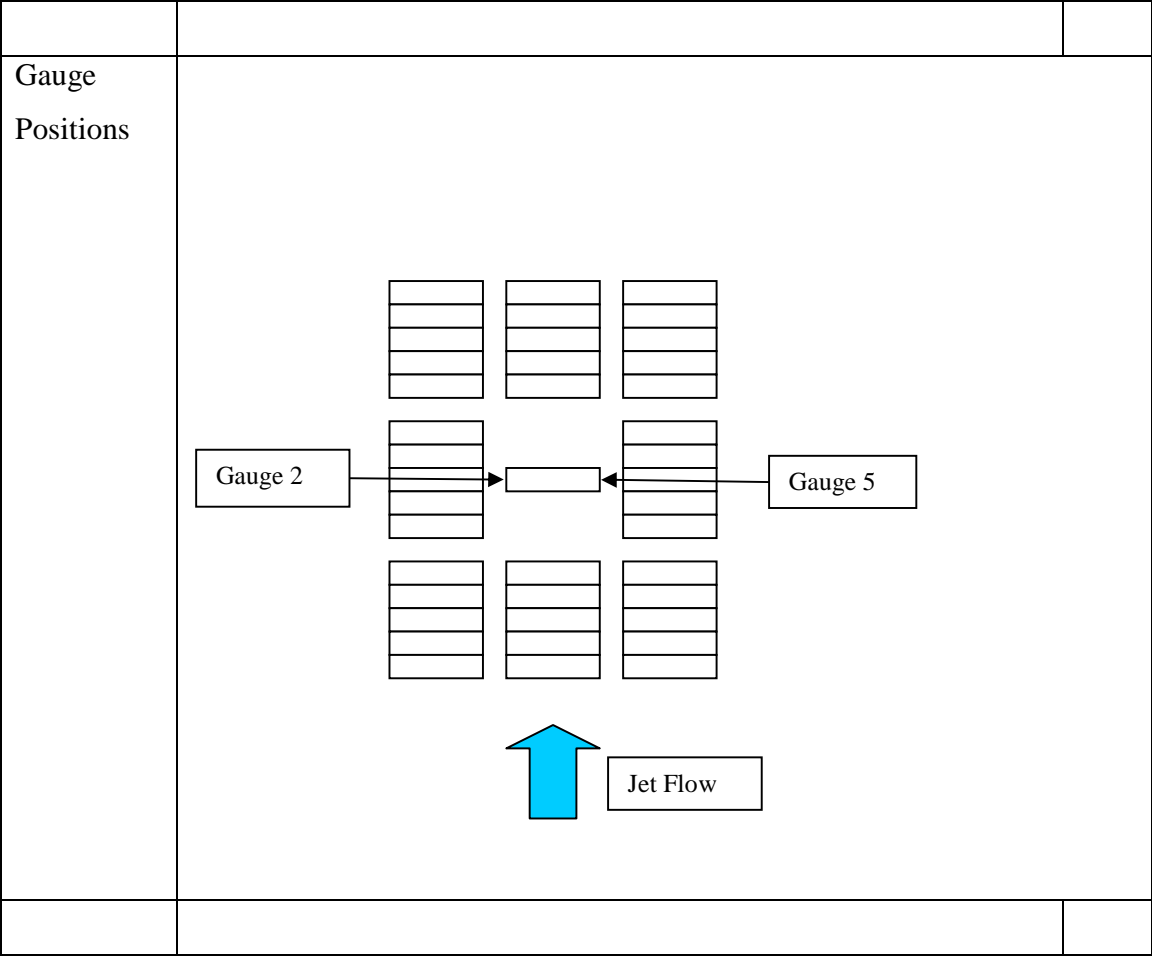
| | |
|----------------------|---|
| <p>Jet footprint</p> |  <p>Shaded blocks are interconnected unshaded are individually supported</p> <p>Jet footprint onto block</p> <p>Jet Flow</p> |
| <p>Comments</p> | <p>The test was carried out with the blocks installed as groups with the centre group of blocks being individually supported and unconnected to the adjacent blocks.</p> |

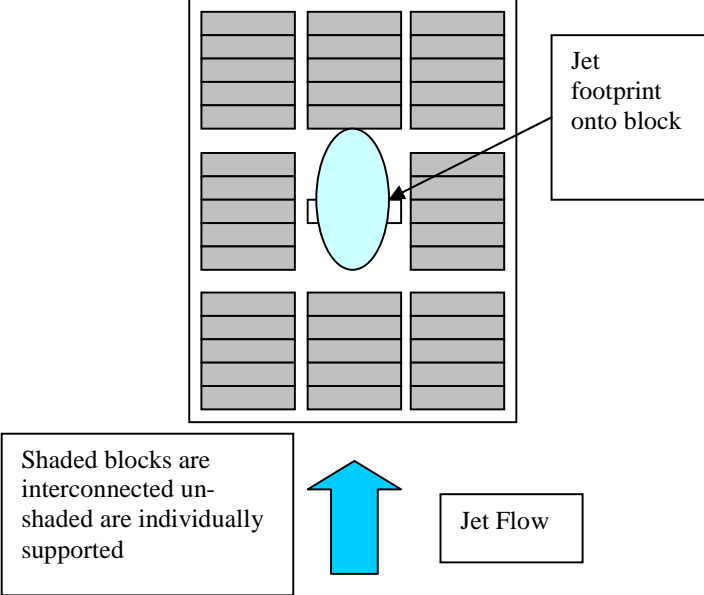
Run 33 Analysis



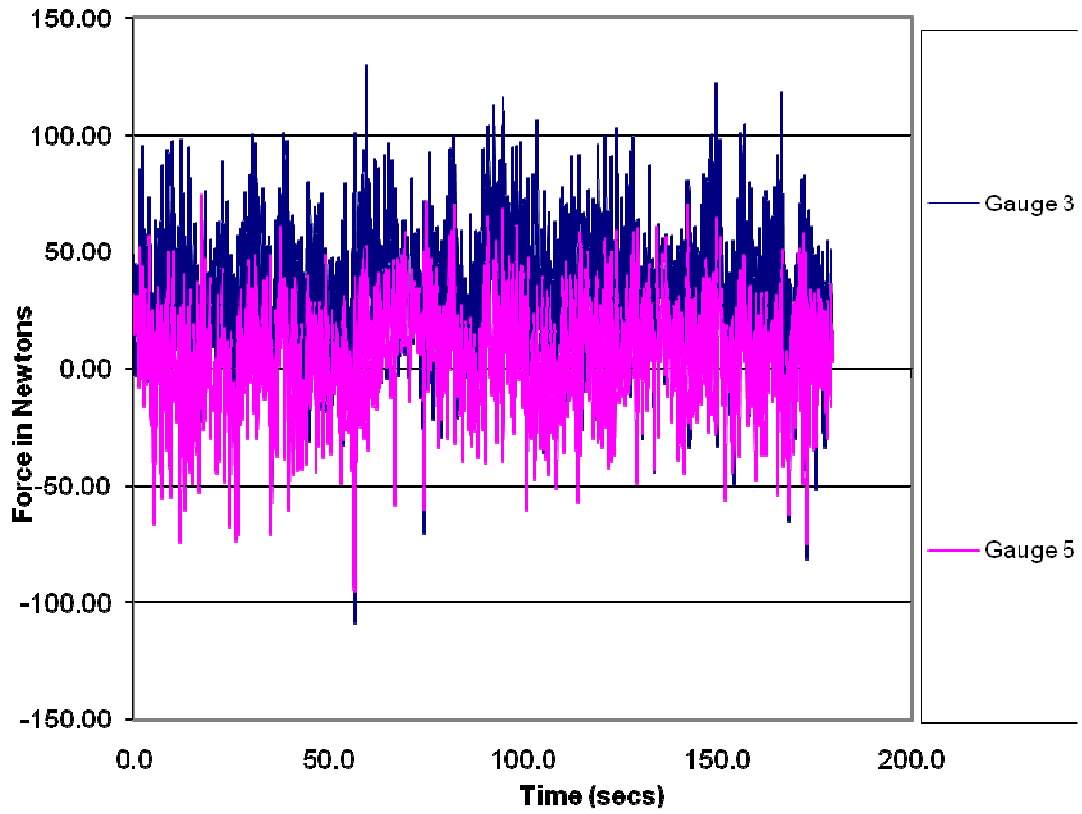
RUN 34

| Run No 34 | | |
|-----------------|--|--|
| Jet Angle | 40 degrees to horizontal | |
| Jet velocity | 2.49 ms ⁻¹ (prototype 11.31ms ⁻¹) | |
| Air Flow | 0 | |
| Seabed Location | Down | |



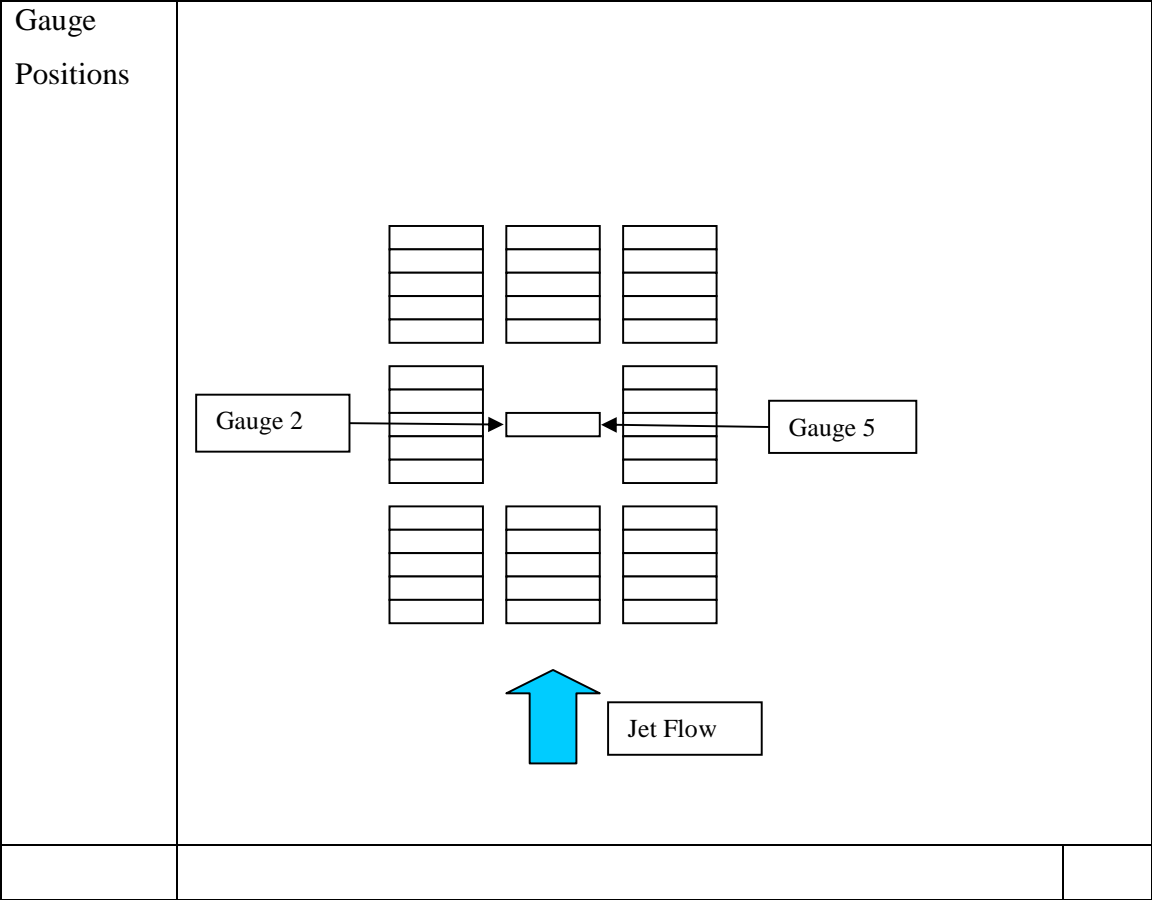
| | |
|----------------------|---|
| <p>Jet footprint</p> |  <p>Shaded blocks are interconnected unshaded are individually supported</p> <p>Jet footprint onto block</p> <p>Jet Flow</p> |
| <p>Comments</p> | <p>The test was carried out with the blocks installed as groups with the centre group of blocks being individually supported and unconnected to the adjacent blocks.</p> |

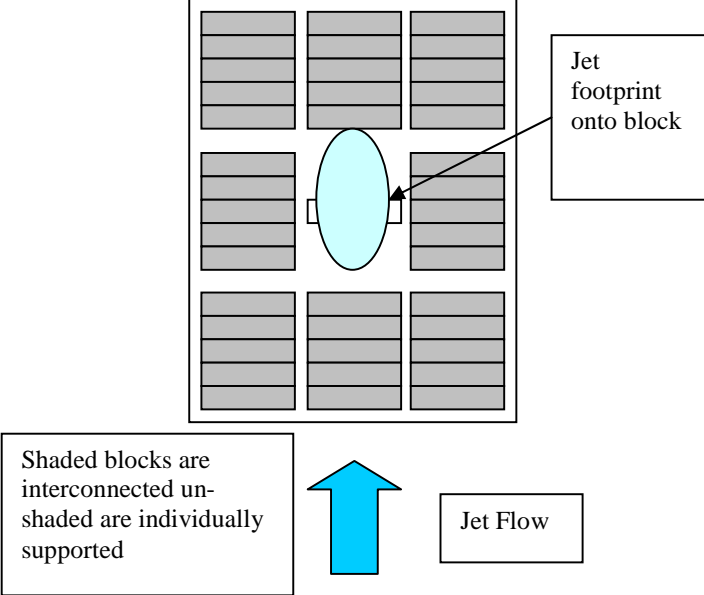
Run 34 Analysis



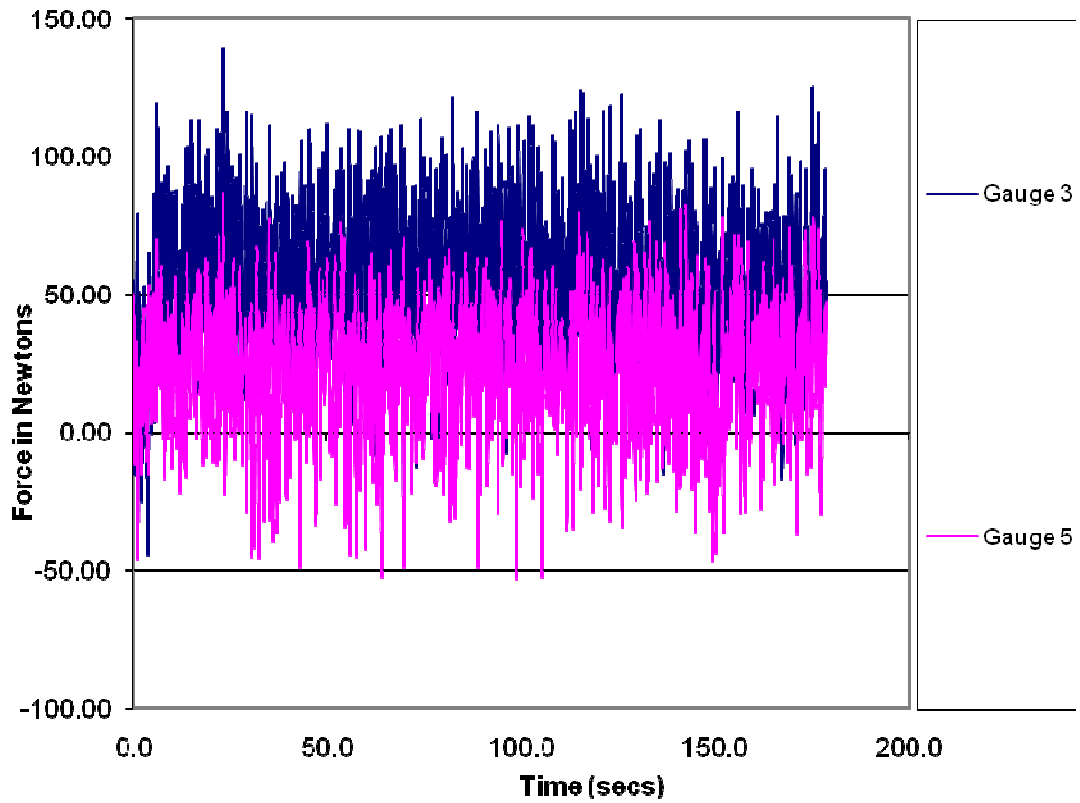
RUN 35

| Run No 35 | | |
|-----------------|--|--|
| Jet Angle | 40 degrees to horizontal | |
| Jet velocity | 2.49 ms ⁻¹ (prototype 11.31ms ⁻¹) | |
| Air Flow | 7% | |
| Seabed Location | Down | |



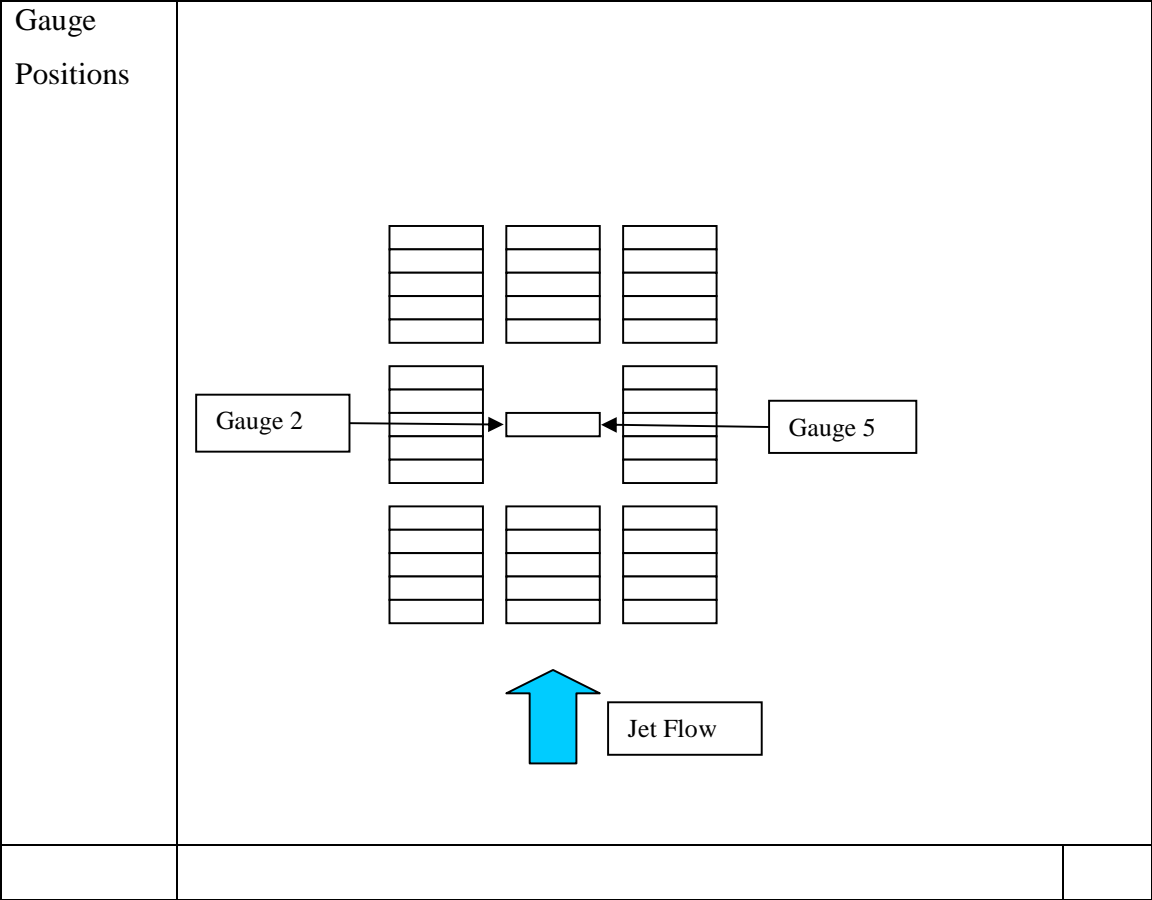
| | |
|----------------------|---|
| <p>Jet footprint</p> |  <p>Shaded blocks are interconnected unshaded are individually supported</p> <p>Jet footprint onto block</p> <p>Jet Flow</p> |
| <p>Comments</p> | <p>The test was carried out with the blocks installed as groups with the centre group of blocks being individually supported and unconnected to the adjacent blocks.</p> |

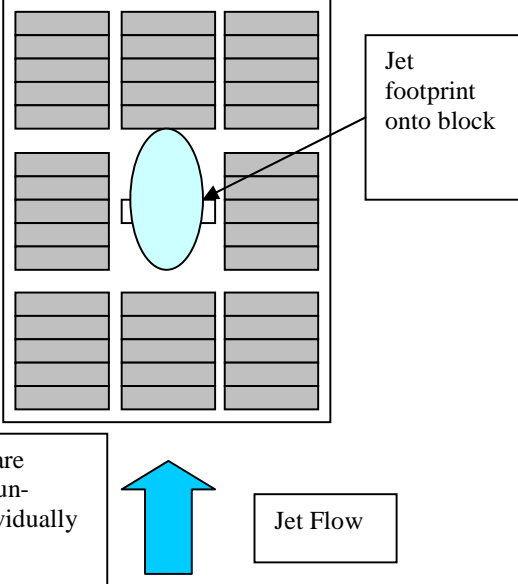
Run 35 Analysis



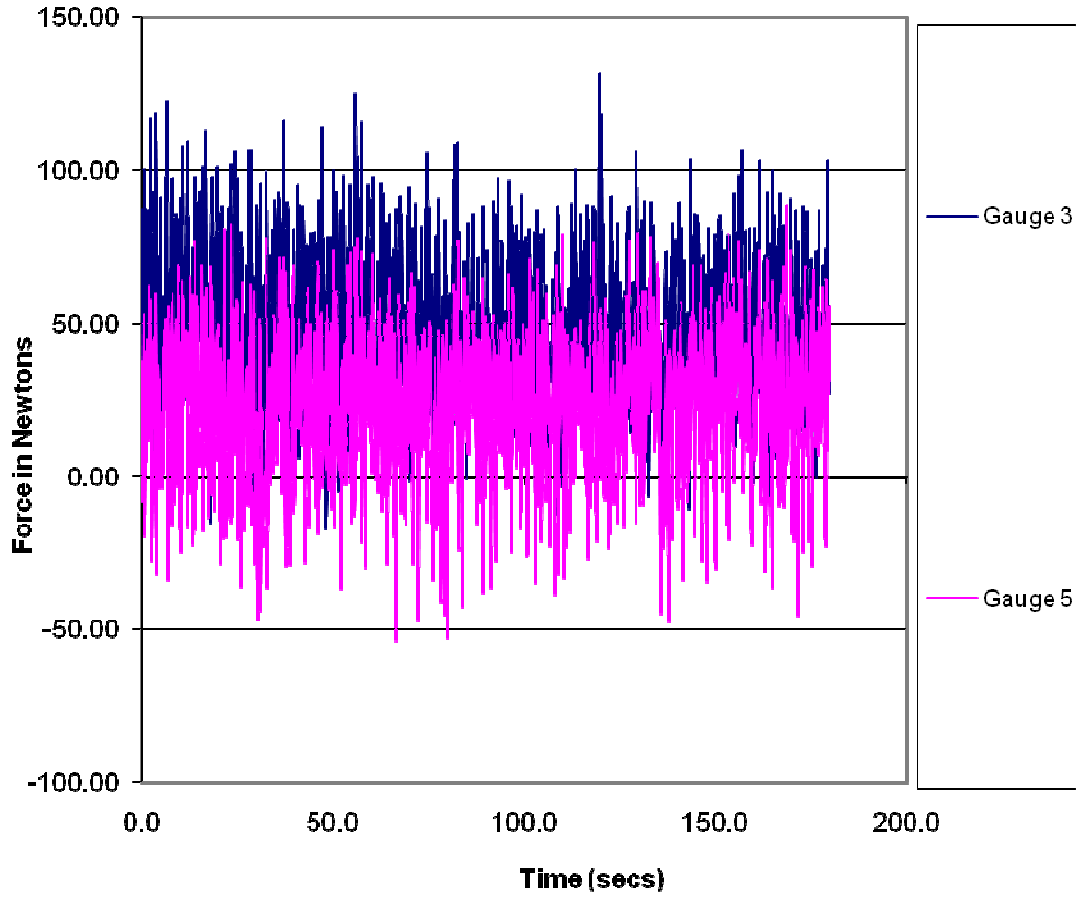
RUN 36

| Run No 36 | | |
|-----------------|--|--|
| Jet Angle | 60 degrees to horizontal | |
| Jet velocity | 2.49 ms ⁻¹ (prototype 11.31ms ⁻¹) | |
| Air Flow | 14% | |
| Seabed Location | Down | |



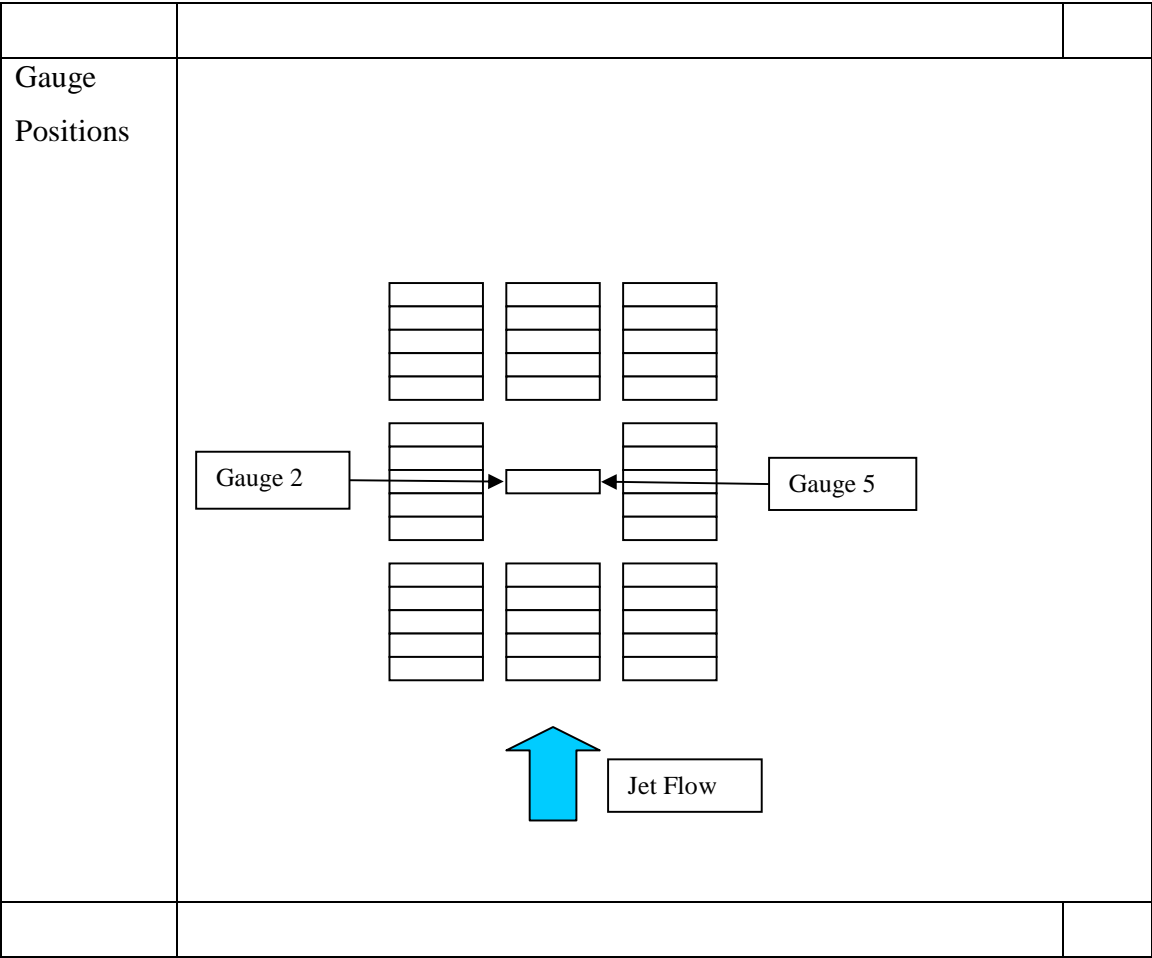
| | |
|----------------------|---|
| <p>Jet footprint</p> |  <p>The diagram shows a 3x3 grid of rectangular blocks. The central block is unshaded, while the other eight blocks are shaded. A cyan oval is positioned over the central block, with an arrow pointing to it from a box labeled 'Jet footprint onto block'. Below the grid, a blue arrow points upwards from a box labeled 'Jet Flow'. To the left of the blue arrow is a box containing the text: 'Shaded blocks are interconnected unshaded are individually supported'.</p> |
| <p>Comments</p> | <p>The test was carried out with the blocks installed as groups with the centre group of blocks being individually supported and unconnected to the adjacent blocks.</p> |

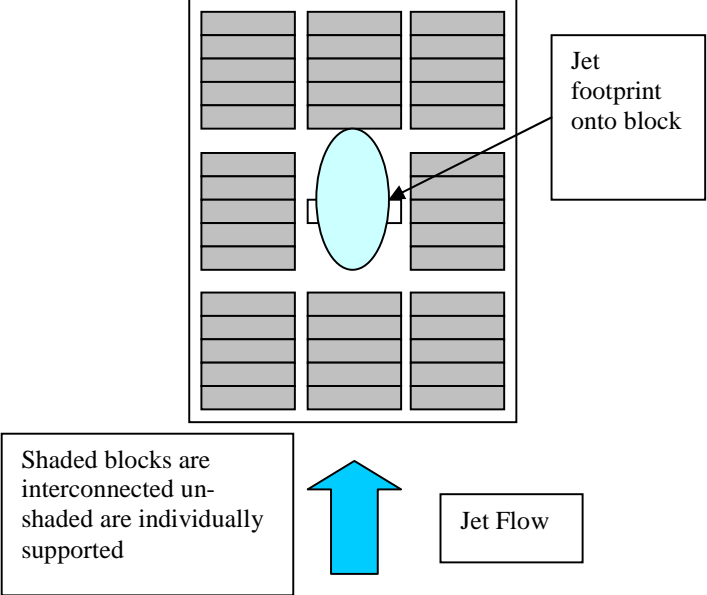
Run 36 Analysis



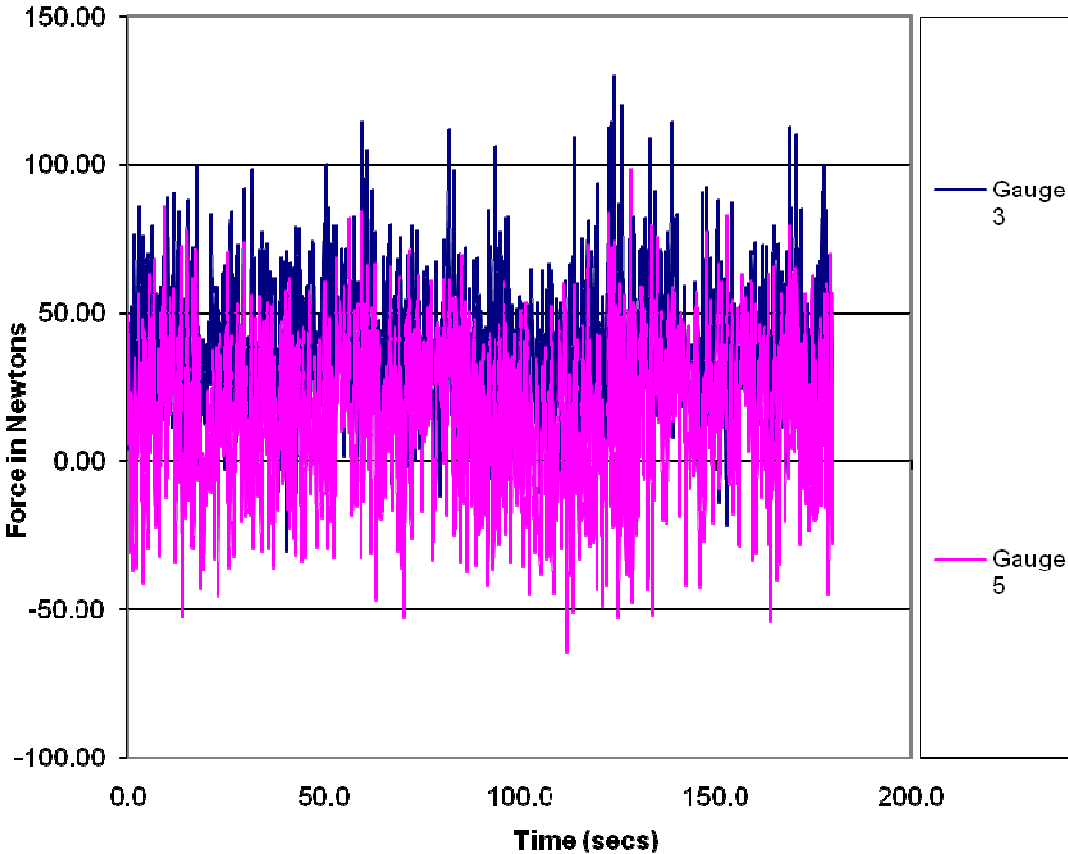
RUN 37

| Run No 37 | | |
|-----------------|--|--|
| Jet Angle | 40 degrees to horizontal | |
| Jet velocity | 2.49 ms ⁻¹ (prototype 11.31ms ⁻¹) | |
| Air Flow | 27% | |
| Seabed Location | Down | |



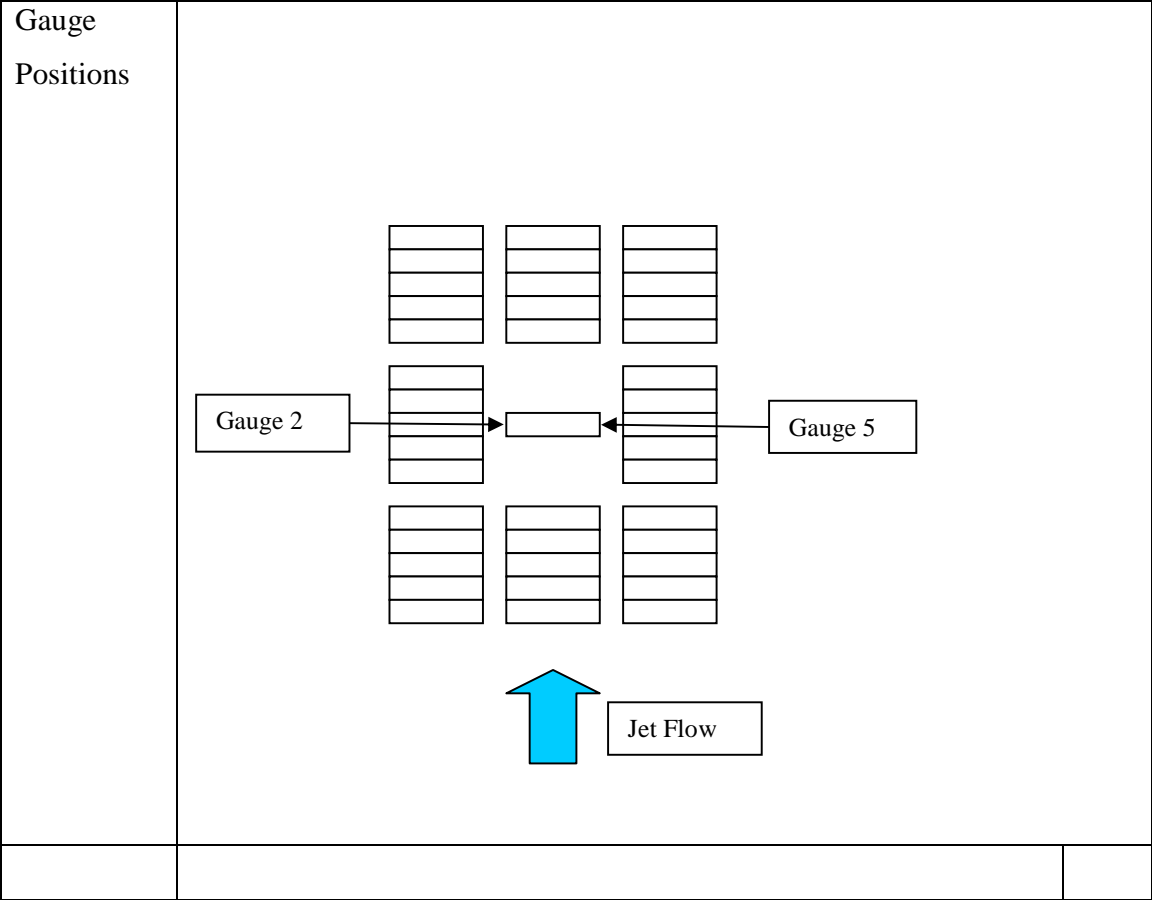
| | |
|----------------------|---|
| <p>Jet footprint</p> |  <p>Shaded blocks are interconnected unshaded are individually supported</p> <p>Jet footprint onto block</p> <p>Jet Flow</p> |
| <p>Comments</p> | <p>The test was carried out with the blocks installed as groups with the centre group of blocks being individually supported and unconnected to the adjacent blocks.</p> |

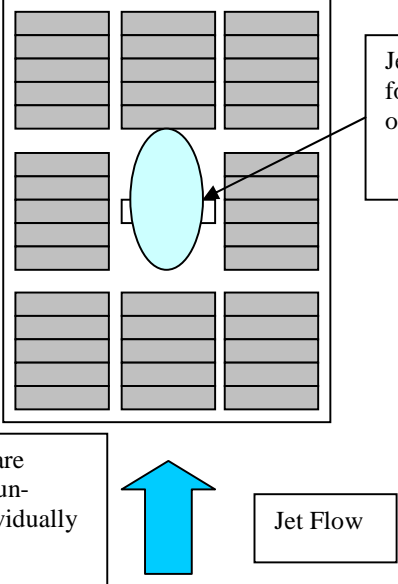
Run 37 Analysis



RUN 38

| Run No 38 | | |
|-----------------|--|--|
| Jet Angle | 40 degrees to horizontal | |
| Jet velocity | 2.49 ms ⁻¹ (prototype 11.31ms ⁻¹) | |
| Air Flow | 0 | |
| Seabed Location | Down | |



| | |
|----------------------|--|
| <p>Jet footprint</p> |  <p>The diagram shows a 3x3 grid of rectangular blocks. The central block is unshaded, while the other eight blocks are shaded. A cyan oval is centered on the unshaded block, and a cyan arrow points upwards from below the grid. A box labeled 'Jet footprint onto block' has an arrow pointing to the cyan oval. A box labeled 'Jet Flow' has an arrow pointing to the cyan arrow. A box below the grid contains the text: 'Shaded blocks are interconnected unshaded are individually supported'.</p> |
| <p>Comments</p> | <p>The test was carried out with the blocks installed as groups with the centre group of blocks being individually supported and unconnected to the adjacent blocks.</p> |

